Polyphosphoesters:

A degradable alternative to polyolefins and poly(ethylene glycol)

Dissertation

Zur Erlangung des akademischen Grades eines

„Doctor rerum naturalium (Dr. rer. nat.)"

Im Promotionsfach Chemie

des Fachbereiches Chemie, Pharmazie, Geowissenschaften (FB09)

der Johannes Gutenberg-Universität

vorgelegt von

Hisaschi Tee

geboren in Frankfurt am Main

JOHANNES GUTENBERG UNIVERSITÄT MAINZ   JG|U   MAX PLANCK INSTITUTE FOR POLYMER RESEARCH

Dekan:

1. Gutachter:

2. Gutachter:

Die vorliegende Arbeit wurde in der Zeit von April 2015 bis Februar 2019 am Max-Planck-Institut für Polymerforschung in Mainz angefertigt. Hiermit versichere ich, die vorliegende Arbeit selbstständig und ohne Benutzung anderer als der angegebenen Hilfsmittel angefertigt zu haben. Alle Stellen, die wörtlich oder sinngemäß aus Veröffentlichungen oder anderen Quellen entnommen sind, wurden als solche eindeutig kenntlich gemacht. Diese Arbeit ist in gleicher oder ähnlicher Form noch nicht veröffentlicht und auch keiner anderen Prüfungsbehörde vorgelegt worden.

Hisaschi Tee

Mainz, Februar 2019

Für meine Familie

„Wer nicht fröhlich beginnt,
kann auch nichts Fröhliches schaffen"

-Jean Paul-

Danksagung

.

Table of content

Abstract

Polyphosphoesters (PPEs) are essential building blocks of life in the nature. They determine life in the form of deoxy- & ribonucleic acid (DNA & RNA), and as pyrophosphates, they store chemical energy in organisms. Thus it would be obvious to find these highly versatile PPEs as an important material class for many applications and especially for the biomedical area, however, compared to other materials they have been relatively scarcely researched up to date. In contrast, polyolefins are commodity polymers, due to cost, low weight, good mechanical properties, and their durability. However, if littered in nature they do not degrade over a period of decades to centuries. Therefore, mimics of polyolefins (and other commodities) based on PPEs are promising alternatives due to their biocompatibility and –degradability. In addition, the chemical versatility of PPEs due to the pentavalent phosphorus allows precise tuning of the desired properties, rendering PPEs as a promising biomaterial. This thesis developed PPEs that can substitute hydrophobic polyolefins, but also very hydrophilic poly(ethylene glycol) by chemical design of the building blocks. PPE-chemistry allows adjusting material properties for individual needs and to adjust the degradation behavior.

Chapter 1 describes the synthesis of Polyethylene mimics of semicrystalline polyphosphoesters (PPE)s with an adjustable amount of non-covalent crosslinks. Acyclic diene metathesis (ADMET) copolymerization of a phosphoric acid triester with a novel phosphoric acid diester monomer was achieved and PPEs with different comonomer ratios and 0%, 20%, 40% and 100% of phosphodiester content were synthesized. The phosphodiester groups result in supramolecular interactions between the polymer chains, with the P-OH-functionality as H-bond donor and the P=O-group as H-bond acceptor. A library of unsaturated and saturated PPEs were prepared and analyzed in detail by NMR spectroscopy, size exclusion chromatography, differential scanning calorimetry, thermogravimetry, rheology, and stress-strain measurements. The introduction of the supramolecular crosslinks into the aliphatic and hydrophobic PPEs proved a significant impact on the materials properties: increased glass transition and melting temperatures were obtained and an increase of the storage modulus of the polymers was achieved. This specific combination of a flexible aliphatic backbone and a supramolecular H-bonding interaction between the chains were maximized in the homopolymer of the phosphodiester monomer, which featured additional properties, such as shape memory properties and polymer samples could be healed after cutting. The P-OH-groups also proved a strong adhesion towards metal surfaces, which was used together with the shape memory function in a model device which responds to a temperature stimulus with

Abstract

shape change. This systematic variation of phosphodiesters/phosphotriesters in polyethylene-mimics further underlines the versatility of the phosphorus chemistry to build up complex macromolecular architectures.

Chapter 2 focuses on the electrospinning of PPEs as a straightforward technique to produce nano- and micrometer sized materials. For the first time, PPEs were used in the electrospinning process and hydrophobic cargo was loaded into the PPE fibers. Fiber mats were produced based on semicrystalline long-chain alkyl PPEs. The effect of H-bonding from phosphoric acid diesters in the polymer chains, which act as noncovalent crosslinks, and their molecular weights were studied. Dexamethasone, an anti-inflammatory drug, was used as a hydrophobic drug which was loaded into the electrospun PPE fibers to study the release under various conditions Degradation studies were conducted, revealing that surface erosion and the selective hydrolytic cleavage of the pendant phenyl-ester was observed at pH 14.

Chapter 3 focuses on the degradation behavior of hydrophobic PPEs containing long aliphatic chains as a fast access to functional and potentially degradable polyethylene mimics. The degradation behavior of such hydrophobic polyphosphoesters (PPEs) is, however, not well studied and by tailoring of the ester stabilities, a precise cleavage of the side or the main chain should be feasible. Herein, we study the hydrolysis at pH 7 and pH 14 of long-chain alkyl polyphosphoesters with phenoxy and ethoxy side chains. Weight loss measurements and differential scanning calorimetry (DSC) was used to follow the degradation. We show that harsh basic conditions are necessary for hydrolysis to phosphoric acid diesters and precise side group hydrolysis is possible by using aromatic phosphoesters side groups. Furthermore, we discovered that such PPEs with an ethoxy side chain can form pyrophosphates with main chain hydrolysis under basic conditions.

Chapter 4 focuses on the preparation of biodegradable polyethylene-mimics by the introduction of pyrophosphate groups into the polymer backbone allowing not only hydrolysis of the backbone but also further degradation by microorganisms. Acyclic diene metathesis polymerization was used to prepare the biodegradable poly(pyrophosphate). The monomer is accessible via a three-step synthesis, in which the pyrophosphate was formed in the last step by DCC-coupling of two phosphoric acid derivatives. The poly(pyrophosphate) was characterized in detail by NMR spectroscopy, size exclusion chromatography, FTIR spectroscopy, differential scanning calorimetry, and thermogravimetry. X-ray diffraction was used to compare the crystallization structure in comparison to analog polyphosphates and showing poly(ethylene)-like structures. In spite of its hydrophobicity and water-insolubility, the pyrophosphate groups exhibited fast

hydrolysis resulting in polymer degradation when films were immersed in water and the hydrolyzed fragments were further biodegraded by microorganisms.

Chapter 5 focuses on the preparation of PPE hydrogels as a substitute for PEG hydrogels. In contrast to the previous chapters, this chapter uses ring-opening polymerization of cyclic phosphates in order to prepare degradable polymer gels. A photocrosslinkable, degradable, PPE, namely poly(methyl ethylene phosphoester) dimethacrylate (PMEP-DMA) was prepared. NMR spectroscopy and infrared spectroscopy was used to characterize the macromonomer. HPLC analysis showed a much higher hydrophilicity for PMEP-DMA compared to PEG-DMA. 10 and 15wt% PMEP hydrogels (HGs) were prepared by photopolymerization of an aqueous solution of the macromonomers. The PPE gels were compared to PEG hydrogels with respect to their swelling and water content and rheology analysis demonstrated viscoelastic characteristics. In contrast to the PEG HGs, the PMEP gels proved a rapid weight loss for the 10wt% PMEP gels and a much slower weight loss for 15wt% PMEP gels during incubation in aqueous media. The release of soluble polymer chains from the network and the formation of phosphoric acid diesters during the hydrolysis protocol was proven. Biocompatibility of the PPE gels was proven with MG-63 osteoblast cells; the PPE HGs further proved no significant cell adhesion similar to the PEG gels, which might find use in biodegradable antifouling surfaces or for drug release systems.
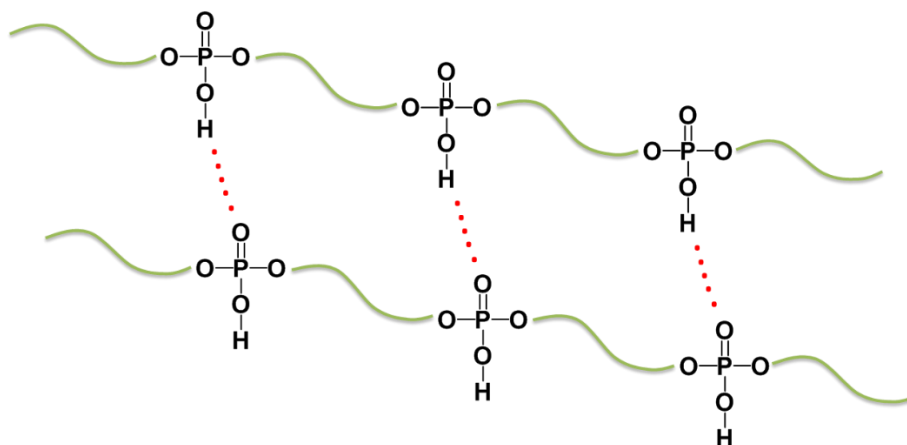
Zusammenfassung

Polyphosphoester (PPEs) sind ein lebenswichtiger Baustein von Leben in der Natur. Sie bestimmen das Leben in Form von Desoxyribonukleinsäure (DNS) und Ribonukleinsäure (RNS) und als Pyrophosphate speichern sie Energie in Organismen. Daher wäre es naheliegend diese vielfältige Materialklasse auch in vielen Anwendungen und Bereichen, vor allem im Biomedizinischen Bereich, wiederzufinden. Jedoch finden PPEs, neben einigen kommerziellen Flammschutzadditiven wenig Verwendung. Dies kann aufgrund der eingeschränkten Synthesemethoden der letzten Jahrzehnte liegen, wodurch die Funktionalität von PPEs nur teilweise genutzt werden konnte. Für viele Biomedizinische Anwendungen ist es jedoch entscheidend, die Anforderungen erfüllen zu können, indem man physikalische und chemische Eigenschaften, sowie das Abbauverhalten und -zeiten präzise einstellt.

Polyphosphoester sind aufgrund ihrer potentiellen Bioabbaubarkeit und –kompatibilität von besonderem Interesse für den Einsatz als Biomaterialien. Ihre Vielfältigkeit ist durch die Pentavalenz des Phosphors gegeben und erlaubt so die gewünschten Eigenschaften genau einzustellen. So kann die Seitenkette genutzt werden um eine hohe Dichte an funktionellen Gruppen einzuführen, die Kette im Polymerrückgrat zwischen den Phosphoestern bestimmt das Kristallisationsverhalten sowie die Hydrophilie oder Hydrophobizität, und das Bindungsmotiv sowie die Gruppen am Phosphoratom sind entscheidend für das Abbauprofil und –verhalten und beeinflussen zusätzlich die Kristallisation und die Hydrophilie.

Im Zuge dieser Doktorarbeit wurden die thermischen und mechanischen Eigenschaften von hydrophoben PPEs durch die Seitengruppe verändert um verschiedene Materialien herzustellen und diese auf Abbaubarkeit und Wirkstofffreisetzung zu untersuchen. Dadurch konnten stabile Polymerfilme oder auch Partikel und Fasern durch Elektrospinning in Mikrometergröße hergestellt werden. Beim Abbau zeigten sich diese PPEs sehr stabil und erst unter harschen basischen Bedingungen konnten Phosphotriester zu Phosphodiester hydrolisieren. Dabei konnten wir einen gezielten Seitenkettenabbau mit Phenoxyseitenketten zeigen, sowie zufällige Haupt- und Seitenkettenhydrolyse mit einer Ethoxyseitenkette, welche bei einer Hauptkettenabspaltung zu Pyrophosphaten weiterreagieren konnten. Daraufhin wurden bioabbaubare PPEs entwickelt indem Pyrophosphatgruppen in die Hauptkette eingebaut wurden, welche nach der Hydrolyse von Bakterien vollständig zu Wasser und Kohlenstoffdioxid abgebaut werden konnten. Desweiteren wurden durch gezielte Strukturänderungen der Hauptkette, hydrophile PPE Hydrogele entwickelt, wobei gezeigt werden konnte, dass diese im Vergleich zu PEG Hydrogelen im neutralen abgebaut werden können.
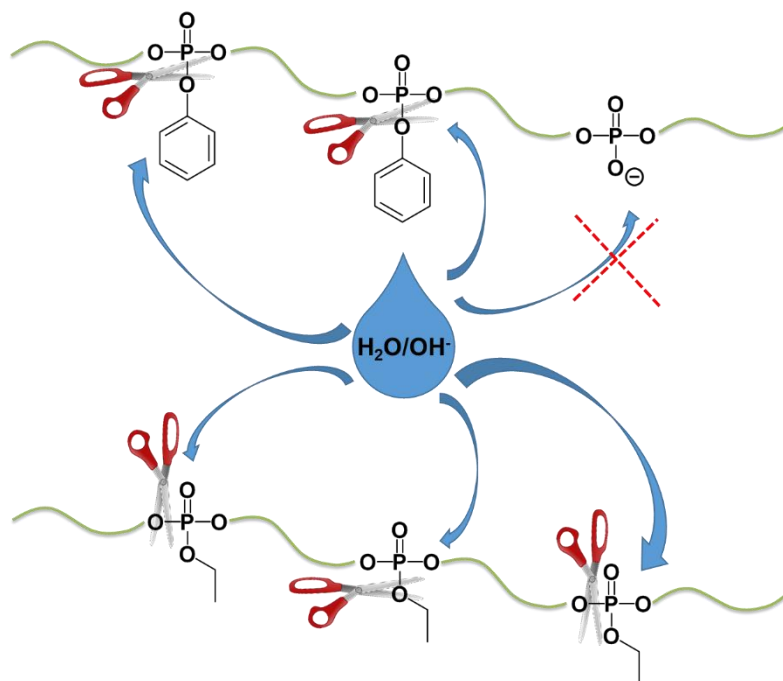
Graphical abstract
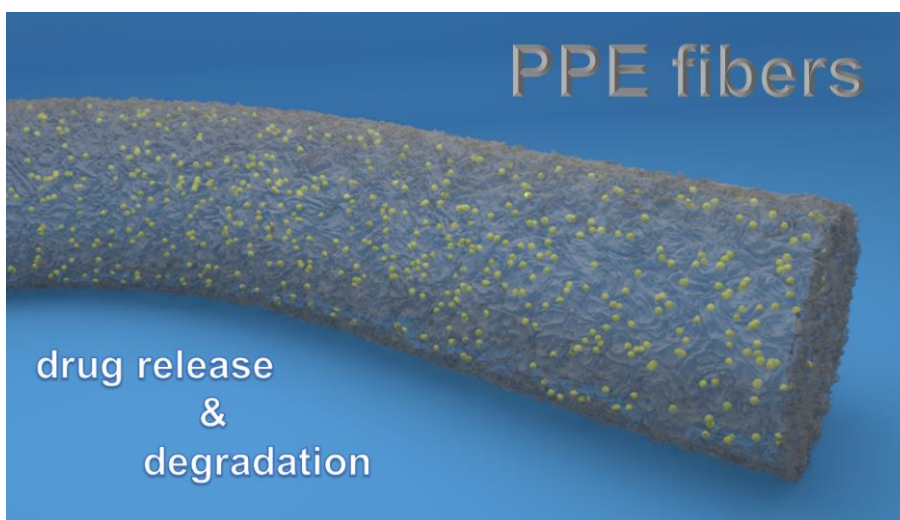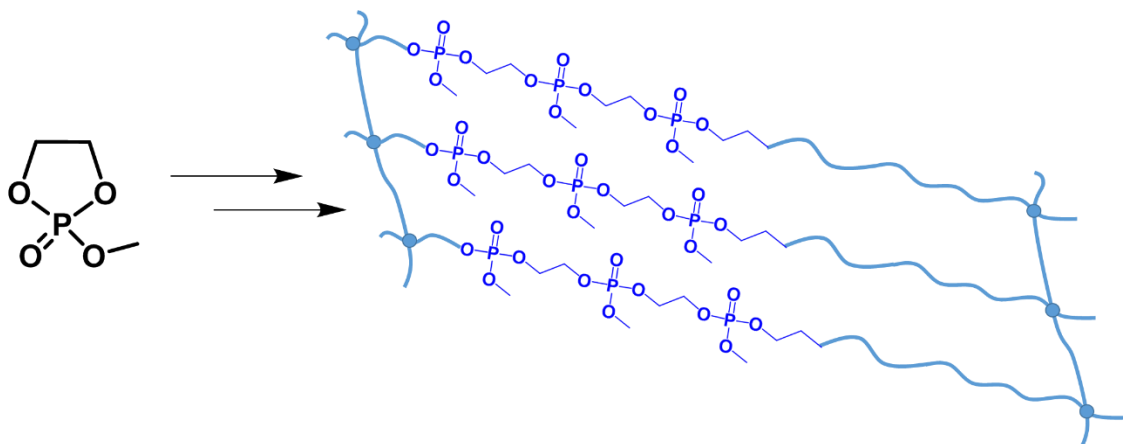
Motivation and Objectives

Degradable Polymers with precise properties are nowadays of great interest in material science and especially for biomedical applications. If littered in nature they won't remain over a period of decades or centuries and in the biomedical field, they will not accumulate in the body after fulfilling their intended task. Degradable polymers have found already several applications if degradation of the device is desired, e.g. for sustained drug release, temporary prostheses, or tissue engineering. For such uses, polyesters, polyamides, or polysaccharide-derivatives and others have been applied, which can be degraded by different enzymes in *vivo*. However, it's necessary to tailor the desired chemical, physical and degradation properties towards the demand in the application. Polyphosphoesters are a polymer class which is especially appealing due to their biocompatibility and versatility which allows the specific adjustment of the desired properties. The nature of the side chain and the spacer of the polymer backbone is a key factor for their crystallization behavior and allows the adjustment of the polymer polarity. Furthermore, the material properties can be strongly influenced with the pendant chains by introduction of a high density of functional groups. Also, the degradation behavior and profile can be altered with the binding motif and moiety around the phosphorus (Figure 1).
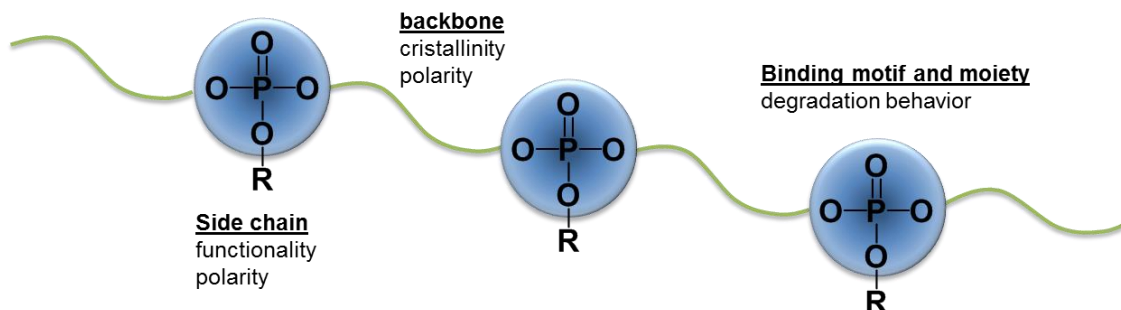

Figure 1. The versatility of polyphosphoesters and the parameters influencing the material properties.

The adjustment of mechanical and thermal properties, polarity and the degradation behavior will give access to advanced PPE-based materials and broaden their application range. Therefore the objectives of the following thesis is the adjustment of mechanical properties, polarity and functionality in PPEs facilitating the preparation of novel materials, and fundamental investigations on the resulting material properties and degradation behavior.

Altering the mechanical properties of hydrophobic polyphosphoesters (Chapter 1)

Degradable polyolefin mimics have attracted great interests due to littering in the environment. Polyphosphoesters with a long alkyl chains between the phosphate groups are chemically similar to poly(olefin)s with the potential degradable phosphoester group in the backbone and therefore an attractive choice. However, the phosphoester in the backbone limits the molecular weight which can be achieved and also acts as a defect in the crystalline part of the polymer resulting in usually brittle materials. **Therefore, the aim of this chapter is to improve the material properties of such polyphosphoester PE-mimics by introducing Hydrogen-bonds (H-bonds) in the side chain with phosphodiesters and to investigate the resulting properties with a saturated or unsaturated alkyl chain in the backbone resulting from acyclic diene metathesis (ADMET) polymerization.**

Degradation of PPE based materials (Chapter 2-3)

Resulting from Chapter 1, PPEs with improved mechanical properties were prepared and were investigated in Chapters 2 & 3 for the development of new materials to broaden the scope of possible applications of PPEs in the biomedical area. Chapter 2 uses Electrospinning as a versatile method to produce microsized particles and fibers with a high surface area to facilitate the investigation on degradation and drug release profile. These materials showed side chain degradation and therefore, in Chapter 3 the degradation of these hydrophobic PPEs with different side chains were conducted on polymer films to investigate the often mentioned biodegradability of PPEs due to the inherent cleavable ester linkages. **Hence, the objective of Chapter 2 & 3 is the investigation on fundamental material properties such as degradation behavior in dependency of the side chain.**

Biodegradable Poly(pyrophosphate) (Chapter 4)

Chapter 2 & 3 showed that the hydrolysis of PPEs is highly dependent to the side chain of PPEs which can result in just side chain cleavage, random cleavage of one side –or main chain or no hydrolysis at all. Since biodegradable polyolefin mimics are a momentous topic to avoid littering, **the objective of Chapter 4 is the development of a biodegradable Polyphosphoester as PE-mimic.**

PPE Hydrogels (Chapter 5)

Hydrogels are an appealing scaffold material for biomedical applications, due to their structural similarity to many extracellular matrixes of many tissues. For the polymer choice in hydrogels poly(ethylene glycol) is one of the most commonly applied hydrogel polymer for tissue engineering and is already FDA approved for several medical applications. However, hydrophilic PPEs were reported to have similar cell –and protein repellent properties, as well as being degradable which avoids bioaccumulation. **Therefore, the objective of Chapter 5 is the development of a novel PPE Hydrogel and the investigation of the degradation profile.**

Introduction

Main-chain poly(phosphoester)s: History, Syntheses, Degradation, Bio-and Flame-Retardant Applications

Foreword

The following introduction is based on the publication "Main-chain Poly(phosphoester)s: History, Syntheses, Degradation, Bio- and Flame-Retardant Applications" and is reproduced and altered with permission from *Progress in Polymer Science* **2017**, vol 73. pp.61-122 (Copyright 2017 Elsevier).
Authors: Kristin N. Bauer, Hisaschi T. Tee, Maria M. Velencoso, Frederik R. Wurm.

The introduction is further based on "Polyphosphoesters: An old biopolymer in a new light." In: "Polymers for Biomedicine: Synthesis, Characterization and Applications", Editor C. Scholz reproduced and altered with permission from John Wiley and Sons Copyright 2017.
Authors: Kristin N. Bauer, Hisaschi T.C. Tee, Evandro M. Alexandrino, Frederik R. Wurm.

Abstract

Nature on planet earth is dominated by polyphosphoesters (PPEs). They structure and determine life in the form of deoxy- & ribonucleic acid (DNA & RNA), and, as pyrophosphates, they store up chemical energy in organisms. Polymer chemistry, however, is dominated by the non-degradable polyolefins and degradable polycarboxylic esters (PCEs) that are produced on a large scale today. Recent work has illustrated the potential of PPEs for future applications beyond flame-retardancy -the main application of PPEs today-, and provided a coherent vision to implement this classic biopolymer in modern applications that demand biocompatibility and degradability as well as the possibility to adjust the properties to individual needs. This comprehensive review summarizes synthetic protocols to PPEs, their applications in biomedicine, e.g. as biodegradable drug carrier or in tissue engineering, and their flame retardant properties. We highlighted recent developments that may make phosphorus-based polymers attractive materials for various future applications.

Main-chain poly(phosphoester)s: History, Syntheses, Degradation, Bio-and Flame-Retardant Applications

1. Introduction

Polyphosphoesters (PPEs), i.e. polyesters based on phosphoric acid derivatives, are omnipresent in nature and all living cells. All life relies on the ability of the C-O-P bond to be stable for a long time but eventually being degradable on demand.[1] The energy-rich phosphorus anhydrides are natures' universal energy storage in the form of adenosine triphosphate (ATP). Controlled cleavage of this bond provides energy for most biochemical reactions. This structure was conserved throughout evolution in all prokaryotes and eukaryotes. Structurally similar but essential for redox-driven bioprocesses, the nicotinamide adenine dinucleotide (NAD$^+$/NADH + H$^+$) redox system also carries a diphosphate (Figure 1). Here, a diphosphate is used to link two functionally different parts of a larger molecule together to form a functional unity used in electron transfer processes. Also, inorganic polyphosphates play an important role in blood coagulation, inflammation, and bone regeneration.[2, 3] Inorganic polyphosphate is structurally very simple, consisting of linear polymers of orthophosphate linked by high-energy phosphoanhydrides bonds (Figure 1). At physiological pH, each internal phosphate unit carries a monovalent negative charge. It is ubiquitous in biology and can vary in polymer length from just a few phosphates to several thousand phosphate units long, depending on the organism and the tissue in which it is synthesized.[4]

PPEs differ from these inorganic polyanhydrides by the organic linker between the phosphorus centers; PPEs can be trivalent, i.e. not charged, or divalent (poly(phosphodiester)s) with a negative charge (*see below*). The most prominent and by far most important examples are the ribonucleic acids and their polymeric forms, DNA and RNA. These macromolecules, as PPEs, encode the genetic information of life and are essential for higher and lower life forms. Both RNA and DNA are PPEs build up from phosphoric acid and derivatives of the carbohydrates ribose or desoxyribose (with the additional nucleobases attached to the anomeric center), respectively (Figure 1).
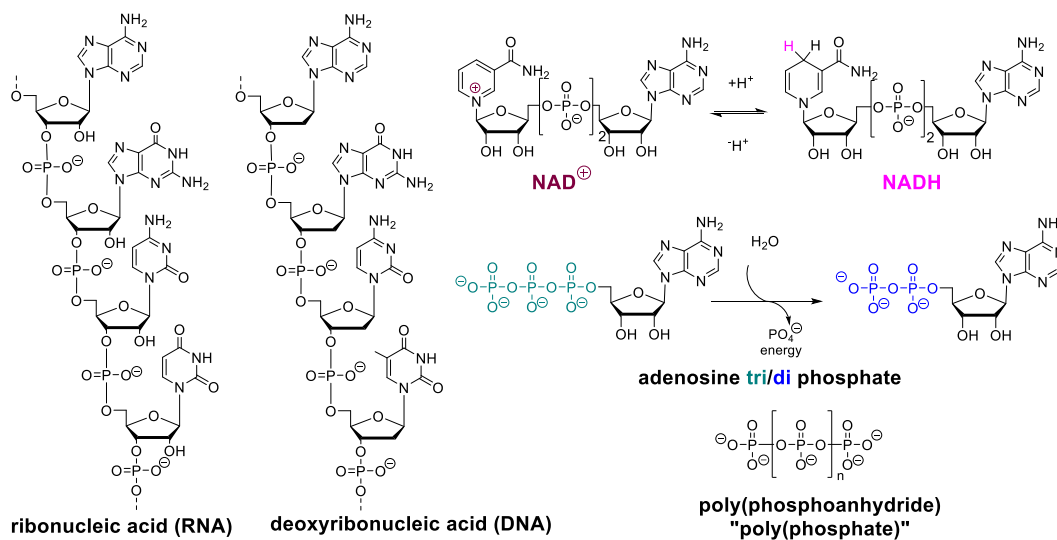
Figure 1. Chemical structures of important phosphorus-containing biomolecules: DNA and RNA sequences, nicotinamide adenine dinucleotide (NADH/NAD+) redox pair containing a diphosphate; adenosine tri/di phosphate (ATP and ADP), essential for the energetic flow in living systems; poly(phosphoanhydride) or inorganic polyphosphate, which is found in platelets.

The negatively charged phosphorus diester in DNA (in combination with the helical double stranded structure) provides long term stability as nucleophilic attacks are unlikely to the anionic charge of the backbone. As natural motif different enzymes are capable of building or degrading phosphoesters. In contrast to DNA, RNA is hydrolyzes much faster, due to the proximity of the additional OH-group on ribose, catalyzing the rapid depolymerization of RNA. The negative charge on the phosphate moiety further allows for interactions with positively charged proteins, the most well-known being histone proteins. These are used for storage and stability purposes.[5] A reduction in positive charge of these proteins plays an important role in the exposing of DNA for other protein-like transcription or translation factors.[5]

Phosphorylation is a general pathway to regulate enzyme activity in cells and hence a multitude of enzymes, the phosphatases, are known with the sole purpose of cleaving several differently substituted phosphoesters.[5] Also, synthetic phosphoesters are expected to be enzymatically degraded inside a living system in addition to the intrinsic susceptibility of ester bonds towards (acidic or basic) hydrolysis. Besides phosphates (i.e. with the structural element PO_4^{3-}), also phosphonates (carrying one stable P-C bond, i.e. PRO_3^{2-}, (Figure 4) are important structural elements in nature. Phosphonic acid derivatives have been identified in various plants, fungi, bacteria, and in some animals.[6] Recent ^{31}P NMR spectroscopic studies proved that up to 30% of

the maritime phosphorous reserve is bound in phosphonic acid derivatives.[7] Also many herbicides, such as the currently heavily discussed glyphosate, are based on phosphonates.

The omnipresence and immense biological importance of phosphoric acid esters makes synthetic PPEs a very promising object of research. These polymers are expected to show a high compatibility with biological systems and potentially low toxicity. Compared to the polyesters based on carboxylic acid esters, phosphorus, in phosphoric acid, can form three stable and divergent bonds in addition to the P=O double bond. This makes not only polyphosphoesters but also the respective *amide*s, a versatile platform for main- and side-chain modification of synthetic polymers, a distinct advantage over carboxylic acid esters, for example (Figure 2).[8] Attachment of side-chain functionalities and labels and therefore modification of material properties is possible in a straightforward way via the pendant group. This avoids main-chain functionalization which has to be conducted for other polycarboxylic acid esters or amides, e.g. in functional lactones or lactams. Also, the intrinsic biodegradability of PPEs can be adjusted via side-chain (and main-chain) modifications.[9]
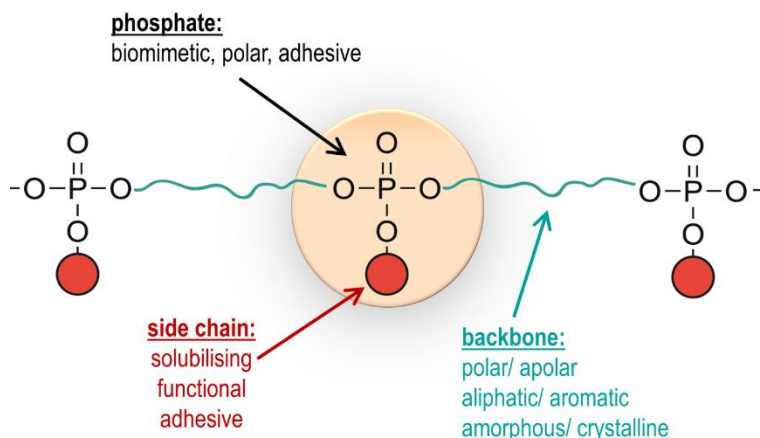

phosphate:
biomimetic, polar, adhesive

side chain:
solubilising
functional
adhesive

backbone:
polar/ apolar
aliphatic/ aromatic
amorphous/ crystalline

Figure 2. The synthetic platform of polyphosphoesters highlighting the handles for the design of future materials.

Polymer chemists have been always taking motifs from nature to synthetics (Figure 3). Polyolefins made it to a commodity material for the modern society with highly efficient catalysts producing polyethylene and polypropylene, for example, on the million ton scale. [10]

Also polyesters and polyamides have made it to commodities in many applications in today's world. Research on these materials[11] is still ongoing with several thousand papers per year covering their synthesis, modification, and application in various areas.[12] On the other hand, PPEs - which are the basis for the living world - remain a niche material on industrial scale and only

few research groups are currently interested in these materials.[13-16] To date, only flame retardant plastics or additives are produced industrially (see sections below). The full potential of synthetic PPEs is only touched in academics. This review summarizes the history of the synthetic achievements towards PPEs based on different monomer types and polymerization mechanisms. We will highlight some - rather forgotten - pathways and summarize the recent trends in PPE-chemistry and applications on academic level. The interested reader is also referred to other reviews and books about PPEs including industrial applications.[8, 17-21]
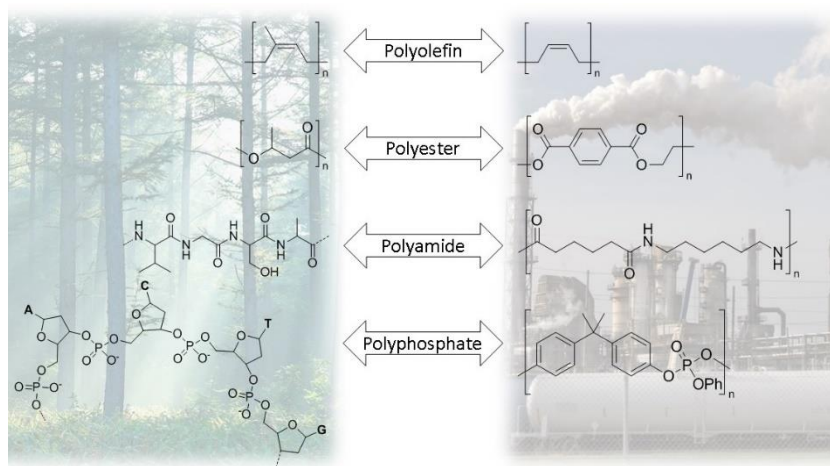
Figure 3. Comparison between the structural motifs of natural occurring polymers (left), and synthetic polymers produced industrially with prominent examples (right)[8] (Reprinted with permission from John Wiley & Sons Inc, Copyright 2015.)

All materials (PPEs) discussed in the actual review carry the phosphorus atoms along the polymer backbone and are separated by organic groups. Polymers with phosphorus in the side-chains, e.g. prepared by the polymerization of vinyl phosphonic acid, will not be touched by this review, however, other recent reviews cover the aspects of those materials.[22] In PPEs, the phosphorus atoms in the polymer backbone are typically in a pentavalent state. , i.e. P(V). Also, polymers with trivalent phosphorus, P(III), have been reported and some interesting candidates will be mentioned throughout this review.

In contrast to their carbon analogues, the polycarboxylic acid esters (PCE), the pentavalency of phosphorus provides an additional linkage per repeating unit, which allows the formation of branched structures or the introduction of functional or solubilizing groups. Depending on the nature of this side group which is connected to the phosphorus atom, PPEs are categorized into different subclasses (Figure 4), namely in polyphosphites (or alkylene H-phosphonates),

polyphosphonates, polyphosphates, and polyphosphoramidates with two phosphoesters (P-O-R) building the main chain and P-H, P-C, P-O, or P-N linkages to the side chain, respectively. Only in a very few studies also the linkage motif along the backbone has been altered, for example to generate branched polyphosphoamidates[23] and linear poly(phosphonate)s with the P-C-bonds in the main chain.[24]
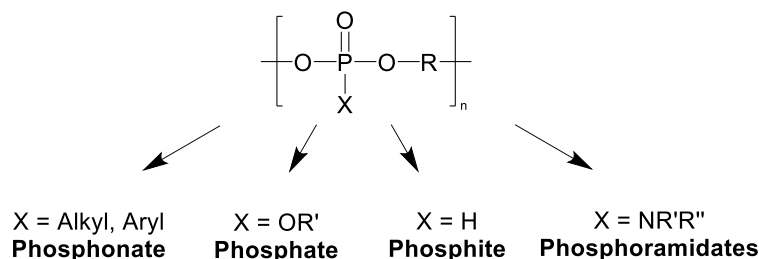

X = Alkyl, Aryl   X = OR'   X = H   X = NR'R"
Phosphonate   **Phosphate**   **Phosphite**   **Phosphoramidates**

**Figure 4. Subclasses of main-chain polyphosphoesters.**

2. PPEs: Synthesis

PPEs can be prepared by various synthetic routes: step-growth or chain growth polymerization can be chosen. Classical polycondensation of phosphoric acid chlorides and diols or transesterification of phosphoesters with diols is applicable. Also polyaddition and acyclic diene metathesis polycondensation have been reported. In addition, for chain-growth strategies, typically ring-opening polymerization of five- or six-membered cyclic phosphoesters is applied (Scheme 1). The polymers prepared by such methods may carry functional (pendant) groups, which allow further postpolymerization modification by different techniques, which will be discussed in this review. By these techniques, PPEs are accessible ranging from very hydrophobic materials to water-soluble polymers or highly crystalline to amorphous materials with variable molecular weights.[25, 26] PPEs with different architectures and polymerization patterns have been prepared, ranging from linear to hyperbranched[27-30] or cyclic[31] homopolymers, copolymers,[32-35] brush copolymers,[36, 37] star polymers,[38-40] and segments in block copolymers,[40-45] or sequenced polymers.[46]
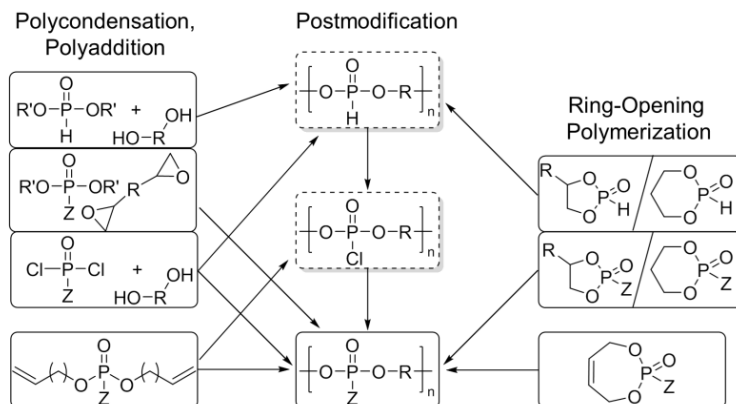
Scheme 1. Overview on the synthetic pathways to PPEs (Z=O-alkyl, O-aryl, alkyl, Cl, H; R= alkyl, aryl).[8] Reprinted with permission from John Wiley & Sons Inc, Copyright 2015.)

1.1   Polycondensation

In 1936 James Arvin reported for the first time the synthesis of aromatic polyphosphates by the polycondensation of phosphorus oxychloride with bisphenol-A.[47] Since then hundreds of reports, especially in the patent literature, on the synthesis of PPEs including polyphosphates,[32, 48] -phosphites, -phosphoramidates,[23, 49] and -phosphonates[50-55] by polycondensation have been published (only a few representative examples are listed here). Also branched and cross-linked materials have been prepared by the use of multifunctional nucleophiles or POCl$_3$.[28, 56] Beside the traditional melt and solution polycondensation the interfacial [50, 52] and the phase-transfer catalyzed[51, 57] polycondensation setups are common techniques.
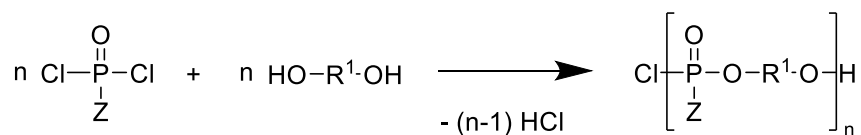
Z = H, O-alkyl, O-aryl, NH$_2$

R^1 = alkyl, aryl

Scheme 2. General protocol for the polycondensation of phosphoric acid dichlorides with diols.

The interfacial polycondensation can also be used to produce PPE- based nanoparticles. Alexandrino *et al.* reported the successful preparation of PPE nanoparticles by interfacial polycondensation of bisphenol A and dichlorophenylphosphate in miniemulsiom (Figure 5)[57].
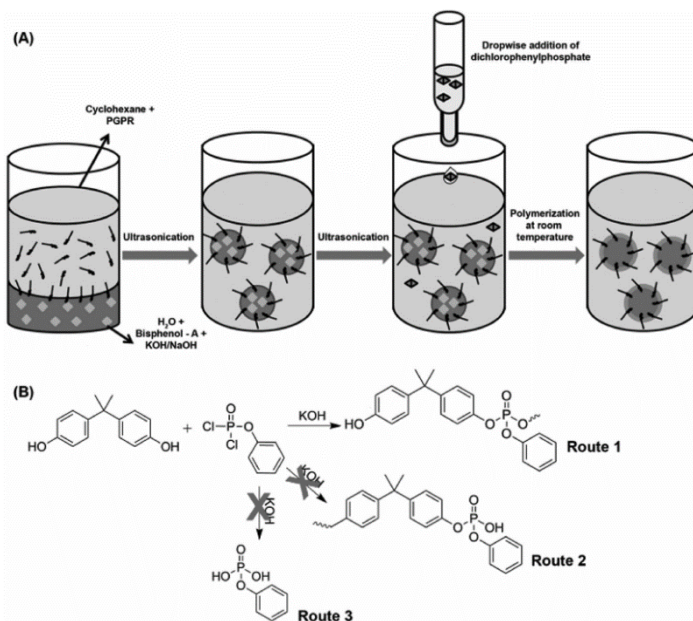
Figure 5: A) Schematic representation of the interfacial polycondensation in inverse miniemulsion applied for the synthesis of PPE colloids. B) Possible side reactions (Routes 2 and 3) that occur during the interfacial polycondensation (Route 1). SEM images of the PPE-articles after redispersion in water/SDS (0.6 wt%): C) KOH or D) NaOH as the osmotic and deprotonation agent. (Reprinted with permission from reference 57. Copyright 2016 Wiley)
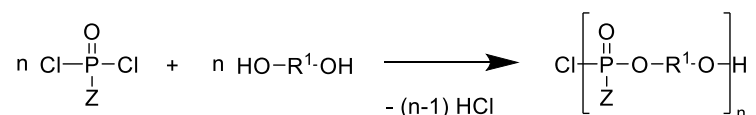
The prepared PPE colloids show diameters of 700 - 900 nm and higher molecular weights than PPEs prepared by classical polycondensation reactions. The particles consist of a well-known flame-retardant and are potentially applicable as additives for flame resistant improvement of other polymers compositions.

Although polycondensation is by far the most widely used approach to PPEs, its application is limited due to several side reactions.[19] They restrict the synthesis of high molecular weight polymers (Scheme 3) and the incorporation of functional groups is challenging.[48] Besides the main reactions between monomers or macromolecules (Scheme 3 Pathway 1.1 and 1.2), which lead to the formation of polyesters, various unwanted side reactions take place resulting in the reduction of yield and molecular weight of the polymer. The reaction between the diol and HCl, which evolves within the polycondensation, leads to the deactivation of the diol and to the cessation of the polyester growth. The hydrolysis of acid chloride groups by traces of water results in the formation of acidic groups, which are not able to participate in the polymerization process anymore. Also cyclic (poly)phosphoesters have been observed, depending on the structure of the
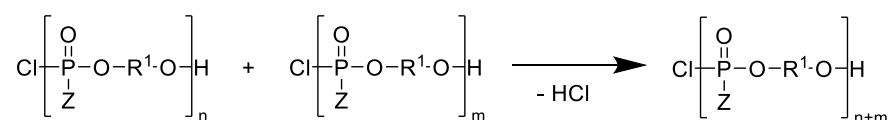
diol. In case of pendant ester linkages, transesterification reactions can take place leading to branched polymers.

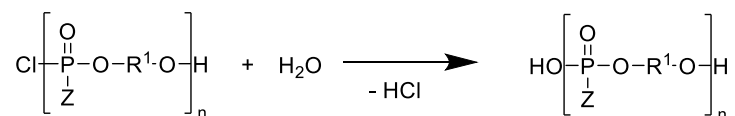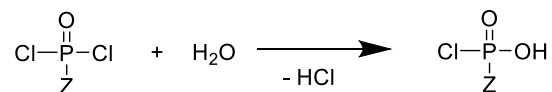**1. Reactions leading to high molecular weights**
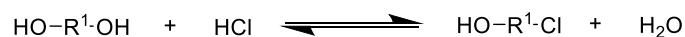
1.1 Polyester formation

$$n \text{ Cl}-\overset{\overset{\text{O}}{\|}}{\underset{\underset{\text{Z}}{|}}{\text{P}}}-\text{Cl} \quad + \quad n \text{ HO}-\text{R}^1\text{-OH} \xrightarrow[- (n-1) \text{ HCl}]{} \text{Cl}\left[\overset{\overset{\text{O}}{\|}}{\underset{\underset{\text{Z}}{|}}{\text{P}}}-\text{O}-\text{R}^1\text{-O}\right]_n\text{H}$$

1.2 Reaction between macromolecules

$$\text{Cl}\left[\overset{\overset{\text{O}}{\|}}{\underset{\underset{\text{Z}}{|}}{\text{P}}}-\text{O}-\text{R}^1\text{-O}\right]_n\text{H} \quad + \quad \text{Cl}\left[\overset{\overset{\text{O}}{\|}}{\underset{\underset{\text{Z}}{|}}{\text{P}}}-\text{O}-\text{R}^1\text{-O}\right]_m\text{H} \xrightarrow[- \text{HCl}]{} \text{Cl}\left[\overset{\overset{\text{O}}{\|}}{\underset{\underset{\text{Z}}{|}}{\text{P}}}-\text{O}-\text{R}^1\text{-O}\right]_{n+m}\text{H}$$

2. Reactions preventing high molecular weights

2.1 Hydrolysis

$$\text{Cl}-\overset{\overset{\text{O}}{\|}}{\underset{\underset{\text{Z}}{|}}{\text{P}}}-\text{Cl} \quad + \quad \text{H}_2\text{O} \xrightarrow[- \text{HCl}]{} \text{Cl}-\overset{\overset{\text{O}}{\|}}{\underset{\underset{\text{Z}}{|}}{\text{P}}}-\text{OH}$$

$$\text{Cl}\left[\overset{\overset{\text{O}}{\|}}{\underset{\underset{\text{Z}}{|}}{\text{P}}}-\text{O}-\text{R}^1\text{-O}\right]_n\text{H} \quad + \quad \text{H}_2\text{O} \xrightarrow[- \text{HCl}]{} \text{HO}\left[\overset{\overset{\text{O}}{\|}}{\underset{\underset{\text{Z}}{|}}{\text{P}}}-\text{O}-\text{R}^1\text{-O}\right]_n\text{H}$$

2.2 Deactivation of the diol

$$\text{HO}-\text{R}^1\text{-OH} \quad + \quad \text{HCl} \rightleftharpoons \text{HO}-\text{R}^1\text{-Cl} \quad + \quad \text{H}_2\text{O}$$

2.3 Formation of cyclic compounds

$$\text{Cl}-\overset{\overset{\text{O}}{\|}}{\underset{\underset{\text{Z}}{|}}{\text{P}}}-\text{Cl} \quad + \quad n \text{ HO}-\text{R}^1\text{-OH} \xrightarrow[- 2 \text{ HCl}]{} \begin{array}{c} \text{R}^1\text{-O} \\ | \\ \text{O}-\text{P}-\text{Z} \\ \| \\ \text{O} \end{array}$$
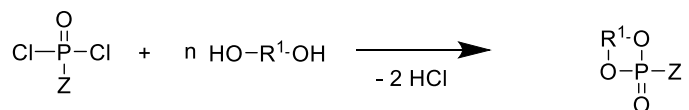
$\text{R}^1 = $ Alkyl, Aryl

$\text{Z} = $ H, alkyl, aryl NR_3

Scheme 3. Reactions during polycondensation of phosphorus dichlorides with diols.[48]

The polycondensation to PPEs also includes the polytransesterification of phosphoric acid diesters with diols (Scheme 4). This strategy is mostly applied for the synthesis of poly(H-phosphonate)s and -(phosphonate)s.
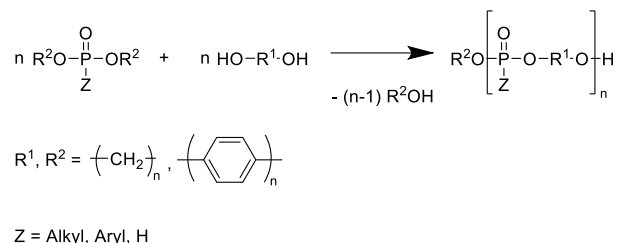

Scheme 4. General scheme of the polytransesterification.[58]

Polytransesterification is not suitable for the direct synthesis of poly(phosphate)s, due to branching., i.e. transesterification with the pendant esters. Nevertheless, poly(phosphates) are also accessible via this method by post polymerization modification of the corresponding poly(H-phosphonate)s.[58, 59] The P-H bond is interesting, as it is inert to the polycondensation conditions, however, allows easy access to functional materials by several post polymerization modifications (Scheme 5).
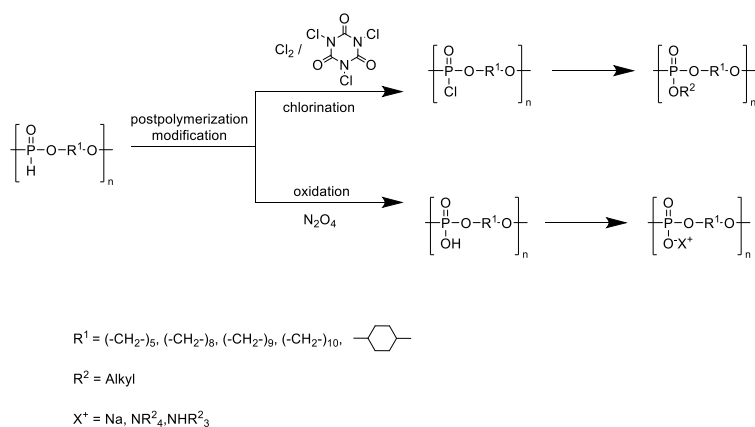
Scheme 5. Post-polymerization modification of poly(H-phosphonate)s.[59, 60]

The hydrolytic instability of the poly(H-phosphonate)s allows an easy transformation of the P-H-bond either by oxidation with N_2O_4 or by chlorination with gaseous chlorine or under milder conditions with trichloroiscyanuric acid[60]. The products can then be transferred into further derivatives (Scheme 5).[61, 62] Also amphiphilic graft copolymers are accessible via the post-polymerization of the poly(H-phosphonate)s (Scheme 6).

m = 1,2
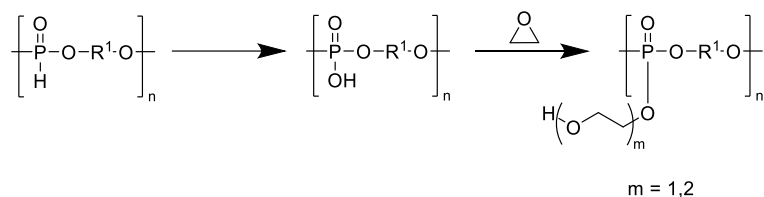
**Scheme 6. Synthesis of amphiphilic graft copolymers (PPE-g-PEO).**

The addition of ethylene oxide proceeds quantitatively to the PEO grafted PPEs (rather short oligomers are grafted under these conditions). Without the addition of an external acid, the reaction stops when all acidic groups are consumed. Longer PEO-chains can be introduced by usage of an external acid.[59, 63] Another efficient post-polymerization modification was achieved by the application of the Atherton-Todd reaction to poly(H-phosphonate)s (Scheme 7).[64-66] Initially, the Atherton-Todd reaction was applied for the synthesis of phosphoamidates by reaction of dialkyl phosphonate with primary amines in the presence of carbon tetrachloride, but was subsequently extended to different nucleophiles throughout the past years.[67]
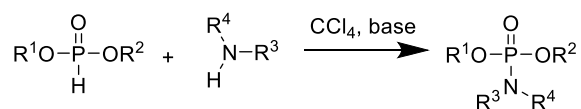
R^1, R^2, R^3, R^4 = Alkyl, Aryl

Scheme 7. General scheme of the Atherton-Todd reaction.

Bogomilova *et al.*, for example, used the Atherton-Todd reaction to bind the anticancer drug mephalan to a water-soluble polymer resulting in a reduced toxicity of the cytostatic while maintaining the therapeutic efficacy (Scheme 8).[68]
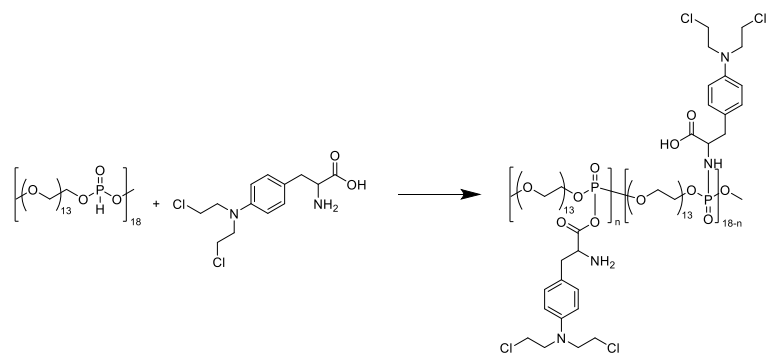
Scheme 8. Reaction pathway for the immobilization of mephalan onto poly(oxyethylene phosphonate) under Atherton-Todd conditions (from Ref 26).
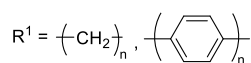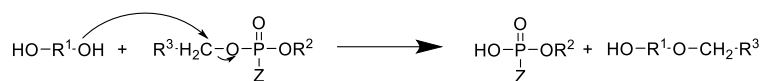
However, the polytransesterification of diesters with diols is plagued with side reactions thus leading to polymers with limited molecular weights. In 1973 Vogt *et al.* reported exhaustively about the side reactions of the polytransesterification of diethyl phosphonate with various diols.[69] Similarly to the side reactions, occurring within the polycondensation reaction between phosphorus dichlorides and diols, the formation of cyclic phosphoesters proceeds also within the polytransesterification process. The reaction of ethylene glycol and dimethyl phosphonate, for example, leads to the formation of oligomers and 2-hydro-2-oxo-1,3,2-dioxaphospholane.[70] Also, the reaction between propylene glycol and dimethyl phosphonate results almost exclusively in the formation of the 2-hydro-2-oxo-1,3,2-dioxaphosphorinane.[71] Besides the formation of cyclic phosphoesters, the formation of cyclic ethers can also be observed within the polytransesterification (Scheme 9).[19, 69]

R^1 = Alkyl, Aryl

Z = H, Alkyl, Aryl
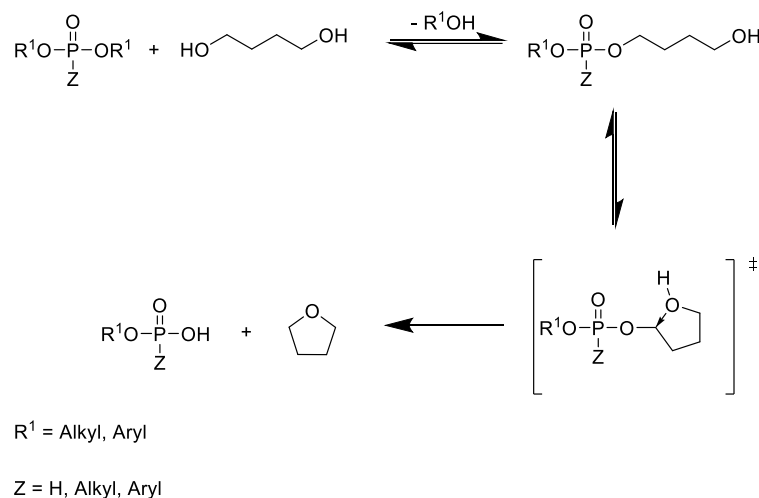
Scheme 9. Formation of tetrahydrofuran during the polytransesterification of phosphorus dialkyls with 1,4-butanediol.[19]

Cyclic ethers are formed by intramolecular cyclization initiated by the nucleophilic attack of the terminal hydroxyl group on the α-carbon. In the course of this ether formation, the ester function is transferred into an acidic P-OH-bond, which cannot undergo further condensation reactions. The amount of the ether formation depends on the diol; in case of 1,4-butanediol the corresponding cyclic ether, i.e. tetrahydrofuran, was formed with a yield of 80%, whereas the usage of 1,5-pentanediol leads to the formation of tetrahydropyrane with only 30% yield.[69]

Another side reaction of the polytransesterification is the dealkylation (Scheme 10).

$R^1 = -(CH_2)_n- , -(C_6H_4)_n-$

R^2, R^3 = Alkyl, Aryl

Z = Alkyl, Aryl, H

**Scheme 10. Dealkylation during the polytransesterification process.**

The main side reaction during the polytransesterification is the dealkylation of the phosphorus diester. Dealkylation occurs due to the nucleophilic attack of the oxygen atom on the α-carbon atom, which represents, besides the phosphorus atom, the second electrophilic center within the phosphoric acid esters. Within this reaction one of the ester functionalities is transformed into an acidic P-OH group, which is not able to participate in the polymerization process anymore and thus limiting the molecular weight of the polymer. To date, many approaches have been published to eliminate or to reduce the side reactions during the polytransesterification. Petrula *et al.* reported about several modified polytransesterification approaches leading to high molecular weight polyphosphoesters.[58, 59, 72, 73]

In 1990 they published a two stage protocol providing poly(H-phosphonate)s with molecular weights up to 3.3×10^4 g mol^{-1} (determined by VPO) by the polycondensation of dimethyl phosphonate with various diols (Scheme 11).[74]
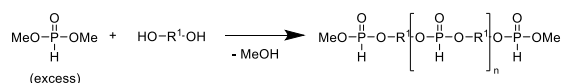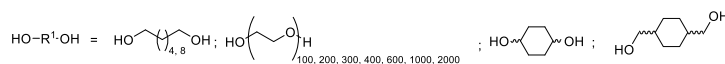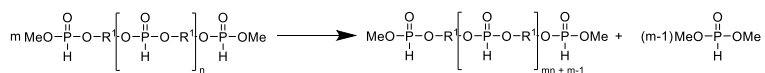

Scheme 11. Synthesis of high molecular weight poly(H-phosphonate)s by a two stage process.[74]

The first stage is conducted with an excess of the dimethyl phosphonate in a temperature range from 120 to 140 °C allowing a complete reaction of the hydroxyl groups with the phosphorus

dimethyl ester. In the first step only oligomers with methyl ester end groups are formed and methanol as side product, which is continuously removed from the reaction mixture by distillation. By this step the side reactions involving hydroxyl groups can be suppressed. After 90% of the theoretical amount of methanol is removed, the temperature is increased to 160- 180 °C. In the second step, high molecular weight polymers are formed by transesterification reactions between the oligomers accompanied by elimination of dialkyl phosphonate.

In 1997 the same group reported about the polycondensation of diphenyl phosphonate with diols such as 1,10-decanediol or tetra(oxyethylene) glycol, leading to high molecular weight poly(H-phosphonate)s with molecular weights up to $M_n = 3 \times 10^4$ g mol^{-1} (determined by membrane osmometry, Scheme 12).[58]

$R^1 = (CH_2)_{10}, (CH_2CH_2O)_3CH_2CH_2$
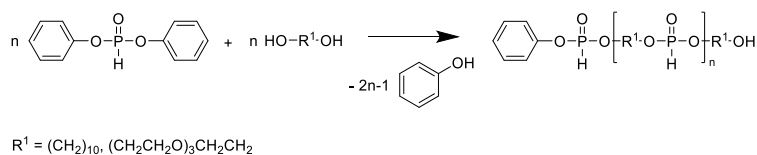
Scheme 12. Polytransesterification of diphenyl phosphonate with diols.

The usage of aromatic esters reduces the dealkylation of the phosphors to a minimum due to the replacement of the sp^3 by a sp^2 carbon that eliminates the possibility of S$_N$2 reactions at this position. Furthermore, diphenyl phosphonate reacts almost irreversibly with alcohols.[75] Therefore the removal of phenol, evolving during the polycondensation process, is not necessary for the synthesis of medium-molecular-mass polymers.

Pretula *et al.* also demonstrated that PPEs can be obtained by the polycondensation of phosphoric acid and a diol, avoiding toxic solvents, catalysts or the use of phosphorus oxychloride.[76-78] Unfortunately, the prepared oligomeric phosphoesters by polycondensation of phosphoric acid and ethylene glycol (P_n= 11 determined by MALDI-ToF MS and NMR spectroscopy) were rather ill-defined and exhibited poor mechanical properties (Scheme 13). However, this strategy is promising and may be optimized to produce PPEs directly from inorganic phosphates or phosphoric acid.
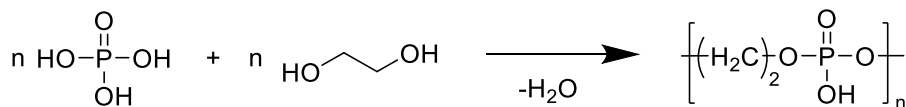
Scheme 13. Direct polycondensation of phosphoric acid with ethylene glycol.
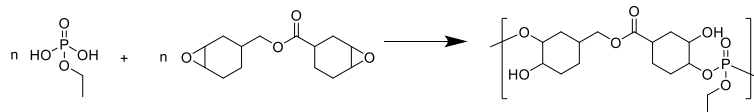
1.2 Polyaddition

Typical approaches to PPEs by polyaddition are reactions of phosphoric acid dichlorides with bisepoxides[79] or bisoxetans[80] using onium salts as catalysts. Poly(phosphates) and -(phosphonates) with reactive pendant chloromethyl groups have been synthesized by Nishikubo *et al.* by polyaddition of aromatic and aliphatic bisepoxides with phosphoric and phosphonic acid dichlorides.[81] Polymers with molecular weights up to 23,000 g mol^{-1} and molecular weight dispersities ranging from M_w/M_n=1.24 to 1.59 were obtained (Scheme 14).

R = Ph, OPh, Me, OMe
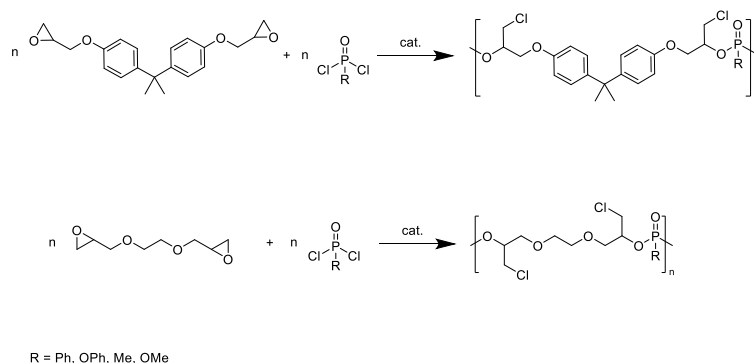
Scheme 14. Synthesis of PPEs by polyaddition of bisepoxides with phosphoric and phosphonic acid dichlorides.

Penczek and co-workers investigated in a series of publications the polyaddition reaction between phosphoric acid and bisepoxides and the associated side reactions [82-85]. The carefully selection of the reactants, namely of 3,4-epoxycyclohexylmethyl-3,4-epoxycyclohexanecarboxylate (ERL) and ethylphosphoric acid allowed the elimination of side reactions and the successful synthesis of PPEs with high molecular weights up to   10^4 g mol^{-1} (determined by VPO, Scheme 15). However, due to the limitation of the starting materials needed for polyadditions, this approach is only of minor relevance. The use of phosphoric acid derivatives is still an attractive idea to omit high-energy intermediates, such as POCl$_3$, and might change the field of PPEs, if new catalysts or synthetic routes are investigated.


Scheme 15. Synthesis of PPEs by polyaddition of ERL with ethylphosphoric acid.

1.3 Ring-opening polymerization (ROP)

Probably the most versatile approach to PPEs is provided by the ring-opening polymerization (ROP) of cyclic phosphoester monomers (CPM, Scheme 16). The polarity of the polymers obtained by this technique range from merely water-soluble[86] to very hydrophobic[87, 88], depending on the character of the pendant group. Furthermore, due to more recent developments towards controlled (or living) polymerization mechanisms for CPMs, linear,[89-92] branched,[93] and hyperbranched,[27] grafted[14, 94] or cross-linked[95] PPEs have been realized by this protocol.

The ROP can proceed via an anionic, cationic or metal-catalyzed insertion mechanism. In general, to date, the anionic polymerization is by far more relevant than the cationic ROP.
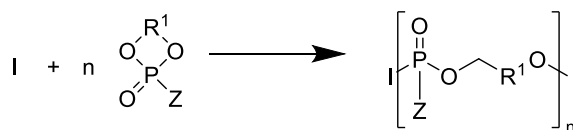

Z = alkyl, aryl, Oalkyl, Oaryl

$R^1 = (-CH_2-)_{2,3}$

Scheme 16. Ring-opening polymerization of cyclic phosphoesters.

Independent from the mechanism, the ideal candidates for the ROP are strained cyclic phosphoesters, with both the phosphorus being tri- or pentavalent. The monomers containing trivalent phosphorus, such as cyclic phosphonates and deoxphostones with variable ring sizes have been intensively studied by Kobayashi *et al.*[96-98] In contrast to the pentavalent monomers, the trivalent phosphorus monomers are exclusively polymerizable by a cationic mechanism.[98] For example the cationic polymerization of 2-phenyl-1,3,2-dioxaphosphephane with methyl iodide as initiator leads to the corresponding poly(phosphonite) with moderate molecular weights (M_n= 3,000 g mol^{-1}, determined by VPO), whereas polymerization under anionic conditions does not proceed at all.[97] The obtained polymers exhibit a wax-like texture and are soluble in polar organic solvents. The monomers based on P(III) have never gained as much attention as their pentavalent counterparts. Nowadays, the interest is focused on the highly strained pentavalent six-membered 2-alkoxy-2-oxo-1,3,2-dioxaphosphorinanes and particularly on the five-membered 2-alkoxy-2-oxo-1,3,2-dioxaphospholanes (see below).[99, 100]

The five- and six-membered cyclic phosphates are accessible by the direct condensation of the appropriate diol with phosphorus oxy chloride and subsequent esterification to introduce a side

chain of choice. In practice, this route (pathway 1 in Scheme 17) is only of minor relevance due to low yields and impure monomers, probably by polycondensation as side reaction. In contrast, the three-step protocol (pathway 2 in Scheme 17) starting with the ring closure by condensation of phosphorus trichloride with a suitable diol, followed by the oxidation of the trivalent phosphorus with oxygen and subsequent esterification is the favored method in most literature reports. The third pathway in Scheme 17 for the synthesis of CPMs is the transesterification of dialkylphosphates with diols, which was used for monomers, in which the pendant group is a hydrogen atom.[71, 101] Of course, this approach is not suitable for the synthesis of cyclic phosphates due to unwanted transesterifications and the formation of branched structures.
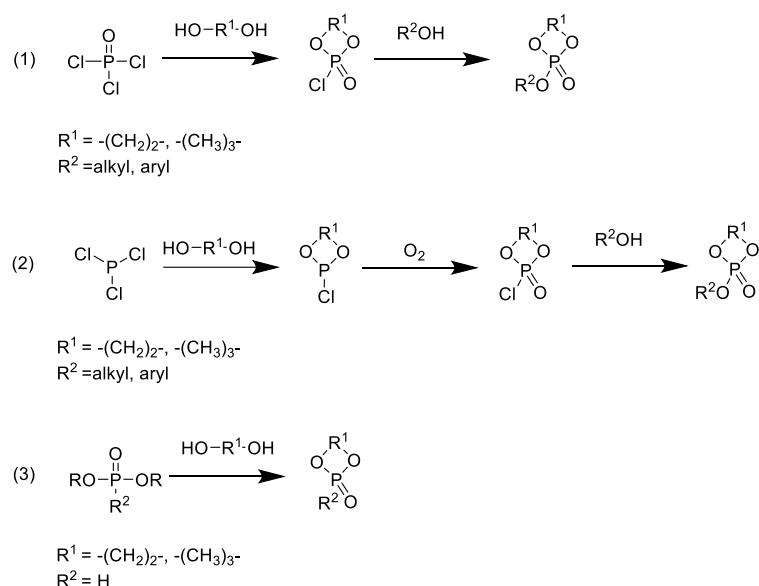
Scheme 17. Different synthetic pathways to cyclic phosphoester monomers.

1.3.1 ROP of Six-Membered Cyclic Phosphates

In the 1960s and 1970s, the ROP of six-membered cyclic phosphoesters has been the center of interest.[102-105] Due to their lower ring strain (2.6 kcal/mol[106] for methoxy-2-oxo-1,3,2-dioxaphosphorinane) compared with the five-membered phosphates (6.7 kcal/mol for methoxy-2-oxo-1,3,2-dioxaphospholane [106]), their synthesis is more robust and the monomers are easier to handle but still reactive enough to be polymerized. First attempts to polymerize 2-ethoxy-2-oxo-1.3.2-dioxaphosphorinane have been made by Munoz *et al.*;[105] the polymerization was conducted thermally at 110-120 °C in the presence of water over several weeks. The polymerization led to viscous polymers with acidic groups soluble in polar solvents such as water or alcohols but

insoluble in diethyl ether or benzene. In the 1970s, the polymerization of cyclic phosphorus-containing compounds has been resumed by Penczek and co-workers, who made intensive progress on elucidating the polymerization mechanism, the thermodynamics and the properties of the final polymers.[107] Two kinds of six-membered cyclic compounds have been investigated in detail, 2-alkoxy- and 2-hydro-2-oxo-1,3,2-dioxaphosphorinanes.[92, 108] The 2-alkoxy-2-oxo-1.3.2-dioxaphosphorinanes can be polymerized either by cationic or anionic ring-opening polymerization.[103, 104] The cationic polymerization can be conducted in bulk as well as in solution above 100 °C using typical cationic initiators such as triphenylcarbenium salts (*e.g.* Ph_3CAsF_6 or Ph_3CSbF_6). The cationic polymerization leads to polymers with low molecular weights with $M_n \leq$ 1,200 g mol^{-1} (determined by VPO). [109]

Intensive investigations on the mechanism of the cationic polymerization have been made by Penczek *et al.* (Scheme 18).[103, 109] The initial step is the nucleophilic attack of the P=O-bond of the monomer at the electrophilic (cationic) initiator and generates a R-O-P-bond leading to a cyclic tetraalkoxy phosphonium cation as the propagating species. In this tetraalkoxy phosphonium cation, the C_4- and C_6-atoms are partially positive charged and thus electrophilic enough to be attacked by the oxygen atom of another monomer (Scheme 18).

Initiation:

teraalkoxyphosphonium cation
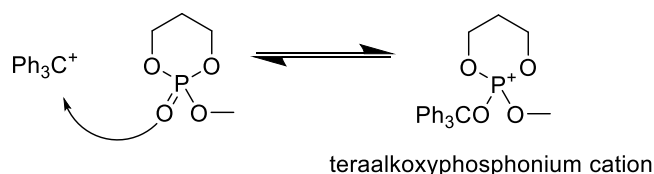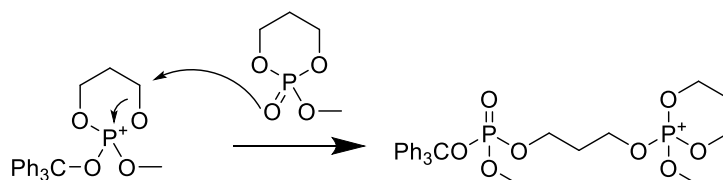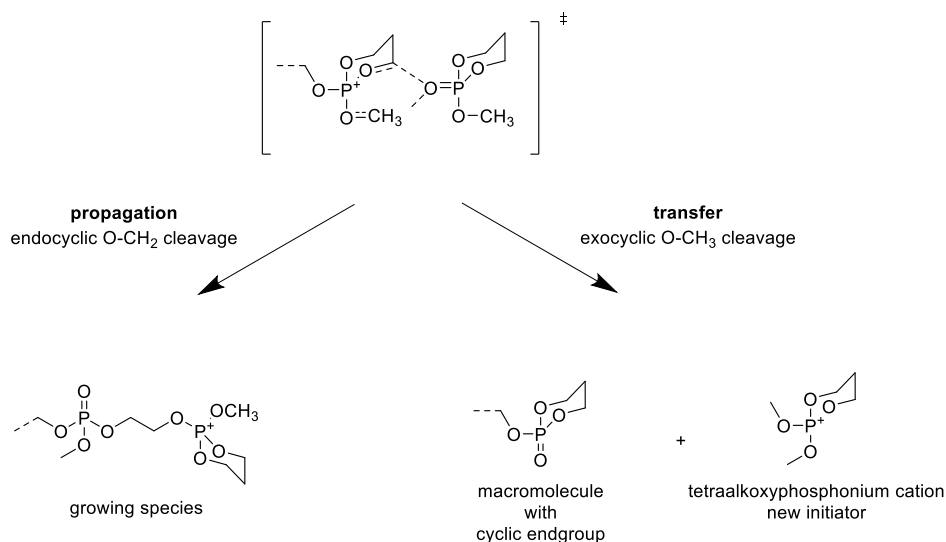
Propagation:

Scheme 18. Mechanism of the cationic polymerization of 2-methoxy-2-oxo-1,3,2-dioxaphosphorinane.

In the propagating step the nucleophilic attack on the partially positive charged carbon atoms results in a transition state that can either lead to a chain growth or to a chain transfer. Chain growth occurs, when an endocyclic CH_2-O-bond is broken (Scheme 19). On the other hand, the passing of the transition state can lead to a chain transfer. In this case an exocyclic O-CH_3-bond is

broken resulting in the formation of a macromolecule with a cyclic end group and a new tetraalkoxy phosphonium cation, which can reinitiate the polymerization. According to the proposed mechanism in the ^{1}H NMR spectra signals at 4.5 ppm (Figure 6) can be observed, that are typical for cyclic structures.

Propagation / Chain Transfer

Scheme 19. Proposed mechanism for the propagation and chain transfer step within cationic polymerization of six-membered cyclic phosphoesters. [103, 109] (Adapted with permission from [103]. Copyright 1977 American Chemical Society.)
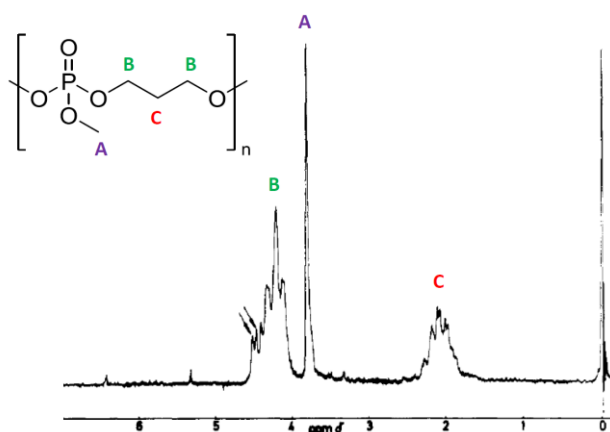

Figure 6. ^{1}H NMR spectrum of poly(2-methoxy-1,3,2-dioxaphosphorinane) showing the presence of some cyclic structures in the macromolecules (the arrows show the region of the contribution of cyclic structures in the linear macromolecule). (Reprinted with permission from reference 109, Copyright 1974 American Chemical Society.)

Besides the chain growth, chain termination can take place: in case of the termination the growing species reacts with a polymer segment, where a non-strained, acyclic teraalkoxyphosphoniumion is built, that cannot initiate further polymerization thus terminating the chain growth (Scheme 20).
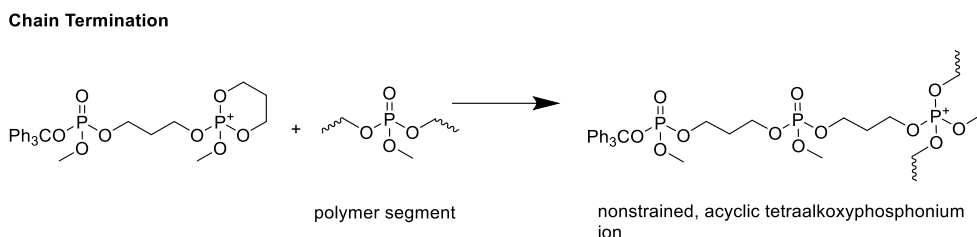
Scheme 20. Branching during the cationic polymerization of 2-methoxy-2-oxo-1.2.3-dioxaphosphorinane.

The only indication of the reaction proposed above comes from the study of the reaction kinetics and from the fact that the measured k_t does not depend on the structure of the anion attached to the growing species.[109] It has to be noted that in most of the older literature molecular weights were determined by VPO, giving no insight in the molar-mass distribution. For many of those systems, a modern revival could be possible with detailed SEC or MALDI-TOF analyses. However, PPEs are sometimes not easy to measure on standard GPCs due to interaction with the column material, thus VPO may still be an alternative.

Beside the cationic polymerization, six-membered phosphates can also be polymerized using anionic initiators (e.g. ^{n}BuLi, ^{t}BuOK, etc.). The mechanism of the anionic polymerization has also been investigated in detail by Penczek's group based on the polymerization of 2-methoxy-2-oxo-1.3.2-dioxaphosphorinane. Here again, the formation of macromolecules with cyclic end groups can be detected preventing the synthesis of high molecular mass polymers (Scheme 21).[104]
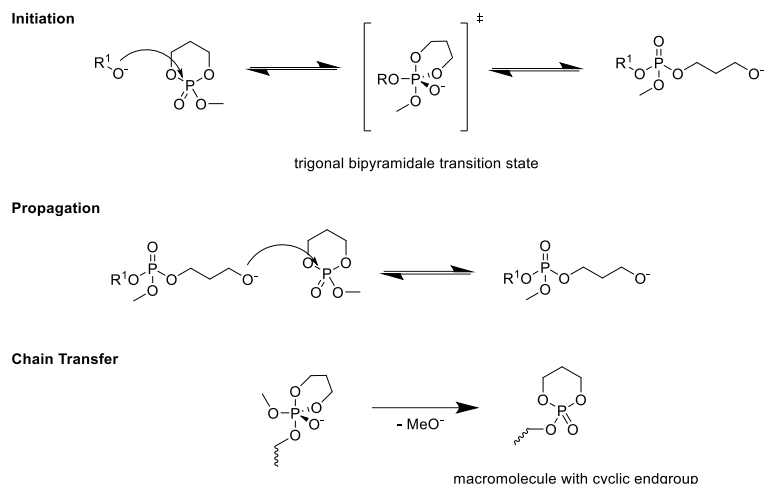
Scheme 21. Proposed mechanism of the anionic polymerization of six-membered cyclic phosphoesters.

The initial reaction is the nucleophilic attack of the initiator at the phosphorus atom, thus leading to a transition state with the geometry of a trigonal bipyramide (Scheme 21). In this transition state, the six-membered cycle is still intact and preferably occupies the axial-equatorial position.[11] Although every P-O-bond could be cleaved it is the axial, which is primarily broken resulting in a new alkoxide anion propagating polymerization.
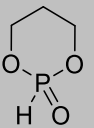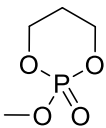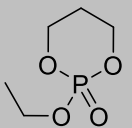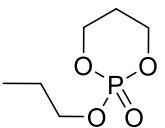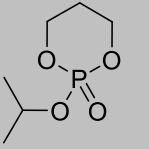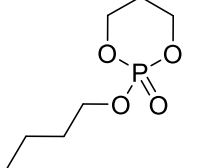
Similar to the cationic polymerization, within the anionic polymerization a terminating chain transfer can occur. This is possible due to the pseudo rotation of the phosphorus compound. It allows a migration of the pendant alkoxy group to the axial position, in which the P-O-bond is preferably cleaved. By this process an alkoxide anion is eliminated, which can again act as initiator, thus leading to macromolecules with cyclic end groups and low molecular mass ($M_n < 10^3$ g mol^{-1} determined by VPO). [104]
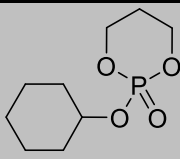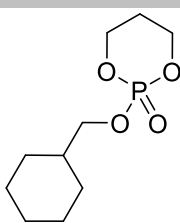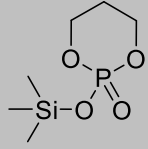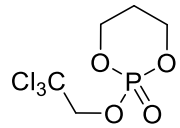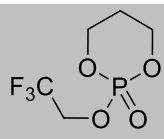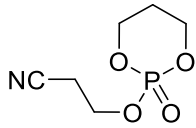
The six-membered 2-hydro-2-oxo-1,3,2-dioxaphosphorinane polymerizes readily to molecular masses up to $M_n = 10^5$ g mol^{-1} (determined by high-speed membrane osmometry) in a temperature range from 45 °C down to -80 °C using common anionic initiators such as ^{t}BuOK, ^{n}BuLi, and ^{i}Pr$_3$Al.[92] The obtained polymers show an enhanced susceptibility to hydrolysis, but also allow an easy post-polymerization modification. By replacing the pendant P-H-bond by a P-C or P-N-bond the hydrolytic stability can be altered as described in the previous paragraph for the post-polymerization modification of poly(H-phosphonate)s obtained by polycondensation reactions. In contrast, the cationic polymerization of the 2-hydro-2-oxo-1,3,2-dioxaphosphorinanes was not reported to date.[92] Today the interest in six-membered phosphates has faded due to the efficient polymerization strategies developed for the five-membered monomers. However, also the 6-membered rings may find a revival with modern polymerization catalysts as one could expect

different hydrophilicity, crystallinity, and hydrolysis kinetics with the backbone based on propylene glycol (compared to the backbone based on ethylene glycol for the 5-membered monomers).

Table 1. Six-membered cyclic phosphoesters used for ring-opening polymerization

Monomer	bp [°C] (mbar)	Mp [°C]	Monomer Yield [%]	Polymerization technique	$M_{n,max}$ [g mol^{-1}]	Ref
	97-98[71] (3.3)	-	79	A,C		[104]
	67 (0.01)	-	40	A,C	1.2×10^5	[104, 110]
	111 (0.9)	-	-	A,C	5×10^4	[103]
	137 (0.7)	-	-	A,C	3.5×10^4	[103]
	103 (0,01)	-	-	A,C		[103]
	111 (0.03)	-	-	A,C	5.4×10^3	[103]

Structure					
(cyclohexyl dioxaphosphorinane structure)	59	-	A,C	1.5×10^4	[103]
(cyclohexylmethyl dioxaphosphorinane structure)	73	-	A,C		[103]
(trimethylsilyloxy dioxaphosphorinane structure)	112 (1.5)	-	-	A,C	[103]
(Cl_3C dioxaphosphorinane structure)	148 (0.07)	-	-	A,C	5.3×10^4	[103]
(F_3C dioxaphosphorinane structure)	120 (0.4)	-	-	A,C	[103]
(NC dioxaphosphorinane structure)	104 (0.07)	-	-	A,C	[103]

A = anionic polymerization, initiators: ^tBuOK, ^nBuLi and $^iPr_3Al$, T

C = Cationic polymerization, initiators: Ph_3CAsF_6 or Ph_3CSbF_6

1.4   Ring-opening polymerization of five-membered cyclic phosphates

The usage of the five-membered dioxaphospholanes as monomers for the PPE-synthesis by ROP also started in the 1960 with the first attempts made by Munoz *et al.* leading to brown, viscous oils with undefined molecular masses.[111]

As time went on, the dioxaphospholanes have almost completely displaced the six-membered dioxaphosphorinanes as monomers for ROP and are now the monomers of choice for the

preparation of PPEs. Their cationic polymerization leads to colored, oily oligomers.[86] In contrast, the anionic ROP with alkoxides as initiators proceeds readily within hours at low temperatures to high molecular mass polymers.[112] The mechanistic details of the anionic polymerization have been studied in detail by Penczek and co-workers using the example of 2-methoxy-2-oxo-1,3,2-dioxaphospholane.[99] Thereby, it was revealed that the polymerization of the five-membered phosphates follows a coordination insertion mechanism similar to that proposed by Teyssié *et al.* for the polymerization of L-lactide and ε-caprolactone.[113, 114] The initial step is the nucleophilic attack of the P=O oxygen of the phosphate monomer on the aluminum atom of the initiator (Scheme 22). This results in the transfer of an isopropoxy group onto the phosphorus atom and the ring opening of the monomer. Propagation proceeds via a pseudoanionic mechanism by insertion of another monomer into the O-Al-bond. Termination is achieved by the addition of an acidic hydrogen (acidic acid).
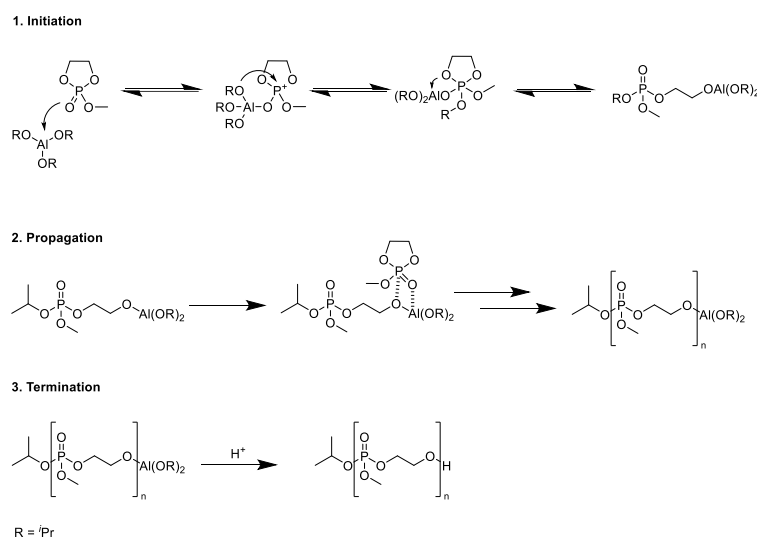
Scheme 22. Mechanism of the anionic ring-opening polymerization of 2-methoxy-2-oxo-1,3,2-dioxaphospholane initiated by aluminum triisopropanolate.

The main difference to the above-mentioned mechanism for the 6-membered analogues is the direct ring-opening after the initiator attack, due to the higher ring strain of the monomer. The high ring-strain of the five-membered monomers suppresses the possible elimination of the side chain attached to the phosphorus atom. Therefore the anionic polymerization of the five-membered in contrast to the six-membered monomers can be conducted under the conditions of a living polymerization, i.e. with absence of transfer and termination reactions. The living nature of

the anionic ROP of the five-membered phosphates was proven by chain extension, i.e. subsequent addition of monomer leading to a restart of the polymerization.[99]

With the anionic ROP established, it was possible to prepare homopolymers of a variety of cyclic phosphoesters with reasonable polymer weights[62, 115, 116] and also copolymers leading to materials with altered properties compared to the homopolymers concerning solubility, biodegradability etc.[33, 34, 117-119] Furthermore, more sophisticated structures such as block copolymers consisting of PPEs and poly(ε-caprolactone)[120] and block copolymers with a brush-like structure[121] containing PEGylated PPE-segments and poly(ε-caprolactone)-blocks.

Iwasaki *et al.* reported about the synthesis of a copolymer consisting of poly(2-ethoxy-1,3,2-dioxaphospholane) (PEEP) and poly(2-isopropoxy-1,3,2-dioxaphospholane) (PIPP) by anionic ROP using triisobutylaluminum as the initiator.[122] Molecular masses up to 1.2 to 1.5 x 10^4 g mol^{-1} with molecular mass distributions of Đ < 1.3 (determined by GPC) were achieved. The copolymers with a composition of 24 % PIPP and 74% PEEP exhibit lower critical solution temperature around 31°C.
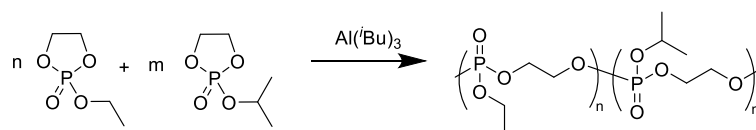
Scheme 23. Synthesis of the thermoresponsive copolymer PIPP-*co*-PEEP.

Furthermore, copolymers of PPEs with other biodegradable polymers have been synthesized (Scheme 24). The most thoroughly investigated and widely used biodegradable polymers are aliphatic polyesters such as poly(lactic acid) (PLA) and poly(ε-caprolactone) (PCL). [119, 123] In particular PLA is a suitable material for applications in the biomedical field. Due to its strong mechanical properties and antimicrobial and antioxidant characteristics, it is appealing as materials for surgical sutures and reconstructive implants. On the other hand, its hydrophobicity and slow degradation limits its application.[119] Leong and associates showed that the copolymerization of lactic acid with phosphoesters allows an adjustability of its hydrophobicity and degradation rate.[119]
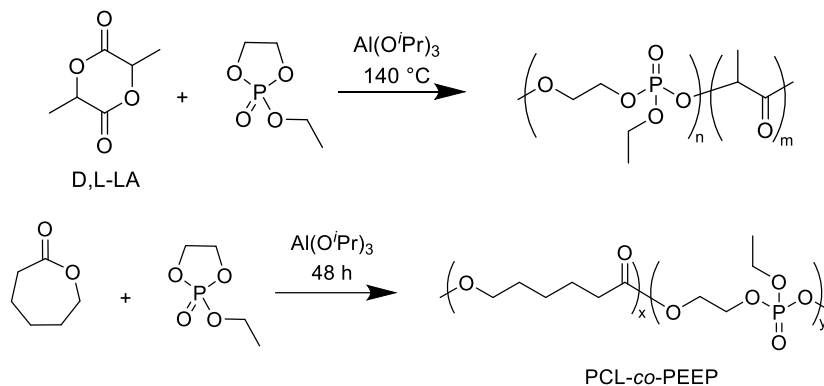
D,L-LA

PCL-*co*-PEEP

Scheme 24. Top: Synthesis of poly(D,L-lactide-co-2-ethoxy-2-oxo-1,3,2-dioxaphospholane) (PLA-co-PEEP). Bottom: Synthesis of poly(ε-caprolactone-*co*-2-ethoxy-2-oxo-1,3,2-dioxaphospholane) (PCL-*co*-PEEP).

The obtained polymers have been used for the formation of microspheres and were loaded with a model protein, BSA. The incorporation of PEEP led to an accelerated degradation of the microspheres and furthermore eliminated the biphasic degradation behavior of PLA. The microspheres showed a constant release of BSA. Leong *et al.* successfully demonstrated the feasibility of encapsulating human β-nerve growth factor, stabilized by bovine serum albumin, in a copolymer of ε-caprolactone and EEP by electrospinning.[118] The copolymer was synthesized by AROP with aluminum triisopropanolate as the initiator.

Furthermore, the formation of block copolymers has been realized by controlled anionic ROP.[120,124] The first report about block copolymers containing a PPE-block was released by Wang *et al.* in 2006.[120] They reported about the synthesis of block copolymers consisting of poly(ε-caprolactone) (PCL) and either poly(2-isopropoxy)-2-oxo-1,3,2-dioxaphospholane (PIPP) and poly(2-ethoxy-2-oxo-1,3,2-dioxaphospholan) (PEEP) respectively. The block copolymers were synthesized via a one-pot, sequential ROP with Al(^{i}OPr)$_3$ as the catalyst.

The obtained block copolymer exhibit a molecular mass dispersity of $Đ = 1.20$ determined by GPC. The GPC curves also showed a slight bimodality towards higher molecular mass indicating the formation of branched structures due to transesterification reactions of the pendant group during the polymerization.

A tremendous simplification of the ROP-process of cyclic phosphoesters has been made by Wang *et al.* in 2006 through employing the co-initiation of stannous octoate (Sn(Oct)$_2$) and alcohols, a common initiation system for lactones, on the polymerization of dioxaphospholanes.[125] The polymerization of cyclic phosphoesters with Sn(Oct)$_2$ also provides a certain biocompatibility, due to the rather low amounts and toxicity of Sn(Oct)$_2$ (which is FDA-approved in many

formulations).[126, 127] However, alternatives to tin-compounds are a demand for future materials, to rule out any long-term toxicity based on the metal additives. Intensive mechanistic studies using MALDI-TOF mass spectrometry on the polymerization of cyclic carboxylic acid esters with $Sn(Oct)_2$ as catalyst published by Penczek and co-workers indicate a coordination-insertion mechanism starting with the formation of the stannous alkoxide as the active initiating species. This initially formed stannous alkoxide reacts with a monomer by means of coordination-insertion and leads to the active chain end, which propagates polymerization by simple monomer insertion into the -Sn-O- bond.[128] On the basis of these studies, Wang *et al.* suggested an analogues mechanism for the polymerization of cyclic phosphoesters catalyzed by $Sn(Oct)_2$ (Scheme 25).[125]
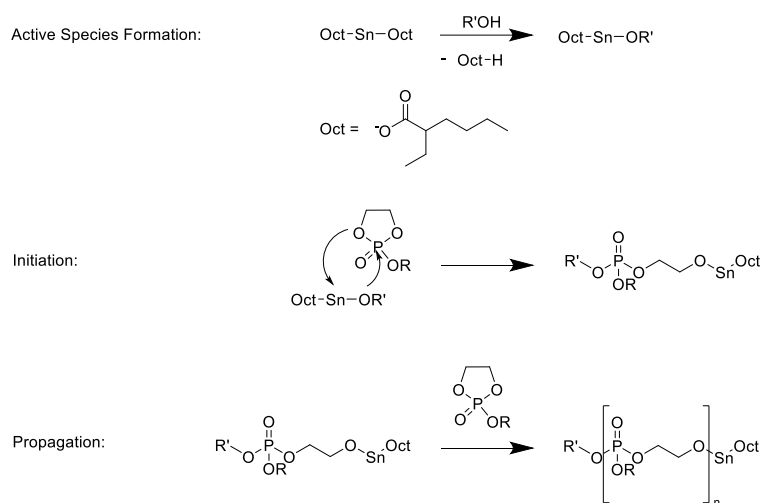
Scheme 25. Proposed mechanism of the ring-opening polymerization of 2-alkoxy-2-oxo-dioxaphospholanes initiated by stannous octoate.[125]

The polymerization can be forced to higher molecular masses by increasing the monomer/initiator ratio. With an increasing monomer conversion the molar-mass dispersity also increases: for conversions less than 70 % M_w/M_n is below 1.2, but increases to 1.5 for monomer conversions up to 95% due to transesterification reactions within the polymerization with $Sn(Oct)_2$. GPC shows besides a shift to higher molar masses, a multimodal molar-mass distribution as well as shoulders towards low molecular masses; the same was also reported for the ROP of cyclic esters.[129, 130] The ROP of cyclic phosphoesters is more complex due to the fact that besides the polymer backbone also the side chain can take part in transesterifications (Scheme 26).
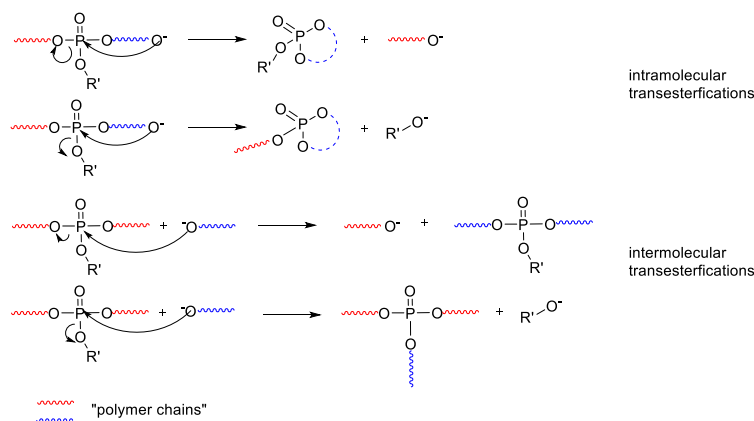
Scheme 26. Schematic depiction of the transesterification reactions of polyphosphoesters during ring-opening polymerization (Adapted with permission from reference 131. Copyright 2012 American Chemical Society.)

This method allows the synthesis of polymers with adjustable molecular masses and Đ < 1,5.[125] In 2010 Iwasaki *et al*. reported about a metal-free catalyzed ROP of cyclic phosphoesters by usage of organic superbases as catalysts, namely 1,8-diazabicyclo[5.4.0]undec-7-ene (DBU) and 1,5,7-triazabicyclo[4.4.0]dec-5-ene (TBD) and alcohols as initiators. [13] Here again, it was possible to employ an established initiator/catalyst-system for ROP of cyclic carboxylic esters [132] on the corresponding phosphoesters. Clément *et al.* reduced the amount of transesterifications to a minimum by using a catalyst-system that consists of DBU and organic Lewis acid thiourea (TU).[131] Mechanistic studies indicated an activation of the initiator by formation of hydrogen bonds to the alcohol functionality resulting in a quasi-anionic ring-opening polymerization.[131-133] The catalysts, DBU, TBD, and DBU/TU, differ by means of the activation mechanisms. DBU exhibits only one activation site, which functions as hydrogen-bond acceptor and therefore activates only the initiator. In contrast, TBD has two activation sites available and can therefore activate the initiator by acting as hydrogen-bond acceptor and simultaneously the CPM by acting as hydrogen-bond donor. The combination of DBU with TU also leads to a catalyst system, which can activate initiator and the cyclic phosphoester monomer (Scheme 34).
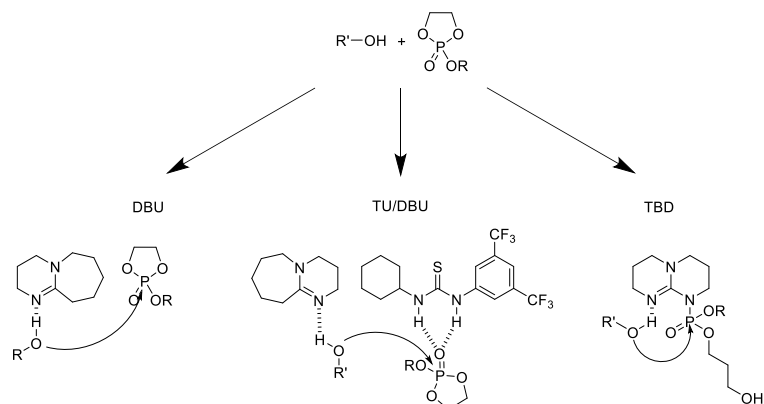
Scheme 27. Activation-mechanism of initiator and/or monomer by DBU, TBD, and TU/DBU.(Adapted with permission from reference 131. Copyright 2012 American Chemical Society.)

For the organocatalytic polymerization molecular masses up to 7×10^4 g mol^{-1} can be achieved with monomodal molar-mass distributions lower than 1.10 and monomer conversion of 98%.[131] Furthermore, by this method metallic catalysts can be avoided, thus making PPEs more attractive as materials for biomedical applications.[134] However, also care has to be taken, to remove unreacted monomer and the also potentially toxic organocatalysts from the final materials.

PPEs have also been synthesized enzymatically in two reports by Wen[135] and Zhuo and coworkers.[136] Porcine pancreas lipase catalyzed the polymerization of ethylene isopropyl phosphate to polymers of about 1 kDa after rather long reaction times (24-120h) and moderate temperatures. The enzymatic synthesis of PPEs is, without doubt, together with the anionic ROP (AROP) the most promising polymerization technique for future applications, meeting the requirements of sustainability.

Our group recently reported on the first living polymerization of cyclic 5-membered phosphonates (Scheme 28).25 In the 2-alkyl-2-oxo-1,3,2-dioxaphospholanes the exocyclic phosphoester is replaced by a phosphonate, whereas the advantageous properties of PPEs such as water-solubility and main chain degradability are preserved. The monomer was synthesized via a two-step synthesis starting with the preparation of the corresponding alkyl dichloro phosphonate. The following polymerization proceeds with a primary alcohol as initiator and DBU as catalyst.
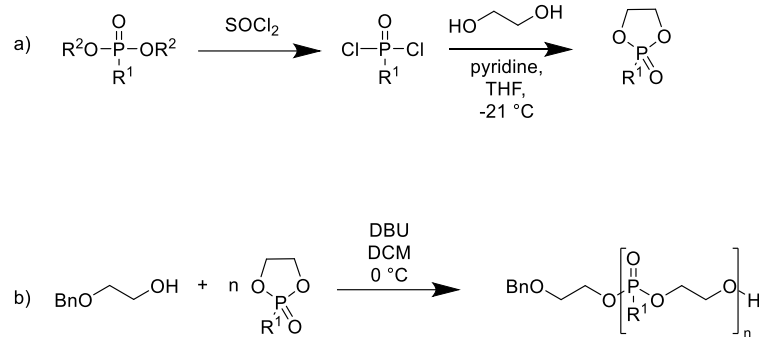
Scheme 28. (a) General synthesis of cyclic phosphonate monomers; (b) polymerization of cyclic phosphonates initiated by 2-(benzyloxy)ethanol and catalyzed by DBU at 0°C in dichloromethane.

Conversions above 90 % can be achieved, while transesterification reactions are reduced to a minimum. In contrast to poly(phosphate)s, within the polymerization process of (phosphonate)s only the main chain can participate in transesterification reactions. It can be distinguished between intra- and intermolecular transesterification resulting in the formation of cycles and termination of the chain growth respectively (

Figure **7**).
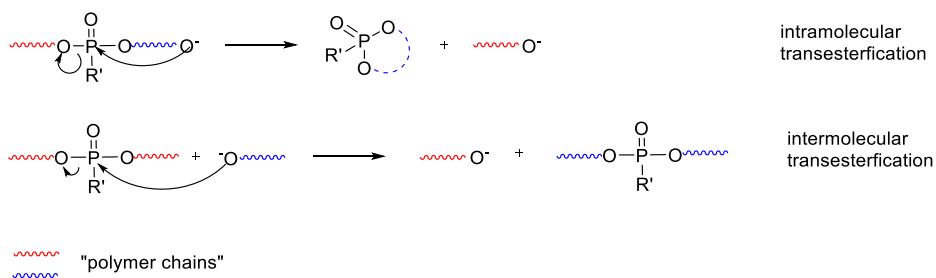
Figure 7. Two possible transesterification reactions during AROP of poly(phosphonate)s.

Very recently we extended the family of cyclic phosphonates to ethyl, propyl, and butyl-substituted structures. They all exhibit an excellent control over polymerization kinetics with full conversion and low molar-mass dispersities.[137] They are currently under deeper investigation concerning their potential in biomedical applications.

With the ROP established and the straightforward synthesis of the five-membered CPMs, it was possible to create more sophisticated polymer architectures especially by varying the pendant group. The thoroughly chosen side chain allows beside a precise adjustability of the hydrophilicity or lipophilicity respectively also a subsequent modification of the polymer.

Iwasaki *et al.*, for example, prepared copolymers consisting of PIPP (Table 2, Entry 9), PChOP (Table 2, Entry 20) and OPBB (Table 2, Entry 27) with adjustable hydrophobicity and functional side chains.[138] The incorporation of OPBB into the polymer allows a subsequent transformation of the PPE-based linear and hydrophobic copolymer into a grafted and amphiphilic polymer by ATRP of 2-methacryloyloxyethyl phosphorylcholine (MPC). Additionally, the cholesteryl-containing units provide a control over the hydrophobicity and the hydrophobic interactions. So, the nature of the pendant group provides the control over solubility and supramolecular architecture. The CPM-synthesis based on the functionalization of COP provides, besides monomers with pendant ester linkages, also the preparation and direct polymerization of phosphoramidates, i.e. CPMs with amine attached to the phosphorus atom (Scheme 29). Previously, poly(phosphoramidate)s were exclusively accessible by post-polymerization modification of the corresponding poly(H-phosphonate).

Zhang *et al.* reported for the first time about the synthesis of a poly(phosphoamidate)s by direct ROP of the corresponding cyclic phospholane amidate monomer (MOEPA, Table 2, Entry 17).[139] Furthermore, the obtained poly(phosphoramidate)s exhibit acid-labile phosphoramidate-bonds along the backbone, thus providing access to phosphoester ionomers by one further step.
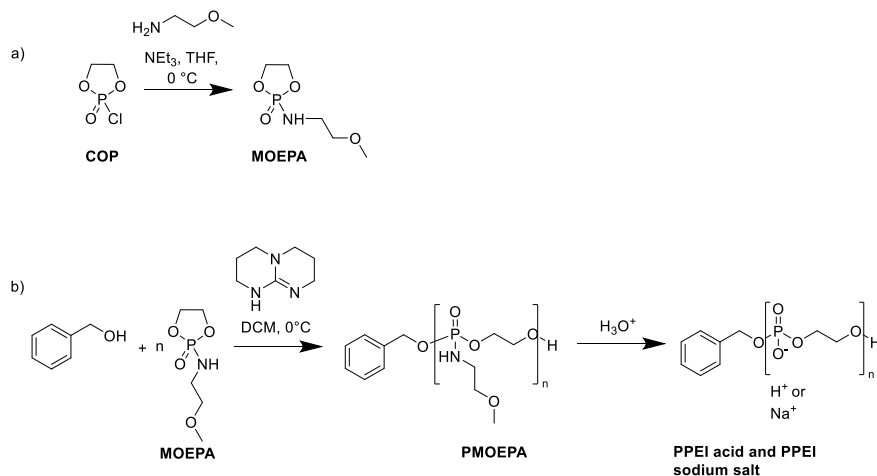
Scheme 29.a) Synthesis of cyclic phospholane amidate monomer and b) Polymerization of MOEPA with TBD as catalyst and benzyl alcohol as initiator and subsequent cleavage of the side chain of PMOEPA.

The presence of functional pendant groups in polymers is of great interest especially for the subsequent modification of polymers. For example, the pendant group in 2-((2,2-dimethyl-1,3-dioxolan-4-yl)methoxy)-1-dioxapholane-2-oxide (GEP, 19 Table 2) can be cleaved under

acidic conditions releasing two hydroxyl groups, which allow a subsequent polymer modification (Scheme 30).[140]
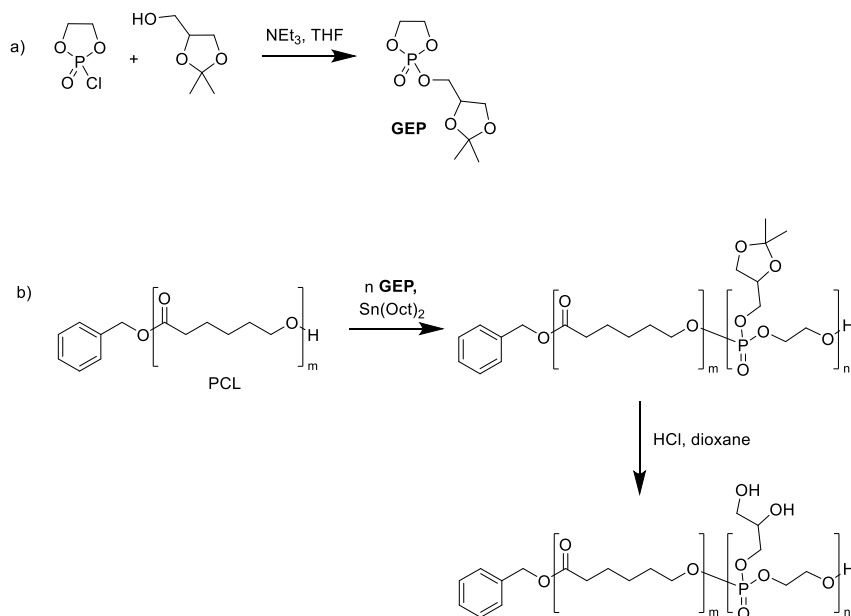
Scheme 30. a) Synthesis of 2-((2,2-dimethyl-1,3-dioxolan-4-yl)methoxy)-1-dioxaphospholane-2-oxide (GEP) and b) polymerization of GEP with Sn(Oct)2 as catalyst and PCL as macroinitiator and subsequent cleavage of the pendant acetal.

Lim *et al.* designed a CPM with a vinyl ether side chain (Scheme 31) as a versatile template for post-polymerization modification allowing besides a functionalization by thiol-ene click reaction also the subsequent introduction of acid labile functionalities, i.e. acetals and thio-acetals respectively.[141] These functionalities are especially appealing for biomedical applications due to their cleavability in acidic environment typical for sites of inflammations, tumors or for the gastrointestinal tract.[142-144]
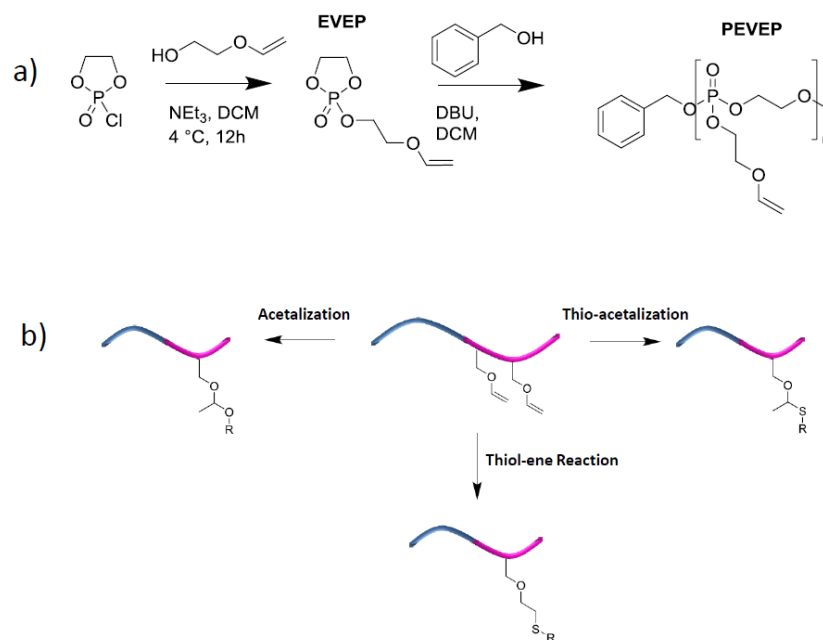
Scheme 31. a) Synthesis of ethylene glycol vinyl ether-1,3,2-dioxaphospholane-2-oxide (EVEP) and b) post-polymerization modification by three different reactions. (Adapted with permission from reference 141. Copyright 2014 American Chemical Society.)

The post-polymerization of PEVEP by thiol-ene reaction with an excess of 2-(2-methoxyethoxy)ethanethiol leads to a quantitative functionalization of the pendant double bond, whereas the acetalization and thioacetalization are accompanied by transesterification reactions and degradation, thus leading to functionalization degrees of only 18 and 8%, respectively. Another two CPMs, namely 2-(but-3-yne-1-yloxy)- and 2-(but-3-en-1-yloxy)-2-oxo-1,3,2-dioxaphospholane (BYP and BeneP, Table 2 entry 24 and 29) with 'clickable' side chains by thiol-ene/yne or azide-alkyne cycloadditions have also been investigated in depth in the Wooley lab (Scheme 32).
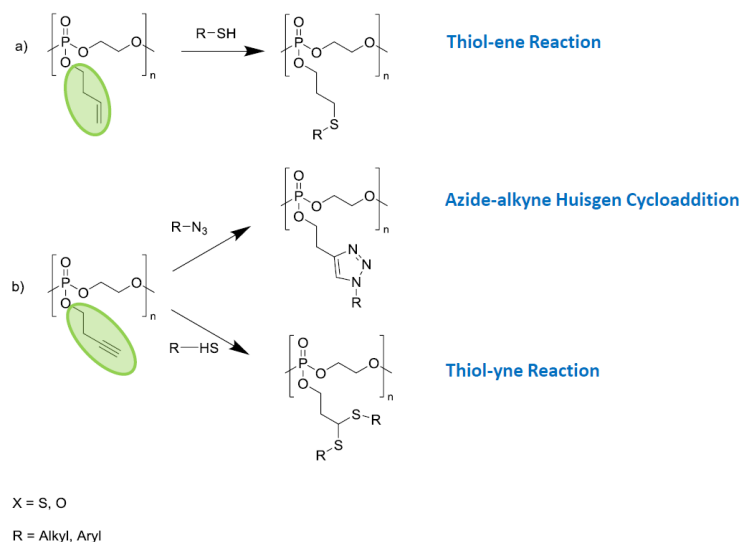
Scheme 32. Post-polymerization modification of poly(2-(but-3-yne-1-yloxy)- and 2-(but-3-en-1-yloxy)-2-oxo-1,3,2-dioxaphospholane) (PBYP and PBeneP, Table 2 entry 24 and 29).

Our group recently reported on the first orthogonally protected PPEs carrying benzyl- and acetal-protected hydroxyl groups in the pendant chains. A new monomer (Table 2, Entry 21) was developed and copolymerized with GEP and EEP (Table 2, Entry 19 and 4). Sequential deprotection under mild acidic conditions or hydrogenation releases the OH-groups selectively.[145] Also hyperbranched PPEs are accessible by ROP of HEEP (Table 2, Entry 22).[27] The inimer HEEP was prepared in high yield and the hyperbranched PPE was obtained by its self-condensing ROP in bulk without catalyst (Scheme 33).
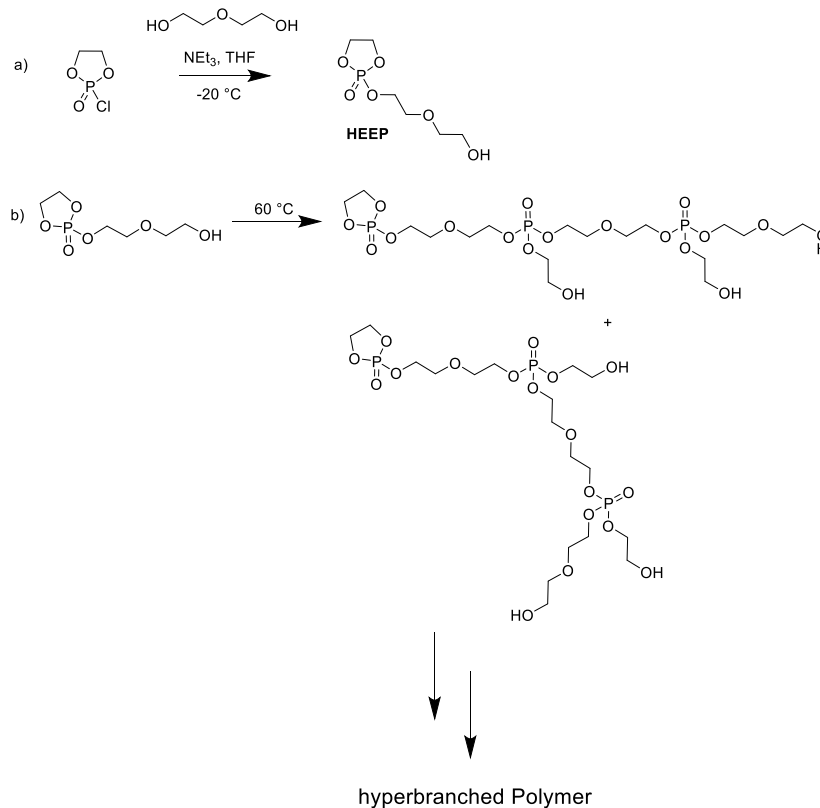
Scheme 33. a) Synthesis of 2-(2-hdroxyethoxy)ethoxy-2-oxo-1,3,2-dioxaphospholane (HEEP) and b) self-condensing ring-opening polymerization at 60 °C.

At 60°C after 14 h the molecular mass of the hyperbranched (hb) *hb*P(HEEP) reached 5,200 g/mol with *Đ*= 1.75. The degree of branching of *hb*P(HEEP) was determined to be 0.47 calculated from quantitative ^{31}P NMR (Figure 8).
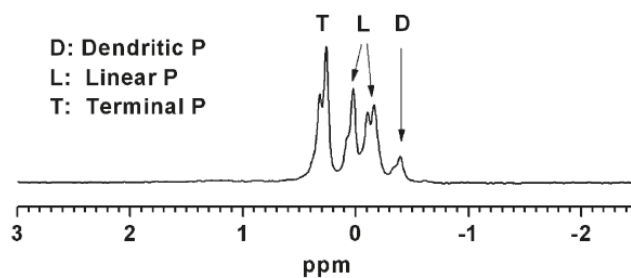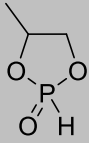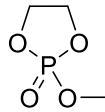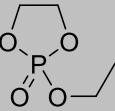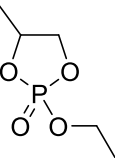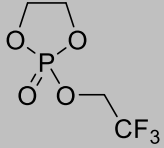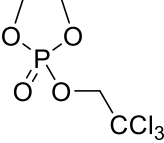
Figure 8. ^{31}P NMR spectra of *hb*PHEEP for the calculation of DB. (Reprinted with permission from reference 27. Copyright 2009 American Chemical Society.)
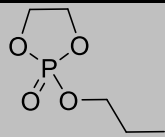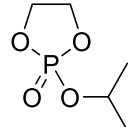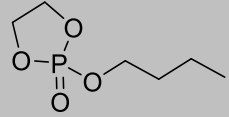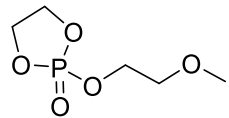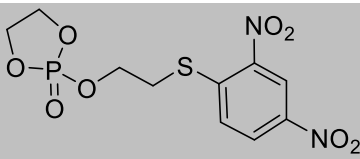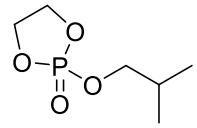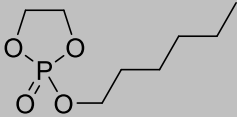
Table 2 gives an overview of the structures, polymerization techniques (PT), which have already been employed on the individual monomer and their availability.
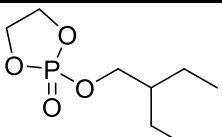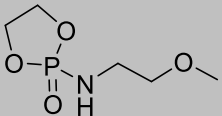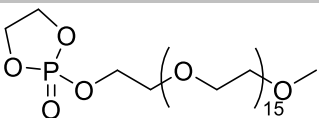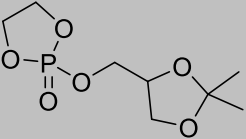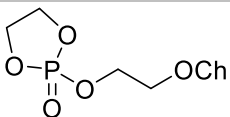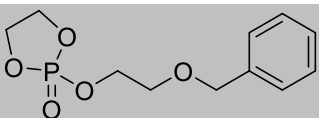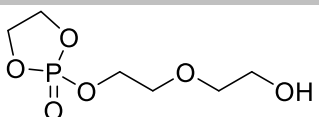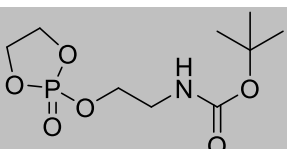
Table 2. Five-membered cyclic phosphates for the ring-opening polymerization.

#	Monomer	Monomer Yield [%]	PT	Name	Ref
2	4-methyl-1,3,2-dioxaphospholane 2-oxide	74	A	- (HMEP)	146
3	2-methoxy-1,3,2-dioxaphospholane 2-oxide	70	A,O,M	MEP	86
4	2-ethoxy-1,3,2-dioxaphospholane 2-oxide	65	A,O,M	EEP	86
5	2-ethoxy-4-methyl-1,3,2-dioxaphospholane 2-oxide	51	O	MEEP	147
6	2-(2,2,2-trifluoroethoxy)-1,3,2-dioxaphospholane 2-oxide	55	A	-	86
7	2-(2,2,2-trichloroethoxy)-1,3,2-dioxaphospholane 2-oxide	80	A	-	86
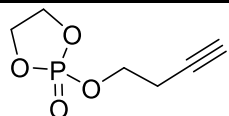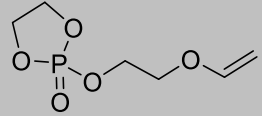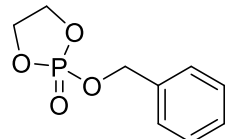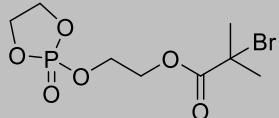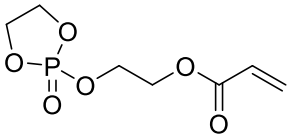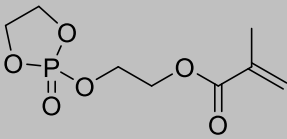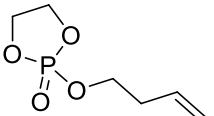
8	2-propoxy-1,3,2-dioxaphospholane 2-oxide	20	A	-	86
9	2-isopropoxy-1,3,2-dioxaphospholane 2-oxide	63	A	**IPP**	86, 148
10	2-butoxy-1,3,2-dioxaphospholane 2-oxide	-	A, O		86
11	2-(2-methoxyethoxy)-1,3,2-dioxaphospholane 2-oxide	78	A	**MOEEP**	124
12	2-(2-((2,4-dinitrophenyl)thio)ethoxy)-1,3,2-dioxaphospholane 2-oxide	36	M	-	149
13	2-isobutoxy-1,3,2-dioxaphospholane 2-oxide	65			131
14	2-(hexyloxy)-1,3,2-dioxaphospholane 2-oxide	-	O	**HEP**	150
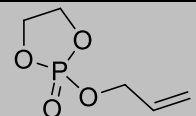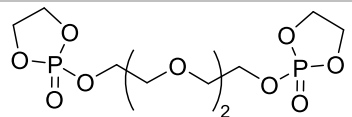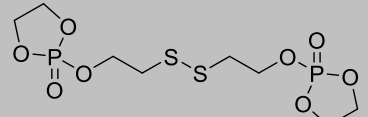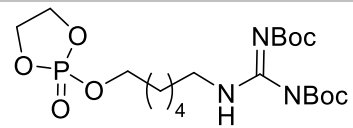
15	2-(2-ethylbutoxy)-1,3,2-dioxaphospholane 2-oxide	73	O	**EBP**	[15]
17	2-((2-methoxyethyl)amino)-1,3,2-dioxaphospholane 2-oxide	63	O	**MOEPA**	[139]
18	2-(2-(2-methoxyethoxy)ethoxy)-1,3,2-dioxaphospholane 2-oxide	70	A	**PPEG**	[121]
19	2-((2,2-dimethyl-1,3-dioxolan-4-yl)methox dioxaphospholane 2-oxide	63	M	**GEP**	[140]
20	2-cholesteryl-1,3,2-dioxaphospholane 2-oxide	32.5	A	**ChOP**	[138]
21	2-(2-(benzyloxy)ethoxy)-1,3,2-dioxaphospholane 2-oxide	87	M	**BnEEP**	[145]
22	2-(2-(2-hydroxyethoxy)ethoxy)-1,3,2-dioxaphospholane 2-oxide	89.7	Thermal polym.	**HEEP**	[27]
23		52.5	M	**EEAPBoc**	[151]

24	2-(but-3-yn-1-yloxy)-1,3,2-dioxaphospholane 2-oxide	30	M, O	**BYP**	[88, 152]
25	2-(2-(vinyloxy)ethoxy)-1,3,2-dioxaphospholane 2-oxide	76	O	**EVEP**	[141]
26	2-(benzyloxy)-1,3,2-dioxaphospholane 2-oxide	-	A	**BP**	[153]
27	2-((2-oxido-1,3,2-dioxaphospholan-2-yl)oxy)etl 2-bromo-2-methylpropanoate	67.1	A	**OPBB**	[138]
28	2-((2-oxido-1,3,2-dioxaphospholan-2-yl)oxy) ethyl acrylate	-	A	**OPEA**	[154]
29	2-((2-oxido-1,3,2-dioxaphospholan-2-yl)o: ethyl methacrylate	97	A	**OPEMA**	[155]
30	2-(but-3-en-1-yloxy)-1,3,2-dioxaphospholane 2-oxide	52	O	**BEneP**	[156]

31	2-(allyloxy)-1,3,2-dioxaphospholane 2-oxide	-	O	**AEP**	[157]
32	2,2'-((oxybis(ethane-2,1-diyl))bis(oxy))bis(1,3,2-dioxaphospholane 2-oxide)		M	**TEGDP**	[95]
33	2,2'-((disulfanediylbis(ethane-2,1-diyl))bis(oxy))bis(1,3,2-dioxaphospholane 2-oxi	-	M	**SSDP**	[158]
34	2-(6-*bis*-Boc-guanidino-hexyloxy)-1,3,2,-dioxaphospholane-2-oxide	79	O	**HexPhos**	[159]

A = anionic polymerization, initiators: ^{t}BuOK, ^{n}BuLi and ^{i}Pr$_3$Al,

O = Organocatalysis, initiators: DBU, TBD, DBU/TU

M = Metallic catalysts, iniator: Sn(Oct)$_2$

1.5 Metathesis Polymerization of unsaturated phosphoesters

High molar-mass PPEs can be prepared by chain or step growth olefin metathesis polymerization.[41, 160-165] Cyclic or linear phosphoesters are readily accessible by esterification of POCl$_3$ and its derivatives. A great advantage of the acyclic monomers compared to the highly strained CPMs is their easy handling and long shelf-life also at room temperature. The unique characteristic of this technique is the combination of the high functional group tolerance of modern ruthenium catalysts with the structural versatility of pentavalent phosphorus, which allows a precise tailoring of the polymer properties and side-chain functionalities.

The acyclic diene (ADMET) and triene metathesis (ATMET) polymerization are polycondensation reactions and follow a step-growth polymerization mechanism.[166] The ADMET is reported so far for acyclic phosphates and phosphonates (with the stable P-C-bond either in the

side chain[162] or the polymer backbone[24]) carrying terminal double bonds. Esterification of unsaturated alcohols with phosphoryl chloride (or derivatives) allows access to difunctional or trifunctional monomers with different arm lengths (Figure 9).

ADMET-Monomers   ATMET-Monomers

n = 2, 4, 9   n = 2,4,9

Z = Oalkyl, Oaryl, alkyl, aryl
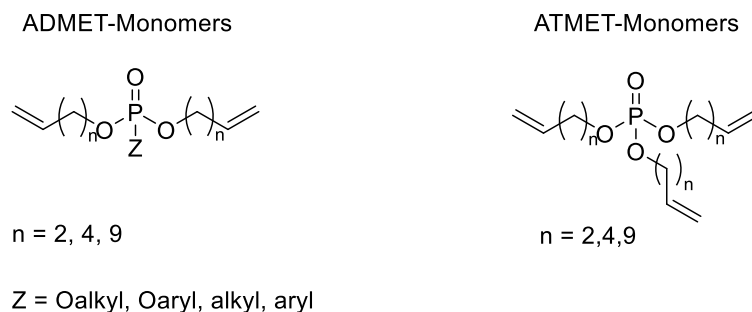
Figure 9. Monomer structures for the acyclic diene (ADMET) and triene (ATMET) metathesis polycondensation.

The polycondensation is promoted by metal carbenes and structurally versatile, linear or branched, unsaturated polyphosphoesters (UPPEs) have been prepared with ethylene as the only byproduct (Scheme 34). With the metathesis approach molecular masses ranging from 7 000 up to 50 000 g mol^{-1} can be obtained with molar-mass distributions of $Đ \approx 2$.[161] Also highly reactive P-Cl-containing monomers can be polymerized via the acyclic diene metathesis polymerization of the monomers di-(buten-3-yl) chlorophosphate and di-(undecen-10-yl) chlorophosphate. Molecular masses ranged from 1,000 to ca. 50,000 g/mol. These highly electrophilic phosphochlorides were post-modified with different nucleophiles, i.e. alcohols, amines, water, and thus allowed the synthesis of side chain polyphosphoamidates, -esters, and free acids from the same starting polymer.[164]

n = 1,2,4,9

Z = Me, OPh, Cl, BODIPY
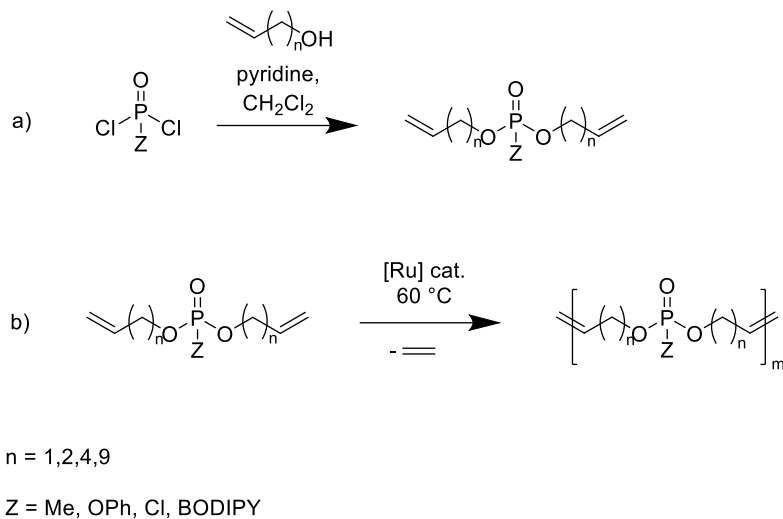
Scheme 34. a) Monomer synthesis for ADMET and ATMET polymerization and b) following ruthenium catalyzed polymerization.

The polymerization of the acyclic dienes can be monitored by NMR spectroscopy, Figure 10 shows this exemplarily for di-(but-3-en-1-yl) chlorophosphate. The polymerization is observed by ^{1}H DOSY NMR spectroscopy: after polymerization the resonances of the terminal double bond protons (a and b) at 5.1 and 5.8 ppm are detected as the end groups of the polymers with a distinct lower diffusion coefficient compared to the monomer. Moreover, as expected, a new peak (c,c') appeared at 5.4 ppm due to formation of internal double bonds. Further, the methylene group next to the phosphorus (d: 4.25 ppm) and the methylene group next to the double bond can be distinguished.

The microstructural adjustability of backbone and side chain allows a facile tailoring of the thermal properties such as melting or glass transition temperatures. The glass transition temperatures decrease with increasing number of methylene groups in the polymer backbone ranging from -30 °C for the poly(phenyl (hex-3-en-1-yl)phosphate) to -70 °C for the poly(phenyl (icos-10-en-1-yl)phosphate). The hydrogenation of the double bonds in the polymer backbone results in a shift of the melting point from -7 °C for the poly(phenyl (icos-10-en-1-yl)phosphate) to 45 °C for the hydrogenated polymer.[161] The respective poly(icos-10-en-1,20-dioxy methylphosphonate)s exhibit melting points up to 70 °C due to the smaller side chain.[162]

The variation of the main chain and thus the distance between the phosphate units (and the P-content) can be adjusted by the length of the unsaturated alcohol used in the monomer synthesis. Due to the „negative neighboring effect" the ADMET polymerization, however, a certain distance between the coordinating oxygen atoms of the phosphate and the double bond is necessary to

achieve a reasonable degree of polymerization.[167] It was found that allyl esters do not undergo ADMET polymerization for linear polymers, however, hyperbranched systems are accessible.[41] Pentavalent phosphorus offers the immediate introduction of three functionalities by esterification of POCl$_3$ with an ω-unsaturated alcohol, making phosphates ideal candidates for ATMET. Hyperbranched PPEs exhibit exceptional scavenging efficiency of singlet oxygen. This system was successfully employed to protect the triplet-triplet annihilation photon upconversion process against singlet oxygen quenching under ambient conditions.[168] They were also investigated as flame-retardant additives for commodity plastics recently.[41]
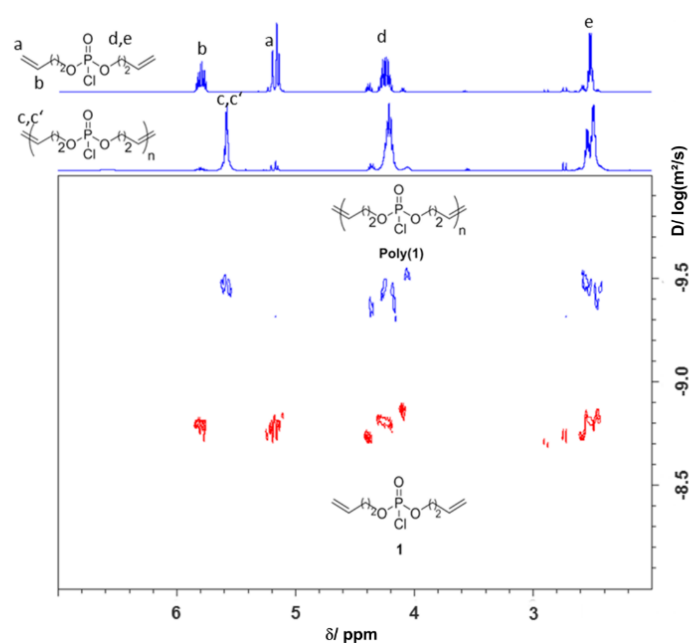
Figure 10. **^{1}H NMR spectrum of monomer 1 (top spectrum of the ^{1}H NMR axis; red signals in the DOSY spectrum) and the respective polymer poly(1) (bottom spectrum of the ^{1}H NMR axis; blue signals of DOSY spectrum) proving the formation of internal double bonds at 5.4 ppm (500 MHz in CDCl$_3$ at 25 °C). (Reprinted with permission from reference 164. Copyright 2014 American Chemical Society.)**

In our recent work, hydrophobic poly(phosphate)s and poly(phosphonate)s were prepared via ADMET polycondensation. Nanoparticles generated by miniemulsion from the corresponding PPEs exhibited strong binding affinity towards a model bone tissue, making this system potentially useful to deliver drugs to the bones. Fluorescent PPEs are accessible by metathesis by a BODIPY-modified phosphate monomer allowing to follow the pathway of nanoparticular drug carrier via

fluorescence microscopy.[169] Another functional ADMET monomer was developed in our group to perform polymer-mediated Horner-Wadsworth-Emmons (HWE) reactions: The usage of linear poly(phosphonate)s minimizes purification efforts because the polymer is converted into a poly(phosphate) during the HWE reaction which can easily be precipitated from the mixture leaving the raw product in the organic supernatant.[170] By this method, several olefins are accessible in high yields.

Polyesters are rarely synthesized by ring-opening metathesis polymerization (ROMP): strained unsaturated lactones could not be initiated by Grubbs type, i.e. Ruthenium-carbenes, catalysts; considerable polymerization was only observed if a Schrock-type catalyst, i.e. Molybdenum-carbene, was employed. For PPEs, however, ROMP was recently investigated for different monomers. The smallest ring systems, and the only ones that have been studied to date are unsaturated seven-membered cyclic phosphonates, phosphates[162, 163] and the nitrogen-containing counterpart.[171] The alkoxy-4,7-dihydro-1,3,2-dioxaphosphepine-2-oxides are accessible via condensation of *cis*-1,4-butene diol and phosphorus dichlorides; for the 1,3,2-diazaphosphepine 2-oxide, *cis*-1,4-butene diamine was used (Scheme 35). The pendant group, resulting from the third ester linkage, can be introduced prior to ring closure. The ring-closure was performed in a dilute THF solution (*ca.* 10 g L^{-1}) with slow addition of the diol *via* a syringe pump to avoid unwanted oligomerization. The ROMP monomers were obtained in reasonable yield (ca. 50-60%) and high purity. In the ^{1}H NMR, it is noteworthy, that the resonances for the protons of the methylene groups next to the phosphonate split up into two distinct signals as they are diastereotopic. This indicates that the phosphonate ring is conformationally locked.
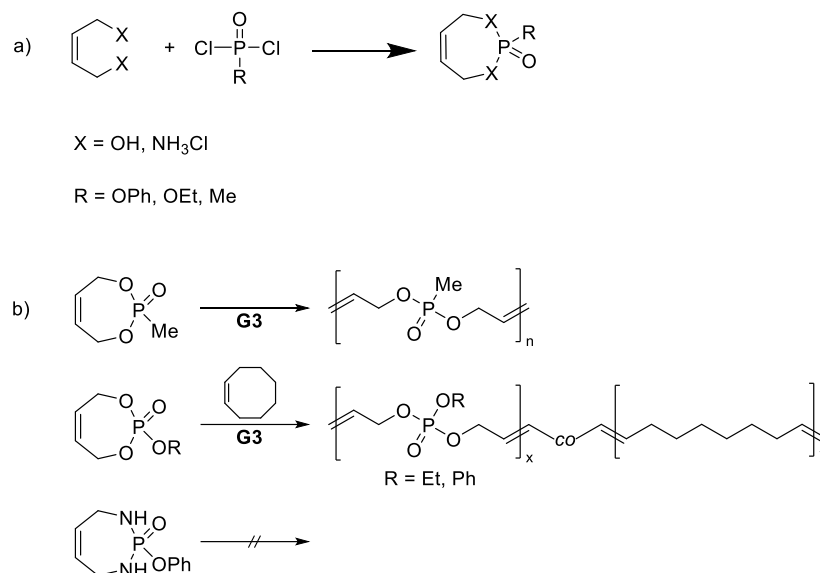
Scheme 35. a) Synthetic approach to 7-membered unsaturated cyclic phosphates and b) homo- and co-polymerization of different ROMP-monomers.

The 1,3,2-diazaphosphepine 2-oxide monomer did not undergo polymerization and was used to terminate a living ROMP of norbornene derivatives.[171] This allows, after acidic hydrolysis of the phosphoamides, the generation of amino-terminated poly(norbornene)s. In the case of the unsaturated seven-membered phosphates (2-phenoxy- and 2-ethoxy-4,7-dihydro-1,3,2-dioxaphosphepine 2-oxide) and phosphonates, polymerization was promoted by the ring-strain in the presence of Grubbs 3rd generation catalyst at ambient temperatures under an argon atmosphere up to 90% monomer conversion. The polymers show a rather broad molecular-mass distribution ($Đ≈2$) and molecular masses up to 5,000 g mol^{-1}. They are amorphous materials with glass transition temperature of ca. -45°C. Also, copolymers with cis-cyclooctene have been prepared to adjust the crystallinity of the copolymers.[162, 163] ROMP allows to prepare poly(phosphonate)s at room temperature under less strict conditions as the anionic polymerization demands. In order to maximize the hydrophilicity of this polyester, the distance between two ester groups needs to be minimized by introducing short alkyl spacers as a linkage. The polyphosphates, which are accessible by ROMP, close the gap of a hypothetical ADMET polymerization of a diallyl phosphate monomer, which does not undergo ADMET polymerization due to the "negative neighboring group effect" of the phosphate ester.[172]

3. Degradation of PPEs

The degradation behavior of polymeric materials is important for many applications, especially in the biomedical field: for tissue engineering, the degradation rate, for example, needs to be designed in the time of the tissue growth, while drug delivery vehicles or nanocarriers need time-dependent release, which should be adjusted by the chemistry. For PPEs several factors are important to consider: hydrophilicity, crystallinity/ glass transition temperature, binding motif around P, and the architecture of the polymer. The degradation rate of PPEs may be adjusted by controlling the chemical structure of the backbone and/or the pendant groups (Figure 11). For PPEs, various enzymes have been reported to degrade phosphoesters in literature,[173-176] depending on their binding motif and their hydrophilicity. In addition, often a combination of hydrolytic and enzymatic degradation of PPEs *in vivo* has to be expected making an *in vitro* simulation only partly reasonable. In addition, it has been found, that degradation products may self-catalyse further degradation.[177] Intensive investigations on the kinetics and mechanisms of the hydrolysis of PPEs at different pH-values have been made by Baran and Penczek using the example of poly(2-methoxy-2-oxo-1,3,2-dioxaphospholane).[9]
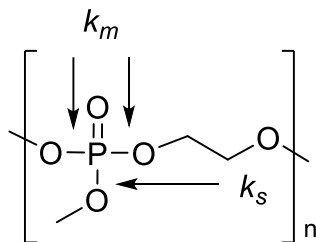
Figure 11. Hydrolysis constants for the phosphoesters in the main chain (k_m) or side chain (k_s) in PPEs.

The investigations revealed that for different pH values the hydrolysis follows different mechanisms: at acidic conditions (pH = 2) the hydrolysis proceeds via a nucleophilic attack of water on the α-carbon atom after activation of the phosphoryl (P=O) bond. Due to the higher accessibility of the carbon atom in the side chain, the ester linkage of the pendant group is cleaved faster than the ester linkages in the main chain. Therefore the cleavage of the side chain can be decelerated by using voluminous side groups. Under weak acidic conditions, hydrolysis does not occur for most phosphate esters.[178] Under basic conditions the nucleophilic attack of the OH⁻ takes place on the central phosphorus atom resulting in a trigonal bipyramidal geometry, wherein the axial position is preferentially broken. Due to the pseudorotation of phosphorus center, the side chain, as well as the polymer backbone, can occupy this position thus resulting in similar rates for

the cleavage of side and main chain (Scheme 36). Due to the simultaneous cleavage of ester linkages in the main chain and side chain, the disruption of the backbone would be accelerated under basic conditions. So the time needed until half of the ester bonds were cleaved have been dramatically faster in basic conditions compared to acidic conditions (6 h at pH 12.30 while 3775 h at pH 3.78). It has to be mentioned that phosphodiesters of phosphoric acid are remarkably stable against hydrolysis,[139] however they may breakdown further by enzymatic degradation.

Recently, Bauer *et al*. studied the hydrolytic degradation of the two most frequently used PPEs, PMEP and PEEP and gave new insights into the degradation mechanism.[179] The degradation process were analyzed by NMR spectroscopy which allowed the identification and quantification of intermediates and degradation products and proved backbiting as the major degradation pathway under basic conditions (Figure 12). The main degradation product was shown to be the diphosphate of ethyl or methyl ethylene phosphate. Chemical modification of the hydroxyl terminus at the polymer end could suppress the degradation and therefore showed the crucial role of the hydroxyl terminus similar to the hydrolytic lability of RNA.
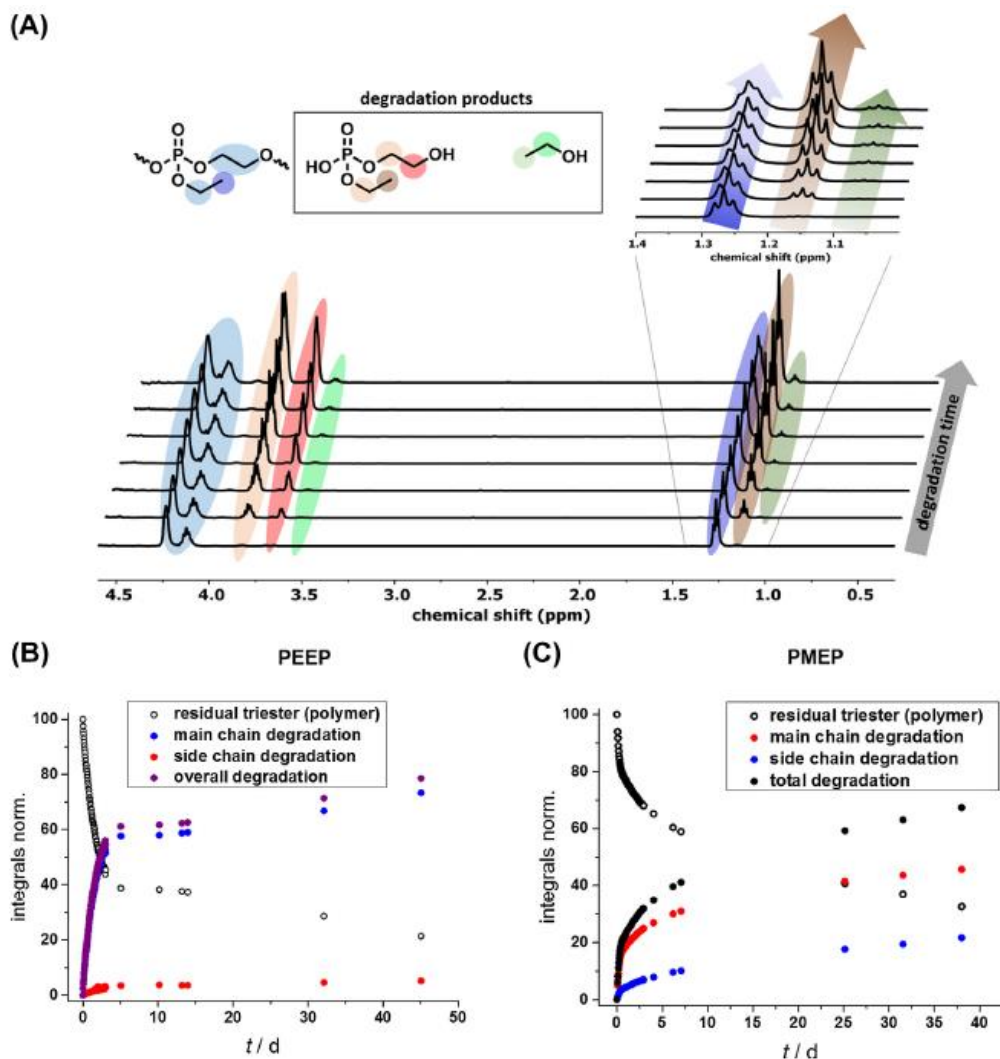
Figure 12. (A) ^{1}H NMR Degradation kinetics of PEEP[93] at basic conditions, revealing the degradation products. (B) Degradation profile of PEEP[93] at pH 11. (C) Degradation profile of PMEP[97] at pH 11. (Reprinted with permission of reference 179. Copyright 2018, with permission from Elsevier.)

Furthermore, these PPEs showed high stability under acidic conditions, as well as enhanced side chain release. This indicates a different degradation mechanism for the acidic degradation as reported by Baran and Penczek.[9]

Iwasaki and coworkers studied the degradation of a hydrogel based on the monomers 2-isopropyl-2-oxo-1,3,2-dioxapholane (IPP) and 2-(2-oxo-1,3,2-dioxaphosphoyloxy)ethyl methacrylate (OPEMA) after radical crosslinking of the methacrylate.[180] The hydrolysis of the hydrogel under acidic conditions (pH 4.0) with almost 60 % weight loss after 15 days was found to be slower, compared to complete degradation under basic conditions (pH 11.0) after 6 days. Under

physiological relevant pH-values, the weight of the hydrogel decreased to 80 % after soaking in PBS for 44 days.

The pH dependence with a dramatically faster degradation in basic conditions on hydrolytic degradation was also in agreement with the work of Wang and coworkers.[181] Additionally, they showed that higher cross linking results in slower degradation rates. After 25 days, the gel with the lowest cross-linking density having the biggest pore sizes and the loosest structure (shown by SEM), degraded completely at pH 7.4. In contrast, gels with higher cross-linking densities did not fully degrade after 106 days under the same conditions.

The dependency of the degradability with the crosslinking density and pH conditions of hydrogels based on PPE was also studied by Zhu *et al*. and showed analogous results as shown above.[182]

1. Hydrolysis under acidic conditions
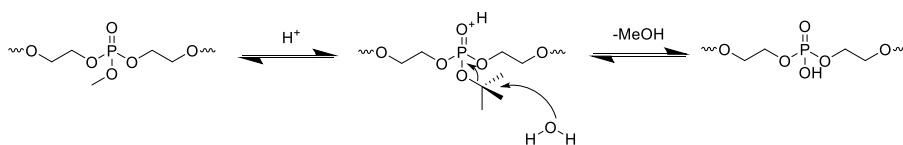
2. Hydrolysis under basic conditions
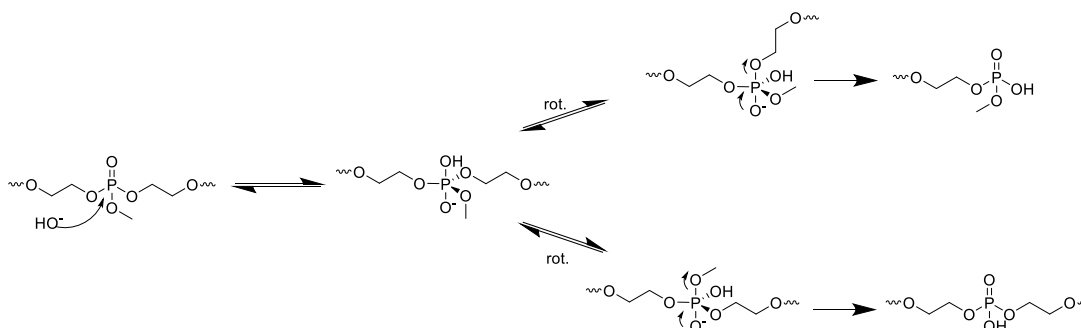
Scheme 36. Hydrolysis of poly(2-methoxy-1,3,2-dioxaphospholane) under 1. acidic and 2. basic conditions.

The introduction of amine-containing side chains to PPEs accelerates their degradation due to the nucleophilic attack on the phosphorus by the pendant amino groups.[16] In several works Leong and coworkers investigated the degradation of PPEs with a propylene glycol backbone and different side groups; they studied the change in the molecular weight distribution over time via GPC.[16, 183, 184] The side groups carried alcohol or amino groups which can attack the phosphate bonds to undergo self-catalytic degradation (Scheme 37). It was found, that PPEs with shorter spacers in the side chain (PPE-MEA in Scheme 37) degraded faster than PPEs with longer spacers (PPE-HA). Since the mechanism of this degradation reactions are based on cyclisation reactions, the degradation rate is really fast when the favored 5-membered cyclic transition state are involved.

While cyclization and with this also the degradation towards smaller or higher membered rings are much slower. Further, the slightly slower degradation rate of PPE3 compared to PPE-EA was attributed to the lower polarity of the side chain.

PPE3

PPE-HA: R=H, m=6
PPE-MEA: R= CH$_3$, m=2
PPE-EA: R=H, m=0
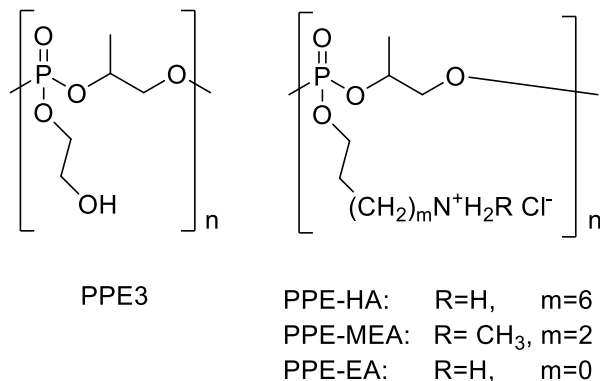
Scheme 37: PPEs with different side chains used for degradation in PBS at 37 °C. (Adapted from reference 185, Copyright 2003, with permission from Elsevier.)
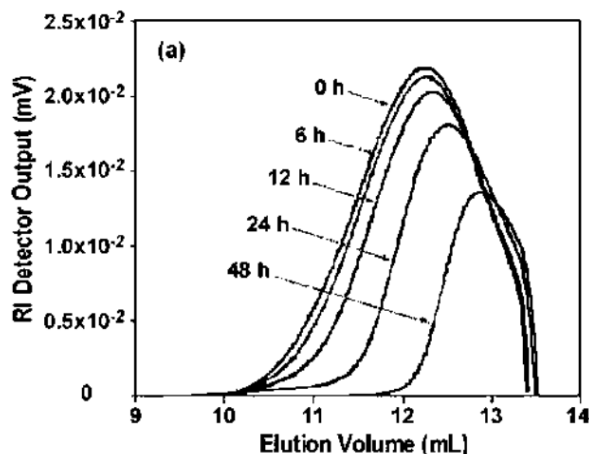
Figure 13: PPE-EA degradation analyzed by GPC. (Reprinted with permission from reference 16. Copyright 2001 American Chemical Society.)

Poly([cholesteryl oxo-carbonylamidoethyl) methyl bis(ethylene) ammonium iodide] ethyl phosphate) (PCEP) is a potential gene carrier and its degradation was studied in PBS (pH 7.4) at 37 °C; the authors found a decrease from M_w=4,000 g/mol to ca. 1,000 g/mol after 2 days of incubation with a multimodal pattern in the GPC elugram.[186] Leong and coworkers designed PPE hydrogels namely poly(6-aminohexyl propylene phosphate) (PPE-HA-ACRL) by conjugation of acrylate groups to the side chains of PPE-HA. The hydrogels showed not only higher mechanical strength but also slower degradation rates with increasing acrylate contents in the macromers.[187]

The same group also studied the protein release from polymer fibers consisting of PCL and PEEP.[188] After incubation of the fibers in distilled water at 37 °C a significant mass loss was observed after one month. While the change of M_w and M_n was negligible after the first 2 months of incubation. In addition, no change of the fiber morphology was observable by SEM. After 3 months of incubation, the weight loss of the copolymer fibers containing 15 molar % of EEP was below 8 %. The release of the protein started with a burst of 20 % and occurred then in a relatively steady manner.

Zhao *et al.* studied the degradation of Poly(lactide –co-ethylphosphate)s at 37 °C and 70 °C and reported a faster degradation rate compared to PLA. Kinetic analysis showed that the degradation occurred in two phases; first the cleavage of the phophoester - lactide linkages followed by cleavage of lactide – lactide bonds with an degradation rate which was several times slower. Accelerated degradation showed lactic acid, phosphoric acid, propylene glycol, and ethanol as final degradation products.[189]

Zhu *et al.* crosslinked PEG phosphoester hydrogels and loaded them with Nile Red: Figure 14 shows the swelling and degradation over time.[190]

Figure 14: Swelling and degradation of PEG-PPE-hydrogels loaded with Nile red. (Reprinted with permission from reference [190]. Copyright 2011 American Chemical Society.)

Ilia and coworkers showed the degradation of PPEs by weight loss of pellets. They synthesized different PPEs by modified inverse phase transfer catalysis.[191] The polymers were pressed to pellets and placed into 4 M NaOH for 8 h. The degradation was then determined by weight loss of the pellets; again, these strong basic conditions only prove a general degradability of the polymers but give no insights to *in vivo* degradation kinetics.

Biodegradation of polymers are catalysed by enzymes *in vitro* or *in vivo* and leads to a breakdown of the substance. Following the IUPAC definition this can be further divided depending on the hazard assessment. The primary biodegradation results in the loss of a specific property of that polymer by alteration of the chemical structure. In the environmentally acceptable, the

biodegradation of the polymer happens until undesirable properties of the polymer are removed. And finally in the ultimate biodegradation the polymer is completely degraded to either fully oxidized or reduced simple molecules such as water, carbon dioxide, nitrate, methane or ammonium. Other reports prove the biodegradability of PPE structures in various applications, rendering PPEs as ideal water-soluble materials for drug delivery or nanocarrier formulations.[21, 192, 193] Poly(phosphoamidate)s (PPAs) with the amidate bond in the side chain can be selectively hydrolyzed to the respective poly(phosphodiester) ionomers, due to the acid-labile amidate bond (Scheme 31). The cleavage of the phosphoramidate bonds is pH-dependent, i.e. under basic conditions (pH = 7.4 and 9.0) it is stable for several days, but is hydrolyzed quantitatively at pH = 1.0 within 10 h, thus making PPAs attractive materials for pH-sensitive drug-delivery systems, particularly in the cancer therapy. It also renders the phosphoramidate bond a potential protective group as it is easily hydrolyzed without scission of the main chain.[194] Interestingly, the resulting polyphosphodiester was very stable under acidic conditions (no degradation observed at pH=1).[139] Wurm *et al.* synthesized a library of novel poly(phosphoroamidate)s (PPDAs) carrying the amidate bond in the main chain and they showed that the pendant P-O bond is selectively cleaved under basic conditions while the P-N bonds are degraded by acidic hydrolysis.[195]

Besides the hydrolysis by acidic or basic pH, the main degradation pathway of PPEs *in vivo* is probably achieved by enzymes, such as phosphatases, phosphodiesterases, etc. Raushel *et al.* reported recently the catalytic hydrolysis of phosphotriesters with lack of an easily hydrolysable bond by phosphotriesterase. They expressed the enzyme from *Escherichia coli* and were able to effectively hydrolyze flame retardants, plasticizers and industrial solvents.[196]

An interesting example of a biodegradable PPE was reported by Chujo and coworkers: they used diphosphoamidite-modified fluorescein as monomer for a polycondensation with diols (Scheme 38).[173] The resulting poly(phosphodiester)s show a low fluorescence, which increased rapidly after degradation with calf intestine phosphatase (see inset in Scheme 38).
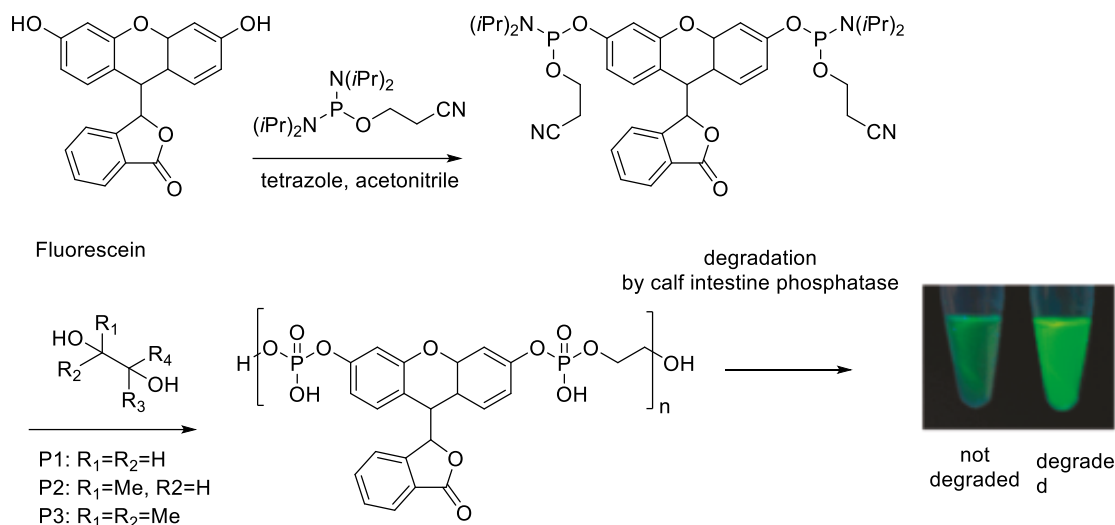
Scheme 38: Biodegradable poly(phosphodiester)s based on fluorescein (Adapted with permission from reference 173. Copyright 2010 American Chemical Society).

Wang *et al*. reported on block copolymers based on PCL and PEEP with a selective degradation of the polyester by lipase, while the PPE remained rather unchanged under these conditions.[175] Additionally, they used phosphodiesterase I for the *in vitro* degradation of the PEEP blocks at pH 8.8. The degradation was demonstrated by sharply reduced proton signals of PEEP blocks in ^{1}H NMR. In another work of Wang *et al*. they used this copolymer to form Doxorubicin (DOX)-loaded vesicles.[197] Incubation of the vesicles with Phosphodiesterase I accelerated the release of DOX to 83.8 % after 140 h, while the release without enzyme was found to be only 30 % after 140 h.

Iwasaki and coworkers used alkaline phosphatase (ALP) in physiological concentration of healthy children and adults (i.e. 72.5 and 220 U/L, respectively) to evaluate the enzymatic degradation of PIOP Hydrogels (Scheme 39) by weight loss.[174] Without ALP the weight of PIOP decreased by 20 % after 40 d and low-molecular-weight compounds similar to the phosphate unit were observed in the aqueous medium.[198] At pH 9.0 the hydrogel reached full degradation after around 100 days. With a concentration of 72.5 U/L of ALP, the hydrogel was completely dissolved after 70 days. With an increase of ALP concentration (220 U/L) the degradation could be accelerated and was completed after a period of 60 days. In general, many reports prove the degradability of PPEs and PPAs under different conditions, but a systematic degradation profile correlated to the molecular structure is still missing *in vitro* and *in vivo*. This might be an important step toward precisely tuned degradable materials.
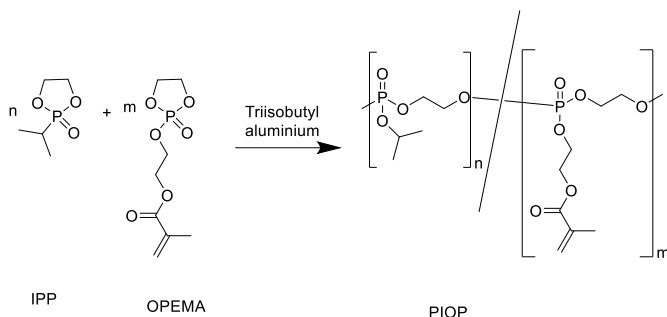
Scheme 39. Synthesis of PIOP from IPP and OPEMA. (Adapted from reference 174, Copyright 2006, with permission from Elsevier.)

4. Biomedical applications of polyphosphoesters

The major challenges in drug delivery are the poor water-solubility of the majority of drugs, their short blood circulation times and the resulting inability to gain access to the site of action at an appropriate dose.[199, 200] The therapeutic effectivity of hydrophobic drugs is often limited by the aforementioned issues. One possibility to overcome these problems is the use of nanocarriers, such as polymeric micelles, for the delivery of hydrophobic drugs. Polymeric micelles are formed by amphiphilic block copolymers, which consist in the simplest case of two different polymers covalently attached to each other and are able to self-assemble spontaneously into micelles in aqueous solution. They exhibit core-shell structures with the hydrophobic core serving as environment for hydrophobic drugs and the hydrophilic shell for stabilization in aqueous solution. The sizes of the micelles typically range from 10 to 50 nm. The micelles can be loaded with drugs by a physical entrapment as well as by covalent bonding to the block copolymer. These micelles possess several features such as enhancing the aqueous solubility of drugs, prolonging the blood circulation time, improving the preferential accumulation at tumor sites by the enhanced permeability and retention effect.[201, 202] To avoid an accumulation of the carrier materials in the body, biodegradable materials are particularly interesting for the design of micellar nanocarriers. With the development of controlled polymerization techniques, PPEs have attracted the interest of a few working groups as promising materials for drug delivery systems. Especially the controlled synthesis of water-soluble PPEs makes them interesting candidates for drug delivery as a potential substitute for the non-degradable poly(ethylene glycol) (PEG). PEG is the gold standard polymer in today's drug delivery community: PEGylated drugs (proteins or low molecular mass drugs), PEGylated liposomes or micelles with the hydrophilic corona based on PEG are dominating the scientific literature.[203-205] This is mainly attributed to the extraordinary

properties of PEG, such as high water-solubility, low protein affinity and easy access to well-defined structures. The commercially available methoxy-PEGs are typically used and modified with various hydrophobic segments, for example. PPEs, however, are typically biocompatible and degradable materials and by the ROP of EEP, also water-soluble PPEs are accessible with the benefits of a living/ controlled polymerization technique. Further developments, such as clickable PPEs[206] for postpolymerization modification or also water-soluble poly(alkyl alkylene phosphonate)s broaden the potential of these biodegradable materials to replace the stable polyethers in the future.

Just recently, our group successfully demonstrated the "stealth effect", i.e. the inhibition of the unspecific cellular uptake of PEGylated and "PPEylated" nanocarriers.[207] It was shown that the modification of polystyrene nanoparticles with both PEG or PEEP either by covalent[207] or adsorptive[208] attachment of the PPEs to the particle surface resulted in a drastically reduced uptake of the particles by cells of the immune system.

This section will highlight several applications of PPEs for drug delivery; we selected representative and more recent examples for various applications. The interested reader may also refer other excellent reviews about PPEs for additional information.[18, 20, 21, 209, 210]

To date, several working groups have published PPE-based drug delivery systems ranging from micellar[211-213] to nanoparticulate structures.[214-217]

Wang *et al.* demonstrated successfully the delivery of siRNA[151, 218] or siRNA[219] combined with paclitaxel to tumor cells both *in vitro* and *in vivo* without activation of the innate immune response or the generation of carrier associated toxicity. The partially degradable carrier system is based on a triblock copolymer consisting of monomethoxy poly(ethylene glycol), poly(ε-caprolactone) and poly(2-aminoethyl ethylene phosphate) (mPEG$_{45}$-*b*-PCL$_{100}$-*b*-PPEEA$_1$,

Scheme **40**).[151, 218] The triblock copolymer was prepared by sequential ROP of lactide and 2-(*N*-*tert*-butoxycarbonylamino) ethoxy-2-oxo-1,3,2-dioxaphopholane, starting with a PEG macroinitiator and Sn(Oct)$_2$ as the respective catalyst and subsequent careful hydrolysis of the protective group to release the pendant amines.
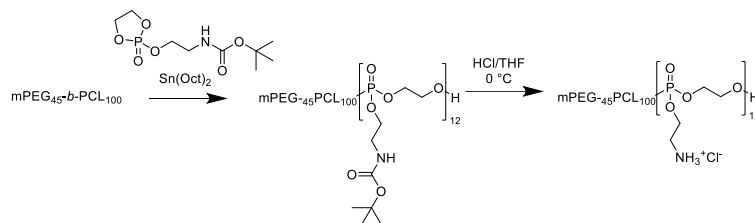
Scheme 40. Synthetic procedure for the synthesis of amphiphilic mPEG45-b-PCL100-PPEEA12 for gene delivery. (Adapted with permission from reference 151. Copyright 2008 American Chemical Society.)

The micellar nanoparticles (MNPs) were prepared by the solvent evaporation method. Wang and coworkers assume a three layered structure for the MNPs with the hydrophobic PCL segment in the inner core and the outer corona consisting of two sublayers (Figure 15). The inner layer of the outer corona includes part of the PEG- and the PPEA-segment and the outer layer is represented by the remaining part of the PEG-block. The siRNA is believed to bind to the cationic layer by electrostatic interaction.
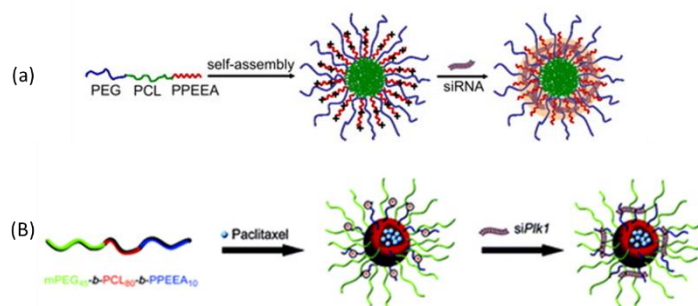
Figure 15. Schematic drawing of self-assembled cationic micellar nanoparticles and loading with (a) siRNA (Reprinted with permission of reference 151. Copyright 2008, with permission from Elsevier.) and (b) siRNA and Paclitaxel (Reprinted with permission from reference [219]. Copyright 2011 American Chemical Society.)

The effective internalization of the micellar carrier system by cancer cells and the subsequent siRNA release resulted in a significant down-regulation of protein expression of these cells. Furthermore, the micelles carrying both siRNA and paclitaxel showed remarkably inhibition of tumor growth in a synergistic way.

Furthermore, Wang *et al.* developed an innovative, dual pH-sensitive anti-cancer drug delivery system based on PPEs with enhanced cytotoxicity in drug-resistant cancer stem cells. As proof of

concept, a polymer doxorubicin-conjugate was used that can react to the tumor extracellular and intracellular pH gradients.[220] The nanocarrier was synthesized via a multi-step protocol (Scheme 41). The final drug carrier contains doxorubicin units that are bound to the polymer via an acid-labile hydrazone bond. The remaining amino groups were reacted with 2,3-dimethylmaleic anhydride resulting in an amide bond that can be cleaved under slightly acidic conditions. Therefore, the resulting drug carrier can change its charge by cleavage of the amide bond in the tumor extracellular environment from negative to positive resulting in an enhanced internalization by the tumor cells. Then, in the more acidic intracellular environment the hydrazone bond is cleaved and doxorubicin is released.
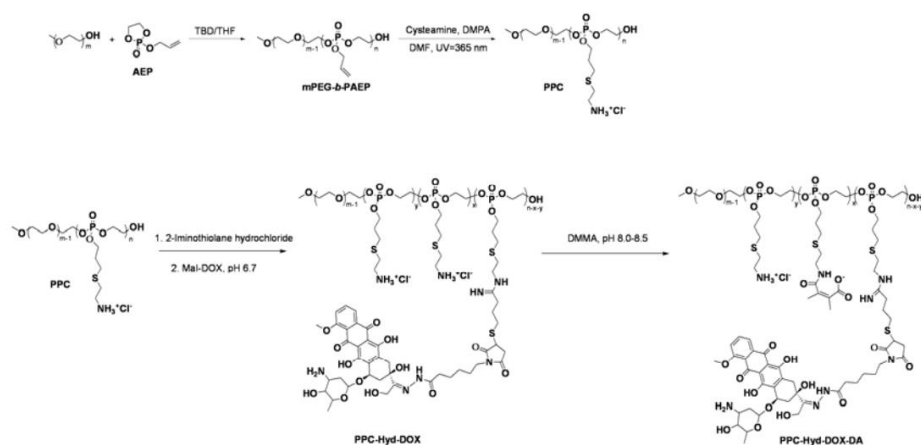
Scheme 41. Synthetic approach to PPC-Hyd-DOX-DA. (Reprinted with permission from reference [220]. Copyright 2011 American Chemical Society.)

The final drug carrier contains doxorubicin units that are bound to the polymer via an acid-labile hydrazone bond. The remaining amino groups were reacted with 2,3-dimethylmaleic anhydride resulting in an amide bond that can be cleaved under slightly acidic conditions (Figure 16A). Therefore, the resulting drug carrier can change its charge by cleavage of the amide bond in the tumor extracellular environment from negative to positive (Figure 16 B) resulting in an enhanced internalization by the tumor cells. Then, in the more acidic intracellular environment, the hydrazone bond is cleaved and the doxorubicin is released (Figure 16C).
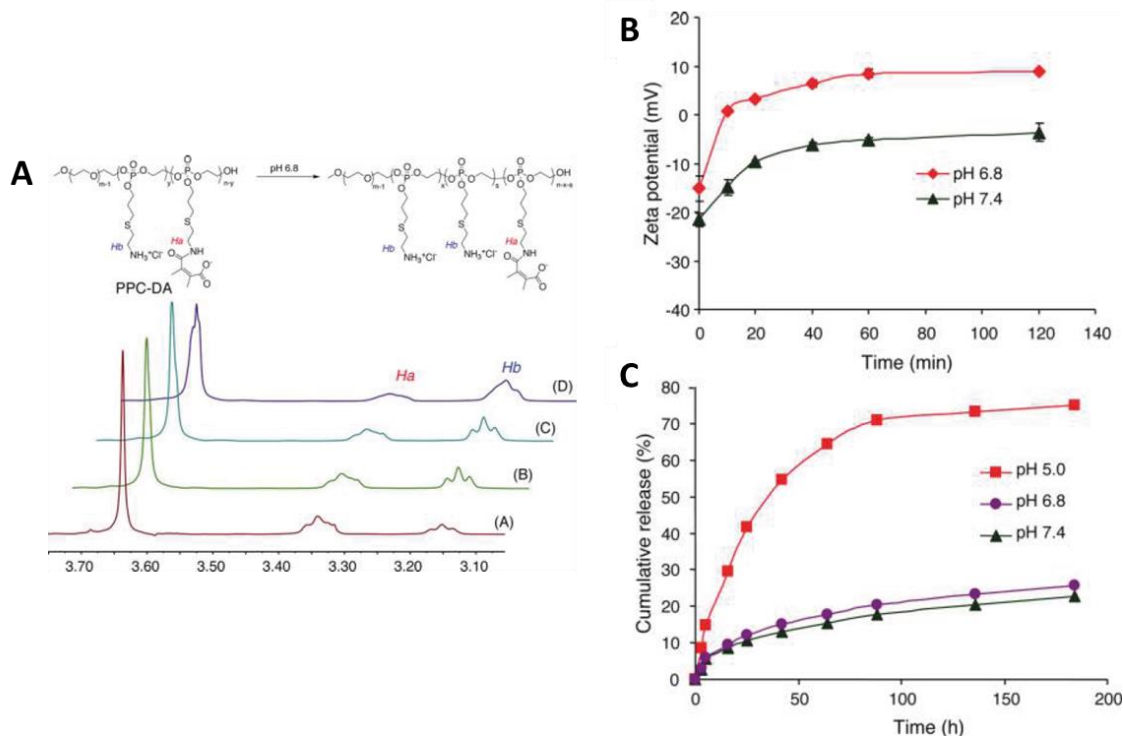
Figure 16. A) ^{1}H NMR spectra of PPC-DA after incubation at pH 6.8 in D$_2$O/DCl (25°C) for different time periods: (A) 0 min, (B) 10 min, (C) 30 min, (D) 60 min. **B)** Zeta potential change of PPC-Hyd-DOX-DA nanoparticles after incubation at pH 7.4 or 6.8 for different time periods. **C)** Time-dependent cumulative release of DOX from PPC-Hyd-DOX-DA NPs at different pH values. (Reprinted with permission from reference [220]. Copyright 2011 American Chemical Society)

The successful release of DOX in the tumor cells at pH = 6.8 has been demonstrated by a sphere formation assay in the SK-3rd cancer stem cell line. The treatment of cancer stem cells with the PPC-Hyd-DOX-DA nanoparticles resulted in a significant lower number of cells in the spheres compared to the treatment with free DOX. To conclude, the dual pH responsive nanoparticles represent an interesting platform for further investigations.

The Wooley lab studied in excellent interdisciplinary collaborations block copolymers with one block consisting of either 'clickable' **PBYP** (Table 2, Entry 23) or **PBEneP** (Table 2, Entry 29) as the basic materials for drug delivery systems.[14, 15, 94, 152, 221-228] The double/triple bonds in the polymer side chains were subsequently functionalized by click reactions, i.e. the thiol-ene/yne reaction and the azide-alkyne-1,3-dipolar cycloaddition.

These block copolymers have two major intentions: the delivery of the hydrophobic anticancer drug paclitaxel and the delivery of antimicrobial silver for the treatment of lung infections.

In 2013 the 1st generation MNPs was published based on an amphiphilic PEG-*b*-PPE-*g*-PTX block copolymer where the PPE-block consists of PBYP (Table 2 entry 23) serving as anchor point for the Paclitaxel (PTX) grafting.[227] Paclitaxel is a potent microtubule-interfering agent for the treatment of breast, non-small lung and advanced ovarian cancers, which belongs to the class of hydrophobic anticancer drugs. One of the major challenges within the application of paclitaxel is the effective delivery through aqueous environment to intracellular targets. Due to its hydrophobicity it exhibits a strong tendency to aggregate, which can lead to complications such as embolism and local toxicity.[229] One efficient approach to overcome the low water-solubility is the usage of degradable micellar nanoparticle carriers.[230] The pendant alkynes in the PBYP-block ensure the grafting of the azide-functionalized PTX by the azide-alkyne cycloaddition

For the micellar nanoparticle formation, the polymer with a loading capacity of 55 wt% and a high water-solubility of 11.3 mg mL^{-1} was used. However, the polymer showed only a low PTX-release of 5% after four days incubation in 20 mM acetate buffer at pH=6. Thus resulting in an 8-to-63 fold lower cytotoxicity against several cancer cell lines compared to the commercial PTX. The low cytotoxicity can be ascribed to the slow dissociation of PTX from the polymer backbone. Therefore, in 2014 the 2nd generation PEO-*b*-PPE-*g*-PTX (G2) was published (Scheme 42), wherein the hydrophobic PBYP- is replaced by a PBEneP-block (Table 2, entry 29).[14] The PBEneP- in contrast to the PBYP-block allows a thermo-induced thiol-ene reaction for the post polymerization modification proceeding without the usage of potentially toxic metal catalysts.
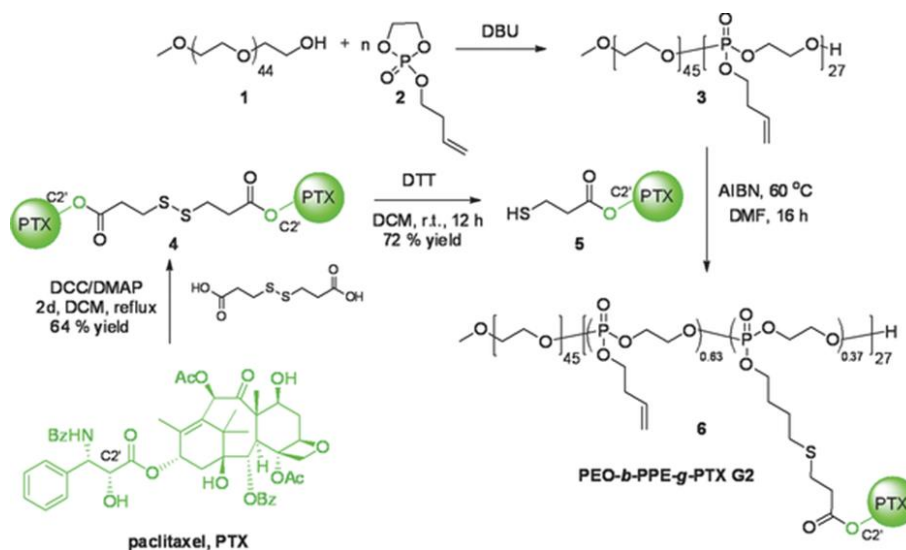
Scheme 42. Synthesis of PEO-*b*-PPE-*g*-PTX G2. (Taken with permission from reference 14. Copyright 2014 Wiley).

In G2 PTX is connected to the polymer backbone via an acid sensitive hydrolytically-labile β-thiopropionate linkage, which ensures a PTX release of 50 wt% after 8 days in PBS buffer at pH=5.5 (under neutral conditions only 25 wt% release). The cytotoxicity of G2 was studied *in vitro* against OVCAR-3 and RAW 264.7 cells. Compared to the first generation PEO-*b*-PPE-*g*-PTX, G2 showed an enhanced, but still 3-to-10 fold lower cytotoxicity compared to the free PTX. Beside the paclitaxel-conjugates, the same group studied different PPE-nanoparticles for the therapy of bacterial infections.[224, 226] Together with the Hunstad lab they prepared silver-bearing degradable nanoparticle consisting of PPE-*block*-poly(L-lactide) and studied the treatment of bacterial infections.[224] The PPE segment in the polymer again consists of PBYP (Table 2 entry 23) that was proven to be suitable for efficient post polymerization modification by thiol-yne reaction. Here, the thiol-yne reaction was performed with 3-mercaptopropanoic acid, which guarantees high water solubility as well as the interaction with silver. Nanoparticles were prepared by direct dissolution in water. The silver loading was performed using three different silver compounds, silver acetate (AgOAc), 1-methyl-3-(3-hydroxypropyl)-4,5-dichloroimidazol-2-ylidene silver(I) acetate (SCC22), or 1-methyl-3-hexyl-4,5-dichloroimidazol-2-ylidene silver(I) acetate (SCC10). It was assumed, that the loading into the nanoparticles occurred by three different mechanisms, i.e. electrostatic interaction with the carboxylate groups, coordination by the sulfur atoms and encapsulation by hydrophobic interactions (Figure 17).
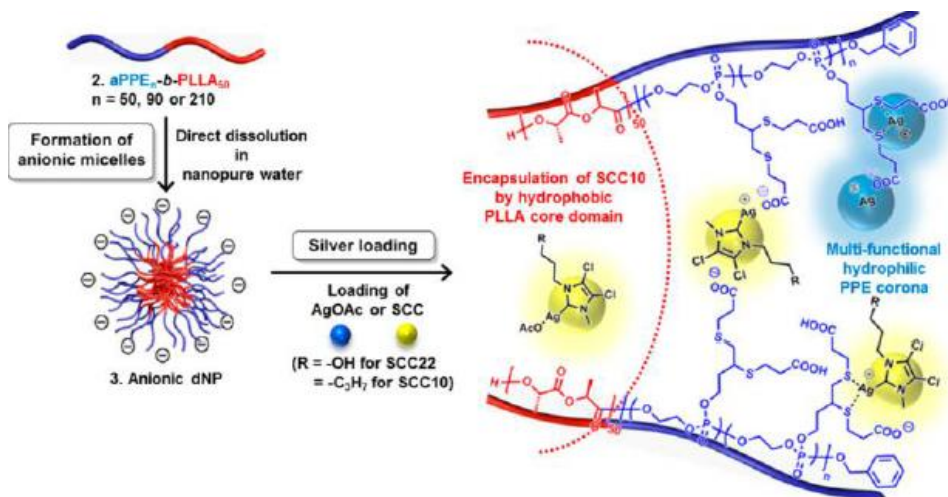
Figure 17. Schematic illustration of the self-assembly of the PPE$_n$-b-PLLA block copolymer into anionic micelles by direct dissolution in water followed by silver loading. (Reprinted with permission from reference [224]. Copyright 2015 American Chemical Society)

The highest loading capacity of 12% was achieved by using SCC22 and a feed ratio of 100 wt % feed amount. For the release kinetics, four samples with the highest loading capacities were chosen and all samples showed a plateau with almost complete silver release on the 3rd day. The degradation of the nanoparticles in aqueous buffer solutions at pH 5.0 or 7.4 at 37 °C was evaluated by DLS measurements and ^{31}P NMR spectroscopy. In both cases, after two weeks the hydrodynamic diameters were significantly decreased and after 35 days ^{31}P NMR spectroscopy showed a distinct shift of the signal from the intact backbone to the degradation product, i.e. phosphoric acid. All in all, the fully degradable silver-bearing nanoparticles show high potential for treatment of bacterial infections and are of high interest for further investigation and development.

A straight forward synthesis of new transporter systems based on oligophosphoesters for drug delivery has been developed by McKinlay *et al.*[159] The presented drug delivery systems are based on a new cyclic phosphate monomer (Table 2, Entry 32) exhibiting a guanidine unit in the pendant chain that can facilitate the cell-penetrating properties. The conjugation of drugs and probe molecules respectively can be achieved by two different strategies (Scheme 43). Cargo molecules containing a nucleophilic functional group, i.e. alcohol, thiol or amine group, can be directly used as initiators in the oligomerization reaction resulting in the cargo-transporter system (Scheme 43B, Strategy 1). Cargo molecules that cannot be conjugated to the oligophosphoester directly in the oligomerization process can be attached to the transporter by postoligomerization strategies. Using this pathway, cargo molecules can attach to be releasable or permanently bound (Scheme 43B, Strategy 2).
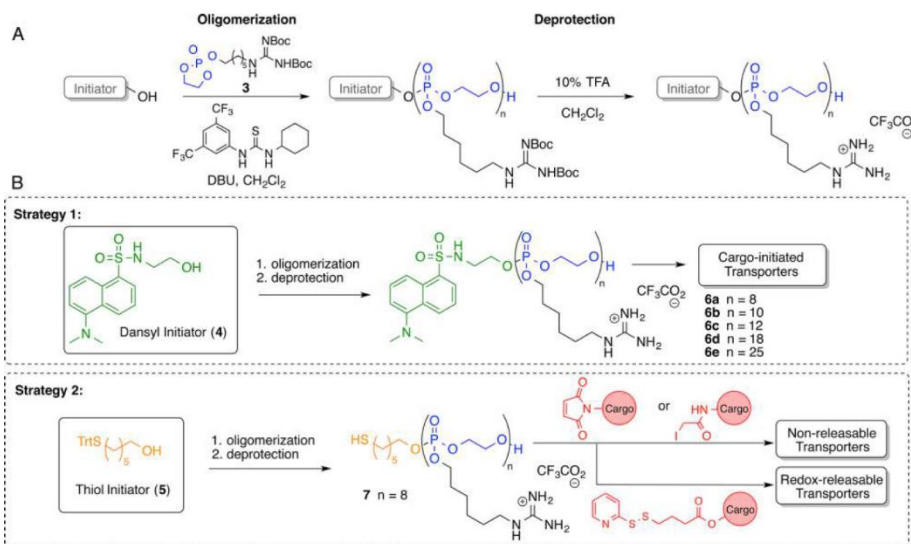
Scheme 43. Overview of synthetic methodologies employed to access guanidinium-rich oligophosphoester transporters. (A) ROP of HexPhos for two step access to guanidinium-functionalized oligophosphoester for drug/probe delivery. (B) Methods of conjugation of drugs or probe molecules to form cell-penetrating oligomeric conjugates. (Reprinted with permission from reference 159. Copyright 2016 American Chemical Society.)

Studies of the length-dependence of the cellular uptake showed a maximum uptake for the HexPhos 10-mer and a in general drastically increased uptake compared to the analogous oligocarbonate (Dansyl-MTC-G_8, Figure 18C) and system and the arginine homopolymer (Dansyl-Arg_8, Figure 18C) (Figure 18A). Cellular uptake was proven in four different cell lines and compared to Dansyl-MTC-G_8 and Dansyl-Arg_8 (Figure 18B).
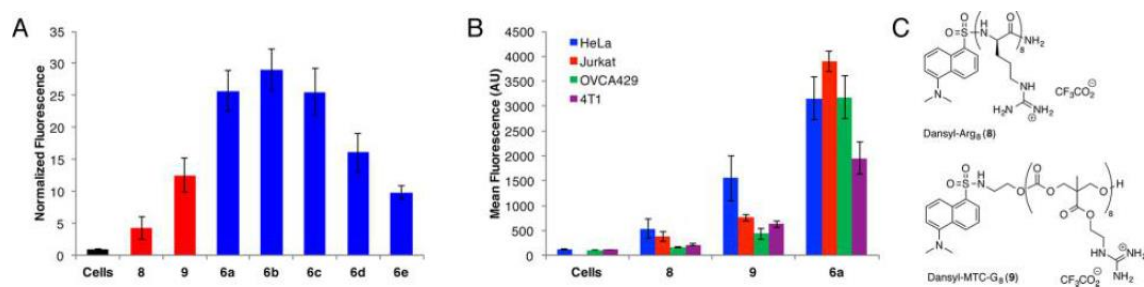
Figure 18.(A) Length dependence of uptake of Dansyl-HexPhos, oligomers 6a−e in HeLa cells compared to Dansyl-Arg8 (8) and Dansyl-MTC-G8 (9). (B) Cell line dependence of uptake of HexPhos8 in HeLa cells (blue), Jurkat cells (red), OVCA429 cells (green), and mouse 4T1 cells (purple). (c) Structures of previously reported transporter systems Dansyl-Arg8 (8) and Dansyl-MTC-G8 (9). (Reprinted with permission from reference 159. Copyright 2016 American Chemical Society.)

Collectively, this study impresses with a plain but clever design of new and efficient drug delivery systems that are accessible via a straightforward synthesis.

Light-responsive amphiphilic hyperbranched PPEs as smart nanocarriers for controlled drug release have been published by Chen *et al*. (Scheme 44) [28, 231] The nanocarriers consist of HPHEEP, (Table 2, entry 22) endcapped with light-sensitive units. The first published polymer contained 2-diazo-1,2-naphthoquinone (DNQ) and the second one contained 1'-(β-carboxyethyl)-3'-3'-dimethyl-6-nitrospiro[indoline-2',2-chromane] (SP-COOH) as light-sensitive unit.
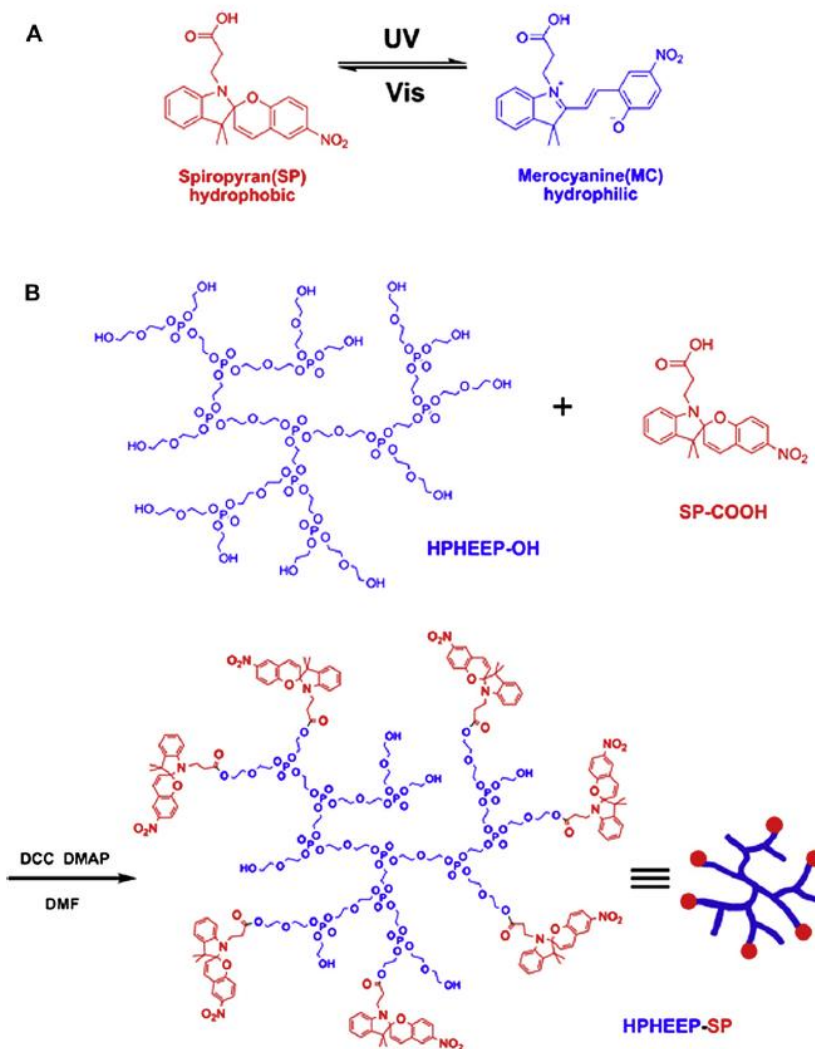
Scheme 44. (A) Photoisomerization of the carboxyl-containing spiropyran. (B) the structure of HPEEP-OH and the synthetic route for HPEEP-SP. (Reprinted from Reference [231], Copyright 2012, with permission from Elsevier)

The next step in the design of smart drug delivery systems is the integration of specific moieties, i.e. for example antigens, proteins or sugars, into the drug carrier which allow a targeted drug delivery to distinct sites in the body. Typical problems associated with systemic drug administration are the even distribution of the pharmaceuticals within the whole body, the lack of drug specific affinity toward a pathological site, the necessity of high drug doses to achieve sufficient local concentrations and the adverse side-effects due to high drug doses. Smart drug delivery systems allowing a targeted transportation of the drug to the affected site, may resolve many of these problems. Up to date some publications about the usage of polyphosphoesters in targeted drug delivery have been published.[232-234] The following paragraph highlights a few of these publications.

The brain is protected against potentially toxic substances by the blood-brain barrier (BBB), which restricts the entry of most pharmaceuticals into the brain. Especially the development of drugs for the treatment of CNS disorders has not kept pace with progress in molecular neurosciences, due to the fact that most new drugs cannot cross the BBB and thus the clinical failure of CNS drugs may be directly linked to a lack of appropriate drug delivery systems. Localized and controlled delivery of drugs at their desired site of action is preferred because it reduces toxicity and increases treatment efficiency.[235]

PPEs are especially appealing as materials for drug delivery to the brain since an enrichment of polymeric drug carriers in the brain can be problematic and PPEs are potentially degradable in this environment. However, up to date there are only a few reports about the usage of PPEs as drug carrier systems for brain targeting.[236, 237] The efficient delivery of paclitaxel to the brain by the usage of transferrin-conjugated PPE hybrid micelles has been demonstrated by Yaping Li *et al.*[238] Micelles consisting of PCL-*b*-PEEP and transferrin-conjugated PEG-*b*-PCL block copolymers have been prepared and loaded with paclitaxel. Transferrin (Tf) can facilitate the transcytosis of coupled nanocarriers through Tf receptor mediated pathway. To investigate the brain delivery properties of the TPM *in vitro* primary brain microvascular endothelial cells (BMECs) were used because they closely represent the barrier property of the BBB. It was shown that the cellular uptake of the TPM nanocarriers in contrast to the unmodified nanocarriers is increased by the factor of two. Furthermore, the cellular uptake of the modified nanocarriers can be inhibited by the addition of free transferrin indicating that the uptake is indeed TfR-mediated (Figure 19A). The anti-glioma activity of the TPM was measured by the survival time of intracranial U-87 MG glioma bearing mice (Figure 19B). Tumor bearing mice were treated either with Taxol®, PM or the modified micelles. Mice treated with PM showed no significantly enhanced survival time

compared to those treated with Taxol®, whereas the survival time of those mice treated with the TPM was significantly prolonged.
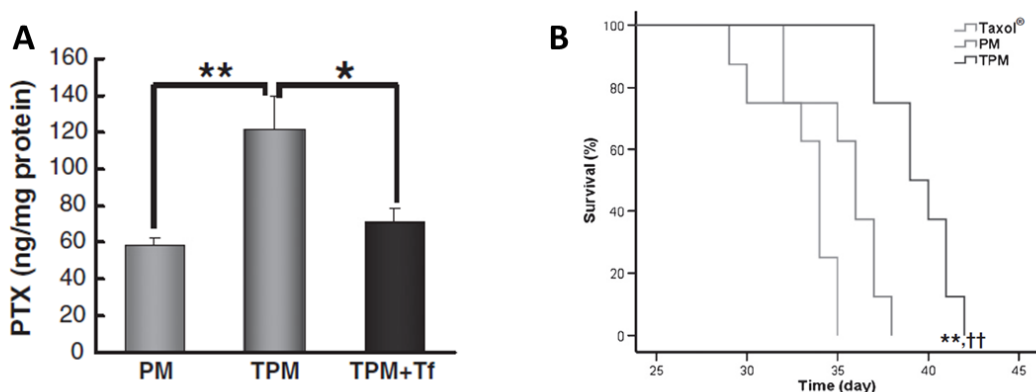
Figure 19. (A) Quantitative determination of the cellular uptake of PTX by BMECs after 1h incubation *$p<0.05$, **$p<0.01$. (B) Kaplan-Meiersurvival curve of mice bearing intracranial U-87 MG glioma. (n=8) **$p<0.01$compared with Taxol®, ††$p<0.01$compared with Taxol®) (Reprinted from reference [238], Copyright 2012, with permission from Elsevier)

With this work, Yaping Li *et al*. have successfully demonstrated the potential of PPE-based targeted delivery and have laid the foundation for further investigations.

A simple, but efficient sheddable ternary acidity-targeted nanoparticular drug delivery system for the delivery of siRNA has been developed by Wang and co-workers.[239] The nanoparticles consist of a ssPEI$_{800}$/siRNA particle core and a ternary negatively charged PEG-*b*-PPE block copolymer that is bound to the particle surface by electrostatic interactions. The outer PEG chain provides a prolonged blood circulation time by minimizing the unspecific interactions of the delivery system with blood components, while the inner PPE-block provides the pH-sensitivity. However, PEGylation also reduces the uptake of the nanoparticle by cancer cells. Therefore, a shedding of the PEG-layer after accumulation at the tumor site is needed which is realized by transferring the PPE-block from a negative to positive charge (Figure 20).
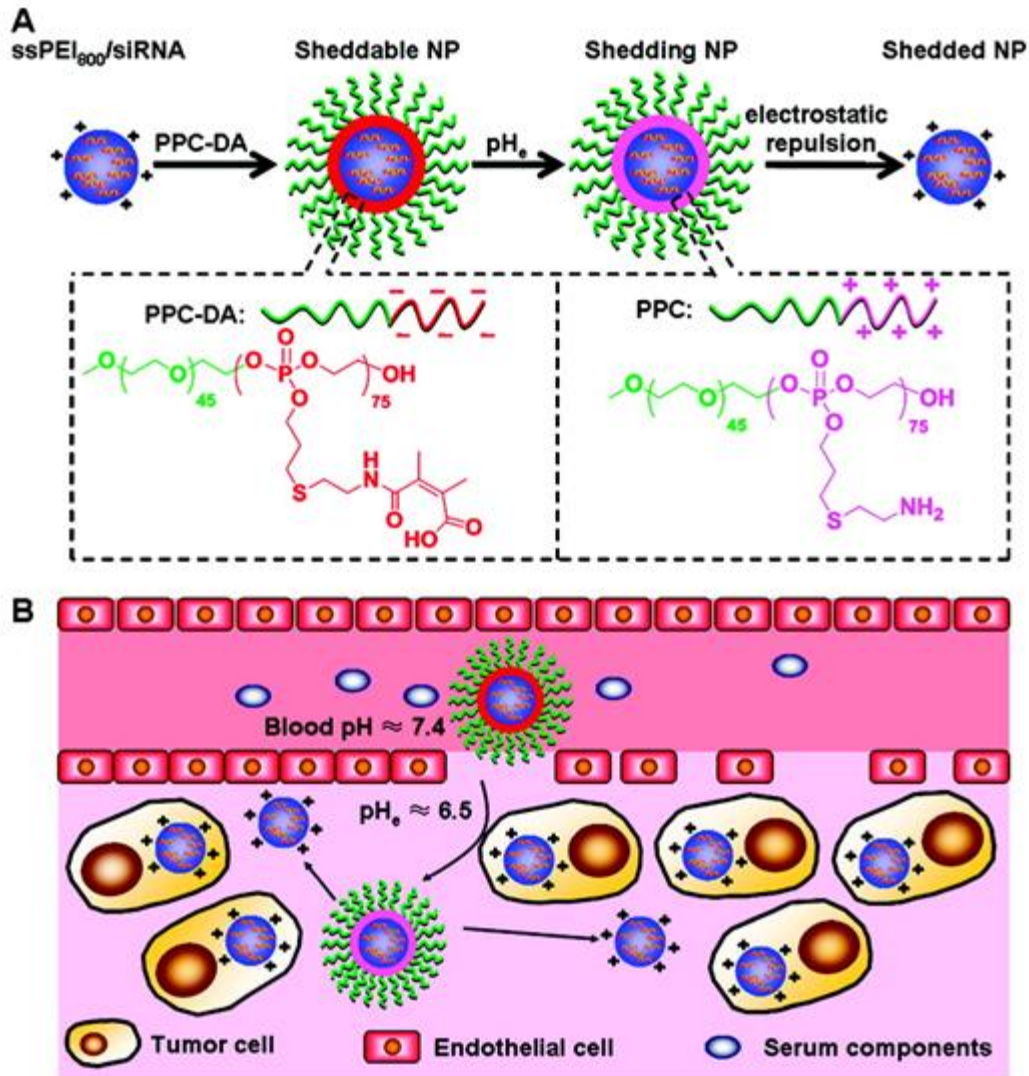
Figure 20: (A) Shielding and deshielding of the positively charged ssPEI800/siRNA nanoparticles by the PEG shell in the acidic environment of the tumor. (B) Schematic illustration of the stealth property and promoted tumoral cell uptake of sheddable nanoparticles. (Taken with permission from reference [239]. Copyright 2012 American Chemical Society.)

The deshielding of the of the PEG shell under slightly acidic conditions was demonstrated by the change of the zeta-potential from ca. -12 mV to 8 mV after incubation with PBS at pH 6.8. Furthermore, the increased cellular uptake after deshielding of the PEG shell under acidic conditions by MDA-MB-231 cells has been proven by incubation of sheddable and unsheddable nanoparticles at pH 7.4 and 6.8. The internalization of the unsheddable nanoparticles was not affected by the pH while the sheddable nanoparticles showed an enhanced cellular uptake at pH

6.8 compared to pH 7.4. Finally, the silencing of polo-like kinase 1 (Plk1) expression of MDA-MB-231 cells at different pHs was studied by using sheddable and unsheddable nanoparticles loaded with siRNA targeting. It was found that the incubation of sheddable nanoparticles with MDA-MB-231 cells at pH 6.8 lead to a significantly improved silencing efficiency of Plk1 expression. In conclusion, Wang *et al.* designed a drug delivery system meeting all requirements that are imposed by modern cancer therapy and that is therefore of high interest for further investigation.

5. PPEs for bone regeneration

The number of people with bone diseases worldwide is drastically increasing. The main causes of those diseases are disability and chronic pain: effective therapeutic systems are urgently needed. Various biomaterials have been developed to facilitate bone regeneration.[240] Even though some of them are efficient for some diseases,[241-243] it remains difficult to establish targeted drug delivery to bone tissue. Among these (bio)materials, both natural and some synthetic polymers are attractive, because of their biocompatibility and biodegradability.[209, 244-248] However, an inherent affinity to bone tissue is only found in a limited number of materials. These include the established antibacterial agent tetracycline[249, 250] and some heavy metals.[251] At present, bisphosphonates are the principal drugs used in the treatment of bone diseases in clinical osteology.[252-254] PPEs have shown excellent biodegradation and flexible plasticity with favorable physicochemical characteristics, and several reports for their use in the field of (bone) tissue engineering have been reported. Moreover, a potential inherent bone adhesion of PPEs was reported proving the attachment of PPE nanoparticles on a model bone tissue, rendering PPEs also interesting for bone regeneration applications.[255] As the result of the attractive osteoinductive potential of phosphate-containing polymers the latest research has been focused into PPE scaffolds for bone tissue regeneration. Furthermore, phosphorus-containing molecules are often used to bind calcium ions and improve bone formation, so PPEs can be used to bind calcium ions and catalyze the deposition of hydroxyapatite.[256] An interesting review has been published 2014 by Mikos and coworkers which gives insight into polymers with backbone phosphates and phosphonate groups and polymers with pendant phosphates and phosphonate groups, for not only bone regeneration, but also for regenerative medicine in overall.[257]

Wang *et al.* modified the surfaces of poly(l-lactic acid) (PLLA) films by spin coating with diblock copolymers consisting of poly(l-lactic acid) and poly (ethyl ethylene phosphate) (PLLA-*b*-PEEP) to study whether PPEs show an osteoinductive effect for potential bone tissue engineering applications.[258] The synthesis of PLLA-*b*-PEEP was achieved by ROP of l-lactide in bulk using

benzyl alcohol as initiator to form hydroxyl terminated PLLA$_{85}$-OH and was further chain-extended with EEP to block copolymers with various PEEP chain lengths.
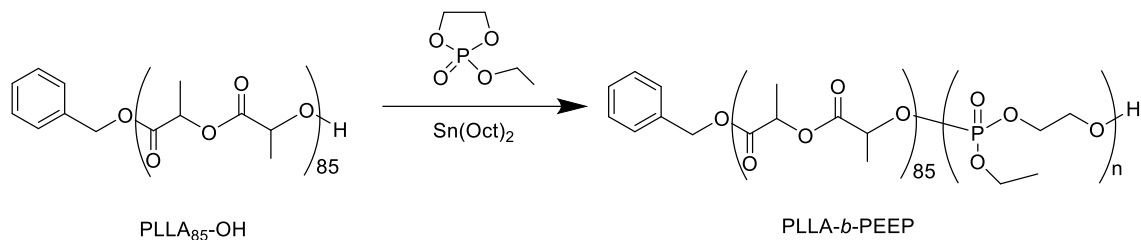
Scheme 45. Synthesis of PLLA-*b*-PEEP.

The enriched phosphorus content on the surface was demonstrated by x-ray photoelectron spectroscopy (XPS) and showed values ranging from 2.09 % to 4.39 % with increasing PEEP length from 58 to 224 units. To study the behavior of osteoblasts on the modified surfaces, the surfaces were seeded with osteoblasts for 4 h, while unattached cells were washed off. The number of osteoblasts attached on the modified surfaces was significantly higher than on unmodified PLLA surfaces and showed an increasing trend with increasing length of PEEP in the block copolymers. The proliferation of osteoblasts was evaluated using 3-(4,5-dimethylthiazol-2-yl)-2,5-diphenyltetrazolium bromide (MTT) assay after 7 days of culture and showed significantly enhanced osteoblast proliferation. Moreover, the PEEP-modified PLLA surfaces can promote cellular functions of osteoblasts including cellular alkaline phosphatase activity and mineral calcium deposits. Additionally, the gene expression of type I collagen and osteocalcin were upregulated on the modified surfaces which further indicates osteoinductivity of PEEP modification.[258] However, it has to be taken into account that besides the P-content also hydrophilicity of the surface was changed by the attachment of the hydrophilic PEEP-segments.

Elisseeff and co-workers synthesized a phosphate-containing and photocrosslinkable macromonomer, poly(ethylene glycol) di[ethyl phosphatidyl (ethylene glycol)methacrylate] (PhosPEG-dMA) which produces a biocompatible and biodegradable hydrogel by light-induced photopolymerization for application on cartilage and bone tissue engineering.[259] They reported the promotion of gene expression, cell-related and scaffold-related mineralization and scaffold degradation rates, that respond to tissue development.[260]
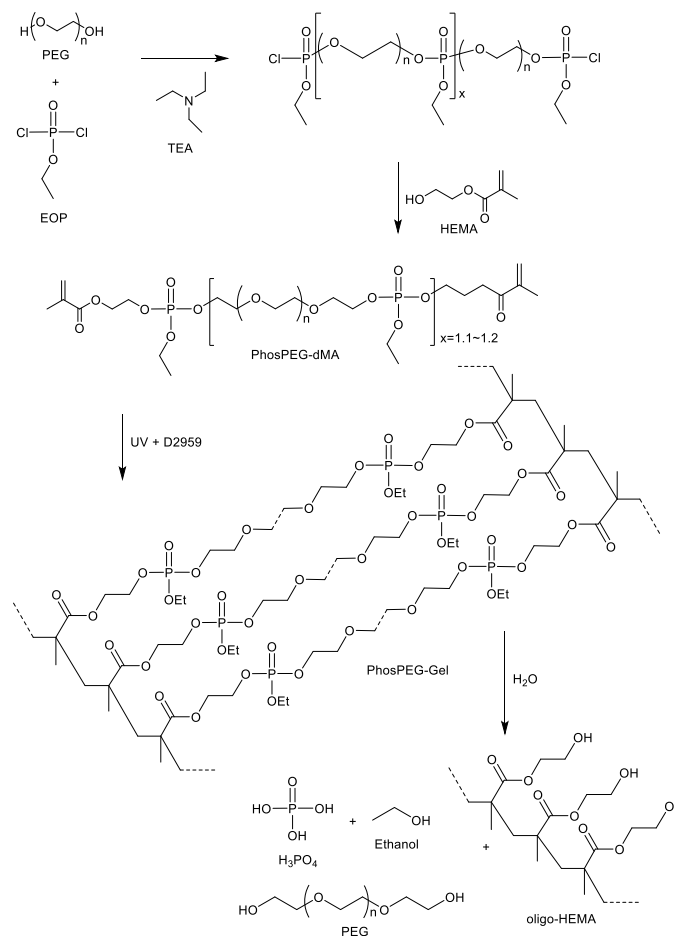
Scheme 46. Scheme of PhosPEG-dMA synthesis, PhosPEG Gel photogelation, and degradation (Reprinted from reference [259], Copyright 2003, with permission from Elsevier.)

The polymer was hydrolytically degradable and the degradation rate was accelerated by the bone-derived enzyme alkaline phosphatase (16.08 % and 22.88 % after 9 weeks). Degradation of the phosphoesters resulted in the collapse of the hydrogel into linear PEG, poly/oligo hydroxyethylmethacrylate (HEMA), ethanol and phosphoric acid. In comparison to the PEG-gels, mineralization of the PPE-containing hydrogels was increased due to the hydroxyapatite-like calcium phosphate deposits of phosphoric acid and the calcium ions. Additionally, the gene expression of bone-specific markers was promoted by a hydrogel containing an intermediate P-concentration. Moreover, an increased secretion of osteocalcin, osteonectin protein, and alkaline phosphatase was observed.[260]

Qiu and co-workers studied biodegradable bone substitutes using unsaturated PPEs based on bis(1,2-propylene glycol) and ethyl dichlorophosphate with *N*-vinyl pyrrolidone (NVP) as cross-linking agent to formulate a injectable paste which can be polymerized *in situ*.[247]
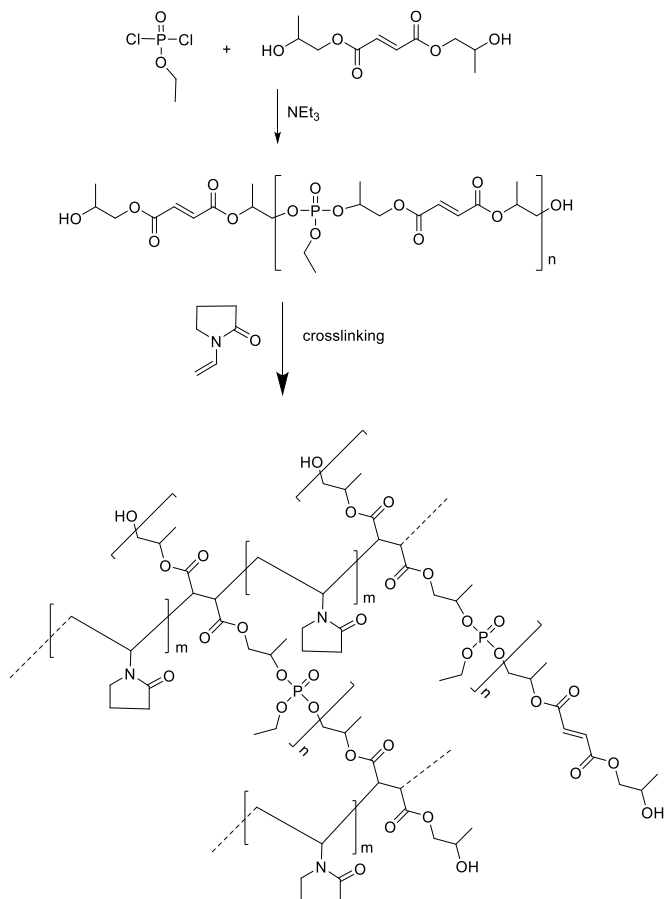
Scheme 47. Schematic illustration for crosslinking of UPPE with NVP.

A porous composite material with mechanical properties sufficient for the replacement of human trabecular bone (5 MPa compressive strength and 50 MPa compressive modulus) was achieved by the incorporation of β-tricalcium phosphate as an osteoconductive matrix and leachable porogen (sodium chloride).[261] Further investigations were conducted concerning the degradation, biocompatibility, and crosslinking.[262, 263]

Bone specific drug delivery is important for the treatment of osseous metastases and osteoporosis: Iwasaki and co-workers studied amphilic polyphosphoester ionomers (CH-PHE) which were immobilized in the membrane of 1,2-dio-leoyl-*sn*-glycero-3-phosphocholine (DOPC) vesicles.[264]
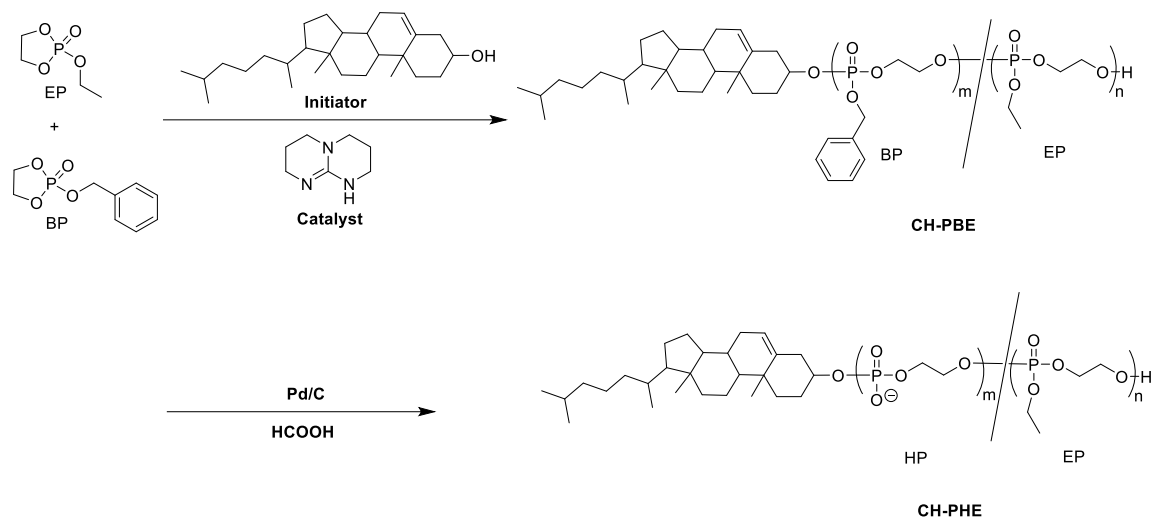
Scheme 48. Synthesis of cholesterol-initiated PPE- ionomers (CH-PHE) (adapted from reference [264]).

By changing the fraction of DOPC and CH-PHE, the stability of the vesicles was improved and the release rate of 5-carboxyfluorescein was controlled. The immobilization with CH-PHE leads further to a reduced enzymatic degradation of DOPC and an increased enzyme tolerance. In addition, the affinity of the PPE-modified vesicles to calcium deposits generated by mouse osteoblastic cells (MC3T3-E1) was significantly enhanced.[264-268] The effect of polymeric phosphates on osteoclasts and osteoblast function and/or survival has been described in several former studies.[265-268] However, in those studies poly(phosphate)s were used, whose structure and properties are quite different from PPEs. To study whether PPEs inhibit osteoclasts growth without affecting osteoblasts the group of Iwasaki synthesized poly(ethylene sodium phosphate) (PEP Na) and tested the effect on human osteoclast function. [269]
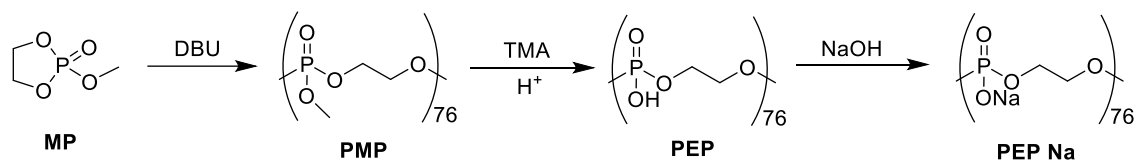
Scheme 49. Syntheses of PEP Na from MP (adapted from reference [269]).

PEP Na was added in different concentrations to osteoclast cultures on thin bone slices to determine the densities of adhered osteoclasts after 24 h. With a concentration higher than 1×10^{-4} mg·mL^{-1} the sizes of cells were reduced and number of adherent osteoclasts decreased significantly indicating that PEP Na and/or degradation products alter molecular metabolism of osteoclasts. Beside that, PEP Na showed excellent short-term biocompatibility with osteoblasts. The group of Iwasaki further used PEP Na to synthesize PEP Na coated PLGA microparticles and

mixed them with α-Ttricalcium phosphate (α-TCP) to stabilize an (o/w) emulsion which set spontaneously in a humidified atmosphere at ambient temperature.[270] The cements had an interconnected macroporous structure due to the degradation of the PLGA microparticles and showed extensive cellular invasion in case of the interconnected macroporous structure in the cement.

Alexandrino *et al*. prepared PPE nanoparticles (NP) by a miniemulsion solvent evaporation protocol,[255] that were previously synthesized via ADMET polycondensation of unsaturated phosphates with a variable number of methylene units between the phosphate and the polymerizable groups. The PPE-NPs were loaded with PTX up to 10 wt% with low size distribution and stable nanoparticle dispersions.
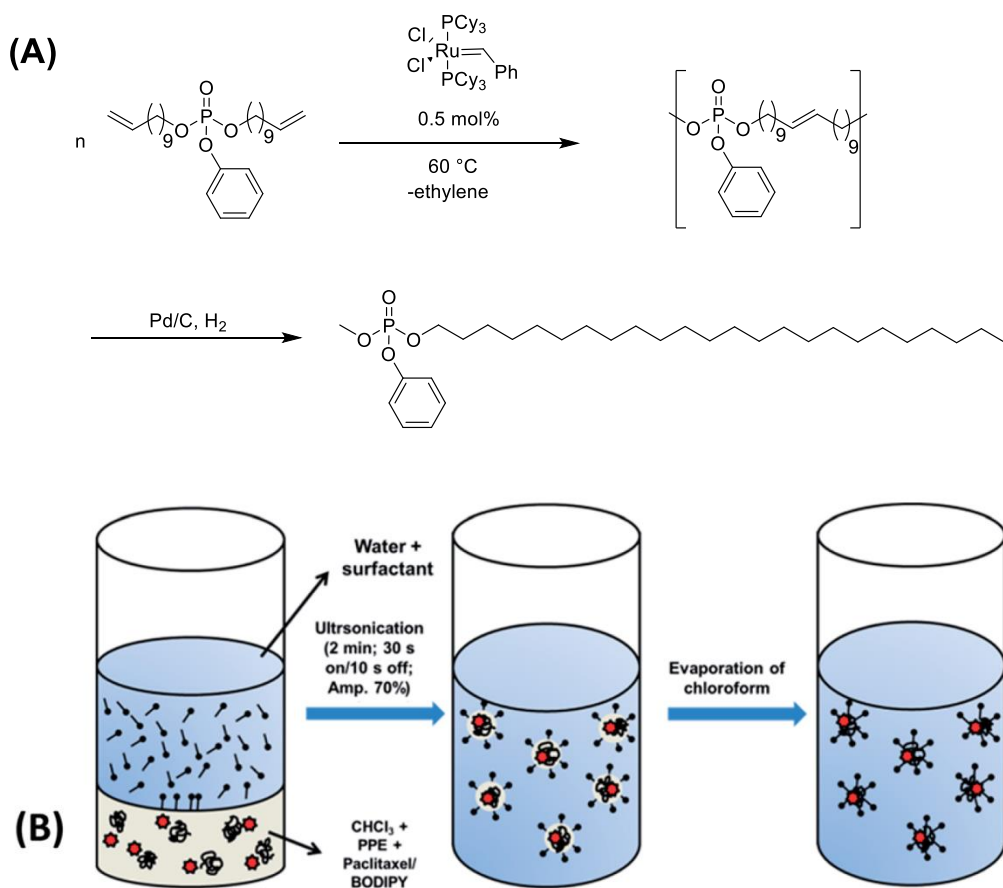
Figure 21. (A) Synthetic scheme of polyphosphoesters (PPE-C20). (B) Illustration of the miniemulsion/solvent-evaporation process for PTX loaded PPE nanoparticles. (taken from reference [255]; Published by The Royal Society of Chemistry.)

These NPs showed potential inherent bone adhesion ability with the efficient adhesion on calcium phosphate bone cement granules. *In vitro* studies against HeLa or osteosarcoma cells (Saos-2) proved that the polyphosphate nanoparticles are nontoxic against those cells up to 600 µg mL^{-1} or 300 µg mL^{-1} respectively, but loaded with paclitaxel a strong cytostatic effect was demonstrated.[255] Yaszemski and coworkers developed a oligo(polyethylene glycol) fumarate (OPF) hydrogel containing negatively charged phosphate groups and investigated this material as a substrate for bone cell attachment and differentiation *in vitro*.[271] Bis(2-(methacryloyloxy)ethyl)phosphate (BP) was used as phosphate-containing molecule and incorporated into the hydrogel and the thermal and mechanical properties were characterized. The compressive moduli of hydrogels were improved from 0.028 to 0.037 MPa with the addition of 310 µmol and decreased with higher concentration of BP. Rheology measurements showed reduced G' and G'' at low frequencies for OPF hydrogel with 5 % BP indicating they are more elastic than the pure hydrogel. Furthermore, it was reported, that the phosphate containing hydrogels improved the differentiation and attachment of human fetal osteoblasts. The hydrogels also support the attachment and differentiation of primary bone marrow stromal cells.

BP

OPF
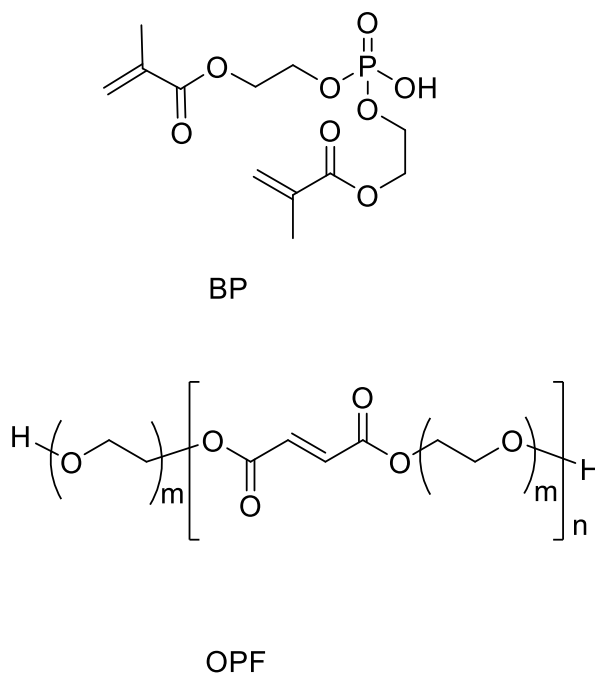
Figure 22. Structure of bis(2-(methacryloyloxy)ethyl) phosphate (BP) and oligo (poly(ethylene glycol) fumarate) (OPF) (adapted from [271], Copyright 2012, with permission from Elsevier.).

6. Conclusions

Main-chain polyphosphoesters –and amides have been reviewed comprehensively. With diverse derivatives of phosphoric acid within the polymer backbone, those materials are versatile candidates for various future applications. Going back to pioneering works in the 1960s, they are mainly used today in flame retardant additives, but their potential in biodegradable polymers with precise degradation profiles or adjustable adhesion has not been fully explored to date.

The PPE and PPA platform was extended in recent years as novel synthetic techniques were introduced, such as living polymerization techniques to water-soluble polyphosphates and –phosphonates with well-defined architectures. Also the potential of controlling materials properties by variation of the binding patterns around the central phosphorus was used in recent works to further adjust materials properties. This is especially important for biomedical applications, such as drug delivery or tissue engineering and further improved flame retardants.

Today's gold standards in biocompatible polymers have a low chemical functionality, such as poly(ethylene glycol) which is used in drug carriers or biodegradable polyesters, such as PLA and PLGA. In contrast, PPEs allow the synthesis of functional polymers using a set of diverse and modular synthetic protocols. Even though PPEs have not found considerable commercial interest in materials science and biomedicine to date, we believe that the current research will lead to considerable innovative materials, which can be commercialized.

The synthesis of PPEs relies on different techniques, depending on the monomer structure, phosphorus center, and the desired polymer properties. Recent advances in controlled polymerization routes, e.g., ROP by organocatalysis and Ruthenium-catalyzed metathesis polymerization, make PPEs readily available on large scale. Also, some first approaches were made employing enzyme catalysis, but still being less efficient than classical polymerization techniques. Several groups use polyfunctional PPEs and use postpolymerization functionalization to prepare biodegradable drug-loaded nanocarriers. As most phosphate monomers are prepared from high-energy products such as phosphoryl chloride, we believe that the next step in the PPE developments is the development of economic and ecological pathways to the monomers and to guarantee their efficient polymerization.

Due to the diverse chemistry of phosphoric acid, the future development of PPEs and PPAs will certainly lead to many fascinating materials.

7. References

1.	Westheimer, F., Why nature chose phosphates. *Science* **1987,** *235* (4793), 1173-1178.
2.	Morrissey, J. H.; Choi, S. H.; Smith, S. A., Polyphosphate: an ancient molecule that links platelets, coagulation and inflammation. *Blood* **2012**.
3.	Schröder, H.; Kurz, L.; Müller, W.; Lorenz, B., Polyphosphate in bone. *Biochemistry (Moscow)* **2000,** *65* (3), 296-303.
4.	Brown, M. R. W.; Kornberg, A., Inorganic polyphosphate in the origin and survival of species. *Proc. Natl. Acad. Sci. U. S. A.* **2004,** *101* (46), 16085-16087.
5.	Krauss, G., *Biochemistry of signal transduction and regulation*. John Wiley & Sons: 2006.
6.	Metcalf, W. W.; van der Donk, W. A., Biosynthesis of phosphonic and phosphinic acid natural products. *Annual review of biochemistry* **2009,** *78* (1), 65-94.
7.	L. L. Clark, E. D. I., R. Benner, Marine organic phosphorous cycling; novel insights from nuclear magnetic resonance. *Am. J. Sci* **1999,** *299* (1), 724-737.
8.	Steinbach, T.; Wurm, F. R., Polyphosphoesters: A New Platform for Degradable Polymers. *Angewandte Chemie International Edition* **2015,** *54* (21), 6098-6108.
9.	Baran, J.; Penczek, S., Hydrolysis of Polyesters of Phosphoric Acid. 1. Kinetics and the pH Profile. *Macromolecules* **1995,** *28* (15), 5167-5176.
10.	Klöpffer, W.; Grahl, B., *Ökobilanz (lca): Ein leitfaden für ausbildung und beruf*. John Wiley & Sons: 2012.
11.	Aksnes, G.; Bergesen, K., Rate studies of cyclic phosphinates, phosphonates and phosphates. *Acta chem. scand* **1966,** *20* (9).
12.	Thomas, C. M., Stereocontrolled ring-opening polymerization of cyclic esters: synthesis of new polyester microstructures. *Chemical Society Reviews* **2010,** *39* (1), 165-173.
13.	Iwasaki, Y.; Yamaguchi, E., Synthesis of Well-Defined Thermoresponsive Polyphosphoester Macroinitiators Using Organocatalysts. *Macromolecules* **2010,** *43* (6), 2664-2666.
14.	Zou, J.; Zhang, F.; Zhang, S.; Pollack, S. F.; Elsabahy, M.; Fan, J.; Wooley, K. L., Poly(ethylene oxide)-block-Polyphosphoester-graft-Paclitaxel Conjugates with Acid-Labile Linkages as a pH-Sensitive and Functional Nanoscopic Platform for Paclitaxel Delivery. *Advanced Healthcare Materials* **2014,** *3* (3), 441-448.
15.	Zhang, S.; Zou, J.; Zhang, F.; Elsabahy, M.; Felder, S. E.; Zhu, J.; Pochan, D. J.; Wooley, K. L., Rapid and Versatile Construction of Diverse and Functional Nanostructures Derived from a Polyphosphoester-Based Biomimetic Block Copolymer System. *Journal of the American Chemical Society* **2012,** *134* (44), 18467-18474.
16.	Wang, J.; Mao, H.-Q.; Leong, K. W., A novel biodegradable gene carrier based on polyphosphoester. *Journal of the American Chemical society* **2001,** *123* (38), 9480-9481.
17.	Penczek, S.; Pretula, J.; Kubisa, P.; Kaluzynski, K.; Szymanski, R., Reactions of H3PO4 forming polymers. Apparently simple reactions leading to sophisticated structures and applications. *Progress in Polymer Science* (0).
18.	Richards, M.; Dahiyat, B. I.; Arm, D. M.; Brown, P. R.; Leong, K. W., Evaluation of polyphosphates and polyphosphonates as degradable biomaterials. *J Biomed Mater Res* **1991,** *25* (9), 1151-1167.
19.	Troev, K. D., *Polyphosphoesters: chemistry and application*. Elsevier: 2012.
20.	Wang, Y.-C.; Yuan, Y.-Y.; Du, J.-Z.; Yang, X.-Z.; Wang, J., Recent Progress in Polyphosphoesters: From Controlled Synthesis to Biomedical Applications. *Macromolecular Bioscience* **2009,** *9* (12), 1154-1164.
21.	Zhao, Z.; Wang, J.; Mao, H.-Q.; Leong, K. W., Polyphosphoesters in drug and gene delivery. *Advanced Drug Delivery Reviews* **2003,** *55* (4), 483-499.

22.   Monge, S.; David, G., *Phosphorus-based Polymers: From Synthesis to Applications*. Royal Society of Chemistry: 2014; Vol. 11.

23.   Liu, Y.; Yan, N.; Li, F.; Chen, P., Synthesis and properties of a novel hyperbranched polyphosphoramidate using an A2 + CB2 approach. *Polymer International* **2013,** *62* (3), 390-396.

24.   Bauer, K. N.; Tee, H. T.; Lieberwirth, I.; Wurm, F. R., In-Chain Poly(phosphonate)s via Acyclic Diene Metathesis Polycondensation. *Macromolecules* **2016,** *49* (10), 3761-3768.

25.   Steinbach, T.; Ritz, S.; Wurm, F. R., Water-Soluble Poly(phosphonate)s via Living Ring-Opening Polymerization. *ACS Macro Letters* **2014,** *3* (3), 244-248.

26.   Huang, S.-W.; Wang, J.; Zhang, P.-C.; Mao, H.-Q.; Zhuo, R.-X.; Leong, K. W., Water-Soluble and Nonionic Polyphosphoester: Synthesis, Degradation, Biocompatibility and Enhancement of Gene Expression in Mouse Muscle. *Biomacromolecules* **2004,** *5* (2), 306-311.

27.   Liu, J.; Huang, W.; Zhou, Y.; Yan, D., Synthesis of hyperbranched polyphosphates by self-condensing ring-opening polymerization of HEEP without catalyst. *Macromolecules* **2009,** *42* (13), 4394-4399.

28.   Chen, S.; Zhang, D.; Cheng, X.; Li, T.; Zhang, A.; Li, J., Preparation and characterization of a novel hyperbranched polyphosphate ester. *Materials Chemistry and Physics* **2012,** *137* (1), 154-159.

29.   Liu, J.; Huang, W.; Pang, Y.; Zhu, X.; Zhou, Y.; Yan, D., Self-Assembled Micelles from an Amphiphilic Hyperbranched Copolymer with Polyphosphate Arms for Drug Delivery. *Langmuir* **2010,** *26* (13), 10585-10592.

30.   Liu, J.; Pang, Y.; Huang, W.; Zhai, X.; Zhu, X.; Zhou, Y.; Yan, D., Controlled Topological Structure of Copolyphosphates by Adjusting Pendant Groups of Cyclic Phosphate Monomers. *Macromolecules* **2010,** *43* (20), 8416-8423.

31.   Stukenbroeker, T. S.; Solis-Ibarra, D.; Waymouth, R. M., Synthesis and Topological Trapping of Cyclic Poly(alkylene phosphates). *Macromolecules* **2014,** *47* (23), 8224-8230.

32.   Chaubal, M. V.; Wang, B.; Su, G.; Zhao, Z., Compositional analysis of biodegradable polyphosphoester copolymers using nmr spectroscopic methods. *Journal of Applied Polymer Science* **2003,** *90* (14), 4021-4031.

33.   Wang, X.-L.; Zhuo, R.-X.; Liu, L.-J., Synthesis and characterization of novel biodegradable poly(carbonate-co-phosphate)s. *Polymer International* **2001,** *50* (11), 1175-1179.

34.   Wen, J.; Zhuo, R.-X., Preparation and characterization of poly(D,L-lactide-co-ethylene methyl phosphate). *Polymer International* **1998,** *47* (4), 503-509.

35.   Zhu, W.; Sun, S.; Xu, N.; Shen, Z., Synthesis, characterization, and properties of poly(ester-phosphoester)s by lanthanum triphenolate-catalyzed ring-opening copolymerization. *Journal of Polymer Science Part A: Polymer Chemistry* **2011,** *49* (23), 4987-4992.

36.   Hao, Y.; He, J.; Zhang, M.; Tao, Y.; Liu, J.; Ni, P., Synthesis and characterization of novel brush copolymers with biodegradable polyphosphoester side chains for gene delivery. *Journal of Polymer Science Part A: Polymer Chemistry* **2013,** *51* (10), 2150-2160.

37.   Yuan, Y.-Y.; Du, Q.; Wang, Y.-C.; Wang, J., One-Pot Syntheses of Amphiphilic Centipede-like Brush Copolymers via Combination of Ring-Opening Polymerization and "Click" Chemistry. *Macromolecules* **2010,** *43* (4), 1739-1746.

38.   Cheng, J.; Ding, J.-X.; Wang, Y.-C.; Wang, J., Synthesis and characterization of star-shaped block copolymer of poly-(ε-caprolactone) and poly (ethyl ethylene phosphate) as drug carrier. *Polymer* **2008,** *49* (22), 4784-4790.

39.   Wu, Q.; Wang, C.; Zhang, D.; Song, X.; Liu, D.; Wang, L.; Zhang, G., Synthesis and micellization of a new amphiphilic star-shaped poly(D,L-lactide)/polyphosphoester block copolymer. *Reactive and Functional Polymers* **2012,** *72* (6), 372-377.

40.   Yang, X.-Z.; Wang, Y.-C.; Tang, L.-Y.; Xia, H.; Wang, J., Synthesis and characterization of amphiphilic block copolymer of polyphosphoester and poly(L-lactic acid). *Journal of Polymer Science Part A: Polymer Chemistry* **2008,** *46* (19), 6425-6434.

41.   Tauber, K.; Marsico, F.; Wurm, F. R.; Schartel, B., Hyperbranched polyphosphoesters as flame retardants for technical and high performance polymers. *Polymer Chemistry* **2014,** *5* (24), 7042-7053.

42.   Gao, H.; Tan, Y.; Guan, Q.; Cai, T.; Liang, G.; Wu, Q., Synthesis, characterization and micellization of amphiphilic polyethylene-b-polyphosphoester block copolymers. *RSC Advances* **2015,** *5* (61), 49376-49384.

43.   Vanslambrouck, S.; Clément, B.; Riva, R.; Koole, L. H.; Molin, D.; Broze, G.; Lecomte, P.; Jérôme, C., Synthesis and tensioactive properties of PEO-b-polyphosphate copolymers. *RSC Advances* **2015,** *5* (35), 27330-27337.

44.   Wang, Y.-C.; Li, Y.; Yang, X.-Z.; Yuan, Y.-Y.; Yan, L.-F.; Wang, J., Tunable Thermosensitivity of Biodegradable Polymer Micelles of Poly(ε-caprolactone) and Polyphosphoester Block Copolymers. *Macromolecules* **2009,** *42* (8), 3026-3032.

45.   Wu, G.-P.; Darensbourg, D. J., Mechanistic Insights into Water-Mediated Tandem Catalysis of Metal-Coordination CO2/Epoxide Copolymerization and Organocatalytic Ring-Opening Polymerization: One-Pot, Two Steps, and Three Catalysis Cycles for Triblock Copolymers Synthesis. *Macromolecules* **2016,** *49* (3), 807-814.

46.   Al Ouahabi, A.; Charles, L.; Lutz, J.-F., Synthesis of Non-Natural Sequence-Encoded Polymers Using Phosphoramidite Chemistry. *J. Am. Chem. Soc.* **2015,** *137* (16), 5629-5635.

47.   James, A. A., Resinous compositions. Google Patents: 1936.

48.   Maiboroda, V. D.; Datskevich, L. A., Polycondensation of phenylphosphoryl dichloride with diethylene glycol. *Polymer Science U.S.S.R.* **1964,** *6* (10), 2113-2117.

49.   Ogawa, T.; Nushimatsu, T.; Minoura, Y., Condensation polymerization of P-phenylphosphonic dichloride with diamines. *Die Makromolekulare Chemie* **1968,** *114* (1), 275-283.

50.   Millich, F.; Carraher, C. E., Interfacial syntheses of polyphosphonate and polyphosphate esters. II. Dependence of yield and molecular weight on solvent volumes and concentrations of comers in basic polymerization of hydroquinone and phenylphosphonic dichloride. *Journal of Polymer Science Part A-1: Polymer Chemistry* **1970,** *8* (1), 163-169.

51.   Imai, Y.; Sato, N.; Ueda, M., Synthesis of aromatic polyphosphonate by phase-transfer catalyzed polycondensation with quaternary onium salts and crown ethers. *Die Makromolekulare Chemie, Rapid Communications* **1980,** *1* (7), 419-422.

52.   Millich, F.; Lambing, L. L., Interfacial sythesis of polyphosphonate and polyphosphate ester. VII. Temperature effects and reaction loci in polycondensations of hydroquinone with phenylphosphonic dichloride and 4-methythiophenyl phosphorodichloridate. *Journal of Polymer Science: Polymer Chemistry Edition* **1980,** *18* (7), 2155-2162.

53.   Schmidt, M.; Freitag, D.; Bottenbruch, L.; Reinking, K., Aromatische polyphosphonate: Thermoplastische polymere von extremer brandwidrigkeit. *Die Angewandte Makromolekulare Chemie* **1985,** *132* (1), 1-18.

54.   Richards, M.; Dahiyat, B. I.; Arm, D. M.; Lin, S.; Leong, K. W., Interfacial polycondensation and characterization of polyphosphates and polyphosphonates. *Journal of Polymer Science Part A: Polymer Chemistry* **1991,** *29* (8), 1157-1165.

55.   Liaw, D.-J.; Shen, W.-C., Synthesis of aromatic polyphosphonate: low temperature solution polycondensation of 4,4′-sulphonyldiphenol with phenoxy dichlorophosphate. *Polymer* **1993,** *34* (6), 1336-1338.

56.   Chen, X.; Jiao, C.; Li, S.; Sun, J., Flame retardant epoxy resins from bisphenol-A epoxy cured with hyperbranched polyphosphate ester. *J Polym Res* **2011,** *18* (6), 2229-2237.

57.   Alexandrino, E. M.; Wagner, M.; Landfester, K.; Wurm, F. R., Polyphosphoester Colloids by Interfacial Polycondensation in Miniemulsion. *Macromolecular Chemistry and Physics* **2016,** *217* (17), 1941-1947.

58.   Pretula, J.; Kaluzynski, K.; Szymanski, R.; Penczek, S., Preparation of Poly(alkylene H-phosphonate)s and Their Derivatives by Polycondensation of Diphenyl H-Phosphonate with Diols and Subsequent Transformations. *Macromolecules* **1997,** *30* (26), 8172-8176.

59.   Penczek, S.; Pretula, J., High-molecular-weight poly(alkylene phosphates) and preparation of amphiphilic polymers thereof. *Macromolecules* **1993,** *26* (9), 2228-2233.

60.   Troev, K.; Naruoka, A.; Terada, H.; Kikuchi, A.; Makino, K., New Efficient Method of Oxidation of Poly(alkylene H-phosphonate)s: A Promising Route to Novel co-Polyphosphoesters. *Macromolecules* **2012,** *45* (14), 5698-5703.

61.   Pretula, J.; Kaluzynski, K.; Penczek, S., Synthesis of poly(alkylene phosphates) with nitrogen-containing bases in the side chains. 1. Nitrogen- and carbon-substituted imidazoles. *Macromolecules* **1986,** *19* (7), 1797-1799.

62.   Kaluzynski, K.; Libisowski, J.; Penczek, S., A New Class of Synthetic Polyelectrolytes. Acidic Polyesters of Phosphoric Acid (Poly(hydroxyalkylene phosphates)). *Macromolecules* **1976,** *9* (2), 365-367.

63.   Biela, T.; Kubisa, P., Oligomerization of oxiranes in the presence of phosphoric acid. Kinetics of model reaction. *Die Makromolekulare Chemie* **1991,** *192* (3), 473-489.

64.   Tzevi, R.; Todorova, G.; Kossev, K.; Troev, K.; Georgiev, E. M.; Roundhill, D. M., Immobilization of bioactive substances on poly (alkylene phosphate) s, 1. Immobilization of 2-phenylethylamine. *Die Makromolekulare Chemie* **1993,** *194* (12), 3261-3269.

65.   Troev, K.; Tsatcheva, I.; Koseva, N.; Georgieva, R.; Gitsov, I., Immobilization of aminothiols on poly (oxyethylene H-phosphonate) s and poly (oxyethylene phosphate) s—An approach to polymeric protective agents for radiotherapy of cancer. *Journal of Polymer Science Part A: Polymer Chemistry* **2007,** *45* (7), 1349-1363.

66.   Troev, K. D.; Mitova, V. A.; Ivanov, I. G., On the design of polymeric 5′-O-ester prodrugs of 3′-azido-2′,3′-dideoxythymidine (AZT). *Tetrahedron Letters* **2010,** *51* (47), 6123-6125.

67.   Le Corre, S. S.; Berchel, M.; Couthon-Gourvès, H.; Haelters, J.-P.; Jaffrès, P.-A., Atherton–Todd reaction: mechanism, scope and applications. *Beilstein Journal of Organic Chemistry* **2014,** *10*, 1166-1196.

68.   Bogomilova, A.; Höhn, M.; Günther, M.; Herrmann, A.; Troev, K.; Wagner, E.; Schreiner, L., A polyphosphoester conjugate of melphalan as antitumoral agent. *European Journal of Pharmaceutical Sciences* **2013,** *50* (3–4), 410-419.

69.   Vogt, W.; Balasubramanian, S., Über die polykondensation von diäthylphosphit mit aliphastischen diolen. *Die Makromolekulare Chemie* **1973,** *163* (1), 111-134.

70.   Zwierzak, A., Cyclic organophosphorus compounds. I. Synthesis and infrared spectral studies of cyclic hydrogen phosphites and thiophosphites. *Canadian Journal of Chemistry* **1967,** *45* (21), 2501-2512.

71.   Oswald, A. A., SYNTHESIS OF CYCLIC PHOSPHOROUS ACID ESTERS BY TRANSESTERIFICATION. *Canadian Journal of Chemistry* **1959,** *37* (9), 1498-1504.

72.   Pretula, J.; Kaluzynski, K.; Szymanski, R.; Penczek, S., Transesterification of oligomeric dialkyl phosphonates, leading to the high-molecular-weight poly-H-phosphonates. *Journal of Polymer Science Part A: Polymer Chemistry* **1999,** *37* (9), 1365-1381.

73.   Pretula, J.; Penczek, S., Poly (ethylene glycol) ionomers with phosphate diester linkages. *Die Makromolekulare Chemie, Rapid Communications* **1988,** *9* (11), 731-737.

74.   Pretula, J.; Penczek, S., High-molecular-weight poly(alkylene phosphonate)s by condensation of dialkylphosphonates with diols. *Die Makromolekulare Chemie* **1990,** *191* (3), 671-680.

75.   Stawinski, J., In Handbook of Organophosphorus Chemistry; Engel, R., Ed. Marcel Dekker: Hoboken, New Jersey: 1992.

76.   Pretula, J.; Kaluzynski, K.; Wisniewski, B.; Szymanski, R.; Loontjens, T.; Penczek, S., H3PO4 in a direct synthesis of oligo–poly(ethylene phosphate)from ethylene glycol. *Journal of Polymer Science Part A: Polymer Chemistry* **2006,** *44* (7), 2358-2362.

77.   Pretula, J.; Kaluzynski, K.; Wisniewski, B.; Szymanski, R.; Loontjens, T.; Penczek, S., Formation of poly(ethylene phosphates) in polycondensation of H3PO4 with ethylene glycol. Kinetic and mechanistic study. *Journal of Polymer Science Part A: Polymer Chemistry* **2008,** *46* (3), 830-843.

78.   Pretula, J.; Kaluzynski, K.; Szymanski, R.; Penczek, S., Polycondensation of H3PO4 with glycerol: From branched structures to hydrolytically reversible gels. *Journal of Polymer Science Part A: Polymer Chemistry* **2014,** *52* (24), 3533-3542.

79.   Minegishi, S.; Komatsu, S.; Kameyama, A.; Nishikubo, T., Novel synthesis of polyphosphonates by the polyaddition of bis(epoxide) with diaryl phosphonates. *Journal of Polymer Science Part A: Polymer Chemistry* **1999,** *37* (7), 959-965.

80.   Minegishi, S.; Tsuchida, S.; Sasaki, M.; Kameyama, A.; Kudo, H.; Nishikubo, T., Synthesis of polyphosphonates containing pendant chloromethyl groups by the polyaddition of bis(oxetane)s with phosphonic dichlorides. *Journal of Polymer Science Part A: Polymer Chemistry* **2002,** *40* (21), 3835-3846.

81.   Nishikubo, T.; Kameyama, A.; Minegishi, S., Novel Syntheses of Poly(phosphonate)s and Poly(phosphate)s by Addition Reactions of Bisepoxides with Phosphonic Dichlorides and Dichlorophosphates. *Macromolecules* **1995,** *28* (14), 4810-4814.

82.   Biedron, T.; Kaluzynski, K.; Pretula, J.; Kubisa, P.; Penczek, S.; Loontjens, T., Synthesis of high molar mass poly (alkylene phosphate) s by polyaddition of diepoxides to difunctional phosphoric acids: Unusual elimination of the side reactions. *Journal of Polymer Science Part A: Polymer Chemistry* **2001,** *39* (17), 3024-3033.

83.   Nyk, A.; Klosinski, P.; Penczek, S., Water-swelling, hydrolyzable gels through polyaddition of H3PO4 to diepoxides. *Die Makromolekulare Chemie* **1991,** *192* (4), 833-846.

84.   Penczek, S.; Kaluzynski, K.; Pretula, J., Addition of H3PO4 to diglycidyl ethers of bisphenol A: Kinetics and product structure. *Journal of Applied Polymer Science* **2007,** *105* (1), 246-254.

85.   Kazanskii, K.; Kuznetsova, V.; Pretula, J.; Penczek, S., Ionizable hydrogels of new type based on poly(ethylene glycol) phosphates. *Polymer Gels and Networks* **1996,** *4* (4), 335-349.

86.   Libiszowski, J.; Kałużynski, K.; Penczek, S., Polymerization of cyclic esters of phosphoric acid. VI. Poly(alkyl ethylene phosphates). Polymerization of 2-alkoxy-2-oxo-1,3,2-dioxaphospholans and structure of polymers. *Journal of Polymer Science: Polymer Chemistry Edition* **1978,** *16* (6), 1275-1283.

87.   Zhai, X.; Huang, W.; Liu, J.; Pang, Y.; Zhu, X.; Zhou, Y.; Yan, D., Micelles from Amphiphilic Block Copolyphosphates for Drug Delivery. *Macromolecular Bioscience* **2011,** *11* (11), 1603-1610.

88.   Wang, Y.-C.; Yuan, Y.-Y.; Wang, F.; Wang, J., Syntheses and characterization of block copolymers of poly(aliphatic ester) with clickable polyphosphoester. *Journal of Polymer Science Part A: Polymer Chemistry* **2011,** *49* (2), 487-494.

89.   Klosinski, P.; Penczek, S., Synthesis of models of teichoic acids by ring-opening polymerization. *Macromolecules* **1983,** *16* (2), 316-320.

90.   Pretula, J.; Kałużyński, K.; Penczek, S., Living reversible anonic polymerization of N,N-diethylamine-1,3,2-dioxaphosphorinan. *Journal of Polymer Science: Polymer Chemistry Edition* **1984,** *22* (6), 1251-1258.

91.   Biela, T.; Kłosiński, P.; Penczek, S., Microstructure of poly(alkylene phosphates) related to biopolymers (teichoic acids). *Journal of Polymer Science Part A: Polymer Chemistry* **1989,** *27* (3), 763-774.

92.   Kałużynski, K.; Libiszowski, J.; Penczek, S., Poly(2-hydro-2-oxo-1,3,2-dioxaphosphorinane). Preparation and NMR spectra. *Die Makromolekulare Chemie* **1977,** *178* (10), 2943-2947.

93.   Yuan, Y.-Y.; Du, J.-Z.; Song, W.-J.; Wang, F.; Yang, X.-Z.; Xiong, M.-H.; Wang, J., Biocompatible and functionalizable polyphosphate nanogel with a branched structure. *Journal of Materials Chemistry* **2012,** *22* (18), 9322-9329.

94.   Zhang, F.; Zhang, S.; Pollack, S. F.; Li, R.; Gonzalez, A. M.; Fan, J.; Zou, J.; Leininger, S. E.; Pavía-Sanders, A.; Johnson, R.; Nelson, L. D.; Raymond, J. E.; Elsabahy, M.; Hughes, D. M. P.; Lenox, M. W.; Gustafson, T. P.; Wooley, K. L., Improving Paclitaxel Delivery: In Vitro and In Vivo Characterization of PEGylated Polyphosphoester-Based Nanocarriers. *Journal of the American Chemical Society* **2015,** *137* (5), 2056-2066.

95.   Xiong, M.-H.; Wu, J.; Wang, Y.-C.; Li, L.-S.; Liu, X.-B.; Zhang, G.-Z.; Yan, L.-F.; Wang, J., Synthesis of PEG-armed and polyphosphoester core-cross-linked nanogel by one-step ring-opening polymerization. *Macromolecules* **2009,** *42* (4), 893-896.

96.   Kobayashi, S.; Hashimoto, T.; Saegusa, T., Alcoholysis Polymerization of Cyclic Acyloxyphosphorane to Polyphosphate Triesters: Polyphosphorylation of Alcohol. *Macromolecules* **1980,** *13* (6), 1650-1654.

97.   Kobayashi, S.; Suzuki, M.; Saegusa, T., Cationic ring-opening polymerization of 2-phenyl-1,2-oxaphospholane (deoxophostone). *Polymer Bulletin* **1981,** *4* (6), 315-321.

98.   Kobayashi, S.; Tokunoh, M.; Saegusa, T., Cationic ring-opening polymerization of 2-phenyl-1,3,2-dioxaphosphepane, a seven-membered cyclic phosphonite. *Macromolecules* **1986,** *19* (2), 466-469.

99.   Penczek, S.; Libiszowski, J., Polymerization of 2-methoxy-2-oxo-1,3,2-dioxaphospholane. Kinetics and polymer microstructure. *Die Makromolekulare Chemie* **1988,** *189* (8), 1765-1785.

100.   Sosnowski, S.; Libiszowski, J.; Słomkowski, S.; Penczek, S., Thermodynamics of the polymerization of ethylene methyl phosphate. *Die Makromolekulare Chemie, Rapid Communications* **1984,** *5* (5), 239-244.

101.   Maffei, M.; Buono, G., A two step synthesis of 2-oxo-2-vinyl 1,3,2-dioxaphospholanes and -dioxaphosphorinanes. *Tetrahedron* **2003,** *59* (44), 8821-8825.

102.   Kałużyński, K.; Penczek, S., Anionic polymerization of 2-Oxo-1,3,2λ5-dioxaphosphorinane. Thermodynamics. *Die Makromolekulare Chemie* **1979,** *180* (10), 2289-2293.

103.   Lapienis, G.; Penczek, S., Cationic Polymerization of 2-Alkoxy-2-oxo-1,3,2-dioxaphosphorinanes (1,3-Propylene Alkyl Phosphates). *Macromolecules* **1977,** *10* (6), 1301-1306.

104.   Łapienis, G.; Penczek, S., Kinetics and thermodynamics of anionic polymerization of 2-methoxy-2-oxo-1,3,2-dioxaphosphorinane. *Journal of Polymer Science: Polymer Chemistry Edition* **1977,** *15* (2), 371-382.

105.   Majoral, J.; Mathis, F.; Munoz, A.; Vives, J.; Navech, J., STUDIES ON CYCLIC ESTERS. 3. POLYMERISATION BY RING OPENING. *BULLETIN DE LA SOCIETE CHIMIQUE DE FRANCE* **1968,** (11), 4455-&.

106.   Dudev, T.; Lim, C., Ring Strain Energies from ab Initio Calculations. *Journal of the American Chemical Society* **1998,** *120* (18), 4450-4458.

107.   Szymanski, R.; Penczek, S., Complexation of sodium cations by polymeric esters of phosphoric acid. *Die Makromolekulare Chemie* **1993,** *194* (6), 1645-1651.

108.   Hu, B.; Zhuo, R.; Fan, C., Synthesis of copolymer of 1,3-dioxan-2-one and 2-hydro-2-oxo-1,3,2-dioxaphosphorinane. *Polymers for Advanced Technologies* **1998,** *9* (2), 145-149.

109.   Lapienis, G.; Penczek, S., Kinetics and Thermodynamics of the Polymerization of the Cyclic Phosphate Esters. II. Cationic Polymerization of 2-Methoxy-2-oxo-1,3,2-dioxaphosphorinane (1,3-Propylene Methyl Phosphate). *Macromolecules* **1974,** *7* (2), 166-174.

110.   Eliel, E. L.; Chandrasekaran, S.; Carpenter, L. E.; Verkade, J. G., Oxygen-17 NMR spectra of cyclic phosphites, phosphates, and thiophosphates. *Journal of the American Chemical Society* **1986,** *108* (21), 6651-6661.

111.   MUNOZ, A.; NAVECH, J.; VIVES, J.; MAJORAL, J., SOME CYCLIC PHOSPHORIC ESTERS. 2. ACTION OF GASEOUS HYDROCHLORIC ACID. *BULLETIN DE LA SOCIETE CHIMIQUE DE FRANCE* **1967,** (9), 3343-&.

112.   Vogt, W.; Pflüger, R., Polymere ester von säuren des Phosphors, 3. Polymerisation des 2-Äthoxy-2-oxo-1,3,2-dioxaphospholans. *Die Makromolekulare Chemie* **1975,** *1* (S19751), 97-110.

113.   Dubois, P.; Jacobs, C.; Jerome, R.; Teyssie, P., Macromolecular engineering of polylactones and polylactides. 4. Mechanism and kinetics of lactide homopolymerization by aluminum isopropoxide. *Macromolecules* **1991,** *24* (9), 2266-2270.

114.   Ouhadi, T.; Stevens, C.; Teyssié, P., Mechanism of ε-Caprolactone polymerization by Aluminum Alkoxides. *Die Makromolekulare Chemie* **1975,** *1* (S19751), 191-201.

115.   Wang, J.; Zhang, P.-C.; Lu, H.-F.; Ma, N.; Wang, S.; Mao, H.-Q.; Leong, K. W., New polyphosphoramidate with a spermidine side chain as a gene carrier. *Journal of Controlled Release* **2002,** *83* (1), 157-168.

116.   Biela, T.; Penczek, S.; Slomkowski, S.; Vogl, O., Racemic and optically active poly(4-methyl-2-oxo-2-hydro-1,3,2-dioxaphospholane). Synthesis and oxidation to the polyacids. *Die Makromolekulare Chemie, Rapid Communications* **1982,** *3* (10), 667-671.

117.   Li, F.; Feng, J.; Zhuo, R., Synthesis and characterization of novel biodegradable poly(p-dioxanone-co-ethyl ethylene phosphate)s. *Journal of Applied Polymer Science* **2006,** *102* (6), 5507-5511.

118.   Chew, S. Y.; Wen, J.; Yim, E. K. F.; Leong, K. W., Sustained Release of Proteins from Electrospun Biodegradable Fibers. *Biomacromolecules* **2005,** *6* (4), 2017-2024.

119.   Wen, J.; Kim, G. J. A.; Leong, K. W., Poly(d,llactide–co-ethyl ethylene phosphate)s as new drug carriers. *Journal of Controlled Release* **2003,** *92* (1–2), 39-48.

120.   Chen, D.-P.; Wang, J., Synthesis and Characterization of Block Copolymer of Polyphosphoester and Poly (ε-caprolactone). *Macromolecules* **2006,** *39* (2), 473-475.

121.   Du, J.-Z.; Chen, D.-P.; Wang, Y.-C.; Xiao, C.-S.; Lu, Y.-J.; Wang, J.; Zhang, G.-Z., Synthesis and Micellization of Amphiphilic Brush−Coil Block Copolymer Based on Poly(ε-caprolactone) and PEGylated Polyphosphoester. *Biomacromolecules* **2006,** *7* (6), 1898-1903.

122.   Iwasaki, Y.; Wachiralarpphaithoon, C.; Akiyoshi, K., Novel thermoresponsive polymers having biodegradable phosphoester backbones. *Macromolecules* **2007,** *40* (23), 8136-8138.

123.   Ozdil, D.; Aydin, H. M., Polymers for medical and tissue engineering applications. *Journal of Chemical Technology & Biotechnology* **2014,** *89* (12), 1793-1810.

124.   Wang, Y.-C.; Shen, S.-Y.; Wu, Q.-P.; Chen, D.-P.; Wang, J.; Steinhoff, G.; Ma, N., Block Copolymerization of ε-Caprolactone and 2-Methoxyethyl Ethylene Phosphate Initiated by Aluminum Isopropoxide: Synthesis, Characterization, and Kinetics. *Macromolecules* **2006,** *39* (26), 8992-8998.

125.   Xiao, C.-S.; Wang, Y.-C.; Du, J.-Z.; Chen, X.-S.; Wang, J., Kinetics and Mechanism of 2-Ethoxy-2-oxo-1,3,2-dioxaphospholane Polymerization Initiated by Stannous Octoate. *Macromolecules* **2006,** *39* (20), 6825-6831.

126.   Garlotta, D., A Literature Review of Poly(Lactic Acid). *Journal of Polymers and the Environment* **2001,** *9* (2), 63-84.

127. Dove, A. P.; Gibson, V. C.; Marshall, E. L.; White, A. J. P.; Williams, D. J., A well defined tin(ii) initiator for the living polymerisation of lactide. *Chemical Communications* **2001,** (3), 283-284.

128. Kowalski, A.; Duda, A.; Penczek, S., Mechanism of Cyclic Ester Polymerization Initiated with Tin(II) Octoate. 2.† Macromolecules Fitted with Tin(II) Alkoxide Species Observed Directly in MALDI−TOF Spectra. *Macromolecules* **2000,** *33* (3), 689-695.

129. Albertsson, A.-C.; Varma, I. K., Recent Developments in Ring Opening Polymerization of Lactones for Biomedical Applications. *Biomacromolecules* **2003,** *4* (6), 1466-1486.

130. Kamber, N. E.; Jeong, W.; Waymouth, R. M.; Pratt, R. C.; Lohmeijer, B. G. G.; Hedrick, J. L., Organocatalytic Ring-Opening Polymerization. *Chemical Reviews* **2007,** *107* (12), 5813-5840.

131. Clément, B.; Grignard, B.; Koole, L.; Jérôme, C.; Lecomte, P., Metal-Free Strategies for the Synthesis of Functional and Well-Defined Polyphosphoesters. *Macromolecules* **2012,** *45* (11), 4476-4486.

132. Pratt, R. C.; Lohmeijer, B. G. G.; Long, D. A.; Waymouth, R. M.; Hedrick, J. L., Triazabicyclodecene: A Simple Bifunctional Organocatalyst for Acyl Transfer and Ring-Opening Polymerization of Cyclic Esters. *Journal of the American Chemical Society* **2006,** *128* (14), 4556-4557.

133. Nederberg, F.; Lohmeijer, B. G. G.; Leibfarth, F.; Pratt, R. C.; Choi, J.; Dove, A. P.; Waymouth, R. M.; Hedrick, J. L., Organocatalytic Ring Opening Polymerization of Trimethylene Carbonate. *Biomacromolecules* **2007,** *8* (1), 153-160.

134. MacMillan, D. W. C., The advent and development of organocatalysis. *Nature* **2008,** *455* (7211), 304-308.

135. Wen, J.; Zhuo, R.-X., Enzyme-catalyzed ring-opening polymerization of ethylene isopropyl phosphate. *Macromolecular Rapid Communications* **1998,** *19* (12), 641-642.

136. He, F.; Zhuo, R. X.; Liu, L. J.; Jin, D. B.; Feng, J.; Wang, X. L., Immobilized lipase on porous silica beads: preparation and application for enzymatic ring-opening polymerization of cyclic phosphate. *Reactive and Functional Polymers* **2001,** *47* (2), 153-158.

137. Wolf, T.; Steinbach, T.; Wurm, F. R., A Library of Well-Defined and Water-Soluble Poly(alkyl phosphonate)s with Adjustable Hydrolysis. *Macromolecules* **2015**.

138. Iwasaki, Y.; Akiyoshi, K., Synthesis and Characterization of Amphiphilic Polyphosphates with Hydrophilic Graft Chains and Cholesteryl Groups as Nanocarriers. *Biomacromolecules* **2006,** *7* (5), 1433-1438.

139. Zhang, S.; Wang, H.; Shen, Y.; Zhang, F.; Seetho, K.; Zou, J.; Taylor, J.-S. A.; Dove, A. P.; Wooley, K. L., A Simple and Efficient Synthesis of an Acid-Labile Polyphosphoramidate by Organobase-Catalyzed Ring-Opening Polymerization and Transformation to Polyphosphoester Ionomers by Acid Treatment. *Macromolecules* **2013,** *46* (13), 5141-5149.

140. Song, W.-J.; Du, J.-Z.; Liu, N.-J.; Dou, S.; Cheng, J.; Wang, J., Functionalized Diblock Copolymer of Poly(ε-caprolactone) and Polyphosphoester Bearing Hydroxyl Pendant Groups: Synthesis, Characterization, and Self-Assembly. *Macromolecules* **2008,** *41* (19), 6935-6941.

141. Lim, Y. H.; Heo, G. S.; Rezenom, Y. H.; Pollack, S.; Raymond, J. E.; Elsabahy, M.; Wooley, K. L., Development of a Vinyl Ether-Functionalized Polyphosphoester as a Template for Multiple Postpolymerization Conjugation Chemistries and Study of Core Degradable Polymeric Nanoparticles. *Macromolecules* **2014,** *47* (14), 4634-4644.

142. Tang, R.; Ji, W.; Panus, D.; Palumbo, R. N.; Wang, C., Block copolymer micelles with acid-labile ortho ester side-chains: Synthesis, characterization, and enhanced drug delivery to human glioma cells. *Journal of Controlled Release* **2011,** *151* (1), 18-27.

143. Lee, E. S.; Shin, H. J.; Na, K.; Bae, Y. H., Poly(l-histidine)–PEG block copolymer micelles and pH-induced destabilization. *Journal of Controlled Release* **2003,** *90* (3), 363-374.

144. Jain, R.; Standley, S. M.; Frechet, J. M., Synthesis and degradation of pH-sensitive linear poly (amidoamine) s. *Macromolecules* **2007,** *40* (3), 452-457.
145. Muller, L. K.; Steinbach, T.; Wurm, F. R., Multifunctional polyphosphoesters with two orthogonal protective groups. *RSC Advances* **2015,** *5* (53), 42881-42888.
146. Oussadi, K.; Montembault, V.; Belbachir, M.; Fontaine, L., Ring-opening bulk polymerization of five- and six-membered cyclic phosphonates using maghnite, a nontoxic proton exchanged montmorillonite clay. *Journal of Applied Polymer Science* **2011,** *122* (2), 891-897.
147. Wurm, F.; Steinbach, T.; Klok, H.-A., One-pot squaric acid diester mediated aqueous protein conjugation. *Chem. Commun.* **2013,** *49* (71), 7815-7817.
148. Iwasaki, Y.; Akiyoshi, K., Design of Biodegradable Amphiphilic Polymers: Well-Defined Amphiphilic Polyphosphates with Hydrophilic Graft Chains via ATRP. *Macromolecules* **2004,** *37* (20), 7637-7642.
149. Wang, Y.-C.; Li, Y.; Sun, T.-M.; Xiong, M.-H.; Wu, J.; Yang, Y.-Y.; Wang, J., Core–Shell–Corona Micelle Stabilized by Reversible Cross-Linkage for Intracellular Drug Delivery. *Macromolecular Rapid Communications* **2010,** *31* (13), 1201-1206.
150. Sun, C.-Y.; Ma, Y.-C.; Cao, Z.-Y.; Li, D.-D.; Fan, F.; Wang, J.-X.; Tao, W.; Yang, X.-Z., Effect of Hydrophobicity of Core on the Anticancer Efficiency of Micelles as Drug Delivery Carriers. *ACS Applied Materials & Interfaces* **2014,** *6* (24), 22709-22718.
151. Sun, T.-M.; Du, J.-Z.; Yan, L.-F.; Mao, H.-Q.; Wang, J., Self-assembled biodegradable micellar nanoparticles of amphiphilic and cationic block copolymer for siRNA delivery. *Biomaterials* **2008,** *29* (32), 4348-4355.
152. Zhang, S.; Li, A.; Zou, J.; Lin, L. Y.; Wooley, K. L., Facile Synthesis of Clickable, Water-Soluble, and Degradable Polyphosphoesters. *ACS Macro Letters* **2012,** *1* (2), 328-333.
153. Iwasaki, Y.; Kawakita, T.; Yusa, S.-i., Thermoresponsive Polyphosphoesters Bearing Enzyme-cleavable Side Chains. *Chemistry Letters* **2009,** *38* (11), 1054-1055.
154. Shao, H.; Zhang, M.; He, J.; Ni, P., Synthesis and characterization of amphiphilic poly(ε-caprolactone)-b-polyphosphoester diblock copolymers bearing multifunctional pendant groups. *Polymer* **2012,** *53* (14), 2854-2863.
155. Ishihara, K.; Ueda, T.; Nakabayashi, N., Preparation of Phospholipid Polylners and Their Properties as Polymer Hydrogel Membranes. *Polym J* **1990,** *22* (5), 355-360.
156. Baeten, E.; Vanslambrouck, S.; Jérôme, C.; Lecomte, P.; Junkers, T., Anionic flow polymerizations toward functional polyphosphoesters in microreactors: Polymerization and UV-modification. *European Polymer Journal* **2016,** *80*, 208-218.
157. Clément, B.; Molin, D. G.; Jérôme, C.; Lecomte, P., Synthesis of polyphosphodiesters by ring-opening polymerization of cyclic phosphates bearing allyl phosphoester protecting groups. *Journal of Polymer Science Part A: Polymer Chemistry* **2015,** *53* (22), 2642-2648.
158. Xiong, M.-H.; Li, Y.-J.; Bao, Y.; Yang, X.-Z.; Hu, B.; Wang, J., Bacteria-Responsive Multifunctional Nanogel for Targeted Antibiotic Delivery. *Advanced Materials* **2012,** *24* (46), 6175-6180.
159. McKinlay, C. J.; Waymouth, R. M.; Wender, P. A., Cell-Penetrating, Guanidinium-Rich Oligophosphoesters: Effective and Versatile Molecular Transporters for Drug and Probe Delivery. *Journal of the American Chemical Society* **2016,** *138* (10), 3510-3517.
160. Malzahn, K.; Marsico, F.; Koynov, K.; Landfester, K.; Weiss, C. K.; Wurm, F. R., Selective Interfacial Olefin Cross Metathesis for the Preparation of Hollow Nanocapsules. *ACS Macro Letters* **2013,** *3* (1), 40-43.
161. Marsico, F.; Wagner, M.; Landfester, K.; Wurm, F. R., Unsaturated Polyphosphoesters via Acyclic Diene Metathesis Polymerization. *Macromolecules* **2012,** *45* (21), 8511-8518.

162. Steinbach, T.; Alexandrino, E. M.; Wahlen, C.; Landfester, K.; Wurm, F. R., Poly(phosphonate)s via Olefin Metathesis: Adjusting Hydrophobicity and Morphology. *Macromolecules* **2014,** *47* (15), 4884-4893.

163. Steinbach, T.; Alexandrino, E. M.; Wurm, F. R., Unsaturated polyphosphoesters via ring-opening metathesis polymerization. *Polymer Chemistry* **2013,** *4* (13), 3800-3806.

164. Steinmann, M.; Markwart, J.; Wurm, F. R., Poly(alkylidene chlorophosphate)s via Acyclic Diene Metathesis Polymerization: A General Platform for the Postpolymerization Modification of Polyphosphoesters. *Macromolecules* **2014,** *47* (24), 8506-8513.

165. Peres, L. B.; Preiss, L. C.; Wagner, M.; Wurm, F. R.; de Araújo, P. H. H.; Landfester, K.; Muñoz-Espí, R.; Sayer, C., ALTMET Polymerization of Amino Acid-Based Monomers Targeting Controlled Drug Release. *Macromolecules* **2016,** *49* (18), 6723-6730.

166. Opper, K. L.; Wagener, K. B., ADMET: metathesis polycondensation. *Journal of Polymer Science Part A: Polymer Chemistry* **2011,** *49* (4), 821-831.

167. Wagener, K. B.; Brzezinska, K.; Anderson, J. D.; Younkin, T. R.; Steppe, K.; DeBoer, W., Kinetics of Acyclic Diene Metathesis (ADMET) Polymerization. Influence of the Negative Neighboring Group Effect. *Macromolecules* **1997,** *30* (24), 7363-7369.

168. Marsico, F.; Turshatov, A.; Peköz, R.; Avlasevich, Y.; Wagner, M.; Weber, K.; Donadio, D.; Landfester, K.; Baluschev, S.; Wurm, F. R., Hyperbranched Unsaturated Polyphosphates as a Protective Matrix for Long-Term Photon Upconversion in Air. *Journal of the American Chemical Society* **2014,** *136* (31), 11057-11064.

169. Marsico, F.; Turshatov, A.; Weber, K.; Wurm, F. R., A Metathesis Route for BODIPY Labeled Polyolefins. *Org. Lett.* **2013,** *15* (15), 3844-3847.

170. Steinbach, T.; Wahlen, C.; Wurm, F. R., Poly (phosphonate)-mediated Horner–Wadsworth–Emmons reactions. *Polymer Chemistry* **2015**.

171. Nagarkar, A. A.; Crochet, A.; Fromm, K. M.; Kilbinger, A. F. M., Efficient Amine End-Functionalization of Living Ring-Opening Metathesis Polymers. *Macromolecules* **2012,** *45* (11), 4447-4453.

172. Steinbach, T.; Schroder, R.; Ritz, S.; Wurm, F. R., Microstructure analysis of biocompatible phosphoester copolymers. *Polymer Chemistry* **2013,** *4* (16), 4469-4479.

173. Tanaka, K.; Kitamura, N.; Chujo, Y., Biodegradable Main-Chain Phosphate-Caged Fluorescein Polymers for the Evaluation of Enzymatic Activity. *Macromolecules* **2010,** *43* (14), 6180-6184.

174. Wachiralarpphaithoon, C.; Iwasaki, Y.; Akiyoshi, K., Enzyme-degradable phosphorylcholine porous hydrogels cross-linked with polyphosphoesters for cell matrices. *Biomaterials* **2007,** *28* (6), 984-993.

175. Wang, Y.-C.; Tang, L.-Y.; Sun, T.-M.; Li, C.-H.; Xiong, M.-H.; Wang, J., Self-assembled micelles of biodegradable triblock copolymers based on poly (ethyl ethylene phosphate) and poly (ϵ-caprolactone) as drug carriers. *Biomacromolecules* **2007,** *9* (1), 388-395.

176. Xiang, D. F.; Bigley, A. N.; Ren, Z.; Xue, H.; Hull, K. G.; Romo, D.; Raushel, F. M., Interrogation of the Substrate Profile and Catalytic Properties of the Phosphotriesterase from Sphingobium sp. Strain TCM1: An Enzyme Capable of Hydrolyzing Organophosphate Flame Retardants and Plasticizers. *Biochemistry* **2015**.

177. Wang, Y.-C.; Tang, L.-Y.; Li, Y.; Wang, J., Thermoresponsive block copolymers of poly (ethylene glycol) and polyphosphoester: thermo-induced self-assembly, biocompatibility, and hydrolytic degradation. *Biomacromolecules* **2008,** *10* (1), 66-73.

178. Whiteside, T.; Carreira, L.; Hilal, S., Estimation of phosphate ester hydrolysis rate constants. II. Acid and general base catalyzed hydrolysis. *QSAR & Combinatorial Science* **2007,** *26* (5), 587-595.

179.   Bauer, K. N.; Liu, L.; Wagner, M.; Andrienko, D.; Wurm, F. R., Mechanistic study on the hydrolytic degradation of polyphosphates. *European Polymer Journal* **2018,** *108*, 286-294.

180.   Iwasaki, Y.; Nakagawa, C.; Ohtomi, M.; Ishihara, K.; Akiyoshi, K., Novel biodegradable polyphosphate cross-linker for making biocompatible hydrogel. *Biomacromolecules* **2004,** *5* (3), 1110-1115.

181.   Du, J.-Z.; Sun, T.-M.; Weng, S.-Q.; Chen, X.-S.; Wang, J., Synthesis and characterization of photo-cross-linked hydrogels based on biodegradable polyphosphoesters and poly (ethylene glycol) copolymers. *Biomacromolecules* **2007,** *8* (11), 3375-3381.

182.   He, J.; Ni, P.; Wang, S.; Shao, H.; Zhang, M.; Zhu, X., Synthesis and physicochemical characterization of biodegradable and pH-responsive hydrogels based on polyphosphoester for protein delivery. *Journal of Polymer Science Part A: Polymer Chemistry* **2010,** *48* (9), 1919-1930.

183.   Huang, S.-W.; Wang, J.; Zhang, P.-C.; Mao, H.-Q.; Zhuo, R.-X.; Leong, K. W., Water-soluble and nonionic polyphosphoester: synthesis, degradation, biocompatibility and enhancement of gene expression in mouse muscle. *Biomacromolecules* **2004,** *5* (2), 306-311.

184.   Wang, J.; Huang, S.-W.; Zhang, P.-C.; Mao, H.-Q.; Leong, K. W., Effect of side-chain structures on gene transfer efficiency of biodegradable cationic polyphosphoesters. *International Journal of Pharmaceutics* **2003,** *265* (1–2), 75-84.

185.   Wang, J.; Huang, S.-W.; Zhang, P.-C.; Mao, H.-Q.; Leong, K. W., Effect of side-chain structures on gene transfer efficiency of biodegradable cationic polyphosphoesters. *International journal of pharmaceutics* **2003,** *265* (1), 75-84.

186.   Wen, J.; Mao, H. Q.; Li, W.; Lin, K. Y.; Leong, K. W., Biodegradable polyphosphoester micelles for gene delivery. *Journal of pharmaceutical sciences* **2004,** *93* (8), 2142-2157.

187.   Li, Q.; Wang, J.; Shahani, S.; Sun, D. D.; Sharma, B.; Elisseeff, J. H.; Leong, K. W., Biodegradable and photocrosslinkable polyphosphoester hydrogel. *Biomaterials* **2006,** *27* (7), 1027-1034.

188.   Chew, S. Y.; Wen, J.; Yim, E. K.; Leong, K. W., Sustained release of proteins from electrospun biodegradable fibers. *Biomacromolecules* **2005,** *6* (4), 2017-2024.

189.   Chaubal, M. V.; Su, G.; Spicer, E.; Dang, W.; Branham, K. E.; English, J. P.; Zhao, Z., In vitro and in vivo degradation studies of a novel linear copolymer of lactide and ethylphosphate. *Journal of Biomaterials Science, Polymer Edition* **2003,** *14* (1), 45-61.

190.   Liu, Z.; Wang, L.; Bao, C.; Li, X.; Cao, L.; Dai, K.; Zhu, L., Cross-Linked PEG via Degradable Phosphate Ester Bond: Synthesis, Water-Swelling, and Application as Drug Carrier. *Biomacromolecules* **2011,** *12* (6), 2389-2395.

191.   Iliescu, S.; Pascariu, A.; Plesu, N.; Popa, A.; Macarie, L.; Ilia, G., Unconventional method used in synthesis of polyphosphoesters. *Polymer bulletin* **2009,** *63* (4), 485-495.

192.   Steinbach, T.; Wurm, F. R., Polyphosphoesters: A new platform for degradable polymers. *Angew. Chem. Int. Ed.* **2015,** *54*, 6098-6108.

193.   Steinbach, T.; Wurm, F. R., Degradable Polyphosphoester-Protein Conjugates:"PPEylation" of Proteins. *Biomacromolecules* **2016,** *17* (10), 3338-3346.

194.   Cankaya, A.; Steinmann, M.; Bülbül, Y.; Lieberwirth, I.; Wurm, F. R., Polyphosphoramidates by ADMET. *Polymer Chemistry* **2016,** *accepted*.

195.   Steinmann, M.; Wagner, M.; Wurm, F. R., Poly (phosphorodiamidate) s by Olefin Metathesis Polymerization with Precise Degradation. *Chemistry-A European Journal* **2016**.

196.   Xiang, D. F.; Bigley, A. N.; Ren, Z.; Xue, H.; Hull, K. G.; Romo, D.; Raushel, F. M., Interrogation of the Substrate Profile and Catalytic Properties of the Phosphotriesterase from Sphingobium sp. Strain TCM1: An Enzyme Capable of Hydrolyzing Organophosphate Flame Retardants and Plasticizers. *Biochemistry* **2015,** *54* (51), 7539-7549.

197. Wang, F.; Wang, Y.-C.; Yan, L.-F.; Wang, J., Biodegradable vesicular nanocarriers based on poly (ε-caprolactone)-block-poly (ethyl ethylene phosphate) for drug delivery. *Polymer* **2009,** *50* (21), 5048-5054.

198. Iwasaki, Y.; Komatsu, S.; Narita, T.; Akiyoshi, K.; Ishihara, K., Biodegradable Phosphorylcholine Polymer Hydrogels Cross-Linked with Vinyl-Functionalized Polyphosphate. *Macromolecular Bioscience* **2003,** *3* (5), 238-242.

199. Haag, R.; Kratz, F., Polymer Therapeutics: Concepts and Applications. *Angewandte Chemie International Edition* **2006,** *45* (8), 1198-1215.

200. Mitragotri, S.; Burke, P. A.; Langer, R., Overcoming the challenges in administering biopharmaceuticals: formulation and delivery strategies. *Nat Rev Drug Discov* **2014,** *13* (9), 655-672.

201. Torchilin, V., Tumor delivery of macromolecular drugs based on the EPR effect. *Advanced Drug Delivery Reviews* **2011,** *63* (3), 131-135.

202. Maeda, H.; Bharate, G. Y.; Daruwalla, J., Polymeric drugs for efficient tumor-targeted drug delivery based on EPR-effect. *European Journal of Pharmaceutics and Biopharmaceutics* **2009,** *71* (3), 409-419.

203. Greenwald, R. B.; Choe, Y. H.; McGuire, J.; Conover, C. D., Effective drug delivery by PEGylated drug conjugates. *Advanced Drug Delivery Reviews* **2003,** *55* (2), 217-250.

204. Harris, J. M.; Chess, R. B., Effect of pegylation on pharmaceuticals. *Nat Rev Drug Discov* **2003,** *2* (3), 214-221.

205. Veronese, F. M.; Pasut, G., PEGylation, successful approach to drug delivery. *Drug Discovery Today* **2005,** *10* (21), 1451-1458.

206. Elsabahy, M.; Zhang, S.; Zhang, F.; Deng, Z. J.; Lim, Y. H.; Wang, H.; Parsamian, P.; Hammond, P. T.; Wooley, K. L., Surface Charges and Shell Crosslinks Each Play Significant Roles in Mediating Degradation, Biofouling, Cytotoxicity and Immunotoxicity for Polyphosphoester-based Nanoparticles. *Scientific Reports* **2013,** *3*, 3313.

207. Schöttler, S.; Becker, G.; Winzen, S.; Steinbach, T.; Mohr, K.; Landfester, K.; Mailänder, V.; Wurm, F. R., Protein adsorption is required for stealth effect of poly (ethylene glycol)-and poly (phosphoester)-coated nanocarriers. *Nature nanotechnology* **2016,** *11* (4), 372-377.

208. Müller, J.; Bauer, K. N.; Prozeller, D.; Simon, J.; Mailänder, V.; Wurm, F. R.; Winzen, S.; Landfester, K., Coating nanoparticles with tunable surfactants facilitates control over the protein corona. *Biomaterials* **2017,** *115*, 1-8.

209. Tian, H.; Tang, Z.; Zhuang, X.; Chen, X.; Jing, X., Biodegradable synthetic polymers: preparation, functionalization and biomedical application. *Progress in Polymer Science* **2012,** *37* (2), 237-280.

210. Huang, Y.; Wang, D.; Zhu, X.; Yan, D.; Chen, R., Synthesis and therapeutic applications of biocompatible or biodegradable hyperbranched polymers. *Polymer Chemistry* **2015**.

211. Li, Y.; Wang, F.; Sun, T.; Du, J.; Yang, X.; Wang, J., Surface-modulated and thermoresponsive polyphosphoester nanoparticles for enhanced intracellular drug delivery. *Sci. China Chem.* **2014,** *57* (4), 579-585.

212. Liu, J.; Huang, W.; Pang, Y.; Zhu, X.; Zhou, Y.; Yan, D., Hyperbranched Polyphosphates for Drug Delivery Application: Design, Synthesis, and In Vitro Evaluation. *Biomacromolecules* **2010,** *11* (6), 1564-1570.

213. Zhu, W.; Du, H.; Huang, Y.; Sun, S.; Xu, N.; Ni, H.; Cai, X.; Li, X.; Shen, Z., Cationic poly(ester-phosphoester)s: Facile synthesis and antibacterial properties. *Journal of Polymer Science Part A: Polymer Chemistry* **2013,** *51* (17), 3667-3673.

214.	Wang, F.; Wang, Y.-C.; Yan, L.-F.; Wang, J., Biodegradable vesicular nanocarriers based on poly(ε-caprolactone)-block-poly(ethyl ethylene phosphate) for drug delivery. *Polymer* **2009,** *50* (21), 5048-5054.

215.	Yuan, Y.-Y.; Mao, C.-Q.; Du, X.-J.; Du, J.-Z.; Wang, F.; Wang, J., Surface Charge Switchable Nanoparticles Based on Zwitterionic Polymer for Enhanced Drug Delivery to Tumor. *Advanced Materials* **2012,** *24* (40), 5476-5480.

216.	Tang, L.-Y.; Wang, Y.-C.; Li, Y.; Du, J.-Z.; Wang, J., Shell-Detachable Micelles Based on Disulfide-Linked Block Copolymer As Potential Carrier for Intracellular Drug Delivery. *Bioconjugate Chemistry* **2009,** *20* (6), 1095-1099.

217.	Sun, C.-Y.; Dou, S.; Du, J.-Z.; Yang, X.-Z.; Li, Y.-P.; Wang, J., Doxorubicin Conjugate of Poly(Ethylene Glycol)-Block-Polyphosphoester for Cancer Therapy. *Advanced Healthcare Materials* **2014,** *3* (2), 261-272.

218.	Mao, C.-Q.; Du, J.-Z.; Sun, T.-M.; Yao, Y.-D.; Zhang, P.-Z.; Song, E.-W.; Wang, J., A biodegradable amphiphilic and cationic triblock copolymer for the delivery of siRNA targeting the acid ceramidase gene for cancer therapy. *Biomaterials* **2011,** *32* (11), 3124-3133.

219.	Sun, T.-M.; Du, J.-Z.; Yao, Y.-D.; Mao, C.-Q.; Dou, S.; Huang, S.-Y.; Zhang, P.-Z.; Leong, K. W.; Song, E.-W.; Wang, J., Simultaneous Delivery of siRNA and Paclitaxel via a "Two-in-One" Micelleplex Promotes Synergistic Tumor Suppression. *ACS Nano* **2011,** *5* (2), 1483-1494.

220.	Du, J.-Z.; Du, X.-J.; Mao, C.-Q.; Wang, J., Tailor-Made Dual pH-Sensitive Polymer–Doxorubicin Nanoparticles for Efficient Anticancer Drug Delivery. *Journal of the American Chemical Society* **2011,** *133* (44), 17560-17563.

221.	Aweda, T. A.; Zhang, S.; Mupanomunda, C.; Burkemper, J.; Heo, G. S.; Bandara, N.; Lin, M.; Cutler, C. S.; Cannon, C. L.; Youngs, W. J., Investigating the pharmacokinetics and biological distribution of silver-loaded polyphosphoester-based nanoparticles using 111Ag as a radiotracer. *Journal of Labelled Compounds and Radiopharmaceuticals* **2015**.

222.	Gustafson, T. P.; Lonnecker, A. T.; Heo, G. S.; Zhang, S.; Dove, A. P.; Wooley, K. L., Poly (d-glucose carbonate) Block Copolymers: A Platform for Natural Product-Based Nanomaterials with Solvothermatic Characteristics. *Biomacromolecules* **2013,** *14* (9), 3346-3353.

223.	Lim, Y. H.; Heo, G. S.; Cho, S.; Wooley, K. L., Construction of a Reactive Diblock Copolymer, Polyphosphoester-block-Poly(l-lactide), as a Versatile Framework for Functional Materials That Are Capable of Full Degradation and Nanoscopic Assembly Formation. *ACS Macro Letters* **2013,** *2* (9), 785-789.

224.	Lim, Y. H.; Tiemann, K. M.; Heo, G. S.; Wagers, P. O.; Rezenom, Y. H.; Zhang, S.; Zhang, F.; Youngs, W. J.; Hunstad, D. A.; Wooley, K. L., Preparation and in Vitro Antimicrobial Activity of Silver-Bearing Degradable Polymeric Nanoparticles of Polyphosphoester-block-Poly(l-lactide). *ACS Nano* **2015,** *9* (2), 1995-2008.

225.	Shen, Y.; Zhang, S.; Zhang, F.; Loftis, A.; Pavía-Sanders, A.; Zou, J.; Fan, J.; Taylor, J. S. A.; Wooley, K. L., Polyphosphoester-Based Cationic Nanoparticles Serendipitously Release Integral Biologically-Active Components to Serve as Novel Degradable Inducible Nitric Oxide Synthase Inhibitors. *Advanced Materials* **2013,** *25* (39), 5609-5614.

226.	Zhang, F.; Smolen, J. A.; Zhang, S.; Li, R.; Shah, P. N.; Cho, S.; Wang, H.; Raymond, J. E.; Cannon, C. L.; Wooley, K. L., Degradable polyphosphoester-based silver-loaded nanoparticles as therapeutics for bacterial lung infections. *Nanoscale* **2015,** *7* (6), 2265-2270.

227.	Zhang, S.; Zou, J.; Elsabahy, M.; Karwa, A.; Li, A.; Moore, D. A.; Dorshow, R. B.; Wooley, K. L., Poly (ethylene oxide)-block-polyphosphester-based paclitaxel conjugates as a platform for ultra-high paclitaxel-loaded multifunctional nanoparticles. *Chemical Science* **2013,** *4* (5), 2122-2126.

228.   Gustafson, T. P.; Lim, Y. H.; Flores, J. A.; Heo, G. S.; Zhang, F.; Zhang, S.; Samarajeewa, S.; Raymond, J. E.; Wooley, K. L., Holistic Assessment of Covalently Labeled Core–Shell Polymeric Nanoparticles with Fluorescent Contrast Agents for Theranostic Applications. *Langmuir* **2014,** *30* (2), 631-641.
229.   Owen, S. C.; Doak, A. K.; Wassam, P.; Shoichet, M. S.; Shoichet, B. K., Colloidal Aggregation Affects the Efficacy of Anticancer Drugs in Cell Culture. *ACS Chemical Biology* **2012,** *7* (8), 1429-1435.
230.   Sun, T.; Zhang, Y. S.; Pang, B.; Hyun, D. C.; Yang, M.; Xia, Y., Engineered Nanoparticles for Drug Delivery in Cancer Therapy. *Angewandte Chemie International Edition* **2014,** *53* (46), 12320-12364.
231.   Chen, C.-J.; Jin, Q.; Liu, G.-Y.; Li, D.-D.; Wang, J.-L.; Ji, J., Reversibly light-responsive micelles constructed via a simple modification of hyperbranched polymers with chromophores. *Polymer* **2012,** *53* (17), 3695-3703.
232.   Wu, J.; Sun, T.-M.; Yang, X.-Z.; Zhu, J.; Du, X.-J.; Yao, Y.-D.; Xiong, M.-H.; Wang, H.-X.; Wang, Y.-C.; Wang, J., Enhanced drug delivery to hepatocellular carcinoma with a galactosylated core-shell polyphosphoester nanogel. *Biomaterials Science* **2013,** *1* (11), 1143-1150.
233.   Wang, Y.-C.; Liu, X.-Q.; Sun, T.-M.; Xiong, M.-H.; Wang, J., Functionalized micelles from block copolymer of polyphosphoester and poly(ε-caprolactone) for receptor-mediated drug delivery. *Journal of Controlled Release* **2008,** *128* (1), 32-40.
234.   Tao, Y.; He, J.; Zhang, M.; Hao, Y.; Liu, J.; Ni, P., Galactosylated biodegradable poly(?-caprolactone-co-phosphoester) random copolymer nanoparticles for potent hepatoma-targeting delivery of doxorubicin. *Polymer Chemistry* **2014,** *5* (10), 3443-3452.
235.   Patel, M. M.; Goyal, B. R.; Bhadada, S. V.; Bhatt, J. S.; Amin, A. F., Getting into the Brain. *CNS Drugs* **2009,** *23* (1), 35-58.
236.   Zhang, G.; Zhang, M.; He, J.; Ni, P., Synthesis and characterization of a new multifunctional polymeric prodrug paclitaxel-polyphosphoester-folic acid for targeted drug delivery. *Polymer Chemistry* **2013,** *4* (16), 4515-4525.
237.   Zhang, P.; Hu, L.; Yin, Q.; Feng, L.; Li, Y., Transferrin-Modified c[RGDfK]-Paclitaxel Loaded Hybrid Micelle for Sequential Blood-Brain Barrier Penetration and Glioma Targeting Therapy. *Molecular Pharmaceutics* **2012,** *9* (6), 1590-1598.
238.   Zhang, P.; Hu, L.; Yin, Q.; Zhang, Z.; Feng, L.; Li, Y., Transferrin-conjugated polyphosphoester hybrid micelle loading paclitaxel for brain-targeting delivery: synthesis, preparation and in vivo evaluation. *Journal of controlled release* **2012,** *159* (3), 429-434.
239.   Yang, X.-Z.; Du, J.-Z.; Dou, S.; Mao, C.-Q.; Long, H.-Y.; Wang, J., Sheddable Ternary Nanoparticles for Tumor Acidity-Targeted siRNA Delivery. *ACS Nano* **2012,** *6* (1), 771-781.
240.   Dimitriou, R.; Jones, E.; McGonagle, D.; Giannoudis, P. V., Bone regeneration: current concepts and future directions. *BMC medicine* **2011,** *9* (1), 66.
241.   Butscher, A.; Bohner, M.; Hofmann, S.; Gauckler, L.; Müller, R., Structural and material approaches to bone tissue engineering in powder-based three-dimensional printing. *Acta Biomaterialia* **2011,** *7* (3), 907-920.
242.   Holzwarth, J. M.; Ma, P. X., Biomimetic nanofibrous scaffolds for bone tissue engineering. *Biomaterials* **2011,** *32* (36), 9622-9629.
243.   Janicki, P.; Schmidmaier, G., What should be the characteristics of the ideal bone graft substitute? Combining scaffolds with growth factors and/or stem cells. *Injury* **2011,** *42*, S77-S81.
244.   Li, B.; Yoshii, T.; Hafeman, A. E.; Nyman, J. S.; Wenke, J. C.; Guelcher, S. A., The effects of rhBMP-2 released from biodegradable polyurethane/microsphere composite scaffolds on new bone formation in rat femora. *Biomaterials* **2009,** *30* (35), 6768-6779.

245. Navarro, M.; Michiardi, A.; Castano, O.; Planell, J., Biomaterials in orthopaedics. *Journal of the Royal Society Interface* **2008,** *5* (27), 1137-1158.

246. Puppi, D.; Chiellini, F.; Piras, A.; Chiellini, E., Polymeric materials for bone and cartilage repair. *Progress in Polymer Science* **2010,** *35* (4), 403-440.

247. Qiu, J. J.; Liu, C. M.; Hu, F.; Guo, X. D.; Zheng, Q. X., Synthesis of unsaturated polyphosphoester as a potential injectable tissue engineering scaffold materials. *Journal of applied polymer science* **2006,** *102* (4), 3095-3101.

248. Rezwan, K.; Chen, Q.; Blaker, J.; Boccaccini, A. R., Biodegradable and bioactive porous polymer/inorganic composite scaffolds for bone tissue engineering. *Biomaterials* **2006,** *27* (18), 3413-3431.

249. Canalis, R. F.; Lechago, J., Tetracycline Bone Labeling An Improved Technique Using Incident Fluorescence. *Annals of Otology, Rhinology & Laryngology* **1982,** *91* (2), 160-162.

250. Pautke, C.; Vogt, S.; Kreutzer, K.; Haczek, C.; Wexel, G.; Kolk, A.; Imhoff, A. B.; Zitzelsberger, H.; Milz, S.; Tischer, T., Characterization of eight different tetracyclines: advances in fluorescence bone labeling. *Journal of anatomy* **2010,** *217* (1), 76-82.

251. Dahl, S.; Allain, P.; Marie, P.; Mauras, Y.; Boivin, G.; Ammann, P.; Tsouderos, Y.; Delmas, P.; Christiansen, C., Incorporation and distribution of strontium in bone. *Bone* **2001,** *28* (4), 446-453.

252. Bartl, R.; Frisch, B.; von Tresckow, E.; Bartl, C., *Bisphosphonates in medical practice: actions-side effects-indications-strategies*. Springer Science & Business Media: 2007.

253. Russell, R. G. G.; Xia, Z.; Dunford, J. E.; Oppermann, U. D. O.; Kwaasi, A.; Hulley, P. A.; Kavanagh, K. L.; Triffitt, J. T.; Lundy, M. W.; Phipps, R. J.; Barnett, B. L.; Coxon, F. P.; Rogers, M. J.; Watts, N. B.; Ebetino, F. H., Bisphosphonates. *Annals of the New York Academy of Sciences* **2007,** *1117* (1), 209-257.

254. Dominguez, L. J.; Di Bella, G.; Belvedere, M.; Barbagallo, M., Physiology of the aging bone and mechanisms of action of bisphosphonates. *Biogerontology* **2011,** *12* (5), 397-408.

255. Alexandrino, E. M.; Ritz, S.; Marsico, F.; Baier, G.; Mailänder, V.; Landfester, K.; Wurm, F. R., Paclitaxel-loaded polyphosphate nanoparticles: a potential strategy for bone cancer treatment. *Journal of Materials Chemistry B* **2014,** *2* (10), 1298-1306.

256. Kretlow, J. D.; Mikos, A. G., Review: mineralization of synthetic polymer scaffolds for bone tissue engineering. *Tissue engineering* **2007,** *13* (5), 927-938.

257. Watson, B. M.; Kasper, F. K.; Mikos, A. G., Phosphorous-containing polymers for regenerative medicine. *Biomedical Materials* **2014,** *9* (2), 025014.

258. Yang, X.-Z.; Sun, T.-M.; Dou, S.; Wu, J.; Wang, Y.-C.; Wang, J., Block Copolymer of Polyphosphoester and Poly(l-Lactic Acid) Modified Surface for Enhancing Osteoblast Adhesion, Proliferation, and Function. *Biomacromolecules* **2009,** *10* (8), 2213-2220.

259. Wang, D.-a.; Williams, C. G.; Li, Q.; Sharma, B.; Elisseeff, J. H., Synthesis and characterization of a novel degradable phosphate-containing hydrogel. *Biomaterials* **2003,** *24* (22), 3969-3980.

260. Wang, D.-A.; Williams, C. G.; Yang, F.; Cher, N.; Lee, H.; Elisseeff, J. H., Bioresponsive phosphoester hydrogels for bone tissue engineering. *Tissue engineering* **2005,** *11* (1-2), 201-213.

261. Zhang, Z.; Feng, X.; Mao, J.; Xiao, J.; Liu, C.; Qiu, J., In vitro cytotoxicity of a novel injectable and biodegradable alveolar bone substitute. *Biochemical and biophysical research communications* **2009,** *379* (2), 557-561.

262. Qiu, J.-J.; He, Z.-X.; Liu, C.-M.; Guo, X.-D.; Zheng, Q.-X., Crosslinking property of an oligomeric unsaturated phosphoester used as a potential injectable biomaterial. *Biomedical Materials* **2008,** *3* (4), 044107.

263. Qiu, J.-J.; Bao, R.; Liu, C.-M., In Vitro Degradation Studies of a Novel Unsaturated Polyphosphoester Based Injectable Bone Repair Material. *Phosphorus, Sulfur, and Silicon* **2008,** *183* (2-3), 815-816.

264. Ikeuchi, R.; Iwasaki, Y., High mineral affinity of polyphosphoester ionomer–phospholipid vesicles. *Journal of Biomedical Materials Research Part A* **2013,** *101* (2), 318-325.

265. Harada, K.; Itoh, H.; Kawazoe, Y.; Miyazaki, S.; Doi, K.; Kubo, T.; Akagawa, Y.; Shiba, T., Polyphosphate-mediated inhibition of tartrate-resistant acid phosphatase and suppression of bone resorption of osteoclasts. **2013**.

266. Müller, W. E.; Tolba, E.; Schröder, H. C.; Wang, X., Polyphosphate: A Morphogenetically Active Implant Material Serving as Metabolic Fuel for Bone Regeneration. *Macromolecular bioscience* **2015**.

267. Müller, W. E.; Wang, X.; Diehl-Seifert, B.; Kropf, K.; Schloßmacher, U.; Lieberwirth, I.; Glasser, G.; Wiens, M.; Schröder, H. C., Inorganic polymeric phosphate/polyphosphate as an inducer of alkaline phosphatase and a modulator of intracellular Ca 2+ level in osteoblasts (SaOS-2 cells) in vitro. *Acta biomaterialia* **2011,** *7* (6), 2661-2671.

268. Wang, X.; Schröder, H. C.; Diehl-Seifert, B.; Kropf, K.; Schlossmacher, U.; Wiens, M.; Müller, W. E., Dual effect of inorganic polymeric phosphate/polyphosphate on osteoblasts and osteoclasts in vitro. *Journal of tissue engineering and regenerative medicine* **2013,** *7* (10), 767-776.

269. Kootala, S.; Tokunaga, M.; Hilborn, J.; Iwasaki, Y., Anti-Resorptive Functions of Poly (ethylene sodium phosphate) on Human Osteoclasts. *Macromolecular bioscience* **2015,** *15* (12), 1634-1640.

270. Iwasaki, Y.; Takahata, Y.; Fujii, S., Self-setting particle-stabilized emulsion for hard-tissue engineering. *Colloids and Surfaces B: Biointerfaces* **2015,** *126*, 394-400.

271. Dadsetan, M.; Giuliani, M.; Wanivenhaus, F.; Runge, M. B.; Charlesworth, J. E.; Yaszemski, M. J., Incorporation of phosphate group modulates bone cell attachment and differentiation on oligo (polyethylene glycol) fumarate hydrogel. *Acta biomaterialia* **2012,** *8* (4), 1430-1439.

Chapter 1

Non-covalent hydrogen bonds tune the mechanical properties of polyphosphoester polyethylene mimics
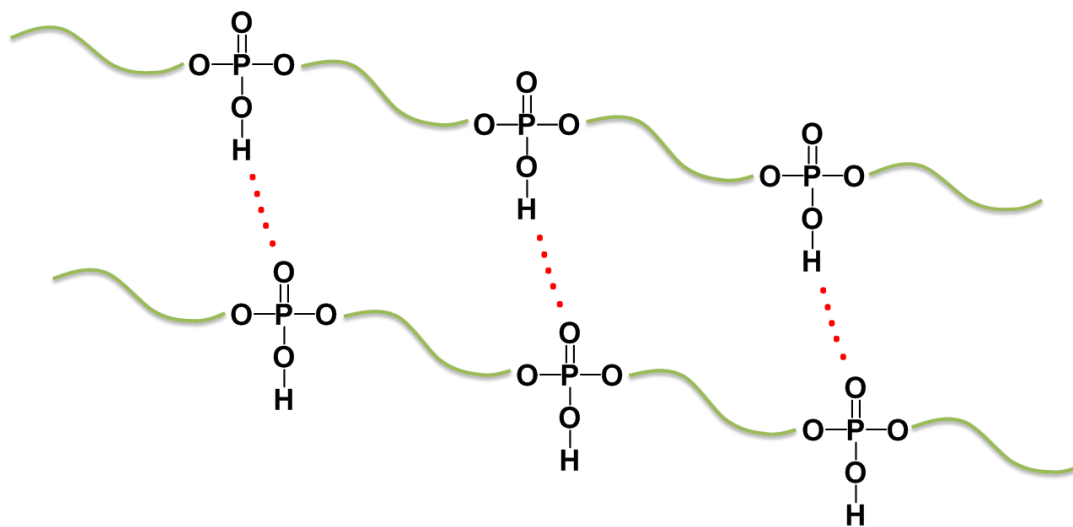
Foreword

The following chapter is based on unpublished results.

Rheology measurements were performed by Andreas Hanewald[1] and Shear lap tests were performed with Alexander Kux[2].

[1] *Max Planck Institute for Polymer Research, Ackermannweg 10, 55128 Mainz, Germany*

[2] *AR Bio-Renewables, Henkel AG & Co. KGaA, Henkelstraße 67, 40589 Düsseldorf, Germany*

Abstract

Polyethylene mimics of semicrystalline polyphosphoesters (PPE)s with an adjustable amount of non-covalent crosslinks were synthesized. Acyclic diene metathesis (ADMET) copolymerization of a phosphoric acid triester (**M1**) with a novel phosphoric acid diester monomer (**M2**) was achieved. PPEs with different comonomer ratios and 0%, 20%, 40% and 100% of phosphodiester content were synthesized. The phosphodiester groups result in supramolecular interactions between the polymer chains, with the P-OH-functionality as H-bond donor and the P=O-group as H-bond acceptor. A library of unsaturated and saturated PPEs were prepared and analyzed in detail by NMR spectroscopy, size exclusion chromatography, differential scanning calorimetry,

thermogravimetry, rheology, and stress-strain measurements. The introduction of the supramolecular crosslinks into the aliphatic and hydrophobic PPEs proved a significant impact on the materials properties: increased glass transition and melting temperatures were obtained and an increase of the storage modulus of the polymers was achieved. This specific combination of a flexible aliphatic backbone and a supramolecular H-bonding interaction between the chains were maximized in the homopolymer of the phosphodiester monomer, which featured additional properties, such as shape memory properties and polymer samples could be healed after cutting. The P-OH-groups also proved a strong adhesion towards metal surfaces, which was used together with the shape memory function in a model device which responds to a temperature stimulus with shape change. This systematic variation of phosphodiesters/phosphotriesters in polyethylene-mimics further underlines the versatility of the phosphorus chemistry to build up complex macromolecular architectures.

1 Introduction

Inspired by nature, supramolecular chemistry uses hydrogen bonding,[1-4] metal-ligand interactions,[5] or donor-acceptor π-π stacking[6] to assemble small molecules or polymers into materials with an extensive range of properties.[7] In nature, complex structures are generated by hydrogen bonding such as are proteins, which fold into specific three-dimensional structures to enable their function, or deoxyribonucleic acid (DNA) with hydrogen bonding between the nucleic acids which plays a crucial role in the double helical structure.[8] The strength of a single hydrogen bond (H-bond) is with ca. 10-40 kJ/mol relatively weak, however, multiple H-bonds result in high cohesive energies which can act as physical cross-links in polymer networks. Due to the temperature sensitivity of H-bonded networks, their viscoelasticity can be changed to give low viscosity melts or more solid-like properties. However, by choose of the H-bonds the material properties can be designed in advance due to weak H-bonds having a fast bond exchange which results in stimuli-responsiveness, while strong H-bonds have a retard bond exchange leading to solid like properties. Several technological concepts such as self-healing,[9] shape-memory processes,[10] and dynamic energy dissipation[11] have been achieved by the incorporation of H-bonds into polymers. H-bonds alter or improve the mechanical properties of a polymer,[12, 13] and are crucial for industrially important polymers like polyurethanes or polyamides.[13-15]

We have been recently working on aliphatic polyethylene (PE) mimics based on P-containing aliphatic polymers. Such polyphosphoesters (PPEs) or polypyrophosphates crystallized similar to polyethylene, but bring the potential to be degradable.[16-18] In linear main-chain PPEs, two phosphoesters build the polymer backbone, while the pendant ester group can be used to tune their chemical functionality.[19, 20] Besides chemical functionality, herein we used the pendant chain to introduce physical crosslinking into a polyphosphoester PE-mimic. Phosphodiester groups were installed into the polymer backbone, with the P-OH-functionality as H-bond donor and the P=O-group as H-bond acceptor. We report the synthesis of aliphatic PPEs with a variable amount of phosphodi- and -triesters via acyclic diene metathesis (ADMET) polymerization of A_2-type phosphodiester or –triester monomers. By the co-monomer ratio, the amount of H-bonding groups in the main chain was adjusted to control the properties of the non-covalent polymer network. As ADMET polymerization produces unsaturated PPEs, with typically a low degree of crystallinity, hydrogenation can be performed to increase their crystallinity.[21] In combination with the supramolecular H-bond interactions, this is another handle to control the mechanical properties of the polymer networks that was studied herein by rheology. Depending on the amount of H-bonding crosslinks, brittle, or ductile materials with healing and shape-memory properties were obtained. This study expands the previous studies on aliphatic PE-mimics to dynamic materials with noncovalent crosslinking, which broaden potential applications.

2   Results and Discussion

Monomer and Polymer Syntheses. To study the influence of noncovalent/supramolecular crosslinking, two different phosphate monomers were prepared. Both monomers were equipped with two C_{11} unsaturated alkyl chains for the linear ADMET polycondensation. **M1** is a phosphotriester carrying additionally a phenoxy side group, while **M2** is a phosphodiester with the P-OH side group, which is able to undergo H-bonding. **M1** was used by our group previously and was synthesized by esterification of phenyl dichlorophosphate with 10-undecen-1-ol in presence of triethylamine.[21] **M2** was prepared by the reaction of phosphorus oxychloride with 2 equivalents of 10-undecen-1-ol followed by hydrolysis of the remaining P-Cl-bond with water. The effect of H-bonding on the properties of **M2** can be already seen between both monomers. **M1** is a viscous liquid with a melting temperature below room temperature, **M2** is a white solid with a melting temperature above room temperature.

Non-covalent hydrogen bonds tune the mechanical properties of polyphosphoester polyethylene mimics

The polymerization and copolymerization of both monomers was accomplished by acyclic diene metathesis polymerization (Figure 1.1a). Polymerization was conducted in bulk without the addition of solvent with mechanical stirring. To adjust the number of physical cross-links and thus to alter the mechanical properties, copolymers with different amounts of **M2** were prepared: 0 mol% (**P1**), 5 mol% (**P1-H$_{0.95}$-co-P2-H$_{0.05}$**), 20 mol% (**P1-H$_{0.80}$-co-P2-H$_{0.20}$**), 40 mol% (**P1-H$_{0.60}$-co-P2-H$_{0.40}$**), or 100 mol% (**P2**). Copolymers with ≤40 mol% **M2** were prepared with Grubbs' first generation catalyst. Copolymers with higher amounts of **M2** were only obtained with Hoveyda-Grubbs first generation catalyst. As the viscosity increased during the polymerization, the temperature was increased from 65 °C up to 90 °C. P(**1$_x$-co-2$_y$**) with x ≤40 mol% were obtained as viscous oils at room temperature. To increase their crystallinity, hydrogenation with 10% Pd/C was performed.
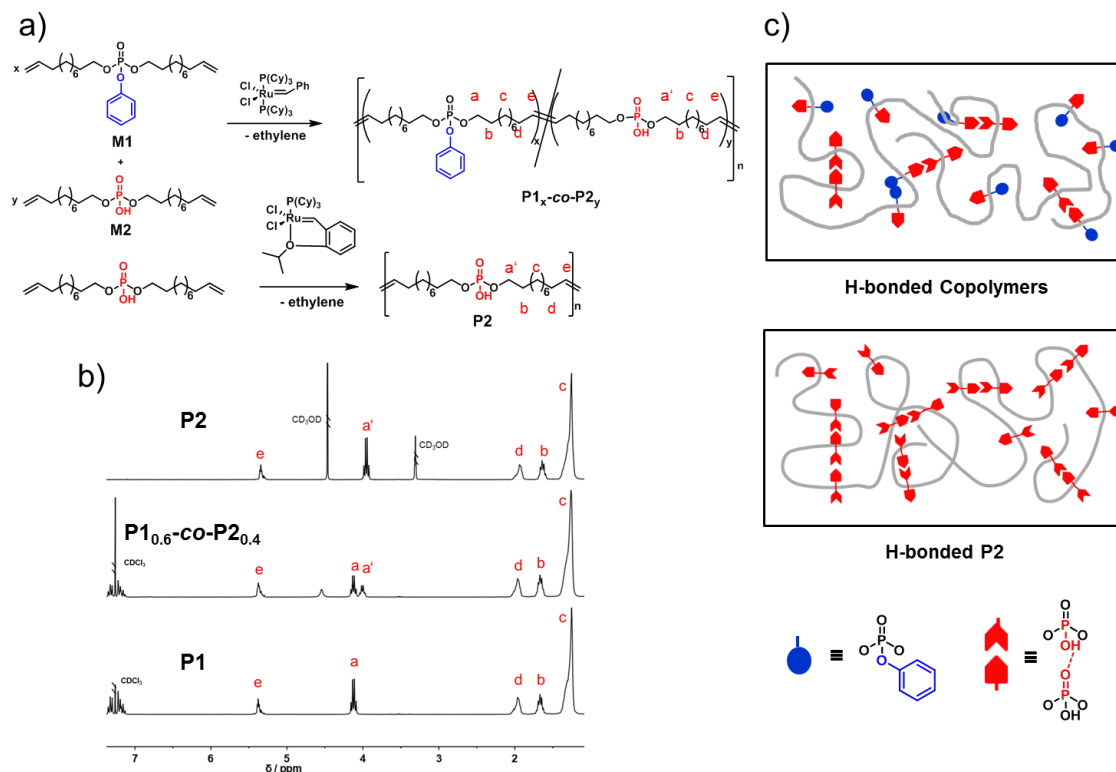
Figure 1.1. Synthesis of non-covalently cross-linked polyphosphoesters. (a) Synthesis of main-chain polyphosphodiesters (P2) and copolymers P(1-co-2) by acyclic diene metathesis polycondensation. (b) ^{1}H NMR spectra of P1, P2 and a copolymer P(1-co-2) with signal assignments. (c) Schematic representation of non-covalently cross-linked PPEs by H-bonding between the P-OH and P=O groups.

^{1}H NMR and ^{31}P NMR was used to confirm the composition of copolymers and showed, that the monomer composition used in the synthesis is found in the polymer product. Figure 1.1b shows the characteristic shift for the protons in the backbone next to the phosphates, which allows the determination of the monomer ratio. For all polymers, SEC proved successful polymerization and molar mass dispersities of ca. 2, as expected for a linear polycondensation, and apparent molar masses (vs. PS standards) between M_n= 4,700 and 11,400 g/mol. For SEC measurement of **P2** the P-OH-groups were converted to the methyl esters by esterification with trimethylsilyldiazomethane to ensure solubilization in THF (the ^{1}H NMR spectra of the methoxylated P2 proved a characteristic doublet at 3.75 ppm, proving successful esterification (cf. Figure 1.49). Also, the other copolymers were esterified and measured again on the SEC, which increased their apparent molar masses, probably to an increased hydrodynamic radius after esterification (cf. Table 1.1.).

Table 1.1. Characterization data of polyphosphoesters prepared in this study.

mol% M2	$M_{n,}$[a] /kg mol^{-1}	M_w/M_n	M_n[b] /kg mol^{-1}	M_w/M_n	T_m[c] /°C	T_c[c] /°C	ΔH_m[c] /J g^{-1}	crystal-linity[d] /%
0	8.0	2.3	n.c.	n.c.	44	40; 24	63	22
5	6.5	2.3	n.d.	n.d.	46	41;27	80	27
20	8.4	2.2	11.4	2.3	48; 53	48	54	18
40	4.7	2.0	8.4	2.8	51, 60	54	50	17
100$_{unsat.}$	n.c.	n.c.	9.8	1.8	51; 80	25	40	14
100	n.c.	n.c.	n.c.	n.c.	93	89	110	37

[a] Determined by SEC in THF vs. polystyrene standards. [b] Determined by SEC in THF vs. polystyrene standards after methoxylation. [c] Determined by DSC with heating/cooling rate of 10 K min^{-1}. Peak T_m determined from the second heating run. [d] From DSC measurements, calculated *vs.* 100 % crystalline polyethylene (293 J g^{-1}).[22]

Two melting peaks were observed with P-OH functionality above 20 %, while the higher peak melting temperature increased significantly with more P-OH functionality compared to the lower peak melting temperature. The crystallinity determined by DSC show no clear trend with increasing H-bonding and XRD diffractograms (Figure 1.61) revealed a similar degree of crystallinity and crystal structure for P(1-H$_x$-*co*-2-H$_y$) (with y≤0.4). TGA indicated a thermal

stability between 260 and 300 °C (Figure 1.55) with a relative high char yield for **P2** which could make this polymer interesting as flame retardant.

2.1   Mechanical Properties.

Tensile stress-strain measurements. From the thermal characterization, the influence of the amount of noncovalent crosslinks on the materials properties was already obvious. The effect of increasing H-bonding groups on the stress-strain behavior of PPEs was investigated. For **P1-H** and **P1-H$_{0.95}$-*co*-P2-H$_{0.05}$** the polymer-films were too brittle to conduct a reproducible measurement with dog-bone specimen. **P1-H$_{0.80}$-*co*-P2-H$_{0.20}$** and **P1-H$_{0.60}$-*co*-P2-H$_{0.40}$** polymer films and dog-bone specimen were still relatively brittle, but already during handling a higher flexibility was obvious. Still, relatively low elongations ranging from $7.3 \pm 0.8\%$ and $9.5 \pm 0.6\%$ were achieved in the stress-strain test before breaking, as expected for a brittle semicrystalline polymer (Figure 1.2a). Both polymers showed a relative low material stiffness with a Young modulus of 0.8 ± 0.2 GPa. In contrast, **P2-H** exhibited an average elongation at break of $100 \pm 30\%$, with a yield strength (σ_y) of 20.5 MPa, as more non-covalent interactions are present in this polymer (Figure 1.2b). Interestingly, the unsaturated analog **P2** proved the highest elongation at break of the investigated samples, namely $640 \pm 45\%$. The yield strength, however, was much lower with 8.6 MPa due to higher chain flexibility of the unsaturated backbone. **P2-H** seems to be tougher itself due to the higher crystallinity and chain arrangement, while **P2** is more ductile and undergoes strain crystallization after passing the yield point. This is in agreement with the measured Young's modulus values of 0.8 ± 0.1 GPa for **P2** and 1.2 ± 0.2 GPa for **P2-H** showing a significantly higher material stiffness for **P2-H**. So we can see in **P2** and **P2-H** that most of the flexibility our PPE gained through H-bonding is lost from the crystallization of our semicrystalline polymers.
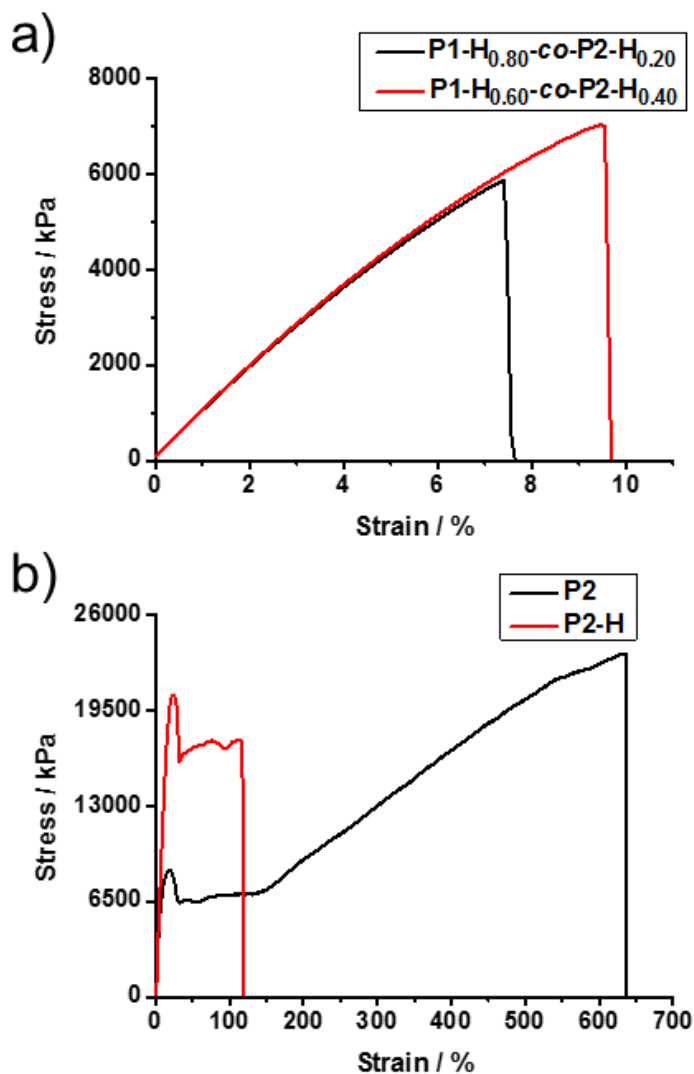
Figure 1.2. Tensile stress-strain curves of (a) P1-H$_{0.80}$-*co*-P2-H$_{0.20}$, P1-H$_{0.60}$-*co*-P2-H$_{0.40}$. (b) P2 and P2-H.

Rheological measurements. In order to probe the softening- and melting behavior of the polymers, we measured the temperature dependencies of their storage G′ and the loss G″ moduli in the range from below the glass transition to a temperature above the melting transition. The temperature sweeps in Figure 1.3 show that higher P-OH amount led to increasing of both glass transition temperatures and melting transition temperatures. Even **P2** with the double bonds along the backbone has a T_m of 50 °C resulting in a solid material at room temperature which was not the case for the unsaturated PPEs with lower amount of hydrogen bonding groups.
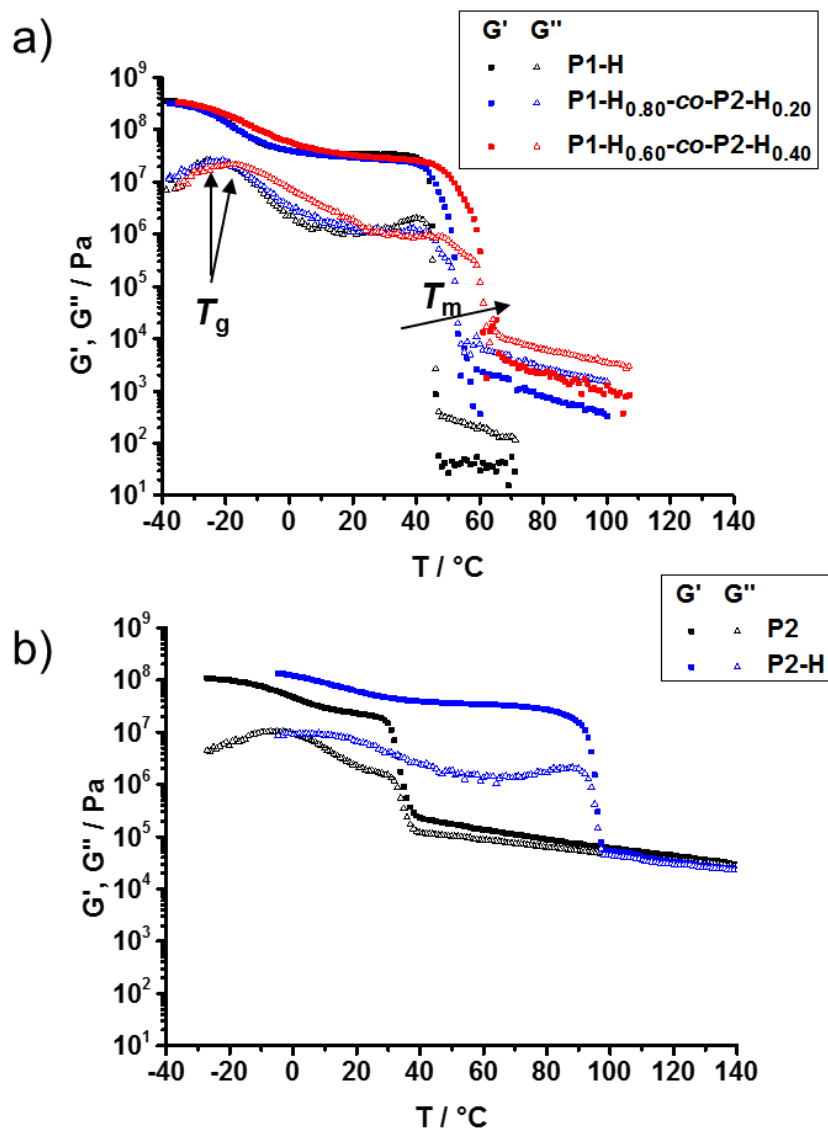
Figure 1.3. Temperature dependencies of the storage G′ and the loss G″ moduli measured on heating from below T_g to above T_m. (a) P1-H, P1-H$_{0.80}$-co-P2-H$_{0.20}$, P1-H$_{0.60}$-co-P2-H$_{0.40}$. (b) P2 and P2-H.

It is interesting to consider and compare the moduli measured at temperatures above the melting temperature where the crystalline parts of the polymers are melted and the polymer chains are able to move. As expected for **P1-H**, G' is much lower than G'' and it shows much lower viscosity compared to **P1-H$_{0.80}$-co-P2-H$_{0.20}$** and **P1-H$_{0.60}$-co-P2-H$_{0.40}$**. G' of **P1-H** without any H-bonding is around 10^3 times lower compared to G' of **P1-H$_{0.60}$-co-P2-H$_{0.40}$**, showing that **P1-H** has more fluid like properties and less elasticity. Even though G' of **P1-H$_{0.60}$-co-P2-H$_{0.40}$** is much higher

due to the H-bonding, tanδ (G''/G') is still <1 indicating a predominantly fluid like material. We next increased the physical crosslinking with 100 mol% of monomer 2 and measured the change in the rheological behavior (Figure 1.3b). Unlike the polymers without H-bonding or low H-bonding G' is larger than G'' at temperatures above the melting transition for **P2**. Furthermore, G' of **P2** is ca. 100 times higher than **P1-H$_{0.60}$-*co*-P2-H$_{0.40}$** and around 10^5 times larger than **P1-H**. Over the entire temperature range G' is larger than G'' showing the strong H-bonding of the phosphates in **P2** which resulted in a solid like behavior even up to 140 °C. After hydrogenation of **P2** the melting temperature was increased by more than 100%. **P2-H** has slightly higher G' and G'' values compared to **P2** below 30 °C due to the more rigid backbone, however, after melting of **P2-H** both polymers show similar values for G' and G''. The dependency of T_m, T_g and G' on the amount of H-bonding groups is summarized in Figure 1.4. A linear increase of thermal properties and storage moduli can be observed for lower OH functionality while the cumulative H-bonding in **P2-H** leads to an extraordinary increase of those.

a)

b)

c)
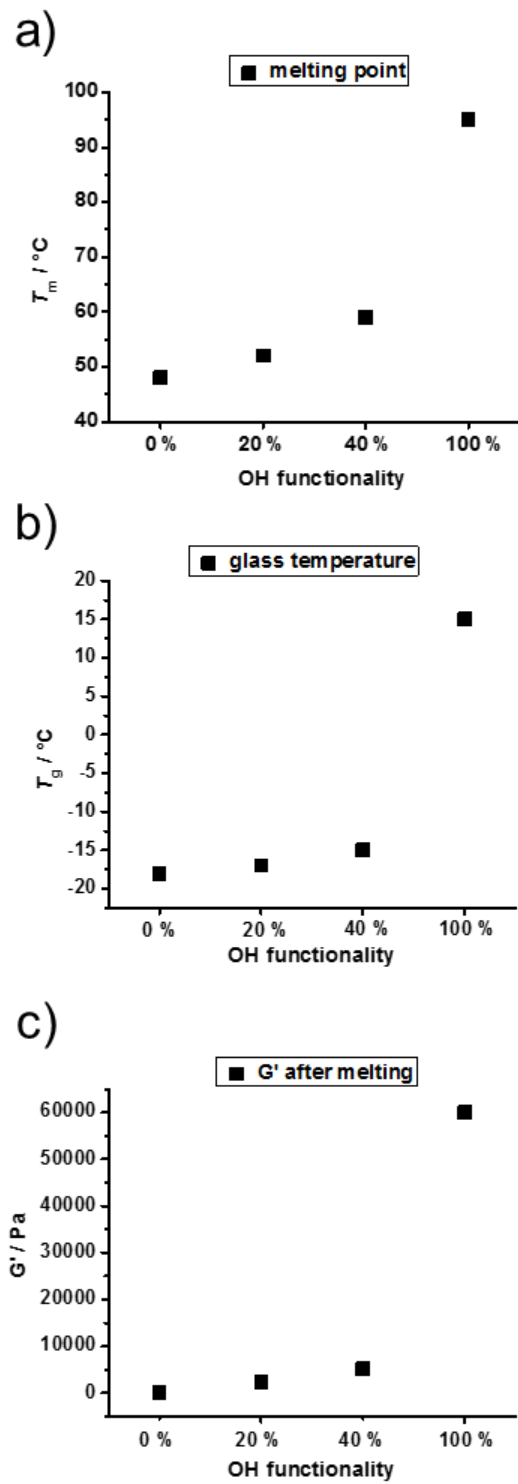
Figure 1.4. Variation of thermal transitions temperatures and G' after melting with increasing hydrogen bonding groups of saturated PPEs. (a) Glass transition temperature. (b) Melting transition temperature. (c) G' after melting.

Shape-recovery and healing. The majority of shape-memory polymers (SMPs) are using phase-segregated morphologies consisting of soft and hard domains. The soft domains will crystallize when cooled under a strained state and under heating those soft domains will melt and trigger the shape-memory transition[23]. Irradiation with light[24, 25], heating through a polymer's glass transition[26] are other ways reported as trigger for shape-memory transitions. In **P2** we use a combination of reversible hydrogen bond association and crystallization in which the strained state can be stabilized by forming a physical crosslinking when cooled due to the slow H-bond exchange as well as crystallization of the soft domains. The release of the strained state is conducted by heating through the melting temperature and by a fast H-bond exchange with heating[27]. A proposed mechanism for the shape-memory and self-healing due to main-chain H-bonding is shown in Figure 1.5c. PPEs with lower amounts of **M2** did not show any shape memory properties. Furthermore, shape memory properties were only found for **P2** and not for **P2-H** (Figure 1.5a). In order to change the shape, **P2** had to be heated above the melting temperature. Once cooled down to room temperature the material kept the shape until the sample was heated again and recovered his old shape. The difference in the melting points of **P2** and **P2-H** and a certain necessary amount of H-bonding groups supports our proposed mechanism in Figure 1.5c. The strained shape is pinned by the crystallization of our cooling PPEs and by a slower H-bonding exchange. When heated above T_m the crystalline parts are melting and the H-bonds can trigger the shape memory.
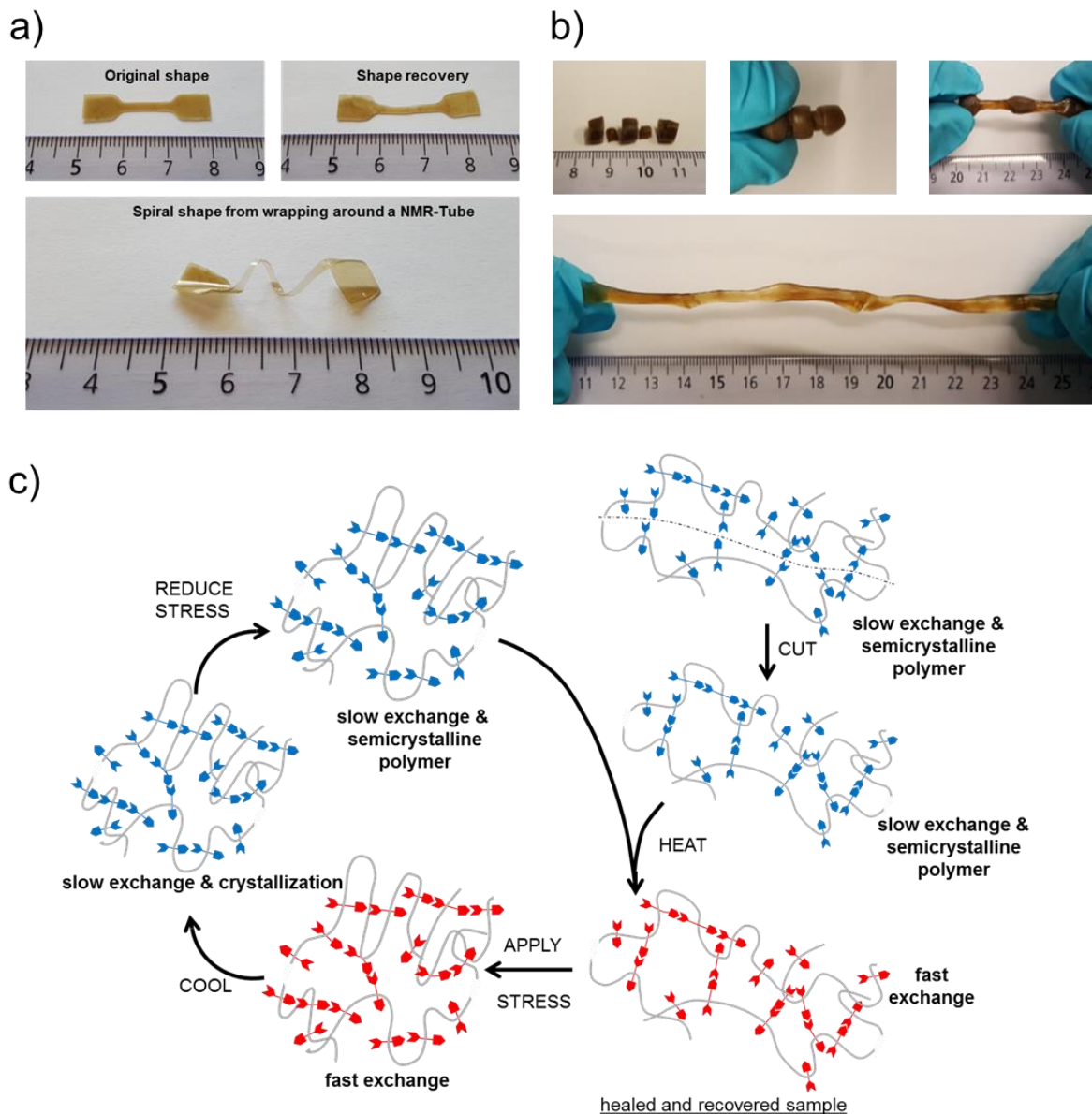
Figure 1.5. (a) Shape-memory properties of P2. A dog bone sample was wrapped and stretched around a NMR-Tube at 70 °C to give a strained spiral shape which maintained its shape at room temperature. The original shape was almost recovered after heating at 70 °C. (b) Healing properties of P2. Cylindrical polymer specimens with different diameters were used to visualize the interfaces. Healed material was obtained after pressing multiple samples at 100 °C together. After healing at 100 °C for 30 min the healed material showed similar elasticity. (c) Proposed self-healing and shape-memory mechanism with breaking and re-association of hydrogen bonds with temperature change.

For healing, specimen with different diameters were used to allow for easily distinguished interfaces. The cut pieces were soften at 100 °C, reattached and then left healing at 100 °C for 0.5 h. The healed polymer showed same stretching like original polymer cylinders (Figure 1.5b).
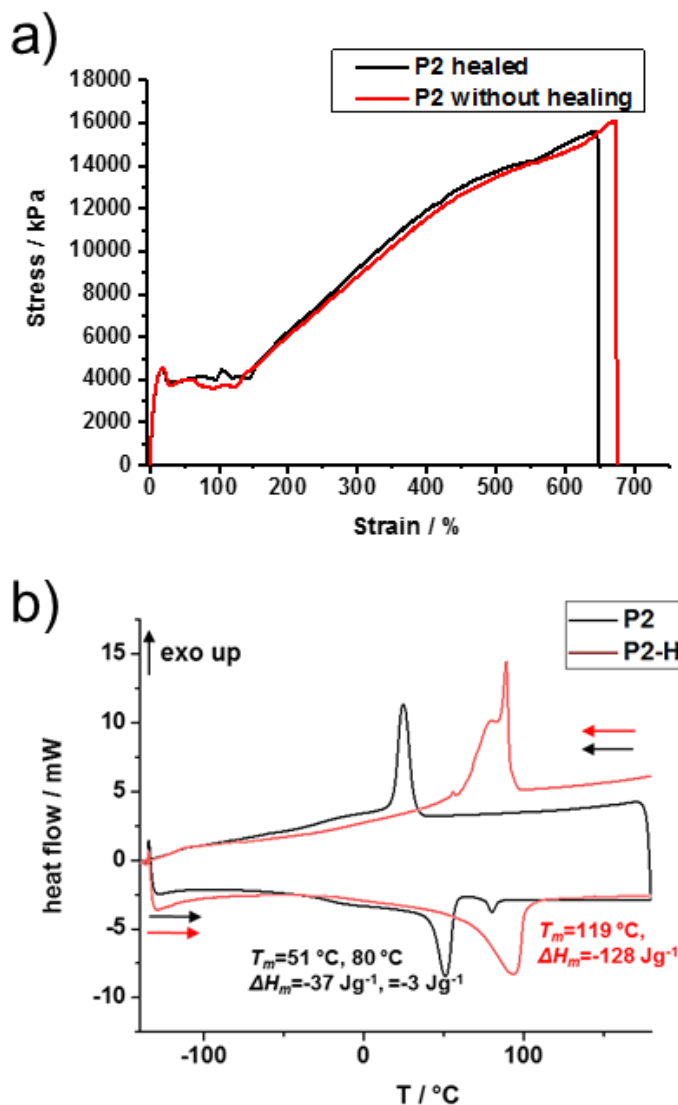
Figure 1.6. (a) Tensile Stress-Strain curves measured for samples of P2 before and after healing. (b) DSC of P2 and P2-H with a heating (second run) and cooling rate of 10 K min⁻¹.

The healing efficiency of **P2** was tested by tensile stress-strain measurements of specimen with and without healing. After cutting the dog bone samples of **P2** and healing at 100 °C the ultimate elongation could be almost recovered with 610 ± 20% (**Fehler! Verweisquelle konnte nicht**

gefunden werden.1.6a). Healing of **P2-H** was not successful probably due to the high melting point (Figure 1.6b). In P2 we have the unique combination of a lower melting point and strong H-bonding to avoid flow of the polymer. At a temperature of 100 °C the polymer chains are melted and the H-bonds exchange fast, allowing the polymer chains to move and the formation of new H-bonds. Once the temperature drops H-bonds will exchange slower and the polymer will crystallize resulting in a completely healed material.

Combination of metal adhesion and shape-memory. The adhesion properties of phosphoric acid esters on hydroxyapatite[28, 29] or metals like alumina[30] are already well known and therefore these materials are often used as dental adhesives or metal coatings. Shear lap test on alumina was conducted for our polymers and showed especially strong adhesive properties for **P2** with a Tension of 22.6 N/mm^2 (Figure 1.62). Figure 1.63 shows the fractures after shear lap test; all polymers except **P2** showed an adhesion fracture which is mostly an undesired fracture. **P2** showed a hybrid fracture, which is desired for many applications due to the balance of adhesion and cohesion strength. These adhesion properties were combined with the shape-recovery process in an easy device that responds to a temperature stimulus with a shape change: **P2** was brought into a rectangular shape and used to glue two pieces of steel together. To these metal plates, a circuit with an LED was installed. This closed circuit was opened, i.e. disconnected by changing the shape of **P2** after heating. In the stressed state, the metal plates are connected (Figure 7 top) and the LED is switched on. When the polymer glue is heated above the melting point, the shape-memory transition was triggered and the polymer disconnected the circuit by moving the two metal plates away from each other (Figure 7 bottom). This combination of adhesion and shape-memory properties might be further expanded to more sophisticated devices or smart materials for tissue engineering (e.g. for an implant or bone adhesion).
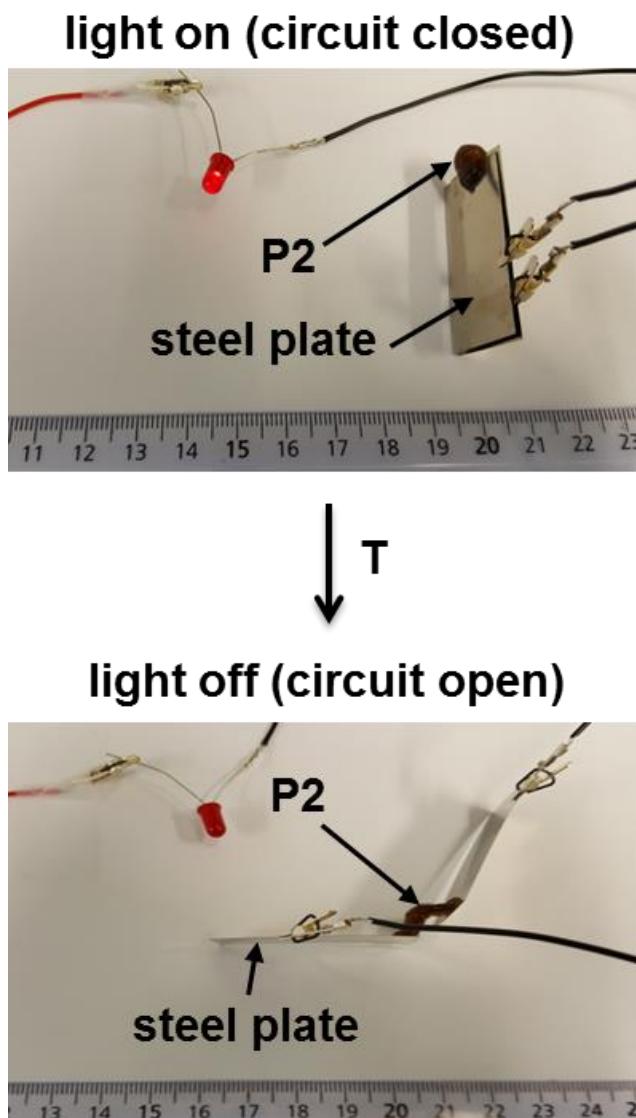
Figure 1.7. Visualization of the shape-memory and adhesive properties of P2: P2 was glued to two metal plates after shape deformation and a circuit was closed to light an LED. After shape-recovery, the metal plates were moved apart to disconnect the circuit.

3   Summary

We prepared non-covalently cross-linked polyphosphoester PE-mimics. PPEs with a variable number of phosphodiester units were prepared by ADMET polycondensation. Polymers with 40 % or lower P-OH functionality were brittle due to the low amount of noncovalent crosslinking. However, they showed linear enhanced viscosity above the melting temperature in rheology with

increasing H-bonding. Furthermore, PPEs with 20 and 40% H-bonding functionality were more flexible and their polymer films could easily be processed to the dog-bone specimen, while PPEs with no H-bonding or just 5 % H-bonding functionality showed low flexibility. Increasing the physical crosslinking density even further by synthesis of PPEs 100 % H-bonding functionality, the impact of the cumulative H-bonds leads to even higher values for tensile stress-strain, thermal transitions and showed viscoelastic properties of a solid after the melting temperature. In addition, with an unsaturated backbone, sufficient H-bonding allowed for efficient healing, rapid shape-memory and strong adhesive properties towards metals. With the adjustable content of noncovalent crosslinking on synthesis, the polymers exhibit tunable mechanical properties depending on P-OH functionality in the main-chain. Combining properties of PPEs like the degradability, a potential inherent bone adhesion, and the osteoinductive potential of phosphate-containing polymers with properties arising from the reversible crosslinking of hydrogen-bonds these PPEs might find application as novel materials for bone tissue regeneration. Furthermore, such materials might also be interesting for flame-retardant coatings or adhesives.

4   Experimental

4.1   General Information

All Solvents and chemicals were purchased from Sigma Aldrich, Acros Organics, or Fluka and used as received unless otherwise stated. Triethylamine was distilled from calcium hydride and stored over molecular sieves (4Å) under argon prior to use. Dry solvents were purchased from Acros Organics or Sigma Aldrich and stored with a septum and over molecular sieves. Deuterated solvents, Grubbs catalyst 1st generation, Hoveyda–Grubbs catalyst 1st generation and Pd/C(10wt%) were purchased from Sigma Aldrich and used as received.

4.2   Instrumentation and Characterization Techniques

SEC. SEC measurements were performed in THF with a PSS SecCurity system (Agilent Technologies 1260 Infinity). Sample injection was performed by a 1260-ALS autosampler (Waters) at 30 °C. SDV columns (PSS) with dimensions of 300×80 mm, 10 μm particle size, and pore sizes of 106, 104, and 500 Å were employed. The DRI Shodex RI-101 detector (ERC) and UV−vis 1260-VWD detector (Agilent) were used for detection. Calibration was achieved using polystyrene standards provided by Polymer Standards Service.

NMR. For nuclear magnetic resonance analysis ^{1}H, ^{13}C, and ^{31}P NMR spectra of the monomers and polymers were recorded on a Bruker AVANCE III 300, 500, or 700 MHz spectrometer. All spectra were measured in CDCl$_3$, CDCl$_3$/MeOD (7:3 or 4:2) or pyridine-d_5 at 298 K. The spectra were calibrated against the solvent signal and analyzed using MestReNova 8 from Mestrelab Research S.L.

DSC. The thermal properties of the synthesized polymers have been measured by differential scanning calorimetry (DSC) on a Mettler Toledo DSC 823 calorimeter. Three scanning cycles of heating-cooling were performed in an N$_2$ atmosphere with a heating and cooling rate of 10 °C min^{-1}.

TGA. TGA was measured on a Mettler Toledo ThermoSTAR TGA/SDTA 851-Thermowaage in a nitrogen atmosphere. The heating rate was 10 °C min^{-1} in a range of temperature between 25 and 600−900 °C.

FTIR. FTIR spectra were recorded in transmission mode accomplished with a Bruker Tensor II (Platinum ATR).

Rheology. Rheology experiments were performed using an Advanced Rheometric Expansion System (ARES, Rheometric Scientific). Plate-plate geometry was used with plate diameters of 6 mm and the gap between plates of 1 mm. The experiments were conducted under dry nitrogen atmosphere. Oscillatory shear deformation was applied under conditions of controlled deformation amplitude, which was kept in the range of the linear viscoelastic response of the studied samples. The temperature dependencies of the storage G′ and the loss G″ moduli were determined at a heating rate of 2°C/min and a constant deformation frequency of 10 rad/s.

Stress-Strain measurements. Stress-Strain behavior was studied using a Zwick Z005 universal testing machine equipped with a 50 N force sensor and 200 N clamping jaws. Dog-bone shaped samples (with 13 mm gauge length and 2 mm width) were cut from compression-mold films. Samples were strained at room temperature and an extension rate of 10 mm/min. For studying the healing properties, dog-bone samples were cut with a knife in the middle. The pieces were softened at 60 °C and reassembled manually and left 12 h at 100 °C before tensile testing.

Shear lap test. Shear lap test was conducted according to ISO 53 283 on a Zwick Z010 with a constant speed of 50 mm/min until the specimen break.

Sample preparation: 2 Aluminum (20/24) plates (80x25x1.8 mm) were heated to 90 °C and melted P(1-H$_x$-co-2-H$_y$) (with y≤0.4) were applied 10 mm along the plate end. Samples were stored for 30 minutes at 90 °C in the oven before they were stored for 2 weeks in the lab before

measurement. For melted $P(1_x$-co-$2_y)$ (with y>0.4) specimen were prepared with a PW 40 E Lab Press at 150 °C and 30 kN and a spacer (300 µm) for 5 minutes. Specimen were stored for one week in the lab before measurement. For polymers with 40 % and less hydrogen bonding functionality the overlap of the aluminum plates were 12 mm and for polymers with more than 40% hydrogen bonding functionality the overlap was 6 mm, due to the force cap.
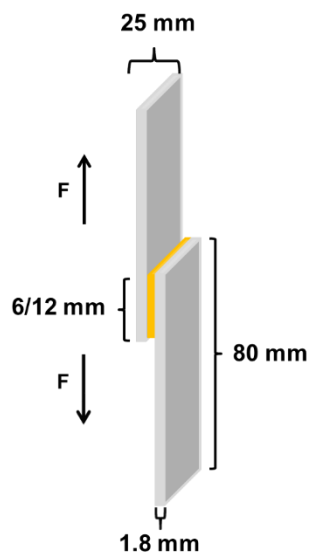
Scheme 1.1. Shear lap test and specimen dimensions.

Compressive strength. The compressive strength of the polymers was determined with a Zwick Roell Materials testing machine Z010. The measurement was conducted according to ISO 5833 E.

Sample preparation: Specimen were produced by melting the polymer into square Teflon molds with 10 holes with a diameter of 6 mm and a height of 3 cm. The cooled cylindrical specimen was then cut to a length of 12 mm with a diameter of 6 mm.

The Preload was 30 N and a speed of 20 mm/min was used until the specimen broke or for ductile samples until a plate distance of 6 mm was reached. The software testXpert II was used recording and evaluating the data.
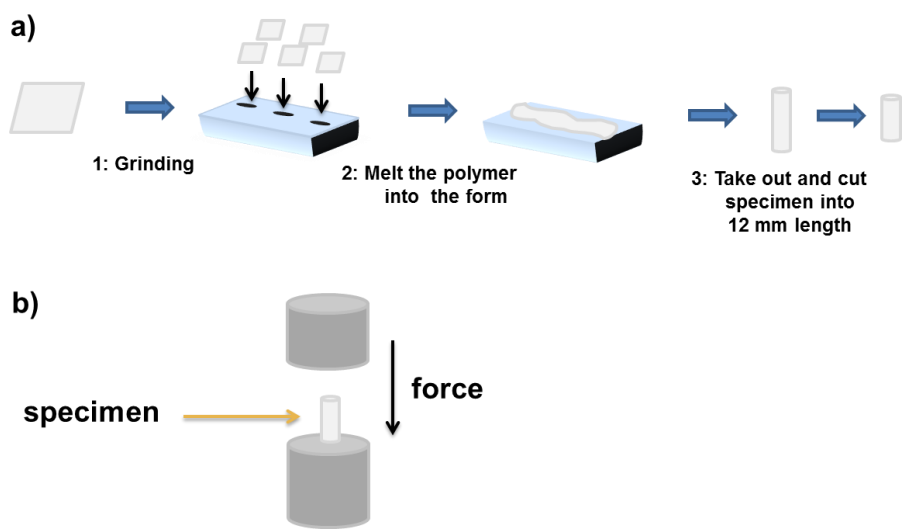
Scheme 1.2. Compressive strength. (a) Specimen preparation. (b) Scheme of measurement.

4.3 Synthetic Procedures

4.3.1 Monomer Synthesis

*Bis-(undec-10-en-1-yl) phenylphosphate (**M1**)*

A 500 mL Schlenk flask, equipped with a stirring bar and a dropping funnel, was charged with phenyl dichlorophosphate (60 g, 0.28 mol), dissolved in dry dichloromethane (150 mL) under an argon atmosphere. The solution was cooled to 0 °C with an ice-bath. 50 mL dry dichloromethane and 1.8 equivalents of triethylamine (71 mL, 0.51 mol) and 101.22 mL (0.51 mol) 10-undecen-1-ol were added over a period of ca. 1 h via the dropping funnel. After the addition, 0.01 equivalents of 4-*N,N*-dimethylaminopyridine (0.34 g) were added and the reaction was stirred overnight at room temperature. The crude mixture was concentrated at reduced pressure, dissolved in diethyl ether and filtered. The organic phase was washed twice with 10 % aqueous hydrochloric acid (HCl) solution and twice with Brine. The organic layer was dried over sodium sulfate, filtered, concentrated at reduced pressure, and purified by chromatography over neutral alumina using dichloromethane as eluent to give an off-white viscous oil (yield: 70.4 %, $R_f(AlOx)$: 0.9 (CH_2Cl_2)). ^{1}H NMR (300 MHz, CDCl$_3$, 298 K): δ = 7.37 − 7,27 (m, 2H), 7.24 − 7.10 (m, *3*H), 5.90 − 5.70 (ddt, *J* = 18 Hz, 12 Hz, 6 Hz, 2H), 5.06 − 4.86 (m, 4H), 4.20 − 4.04 (m, 4H), 2.10 − 1.95 (m, 4H), 1.74 − 1.60 (m, 4H), 1.46 − 1.16 (m, 24H) ppm. ^{13}C NMR (75 MHz, CDCl$_3$, 298 K) δ = 139.11,

129.63, 124.88, 119.99, 119.93, 114.15, 68.56, 68.48, 33.78, 30.25, 30.16, 29.41, 29.36, 29.08, 29.06, 28.90, 25.36 ppm. ^{31}P {H} NMR (121 MHz, CDCl$_3$, 298 K): δ = -6.10 ppm.

Bis-(undec-10-en-1-yl) phosphate (M2)

A 500 mL Schlenk flask, equipped with a stirring bar and a dropping funnel, was charged with phosphorus oxychloride (26.87 g, 0.18 mol), dissolved in dry dichloromethane (60 mL) under an argon atmosphere. The solution was cooled to 0 °C with an ice-bath. 40 mL dry dichloromethane and 2 equivalents of triethylamine (48.59 mL, 0.36 mol) and 1.99 equivalents (70.05 mL, 0.36 mol) 10-undecen-1-ol were added over a period of ca. 1 h via the dropping funnel. After stirring overnight, the precipitated triethyl ammonium hydrochloride was removed by filtration. The filtrate containing the dialkylene chlorophosphate in dichloromethane was stirred vigorously and an excess of water (ca. 100 mL) was added to the mixture. The acidic aqueous phase was exchanged every day with fresh water until the reaction was finished. The reaction was acidified until phase separation occurs. The organic layer was separated from water, dried with Na$_2$SO$_4$ and the dichloromethane was evaporated *in vacuo*. The viscous residue was dissolved in hexane (100 mL) at room temperature and kept at -20 °C to allow precipitation. The product was filtered, washed with cold hexane and a colorless solid was obtained (yield: 86 %, 63.30 g). ^{1}H NMR (300 MHz, CDCl$_3$, 298 K): δ = 8.53 (s, 1H), 5.90 – 5.71 (ddt, *J*= 18 Hz, 12 Hz 6 Hz, 2H), 5.05 – 4.87 (m, 2H), 4.08 – 3.95 (q, *J*= 6 Hz, 4H), 2,10 – 1.96 (m, 4H), 1.76 – 1.59 (m, 4H), 1.45 – 1.19 (m, 24H) ppm. ^{13}C NMR (75 MHz, Chloroform-*d*) δ = 139.17, 114.13, 67.72, 67.65, 33.80, 30.23, 30.13, 29.47, 29.41, 29.15, 29.11, 28.92, 25.43 ppm. ^{31}P {H} NMR (121 MHz, CDCl$_3$, 298 K): δ = 1.09 ppm.

4.3.2   Polymer synthesis

*Representative procedure for the ADMET bulk polymerization of **M1** and copolymerization with **M2** up to 40%.*

P1. In a vacuum reactor **M1** (100 g) and for copolymers the analog equivalent of **M2** and the Grubbs catalyst 1st generation (0.3 mol%) were mixed under an argon atmosphere. Polymerization was carried out at reduced pressure (first membrane pump (5 h, 50 mbar) then oil pump (1 mbar)) to remove ethylene gas evolving during the metathesis reaction, at 65 °C for 1 h and 85 °C for 16-48 h. The crude mixture was dissolved in CH$_2$Cl$_2$, treated with *tris*-(hydroxymethyl) phosphine (10 eq with respect to the catalyst) and 2 mL of Et$_3$N. After stirring for 1 h water was added in the

same volume to the organic phase and the solution was stirred overnight. The organic layer was washed twice with 5 % aqueous HCl and brine to remove the catalyst residue. The water layer was extracted with CH_2Cl_2 several times until the emulsion disappeared and the water layer got clear. The combined organic phase was dried over sodium sulfate (Na_2SO_4), filtered and concentrated at reduced pressure. (yields typically: 95 %). ^{1}H NMR: (300 MHz, $CDCl_3$, 298 K): δ = 7.38 – 7.27 (m), 7.24 – 7.11 (m), 5.47 – 5.26 (m), 4.20 – 4.05 (m), 2.10 – 1.87 (m), 1.75 – 1.57 (m), 1.45 – 1.12 (m) ppm. ^{31}P {H} NMR (202 MHz, $CDCl_3$, 298 K): δ = -6.10 ppm.

P1$_{0.95}$-*co*-P2$_{0.05}$

The reaction was carried out following the general procedure above with **M2** (450 mg, 1.12 mmol) and **M1** (10.17 g, 21.24 mmol) for 24 h (yield: 92%). ^{1}H NMR (500 MHz, $CDCl_3$, 298 K) δ = 7.36 – 7.28 (m), 7.24 – 7.12 (m), 5.39 – 5.36 (m), 5.36 – 5.32 (m), 2.06 – 1.92 (m), 1.70 – 1.61 (m), 1.38 – 1.18 (m) ppm. ^{31}P {H} NMR (202 MHz, $CDCl_3$, 298 K): δ = 0.85, -6.11 ppm.

P1$_{0.80}$-*co*-P2$_{0.20}$

The reaction was carried out following the general procedure above with **M2** (8.00 g, 19.87 mmol) and **M1** (38.05 g, 79.49 mmol) for 46 h (yield: 94 %). ^{1}H NMR: (300 MHz, $CDCl_3$, 298 K): δ = 7.38-7.28 (m), 7.24 – 7.10 (m), 5.45 – 5.30 (m), 4.20 – 4.06 (m), 4.06 – 3.92 (m), 2.09 – 1.86 (m), 1.79 – 1.55 (m), 1.48 – 1.14 (m) ppm. ^{13}C NMR (75 MHz, $CDCl_3$, 298 K) δ 130.32, 129.86, 129.65, 124.90, 120.00, 119.94, 68.61, 68.52, 32.62, 30.27, 30.18, 29.66, 29.47, 29.41, 29.18, 29.10, 27.23, 25.38 ppm. ^{31}P {H} NMR (121 MHz, $CDCl_3$, 298 K): δ = 1.14, -6.14 ppm.

P1$_{0.60}$-*co*-P2$_{0.40}$

The reaction was carried out following the general procedure above with **M2** (17.00 g, 42.23 mmol) and **M1** (30.32 g, 63.35 mmol) for 46 h (yield: 89 %). ^{1}H NMR: (300 MHz, $CDCl_3$, 298 K): δ = 7.37 – 7.28 (m), 7.24 – 7.10 (m), 5.45 – 5.28 (m), 4.19 – 4.07 (m), 4.06 – 3.93 (m), 2.07 – 1.87 (m), 1.75 – 1.57 (m), 1.44 – 1.16 (m) ppm. ^{13}C NMR (75 MHz, $CDCl_3$, 298 K) δ = 130.32, 129.87, 129.65, 124.91, 120.00, 119.94, 68.62, 68.53, 67.63, 32.61, 30.26, 30.17, 29.66, 29.47, 29.18, 29.10, 27.23, 25.45, 25.3 ppm. ^{31}P {H} NMR (121 MHz, $CDCl_3$, 298 K): δ = 1.04, -6.13 ppm.

*Representative procedure for the ADMET bulk polymerization of **M2**.*

P2. In a vacuum reactor **2** (60 g, 149 mmol) was melted at 40 °C then Hoveyda –Grubbs catalyst 1st generation (0.3 mol%) were mixed under an argon atmosphere. Polymerization was carried out at reduced pressure (first membrane pump (5 h, 50 mbar) then oil pump (1 mbar)) to remove ethylene gas evolving during the metathesis reaction, at 65 °C for 1 h and 90 °C for 16-72 h. The

polymer was not further purified after synthesis (yield: quantitative). ^{1}H NMR: (300 MHz, CDCl$_3$:CD$_3$OD 4:2, 298 K): δ = 5.29 – 4.93 (m), 3.90 – 3.57 (m), 1.92 – 1.58 (m), 1.55 – 1.28 (m), 1.30 – 0.75 (m) ppm. ^{13}C NMR (75 MHz, CDCl$_3$:CD$_3$OD 4:2, 298 K) δ = 130.02, 67.09, 67.01, 32.26, 30.03, 29.93, 29.33, 29.21, 29.13, 28.88, 28.82, 25.19 ppm. ^{31}P {H} NMR (121 MHz, CDCl$_3$:CD$_3$OD 4:2, 298 K): δ = -0.06, -0.79, -1.32 ppm.

P1$_{0.05}$-*co*-P2$_{0.95}$

The reaction was carried out following the general procedure above with **M2** (8.00 g, 30.50 mmol) and **M1** (543.2 mg, 1.61 mmol) for 20 h (yield: quantitative). ^{1}H NMR: (300 MHz, CDCl$_3$:CD$_3$OD 5:1, 298 K): δ = 7.37 – 7.27 (m), 7.20 – 7.11 (m), 5.44-5.24 (m), 4.16 – 4.06 (m), 4.05 – 3.88 (m), 2.07 – 1.83 (m), 1.77 – 1.53 (m), 1.45 – 1.12 (m) ppm. ^{31}P {H} NMR (121 MHz, CDCl$_3$:CD$_3$OD 5:1, 298 K): δ = 0.03, -0.71, -1.19, -6.62 ppm.

Representative procedure for catalytic hydrogenation

P1-H. A Schlenk flask was charged with **P1** and dissolved in toluene (ca. 12 wt%). The air was removed by reduced pressure and flushing the schlenk flask with argon. 10 wt% of 10 % Pd/C catalyst were added, the schlenk flask was evacuated and flushed with hydrogen from a balloon. Hydrogenation was then performed with a hydrogen balloon under vigorous stirring at room temperature until ^{1}H NMR showed the removal of the double bond signals. The solution was filtered over celite and the polymer was obtained as a solid after solvent evaporation in a yield of 80 %. ^{1}H NMR: (300 MHz, CDCl$_3$, 298 K): δ = 7.38 – 7.27 (m), 7.24 – 7.11 (m), 5.47 – 5.26 (m), 4.20 – 4.05 (m), 2.10 – 1.87 (m), 1.75 – 1.57 (m), 1.45 – 1.12 (m) ppm. ^{13}C NMR (176 MHz, CDCl$_3$, 298 K) δ = 150.88, 129.66, 124.91, 120.02, 119.99, 68.59, 68.55, 30.28, 30.24, 29.76, 29.70, 29.61, 29.54, 29.14, 25.43 ppm. ^{31}P {H} NMR (283 MHz, CDCl$_3$, 298 K): δ = -6.10 ppm.

P1-H$_{0.95}$-*co*-P2-H$_{0.05}$

Hydrogenation of **P1$_{0.95}$-*co*-P2$_{0.05}$** (yield: 90 %). ^{1}H NMR (300 MHz, CDCl$_3$, 298 K) δ = 7.38 – 7.27 (m), 7.23 – 7.10 (m), 4.20 – 4.05 (m), 1.75 – 1.60 (m), 1.48 – 1.14 (m). ^{13}C NMR (75 MHz, CDCl3, 298 K) δ = 129.64, 124.89, 120.01, 119.94, 68.60, 68.52, 30.27, 30.18, 29.73, 29.68, 29.58, 29.51, 29.11, 25.39 ppm. ^{31}P {H} NMR (121 MHz, CDCl$_3$, 298 K): δ = -6.11 ppm

P1-H$_{0.80}$-*co*-P2-H$_{0.20}$

Hydrogenation of **P1$_{0.80}$-*co*-P2$_{0.20}$** (yield: 92 %). ^{1}H NMR: (500 MHz, CD$_2$Cl$_2$, 298 K): δ = 7.38 – 7.31 (m), 7.22 – 7.14 (m), 4.18 – 4.04 (m), 4.02 – 3.90 (m), 1.72 – 1.56 (m), 1.45 – 1.08 (m) ppm. ^{13}C NMR (126 MHz, CD$_2$Cl$_2$, 298 K) δ = 68.56, 68.51, 53.63, 53.41, 53.19, 52.98, 30.25, 30.20,

29.74, 29.72, 29.68, 29.59, 29.52, 29.12, 25.41 ppm. ^{31}P {H} NMR (202 MHz, CD$_2$Cl$_2$, 298 K): δ = 0.77, -0.90, -6.22 ppm.

P1-H$_{0.60}$-*co*-P2-H$_{0.40}$

Hydrogenation of **P1$_{0.60}$-*co*-P2$_{0.40}$**. After filtration over Celite, Soxhlet extraction with CHCl$_3$ of Celite and coal from catalyst was necessary to increase the yield (yield: 81 %). ^{1}H NMR: (500 MHz, CD$_2$Cl$_2$, 298 K): δ = 7.39 – 7.30 (m), 7.24 – 7.14 (m), 4.19 – 4.04 (m), 4.03 – 3.88 (m), 1.72 – 1.57 (m), 1.453 – 1.10 (m) ppm. ^{13}C NMR (75 MHz, CDCl$_3$, 298 K) δ = 129.65, 124.90, 120.01, 119.94, 68.63, 68.54, 30.27, 30.18, 29.72, 29.51, 29.11, 25.39 ppm. ^{31}P {H} NMR (202 MHz, CD$_2$Cl$_2$, 298 K): δ = 0.51, -6.23 ppm.

P2-H

2 g **P2** was dissolved in 40 mL of Toluene:Methanol 7:3 at 40 °C and then transferred into an hydrogenation tube. The polymer solution was degassed for 10 minutes by bubbling argon under vigorous stirring. 4,4 mg of the hydrogenation catalyst precursor [(PCy3)3Cl2Ru=CHOEt] (synthesized from Grubbs catalyst 1st generation with ethyl vinyl ether)[31] was added and the solution again degassed for 2 minutes. Hydrogenation was then performed in a high pressure reactor at 40 °C and 60 bar H$_2$ overnight. After hydrogenation, the solvent was removed under reduced pressure to give P2 in quantitative yield. NMR measurement were prepared by dissolving 0.1 mL of the reaction mixture before removing the solvent in 0.5 mL CDCl$_3$:MeOD 4:2. Dissolving P2-H again was not accessible for any tested solvent. ^{1}H NMR: (300 MHz, CDCl$_3$:CD$_3$OD 4:2, 298 K): δ = 3.89 – 3.70 (m), 1.55 – 1.38 (m), 1.28 – 0.82 (m) ppm. ^{31}P {H} NMR (121 MHz, CDCl$_3$:CD$_3$OD 4:2, 298 K): δ = 3.28 ppm.

4.3.3 Esterification of P2-units to P3-units.

P1-H$_{0.80}$-*co*-P3-H$_{0.20}$. **P1-H$_{0.80}$-*co*-P2-H$_{0.20}$** (100 mg) was dissolved in 1.4 mL chloroform + 0.6 mL methanol at 35 °C. 2 M Trimethylsilyldiazomethane in diethylether (2 eq. to P-OH funct., 51 μL, 0.5 mmol) was added and the reaction was stirred for 30 min at 25 °C. Solvents and excess trimethylsilyldiazomethane were removed at reduced pressure. ^{1}H NMR (300 MHz, CDCl$_3$, 298 K) δ = 7.38 – 7.09 (m), 4.18 – 4.08 (m), 4.08 – 3.93 (m), 3.75 (d, *J* = 12 Hz), 1.79 – 1.47 (m), 1.44 – 1.08 (m) ppm. ^{31}P NMR (121 MHz, CDCl$_3$, 298 K) δ = 0.40, -6.11 ppm.

P1-H$_{0.60}$-*co*-P3-H$_{0.40}$

The reaction was carried out following the general procedure above with **P1-H$_{0.80}$-co-P3-H$_{0.20}$** using 102μL (1.0 mmol) Trimethylsilyldiazomethane-solution. ^{1}H NMR (300 MHz, Chloroform-d) δ = 7.38 – 7.10 (m), 4.19 – 4.08 (m), 4.08 – 3.93 (m), 3.75 (d, J = 12 Hz), 1.74 – 1.58 (m), 1.42 – 1.14 (m) ppm. ^{31}P NMR (121 MHz, CDCl$_3$, 298 K) δ = 0.39, -6.12 ppm.

P3

The reaction was carried out following the general procedure above with **P1-H$_{0.80}$-co-P3-H$_{0.20}$** using 272 μL (2.7 mmol) Trimethylsilyldiazomethane-solution. ^{1}H NMR (300 MHz, CDCl$_3$, 298 K) δ = 5.43 – 5.30 (m,), 4.09 – 3.94 (m), 3.75 (d, J = 11.1 Hz), 2.15 – 1.84 (m), 1.75 – 1.60 (m), 1.38 – 1.24 (m) ppm. ^{31}P NMR (121 MHz, CDCl$_3$, 298 K) δ = 1.40, 0.39 ppm.

4.4 ^{1}H, ^{13}C, ^{31}P NMR spectra

4.4.1 Monomer NMR spectra
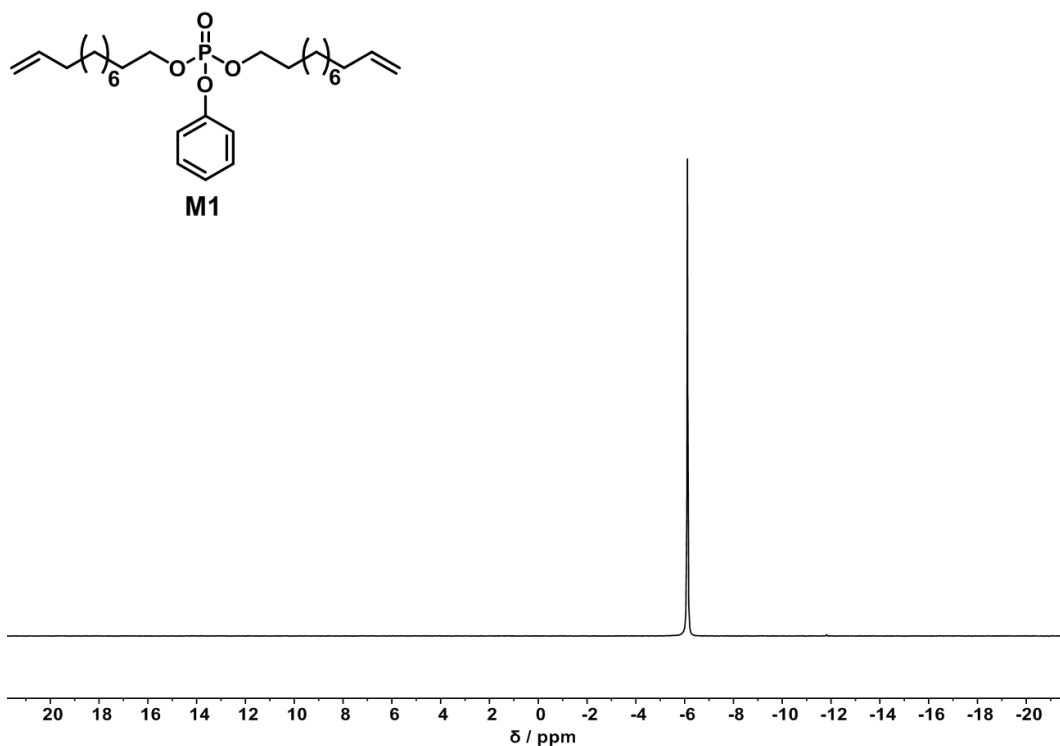
Figure 1.8. ^{31}P (121 MHz) NMR spectra of M1 in CDCl$_3$ at 298 K.
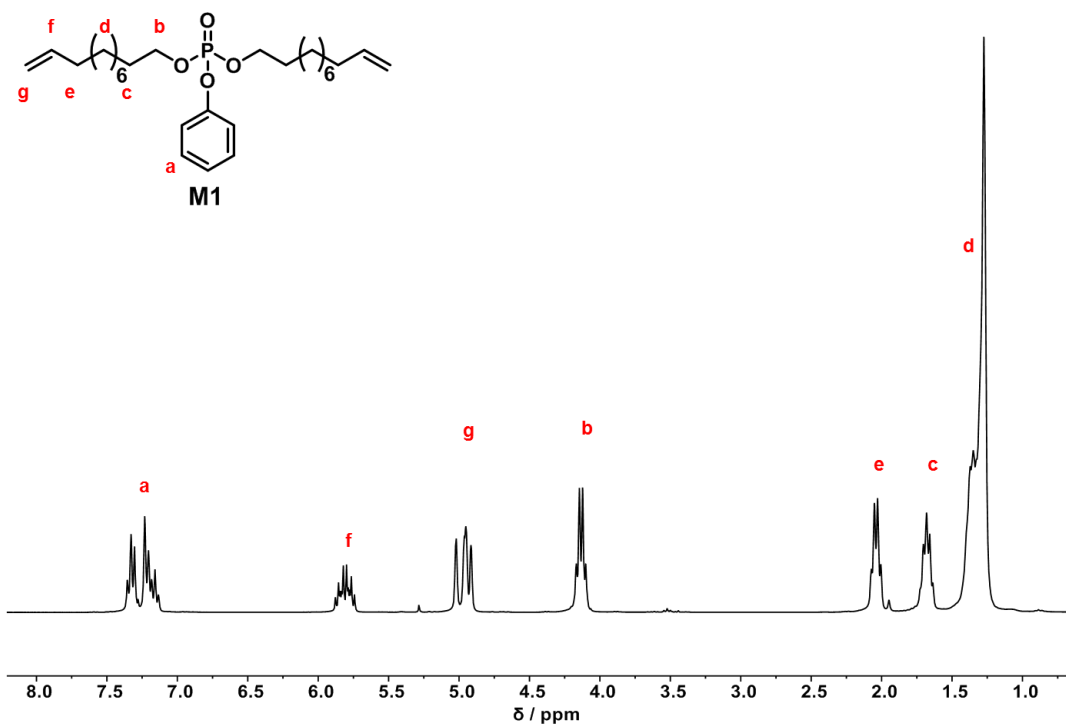
Figure 1.9. ^{1}H (300 MHz) NMR spectra of M1 in CDCl$_3$ at 298 K.
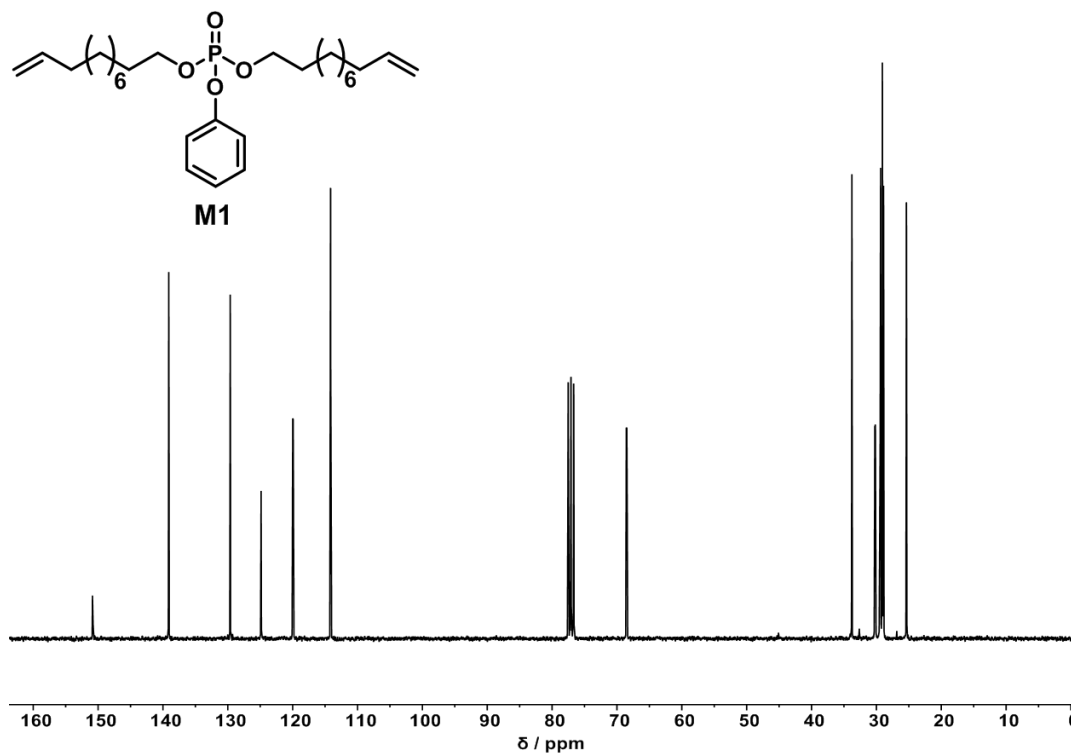
Figure 1.10. ^{13}C (75 MHz) NMR spectra of M1 in CDCl$_3$ at 298 K.
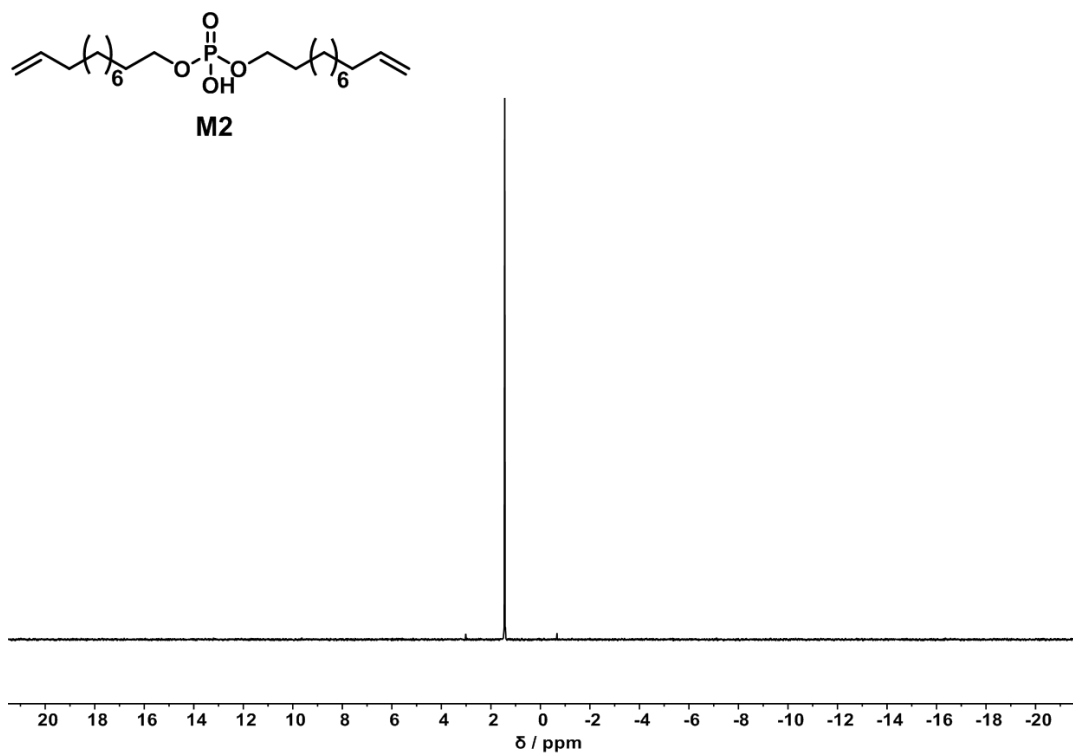
Figure 1.11. ^{31}P (121 MHz) NMR spectra of M2 in CDCl$_3$ at 298 K.
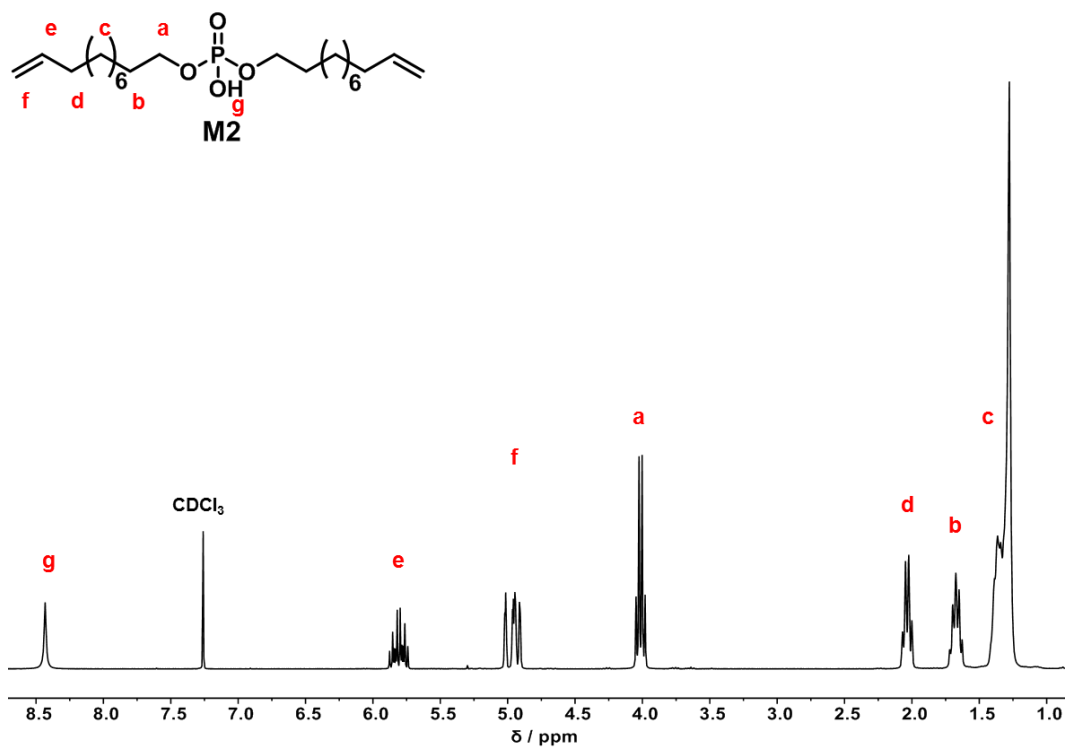
Figure 1.12. ^{1}H (300 MHz) NMR spectra of M2 in CDCl$_3$ at 298 K.
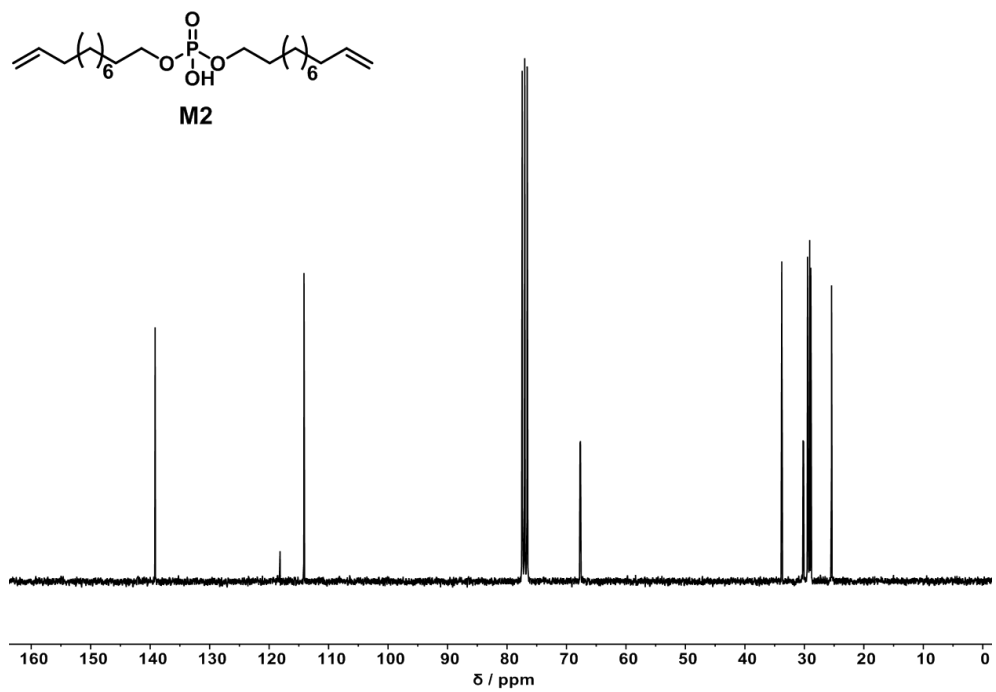
Figure 1.13. ^{13}C (75 MHz) NMR spectra of M2 in CDCl$_3$ at 298 K.

4.4.2 Polymer NMR Spectra
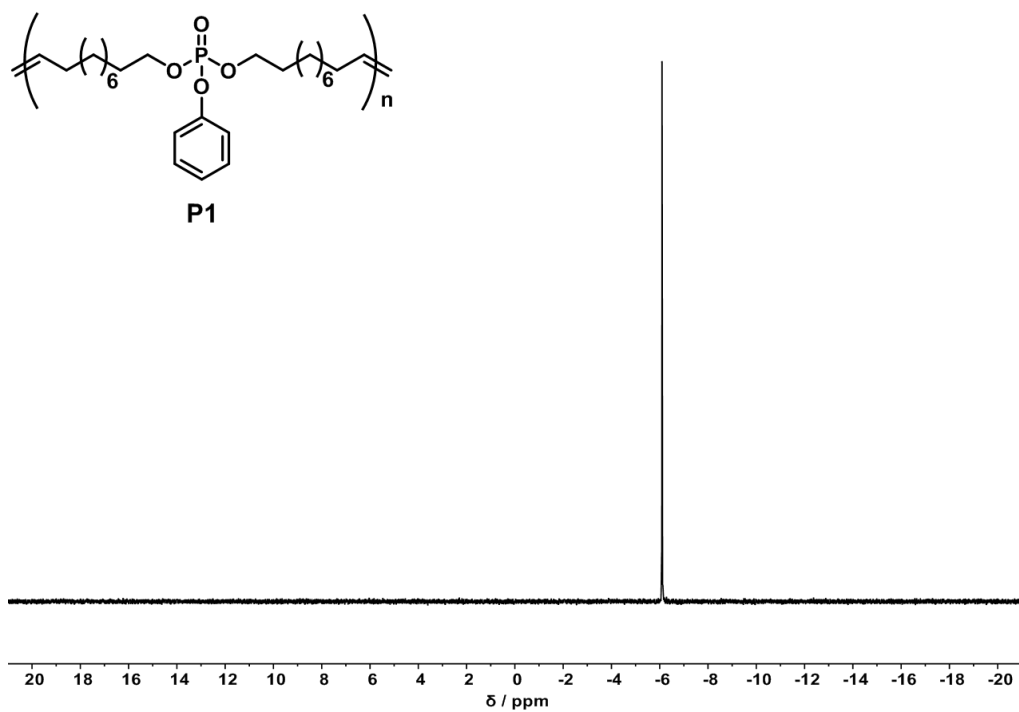
Figure 1.14. ^{31}P (121 MHz) NMR spectra of P1 in CDCl$_3$ at 298 K.
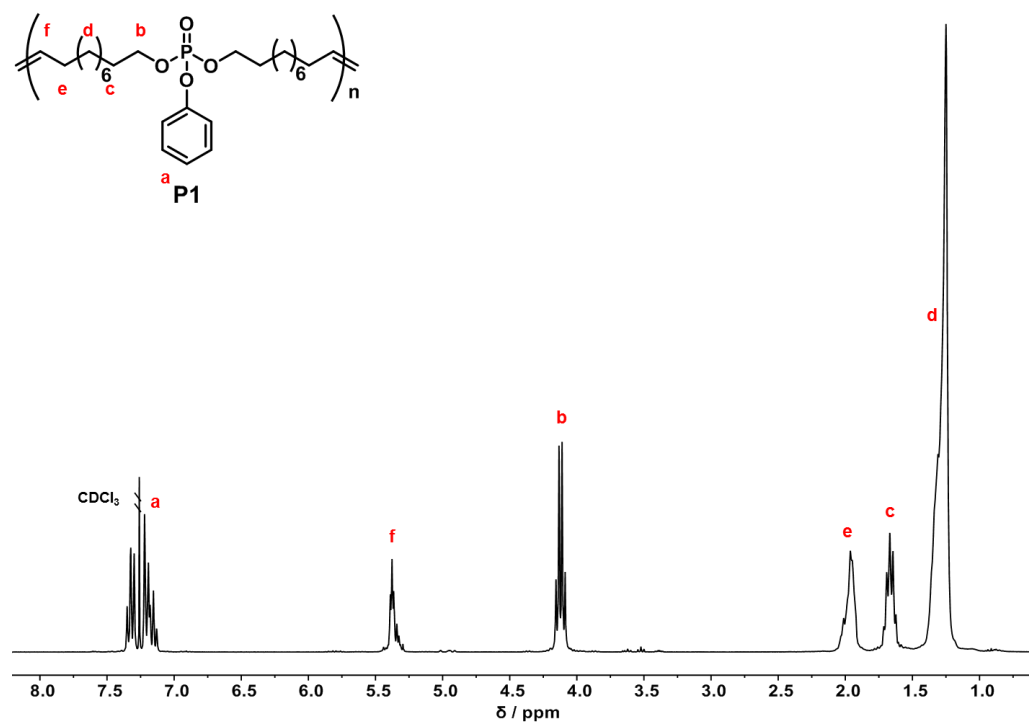
Figure 1.15. ^{1}H (300 MHz) NMR spectra of P1 in CDCl$_3$ at 298 K.
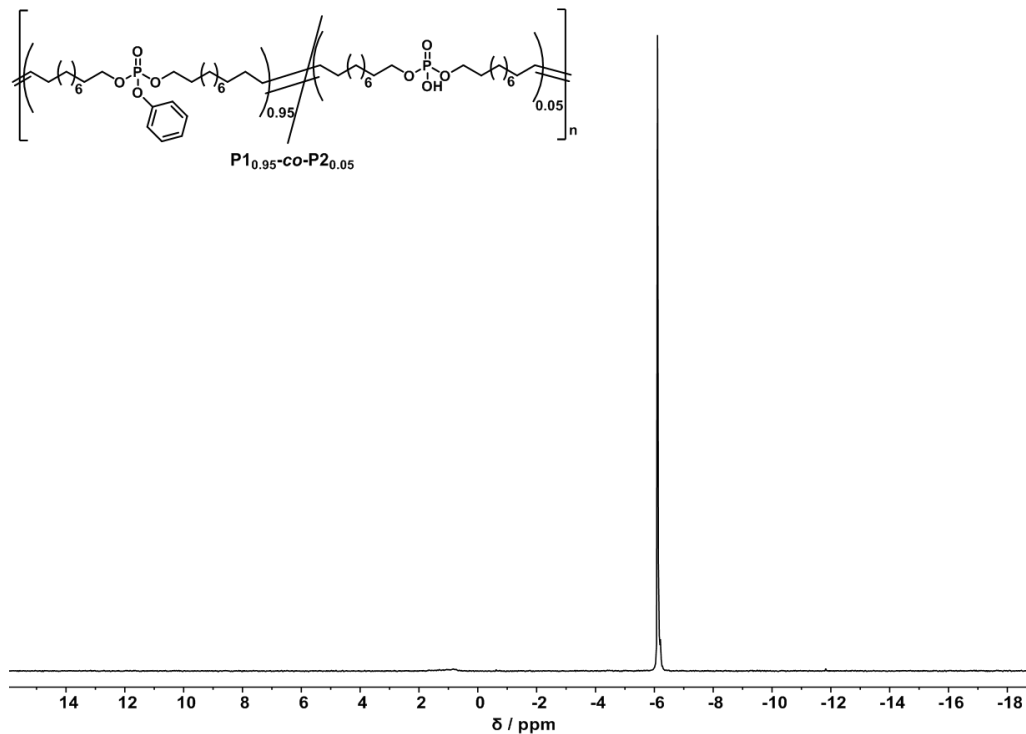
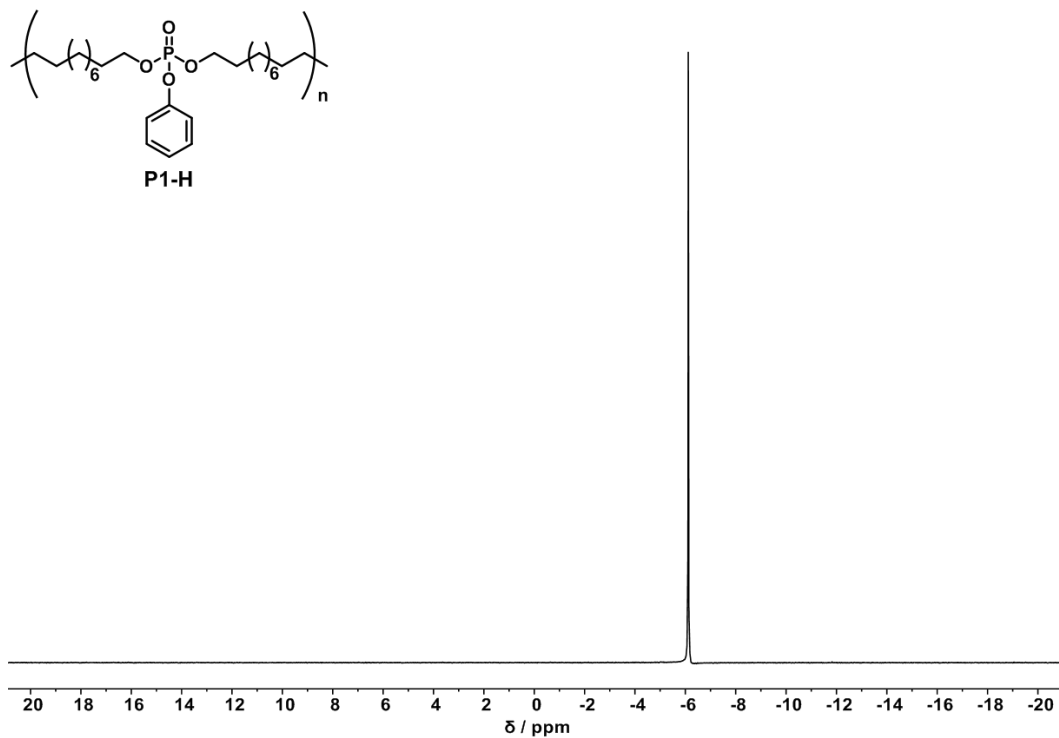**Figure 1.16. ^{31}P (202 MHz) NMR spectra of P1$_{0.95}$-co-P2$_{0.05}$ in CDCl$_3$ at 298 K.**
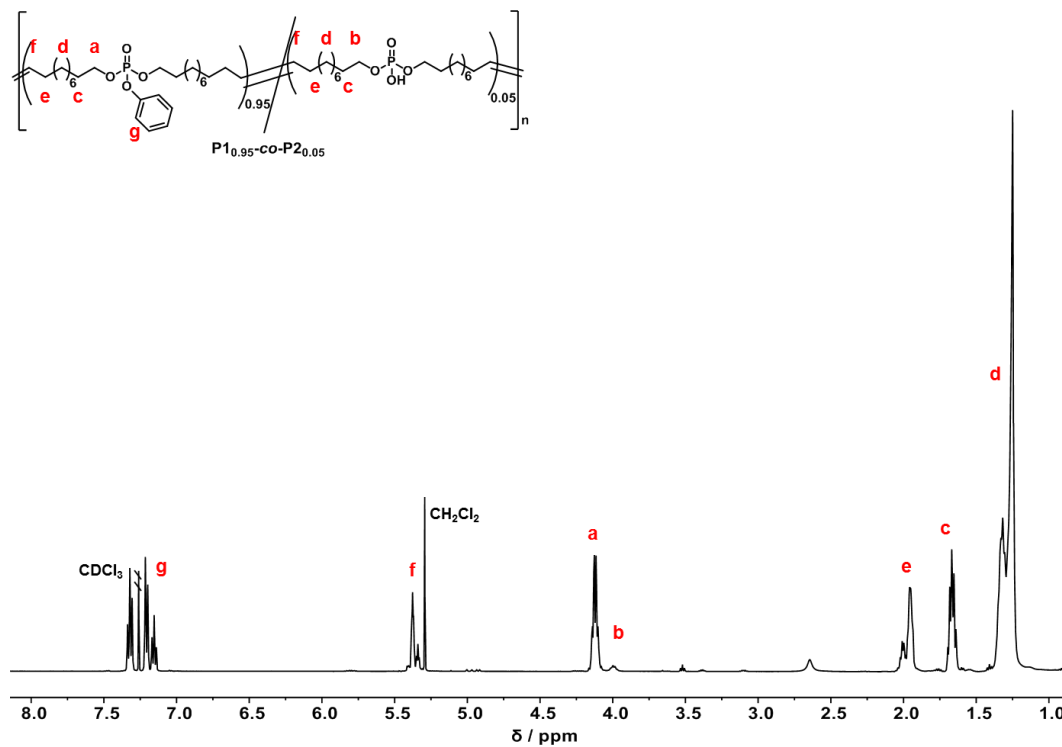
Figure 1.17. ^{1}H (500 MHz) NMR spectra of $P1_{0.95}$-co-$P2_{0.05}$ in CDCl$_3$ at 298 K.
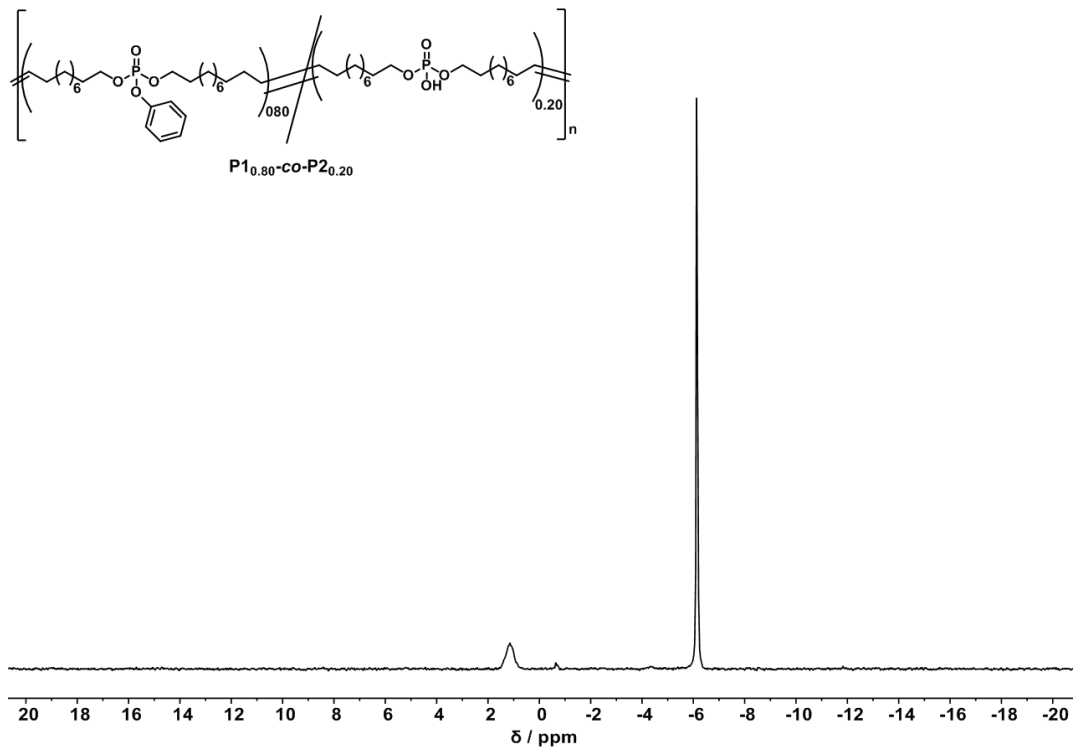
Figure 1.18. ^{31}P (121 MHz) NMR spectra of $P1_{0.80}$-co-$P2_{0.20}$ in CDCl$_3$ at 298 K.
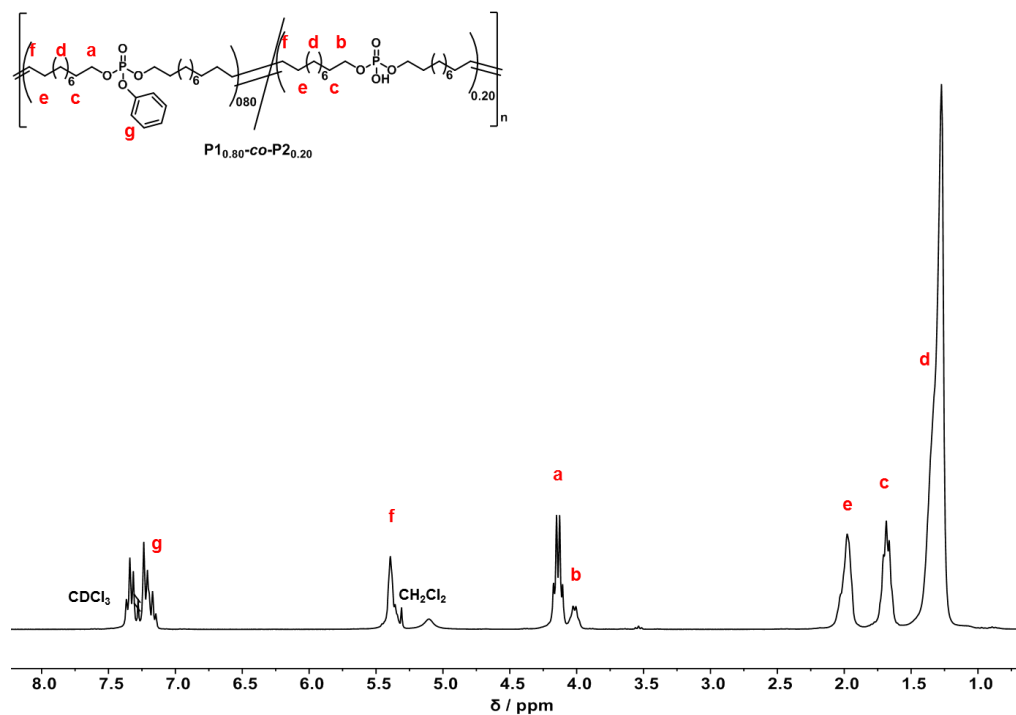
Figure 1.19. ^{1}H (300 MHz) NMR spectra of P1$_{0.80}$-*co*-P2$_{0.20}$ in CDCl$_3$ at 298 K.
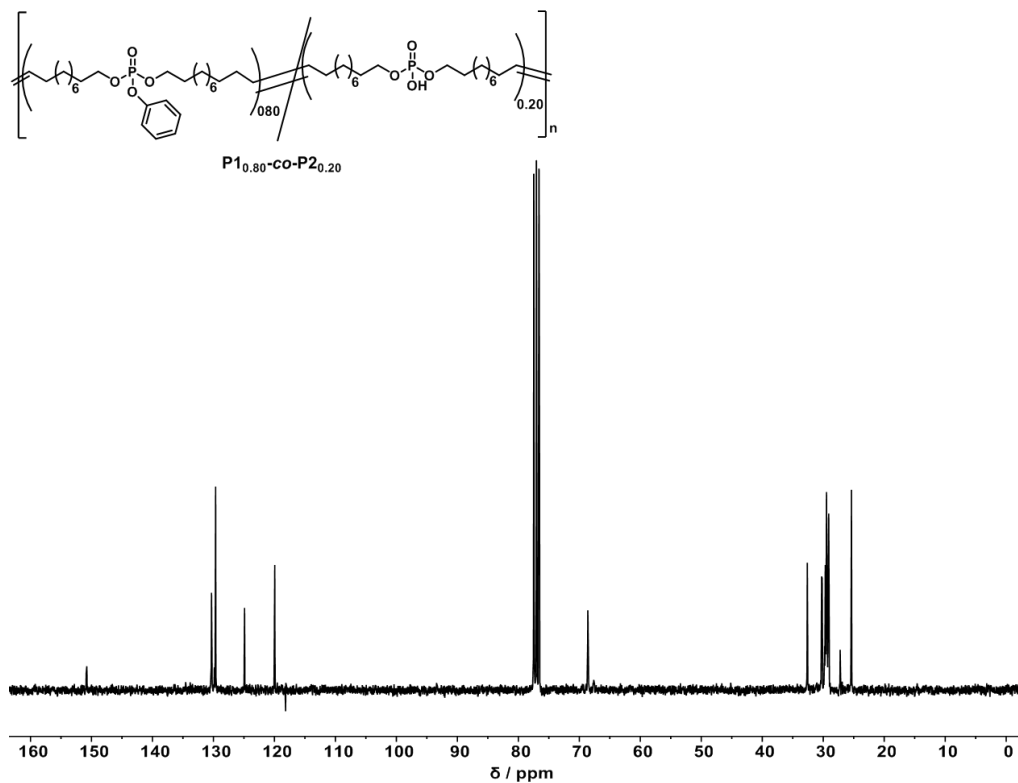
P1$_{0.80}$-*co*-P2$_{0.20}$

Figure 1.20. ^{13}C (75 MHz) NMR spectra of P1$_{0.80}$-*co*-P2$_{0.20}$ in CDCl$_3$ at 298 K.
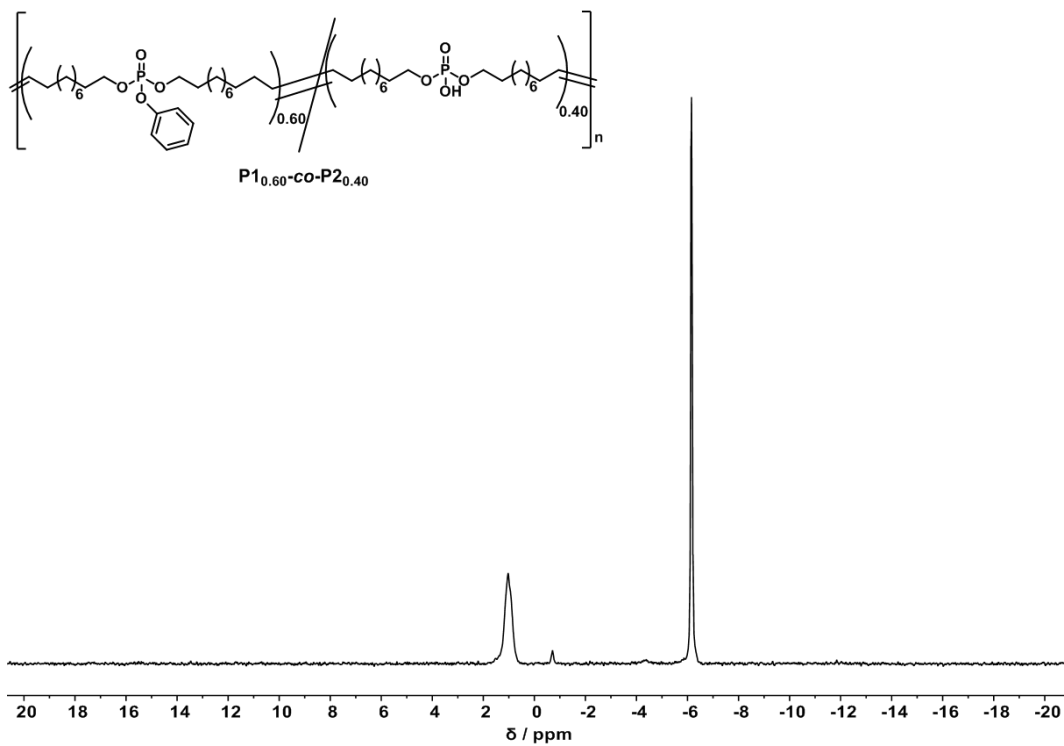
Figure 1.21. ^{31}P (121 MHz) NMR spectra of P1$_{0.60}$-*co*-P2$_{0.40}$ in CDCl$_3$ at 298 K.
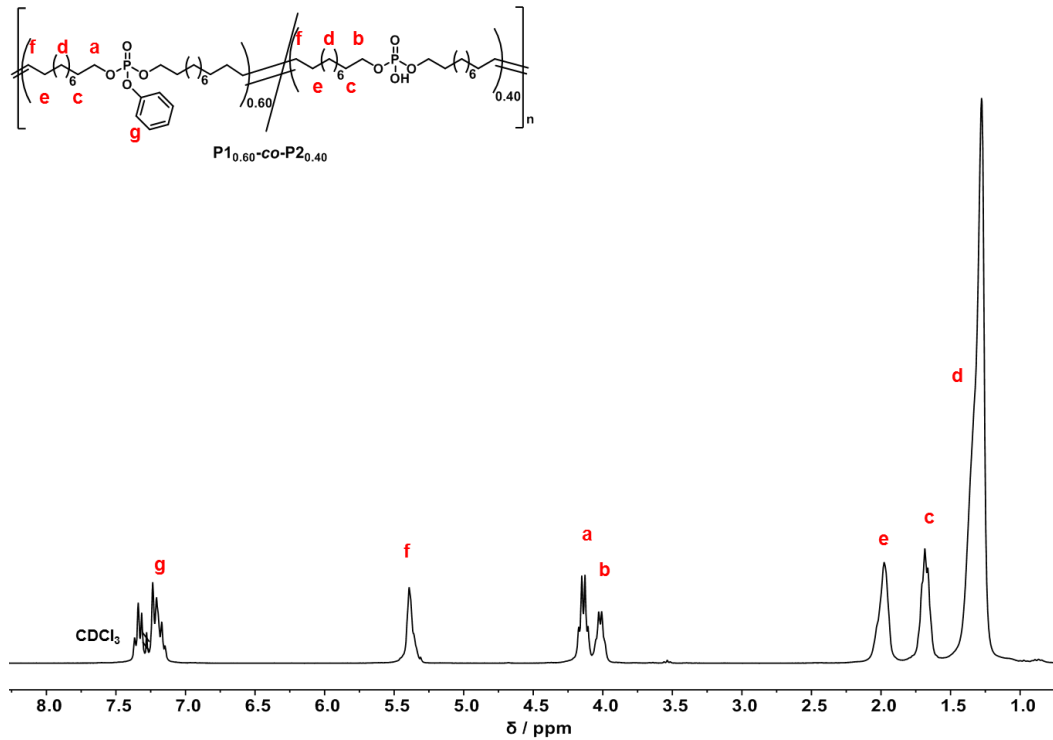
Figure 1.22. ^{1}H (300 MHz) NMR spectra of P1$_{0.60}$-*co*-P2$_{0.40}$ in CDCl$_3$ at 298 K.
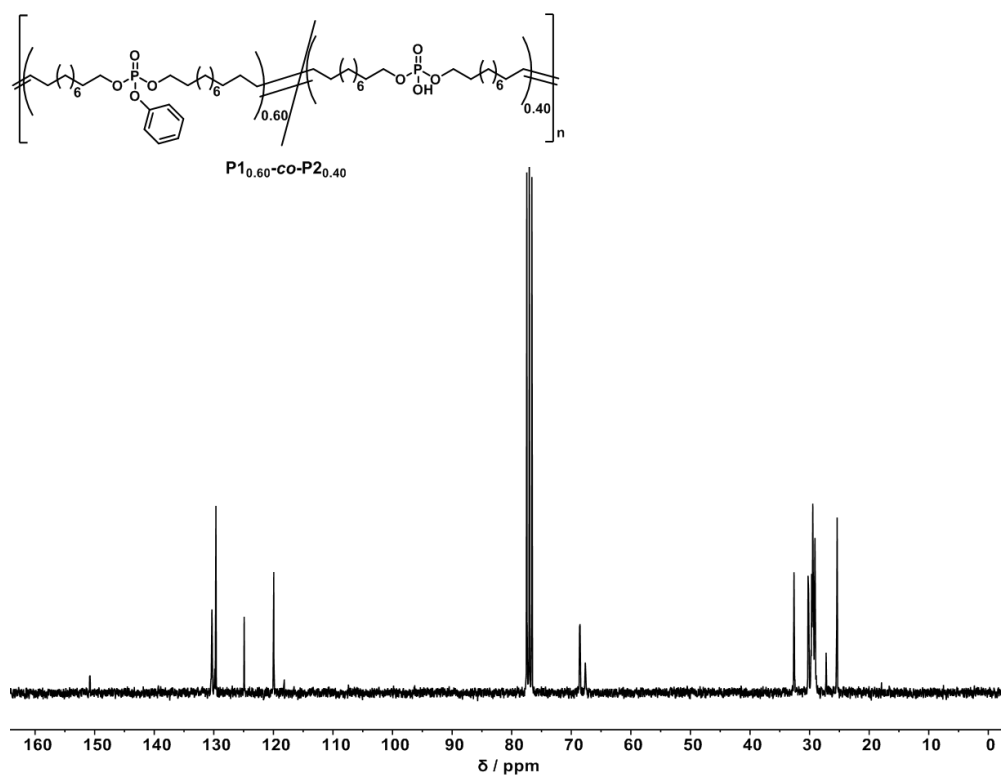
P1$_{0.60}$-co-P2$_{0.40}$

Figure 1.23. ^{13}C (75 MHz) NMR spectra of P1$_{0.60}$-co-P2$_{0.40}$ in CDCl$_3$ at 298 K.
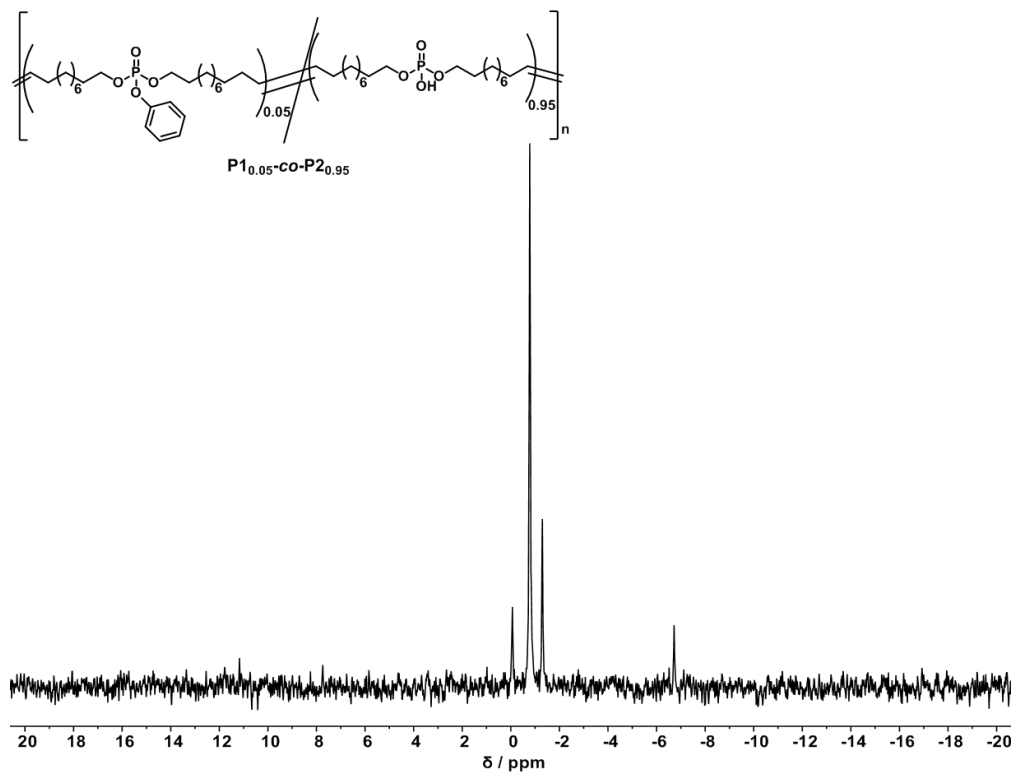
P1$_{0.05}$-co-P2$_{0.95}$

Figure 1.24. ^{31}P (121 MHz) NMR spectra of P1$_{0.05}$-*co*-P2$_{0.95}$ in CDCl$_3$ at 298 K.
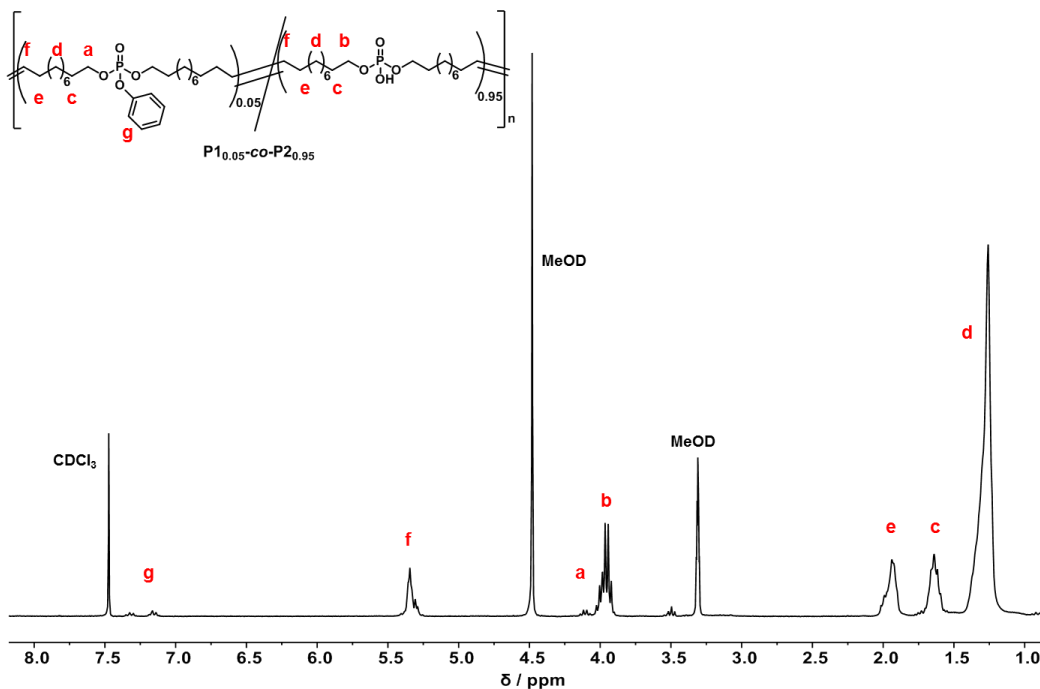
Figure 1.25. ^{1}H (300 MHz) NMR spectra of P1$_{0.05}$-*co*-P2$_{0.95}$ in CDCl$_3$ at 298 K.
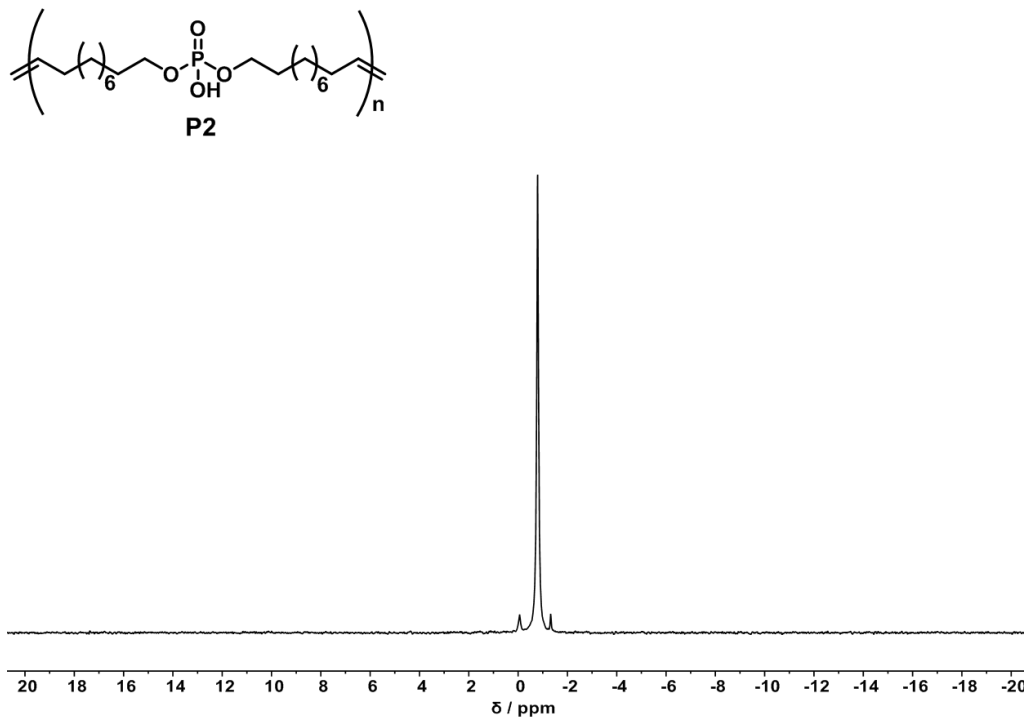
Figure 1.26. ^{31}P (121 MHz) NMR spectra of P2 in CDCl$_3$:CD$_3$OD 4:2 at 298 K.
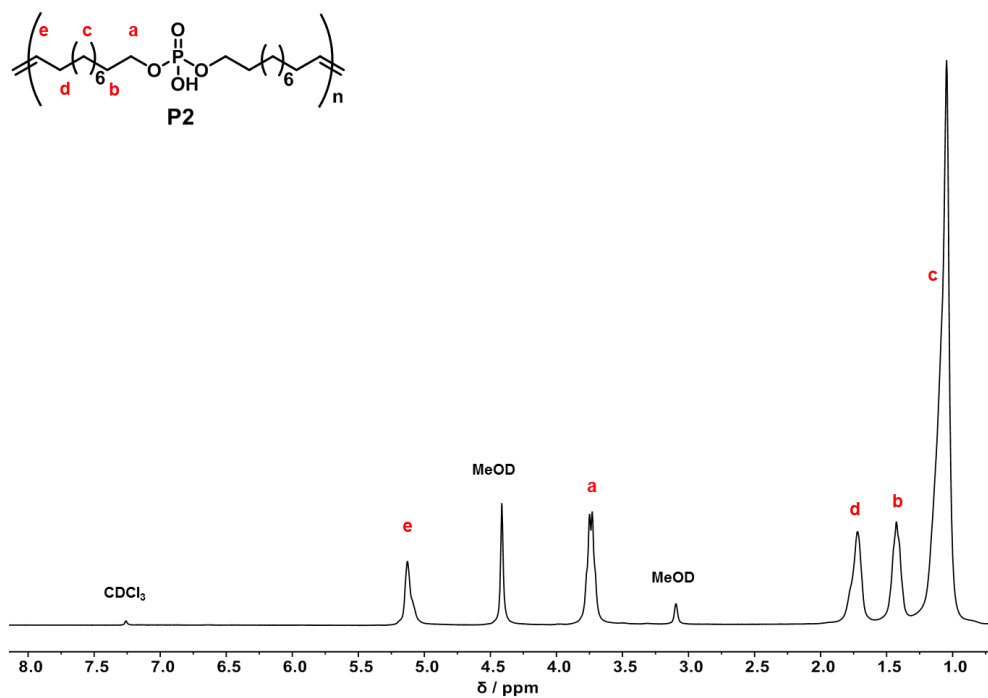
Figure 1.27. ^{1}H (300 MHz) NMR spectra of P2 in CDCl$_3$:CD$_3$OD 4:2 at 298 K.
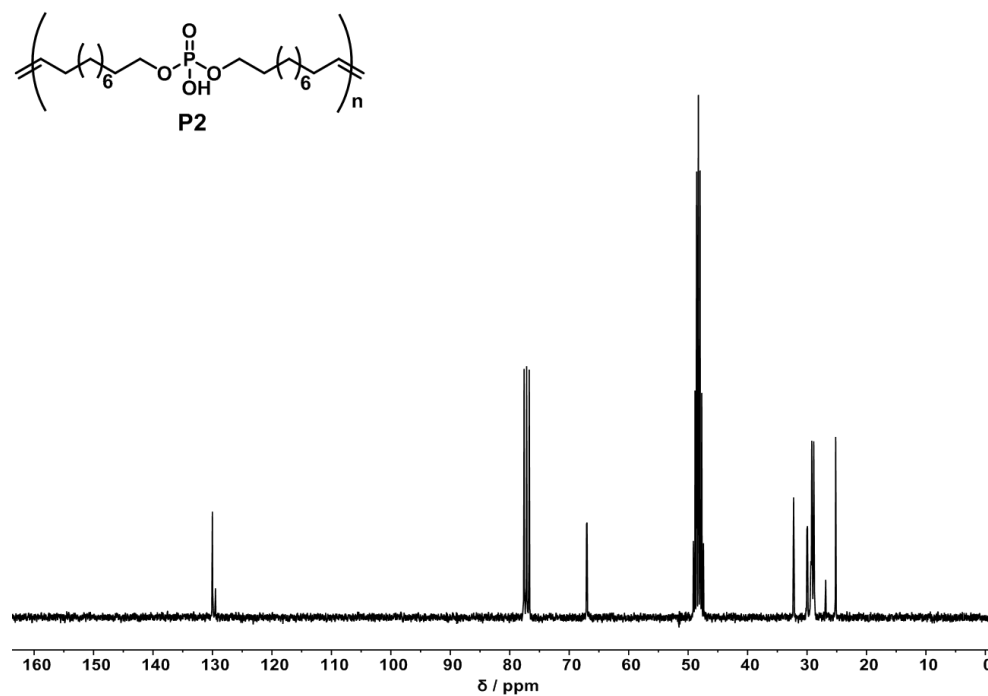
Figure 1.28. ^{13}C (75 MHz) NMR spectra of P2 in CDCl$_3$:CD$_3$OD 4:2 at 298 K.

Figure 1.29. ^{31}P (283 MHz) NMR spectra of P1-H in CDCl$_3$ at 298 K.
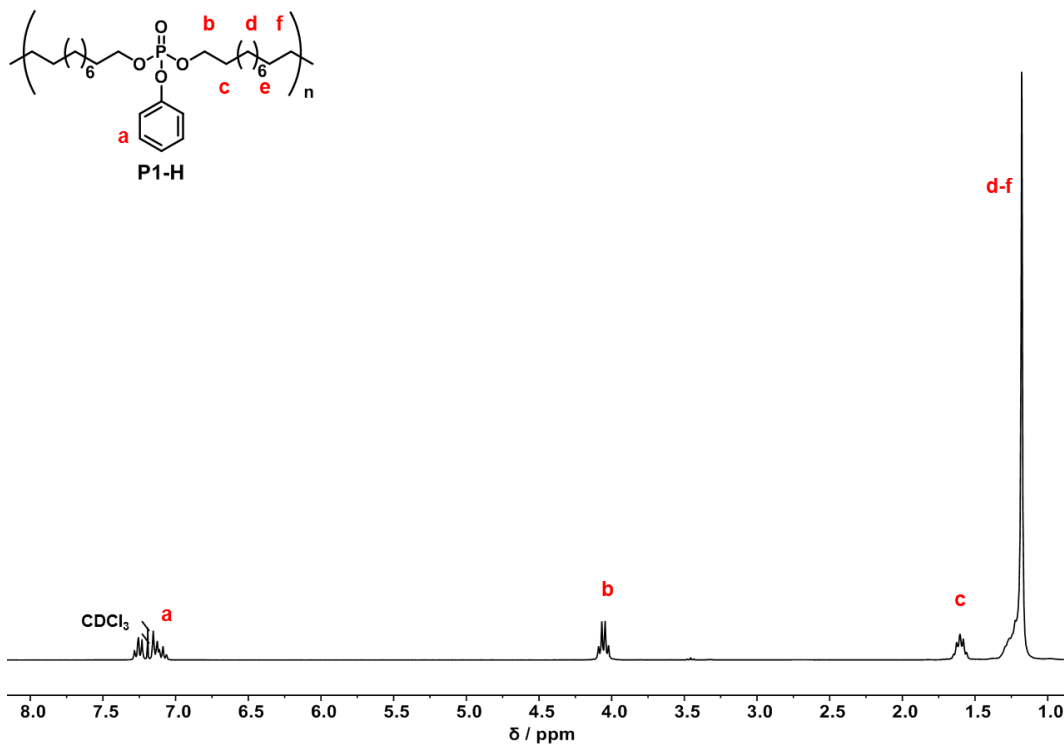
Figure 1.30. ^{1}H (300 MHz) NMR spectra of P1-H in CDCl$_3$ at 298 K.
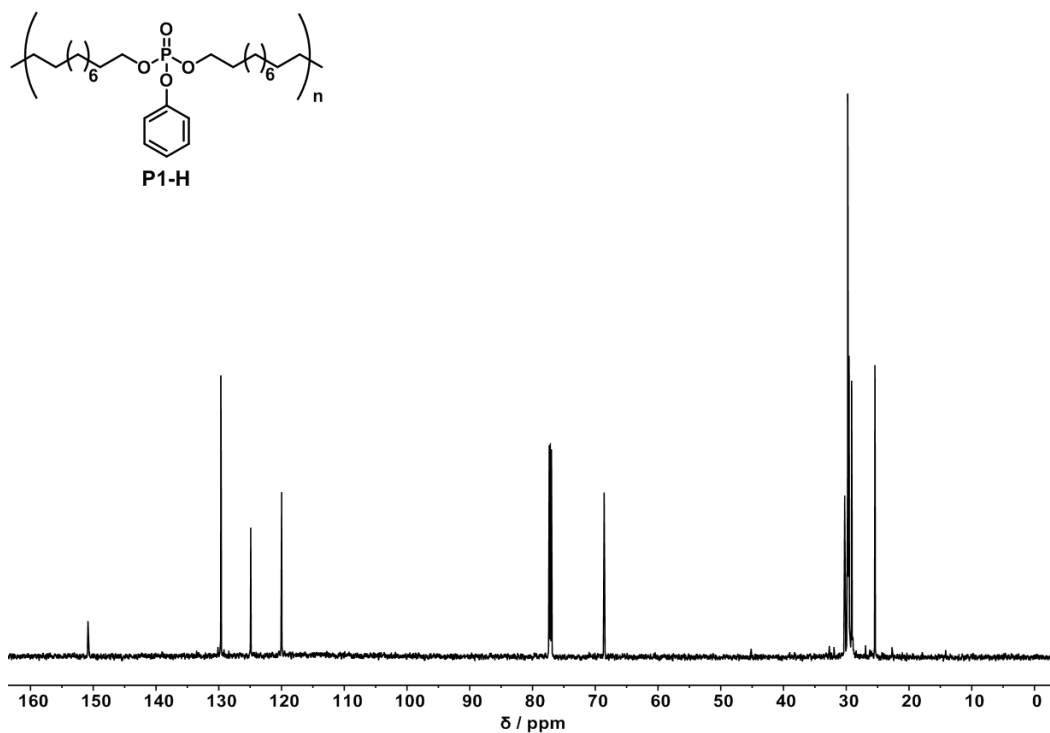
Figure 1.31. ^{13}C (176 MHz) NMR spectra of P1-H in CDCl$_3$ at 298 K.
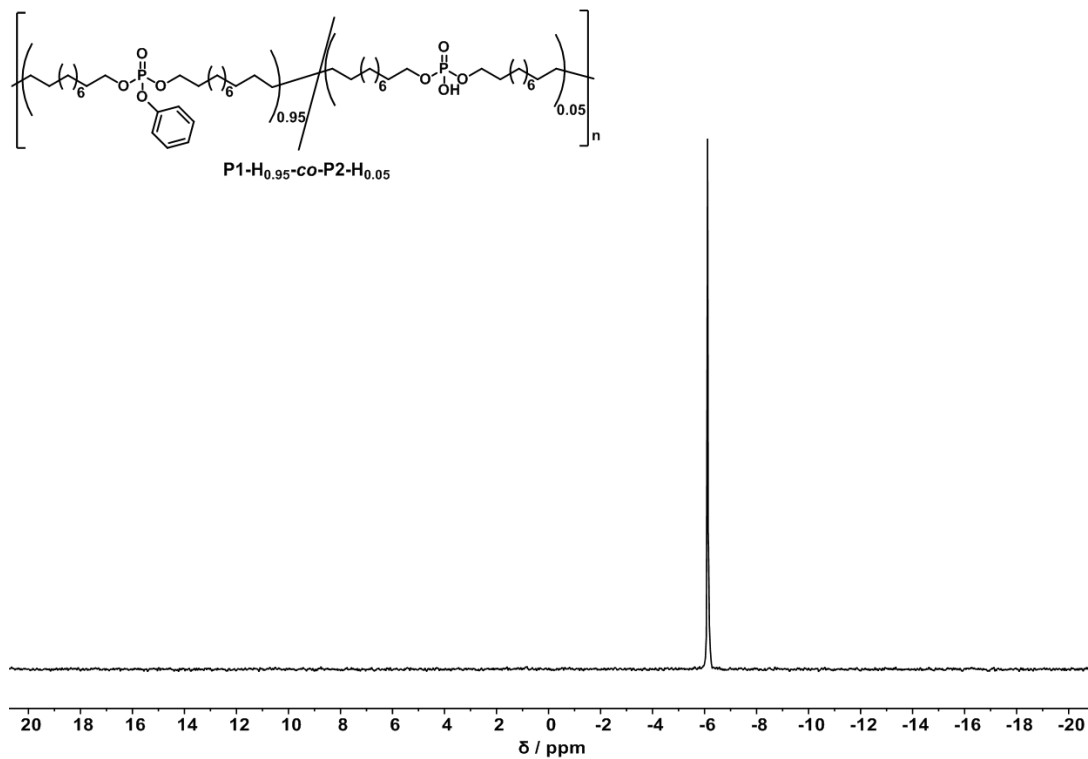
Figure 1.32. ^{31}P (121 MHz) NMR spectra of P1-H$_{0.95}$-co-P2-H$_{0.05}$ in CDCl$_3$ at 298 K.
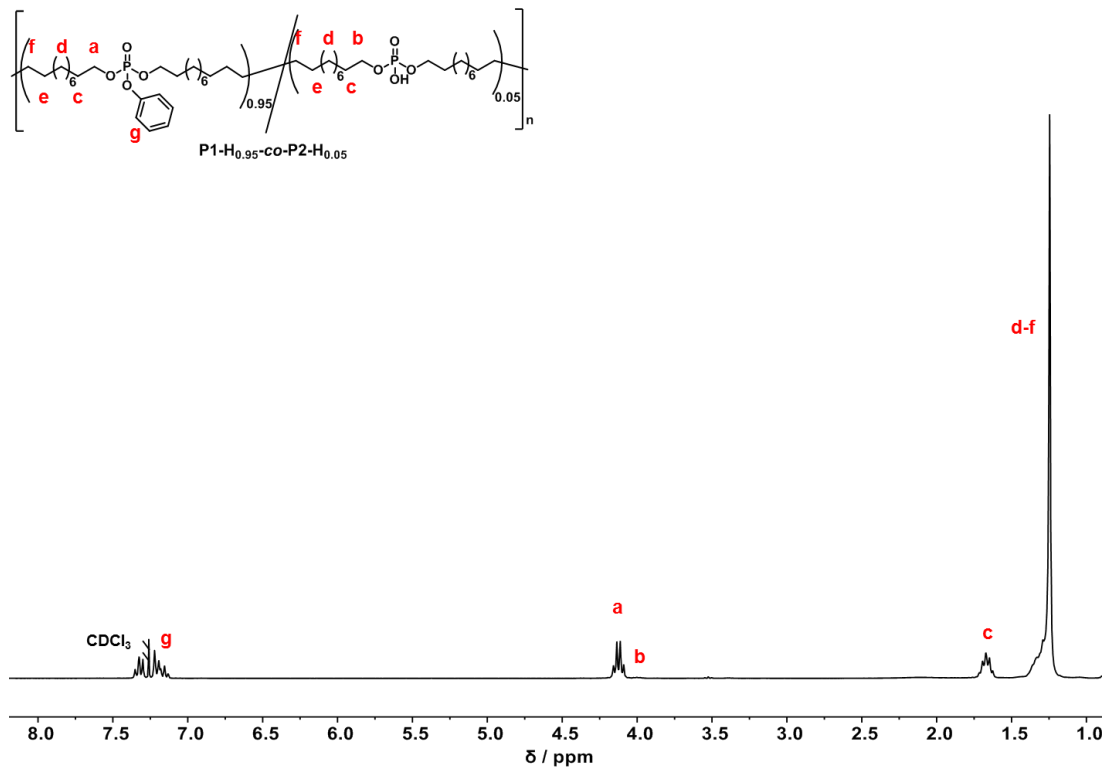
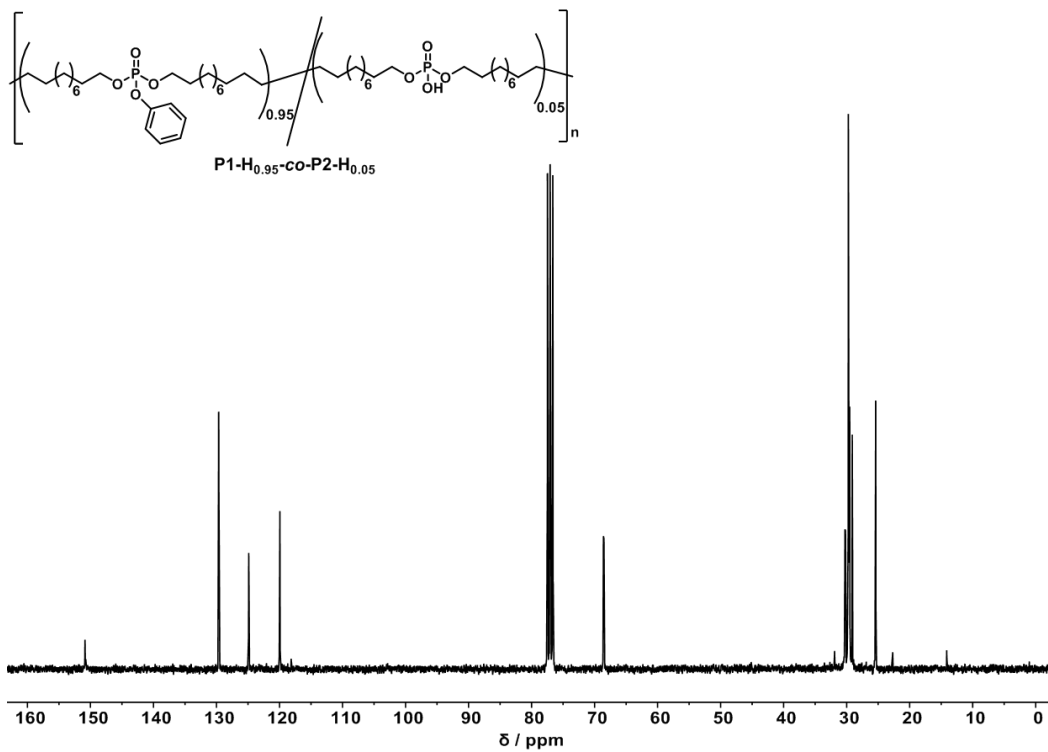**Figure 1.33. ^{1}H (300 MHz) NMR spectra of P1-H$_{0.95}$-co-P2-H$_{0.05}$ in CDCl$_3$ at 298 K.**

Figure 1.34. ^{13}C (75 MHz) NMR spectra of **P1-H$_{0.95}$-*co*-P2-H$_{0.05}$** in CDCl$_3$ at 298 K.
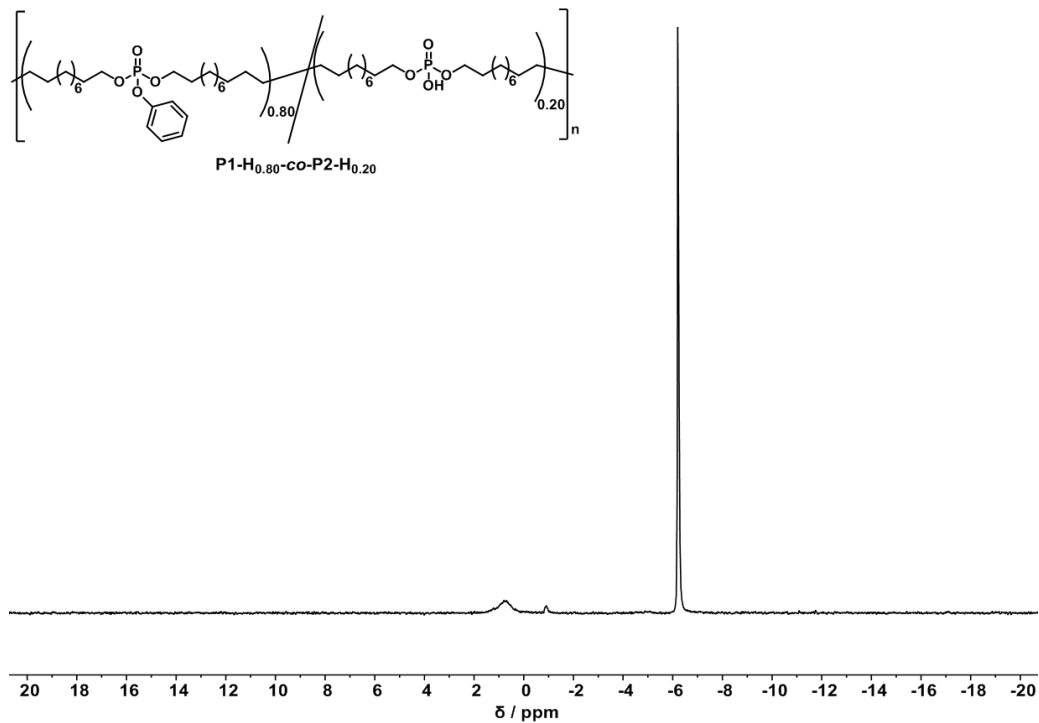
Figure 1.35. ^{31}P (202 MHz) NMR spectra of **P1-H$_{0.80}$-*co*-P2-H$_{0.20}$** in CD$_2$Cl$_2$ at 298 K.
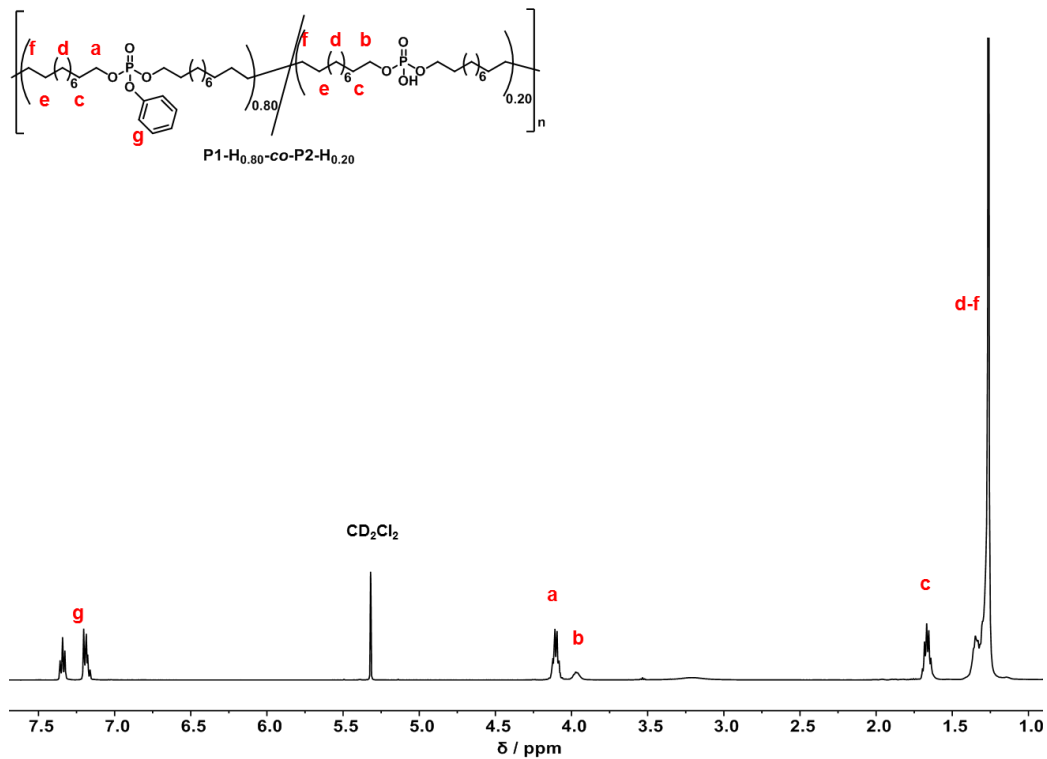
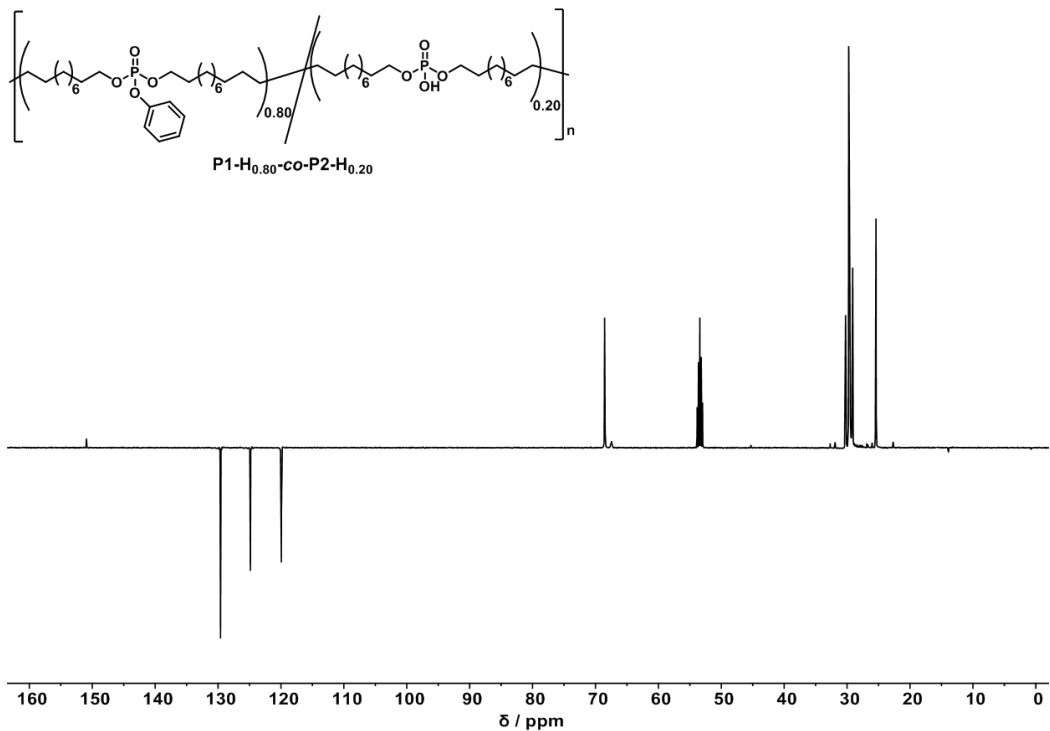**Figure 1.36.** ^{1}H (500 MHz) NMR spectra of P1-H$_{0.80}$-*co*-P2-H$_{0.20}$ in CD$_2$Cl$_2$ at 298 K.

Figure 1.37. ^{13}C (126 MHz) NMR spectra of P1-H$_{0.80}$-*co*-P2-H$_{0.20}$ in CD$_2$Cl$_2$ at 298 K.
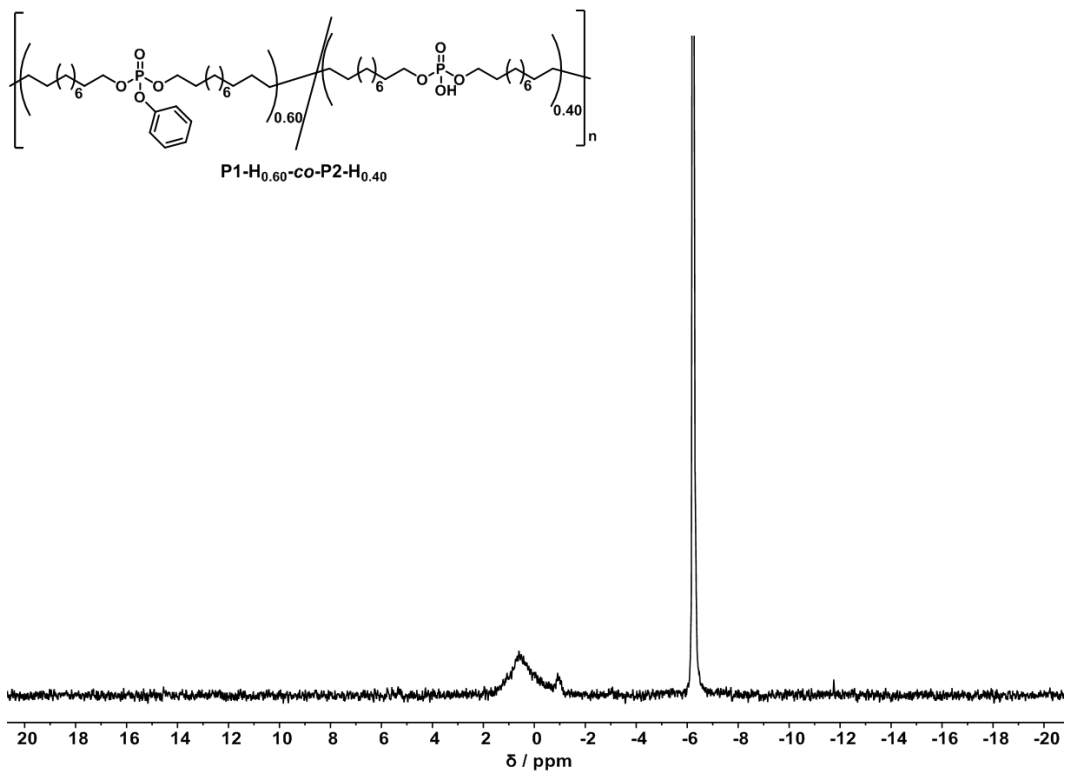
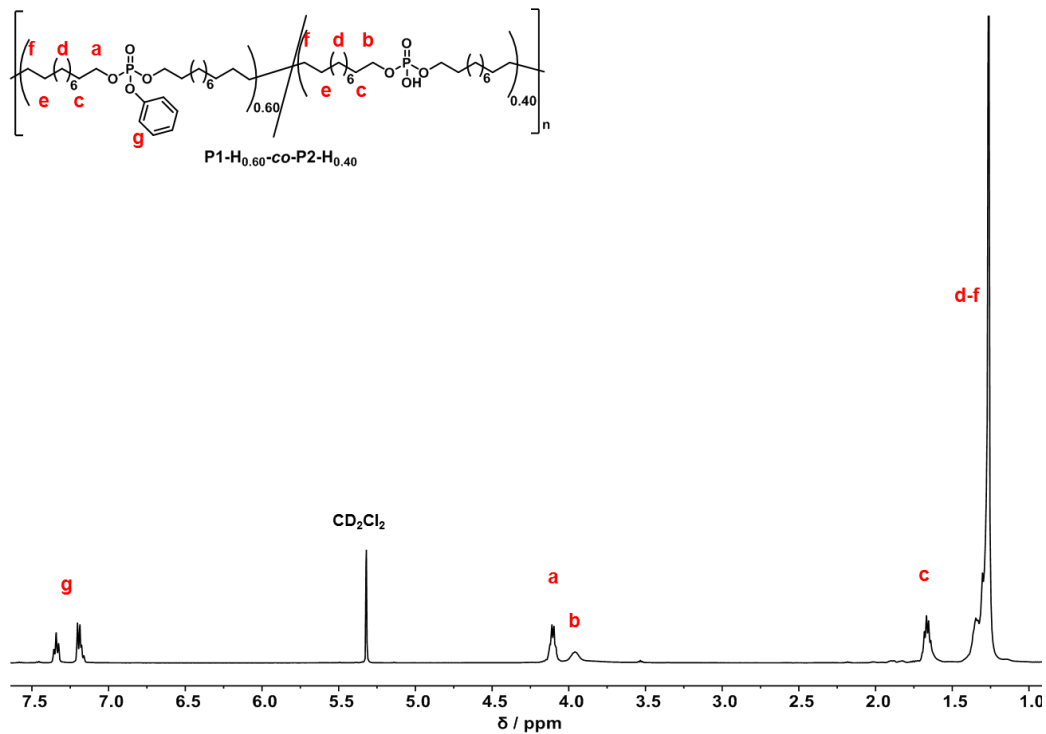**Figure 1.38.** ^{31}P (202 MHz) NMR spectra of P1-H$_{0.60}$-*co*-P2-H$_{0.40}$ in CD$_2$Cl$_2$ at 298 K.

Figure 1.39. ^{1}H (500 MHz) NMR spectra of P1-H$_{0.60}$-*co*-P2-H$_{0.40}$ in CD$_2$Cl$_2$ at 298 K.
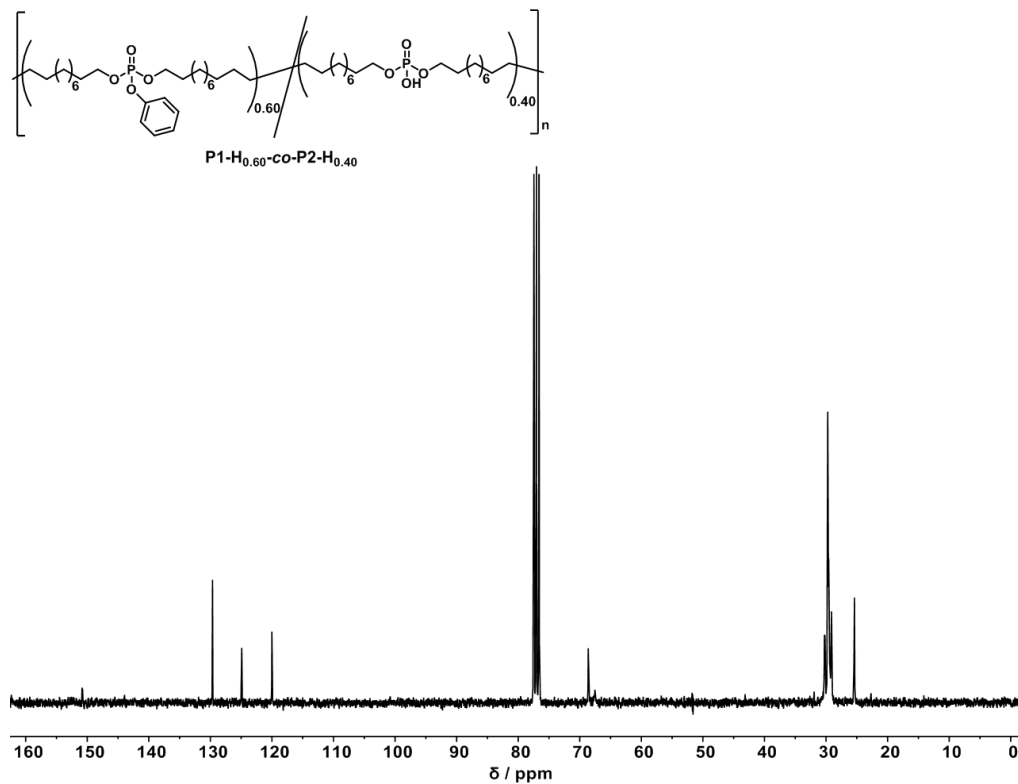
Figure 1.40. ^{13}C (75 MHz) NMR spectra of P1-$H_{0.60}$-*co*-P2-$H_{0.40}$ in $CDCl_3$ at 298 K.
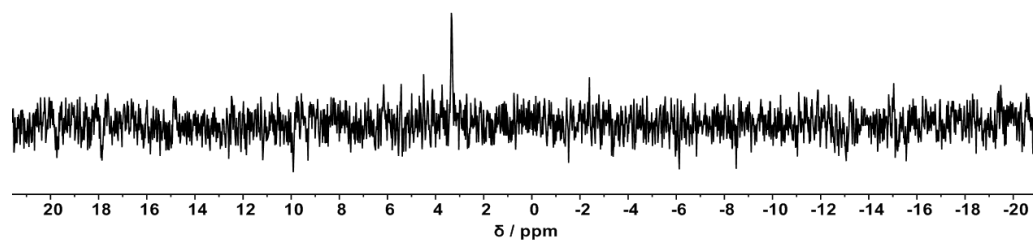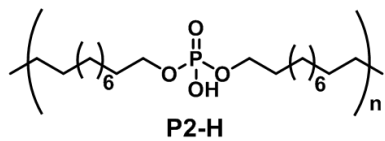
Figure 1.41. ^{31}P (121 MHz) NMR spectra of P2-H in $CDCl_3$:CD_3OD 4:2 at 298 K
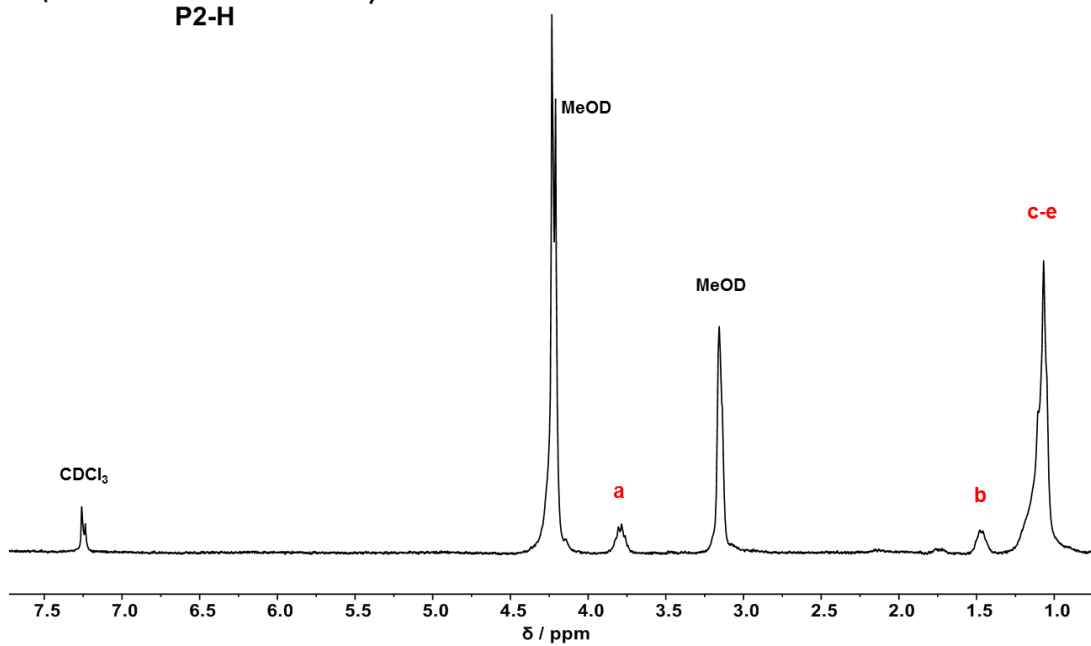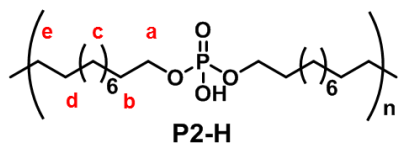
Figure 1.42. ^{1}H (300 MHz) NMR spectra of P2-H in CDCl$_3$:CD$_3$OD 4:2 at 298 K

4.4.3 Esterified Polymer NMR Spectra
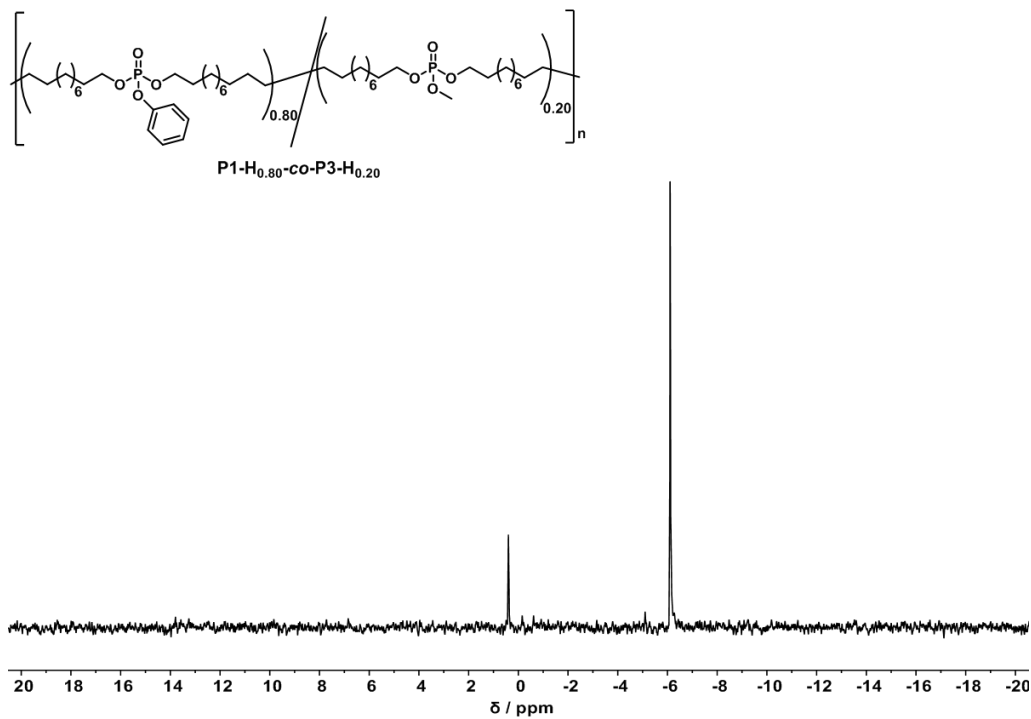
Figure 1.43. ^{31}P (121 MHz) NMR spectra of P1-H$_{0.80}$-co-P3-H$_{0.20}$ in CDCl$_3$ at 298 K.
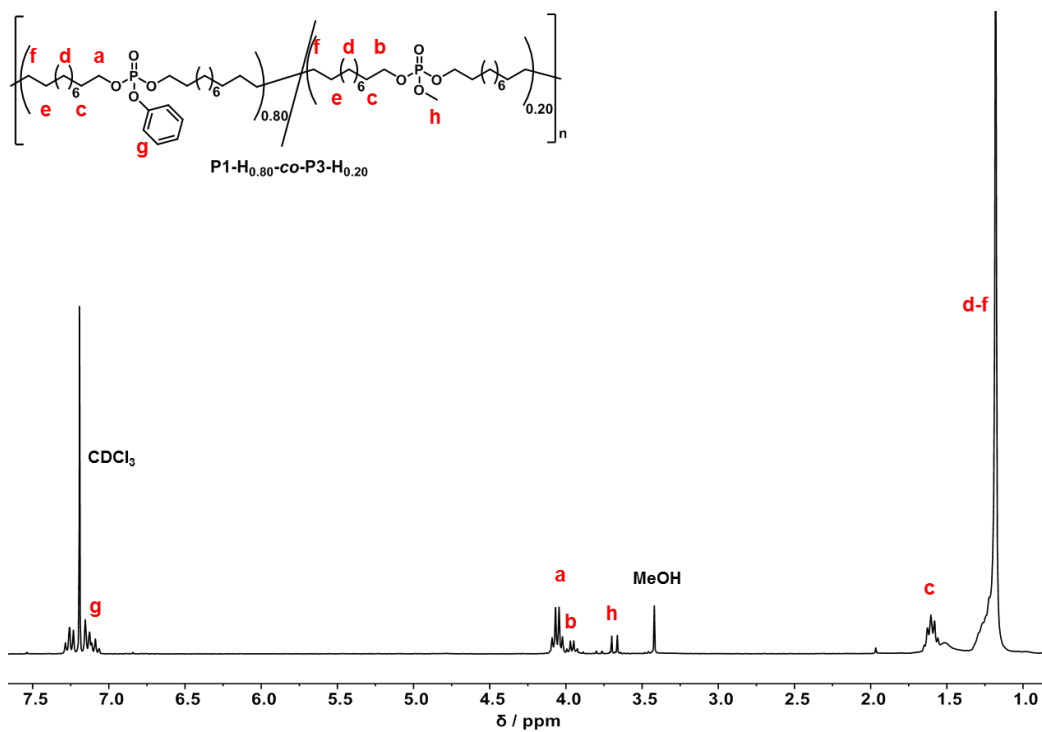
Figure 1.44. ^{1}H (300 MHz) NMR spectra of P1-H$_{0.80}$-co-P3-H$_{0.20}$ in CDCl$_3$ at 298 K.
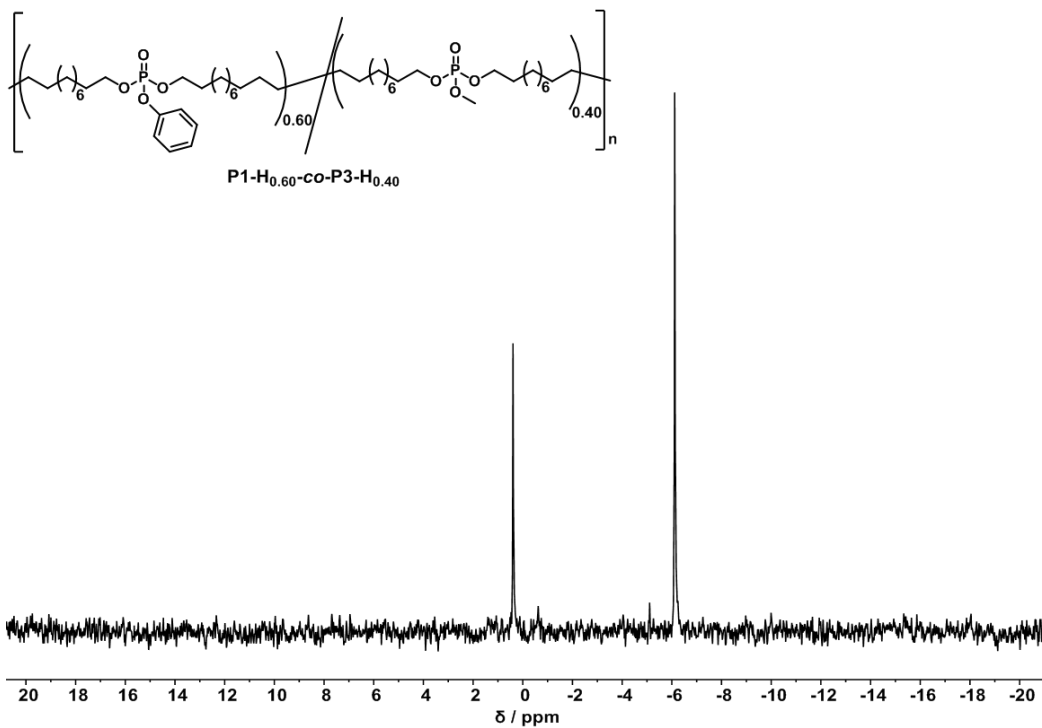
Figure 1.45. ^{31}P (121 MHz) NMR spectra of P1-H$_{0.60}$-co-P3-H$_{0.40}$ in CDCl$_3$ at 298 K.
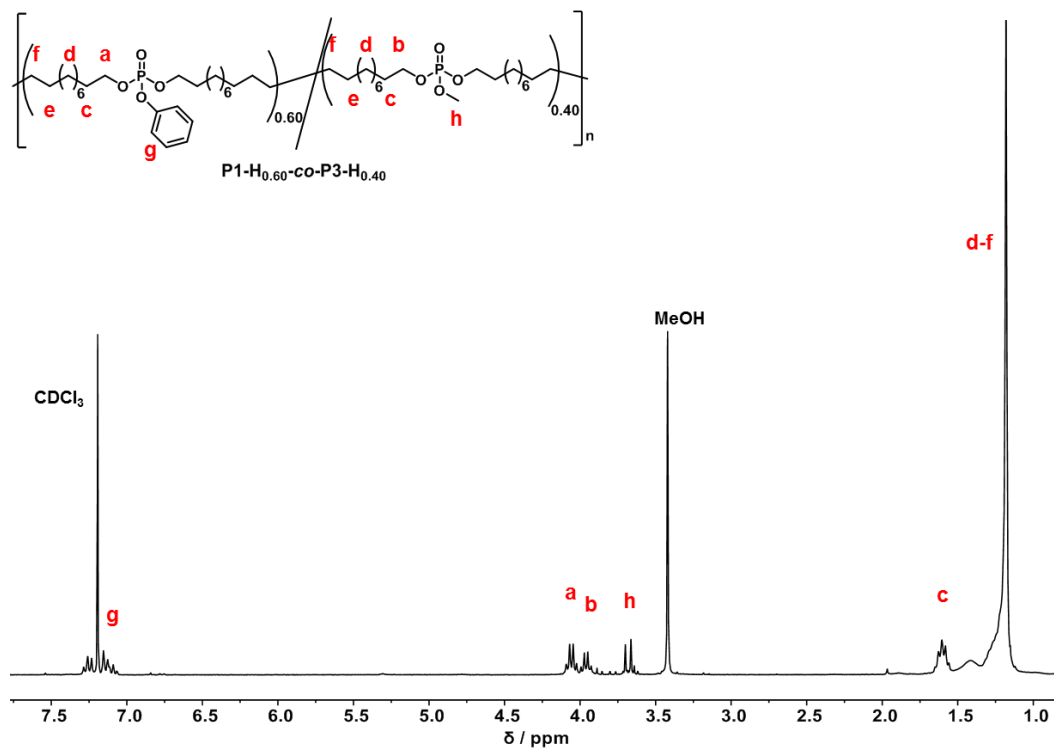
Figure 1.46. ^{1}H (300 MHz) NMR spectra of P1-H$_{0.60}$-co-P3-H$_{0.40}$ in CDCl$_3$ at 298 K.
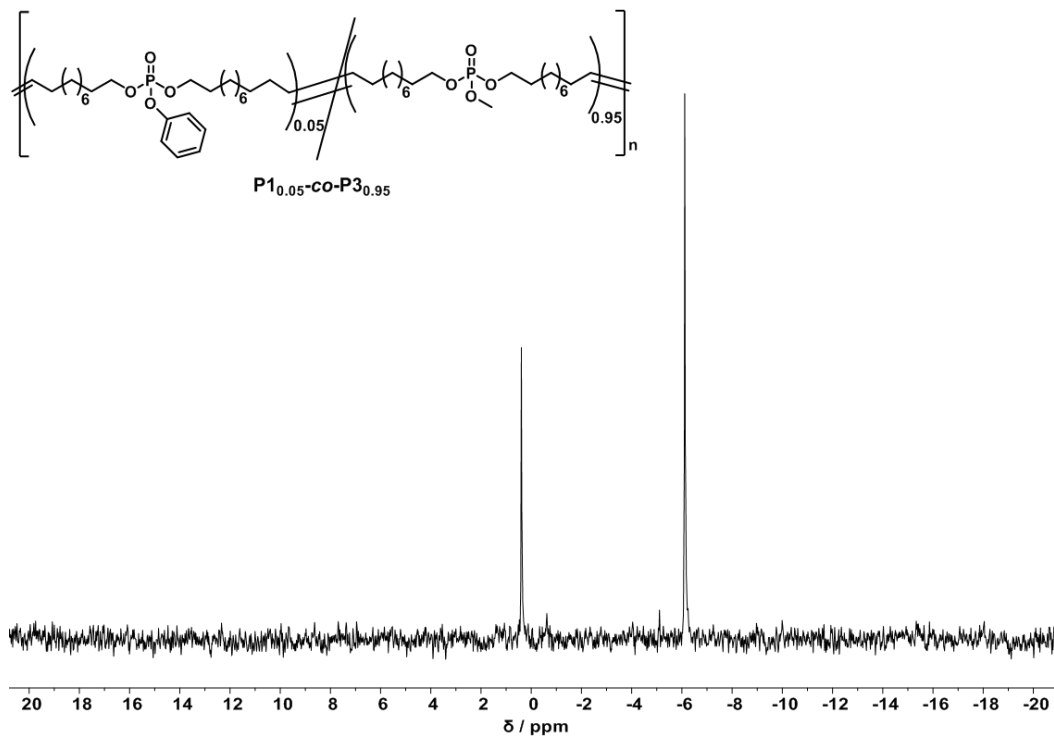
Figure 1.47. ^{31}P (121 MHz) NMR spectra of P1$_{0.05}$-co-P3$_{0.95}$ in CDCl$_3$ at 298 K.
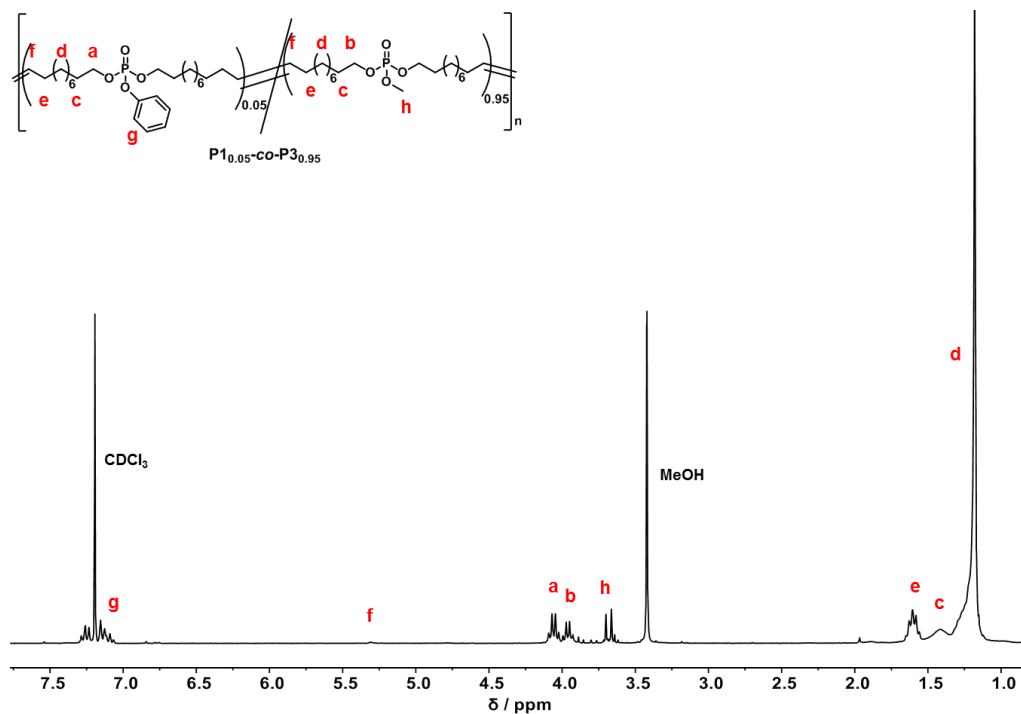
Figure 1.48. ^{1}H (300 MHz) NMR spectra of P1$_{0.05}$-co-P3$_{0.95}$ in CDCl$_3$ at 298 K.
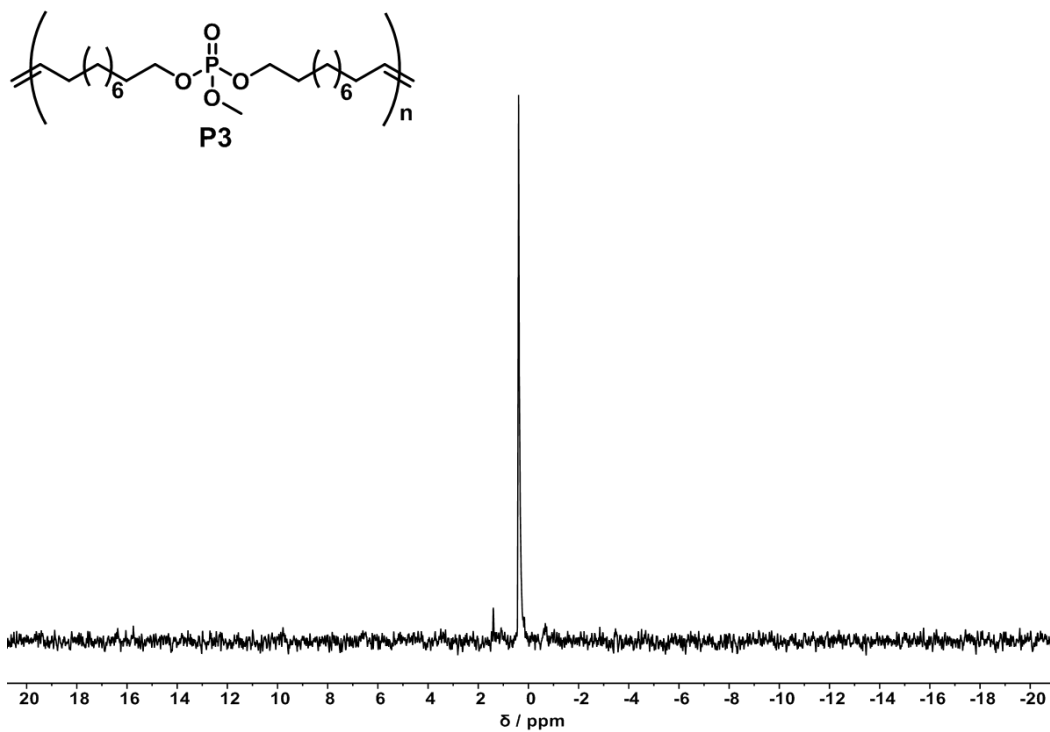
Figure 1.49. ^{31}P (121 MHz) NMR spectra of P3 in CDCl$_3$ at 298 K.
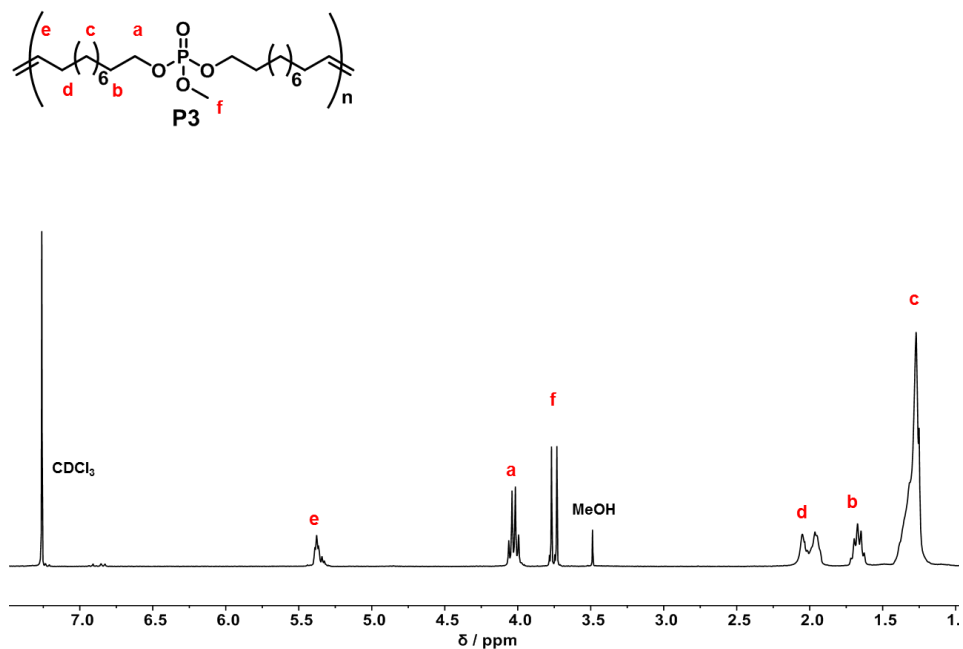
Figure 1.50. ¹H (300 MHz) NMR spectra of P3 in CDCl₃ at 298 K.

4.5   DSC, TGA
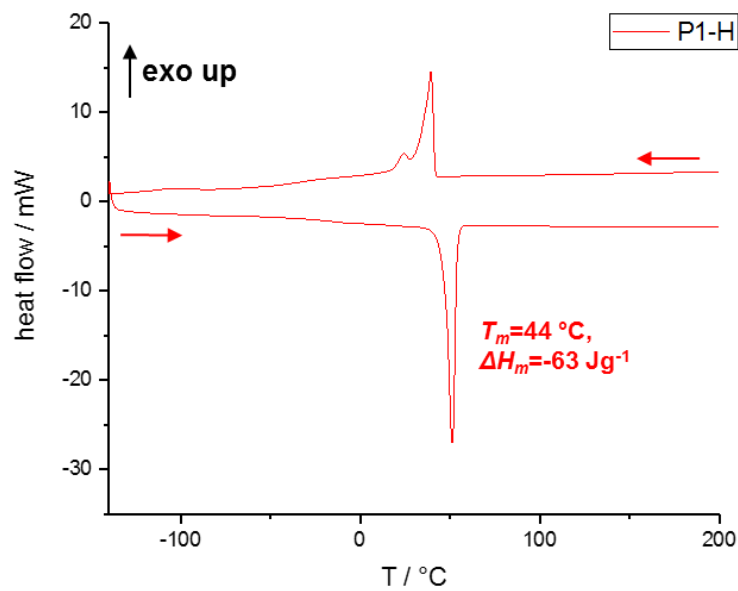
Figure 1.51. DSC of P1-H with a heating (second run) and cooling rate of 10 K min⁻¹.
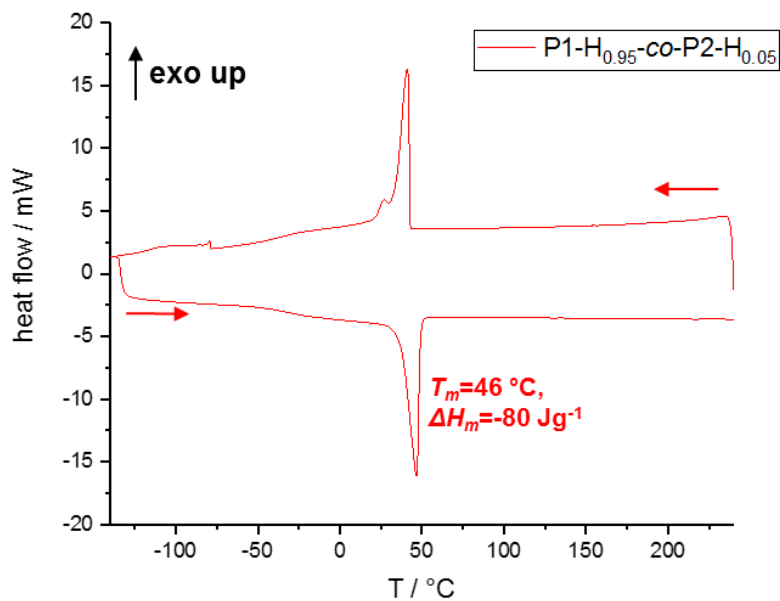
Figure 1.52. DSC of P1-H$_{0.95}$-*co*-P2-H$_{0.05}$ with a heating (second run) and cooling rate of 10 K min^{-1}.
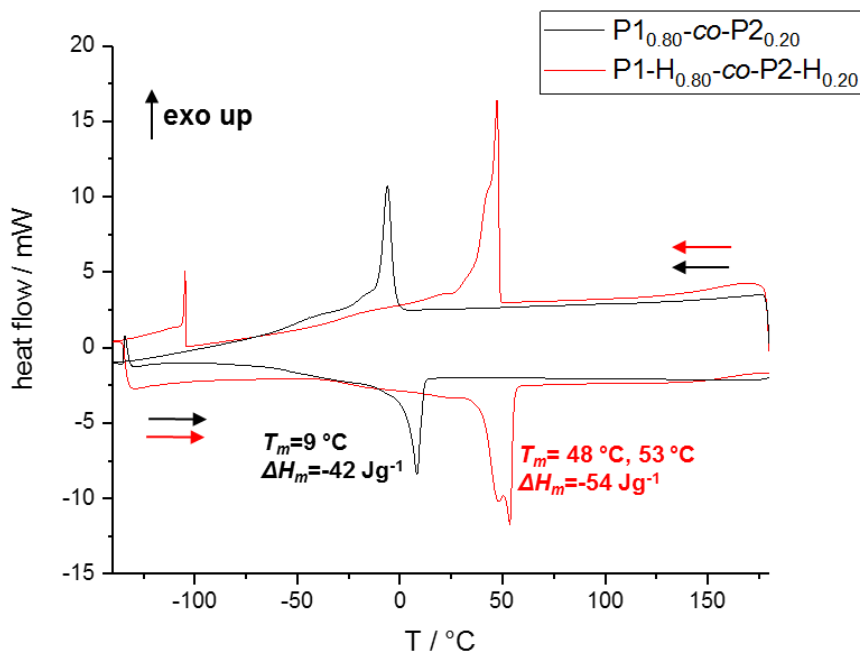
Figure 1.53. DSC of P1$_{0.80}$-*co*-P2$_{0.20}$ and P1-H$_{0.80}$-*co*-P2-H$_{0.20}$ with a heating (second run) and cooling rate of 10 K min^{-1}.
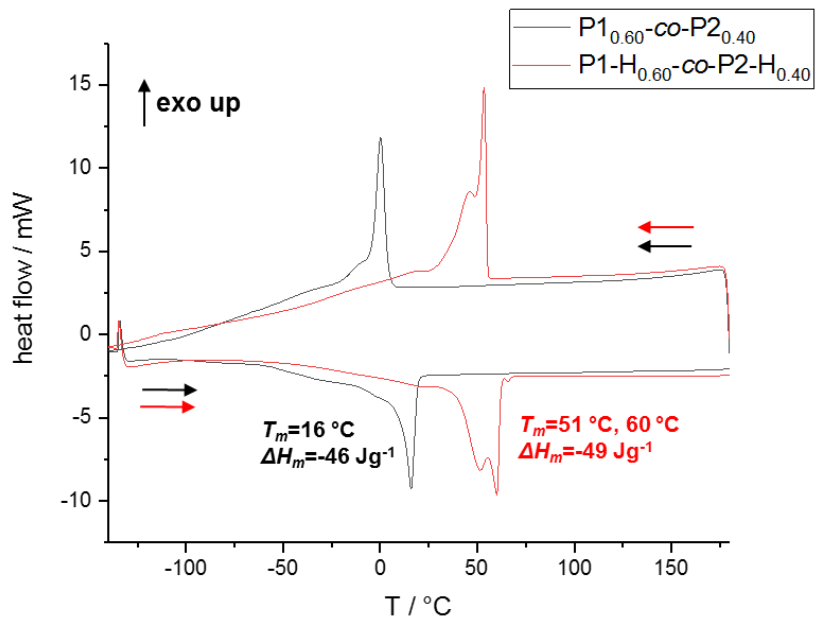
Figure 1.54. DSC of P1$_{0.60}$-*co*-P2$_{0.40}$ and P1-H$_{0.60}$-*co*-P2-H$_{0.40}$ with a heating (second run) and cooling rate of 10 K min^{-1}.
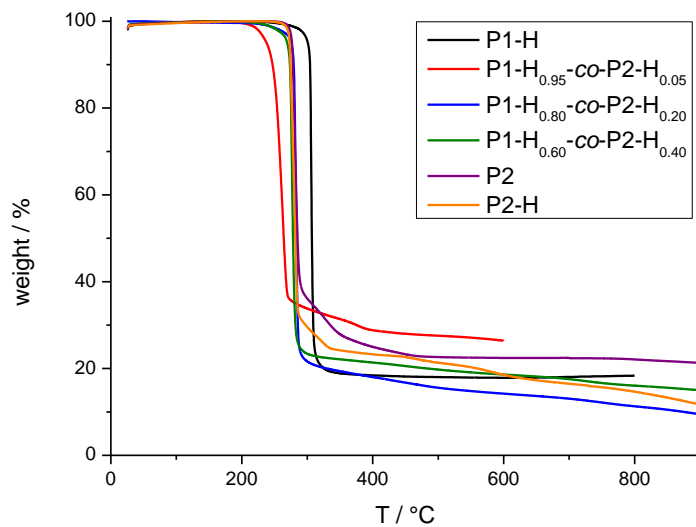
Figure 1.55. TGA of P1-H, P1-H$_{0.95}$-*co*-P2-H$_{0.05}$, P1-H$_{0.80}$-*co*-P2-H$_{0.20}$, P1-H$_{0.60}$-*co*-P2-H$_{0.40}$, P2, and P2-H with a heating rate of 10 K min^{-1}.

4.6   Size exclusion chromatography
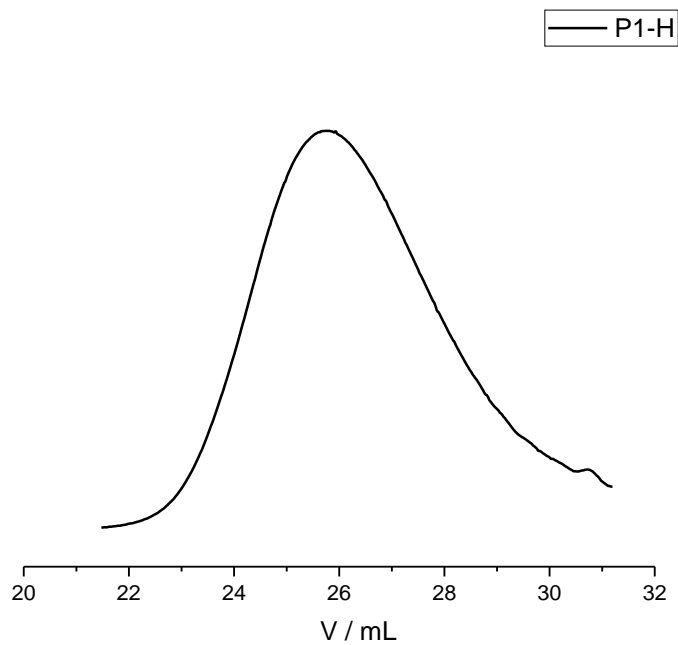
Figure 1.56. SEC Elugram of P1-H in THF (RI detection).
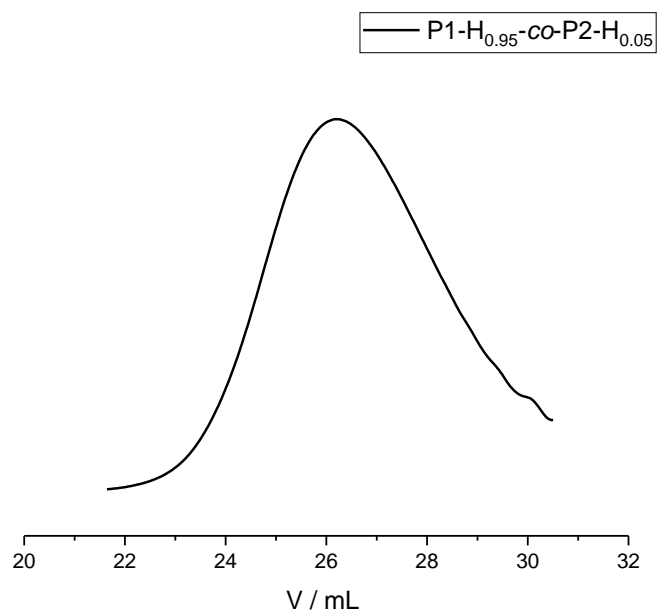
Figure 1.57. SEC Elugram of P1-H$_{0.95}$-*co*-P2-H$_{0.05}$ in THF (RI detection).
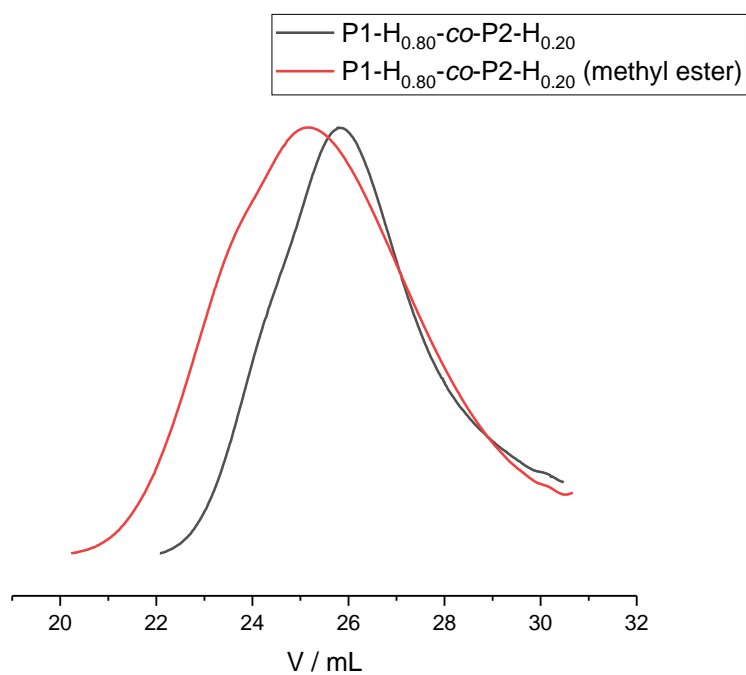
Figure 1.58. SEC Elugram of P1-H$_{0.80}$-*co*-P2-H$_{0.20}$ before and after esterification in THF (RI detection).
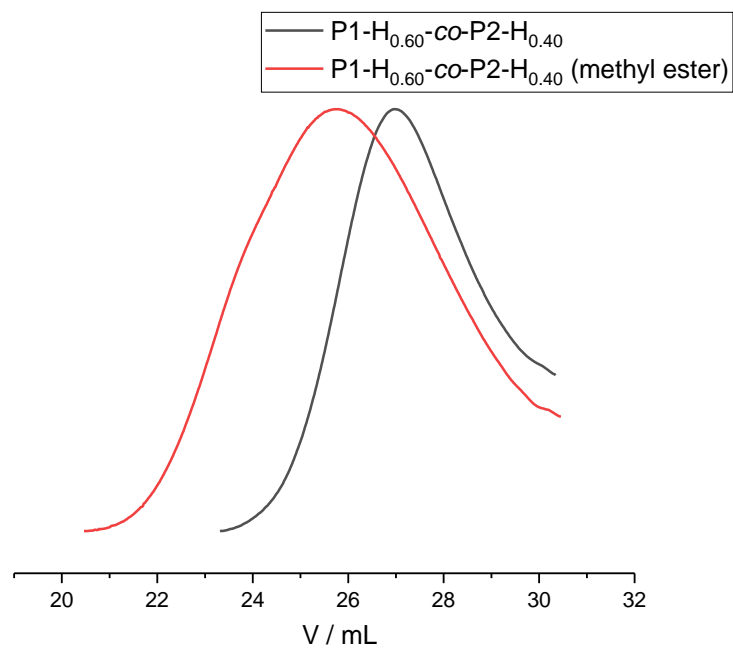
Figure 1.59. SEC Elugram of P1-H$_{0.60}$-*co*-P2-H$_{0.40}$ before and after esterification in THF (RI detection).
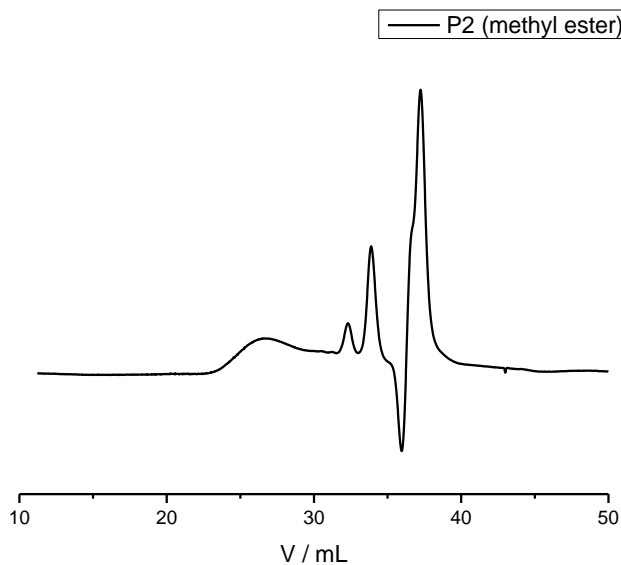
Figure 1.60. SEC Elugram of P2 after esterification in THF (RI detection).

4.7 XRD
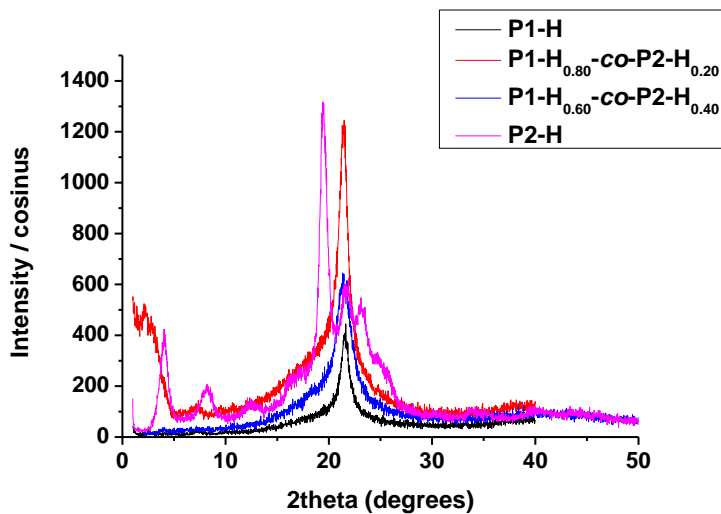
Figure 1.61. X-ray diffractograms of P1-H, P1-H$_{0.80}$-*co*-P2-H$_{0.20}$, P1-H$_{0.60}$-*co*-P2-H$_{0.40}$ and P2-H.

4.8 Shear lap test, compressive strength
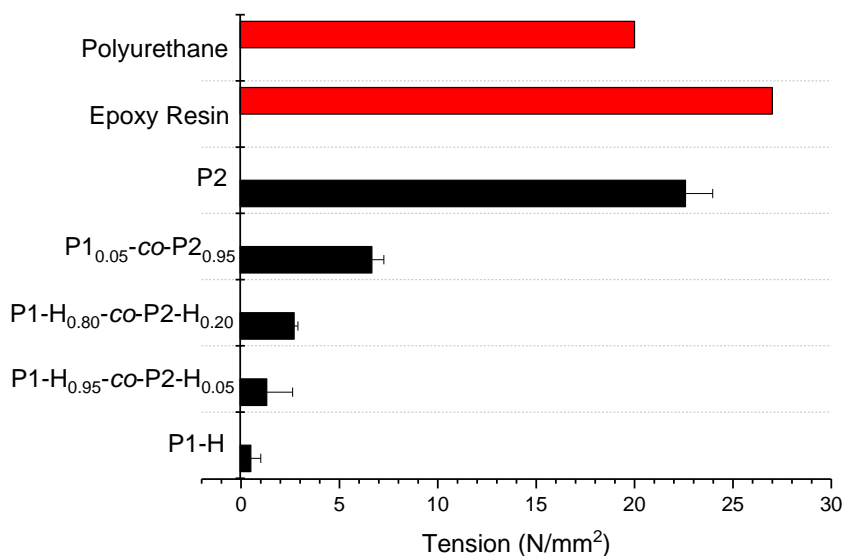
Figure 1.62. Adhesion of PPEs. Shear lap test of P1-H, P1-H$_{0.95}$-*co*-P2-H$_{0.05}$, P1-H$_{0.80}$-*co*-P2-H$_{0.20}$, and P2 on aluminum plates. The Values from polyurethane and epoxy resin are taken from the literature for comparison.[32]
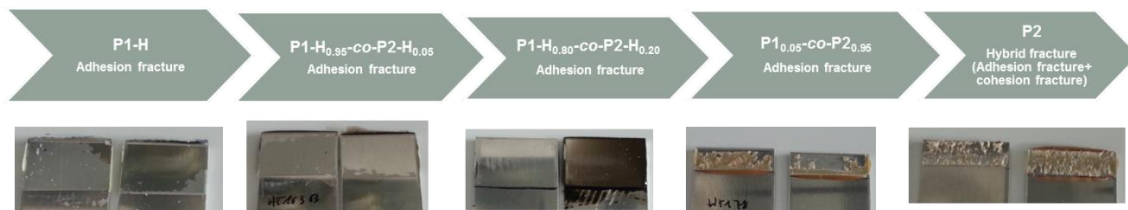
Figure 1.63. Images of PPEs with variable OH-group-content after shear lap test on aluminum plates.
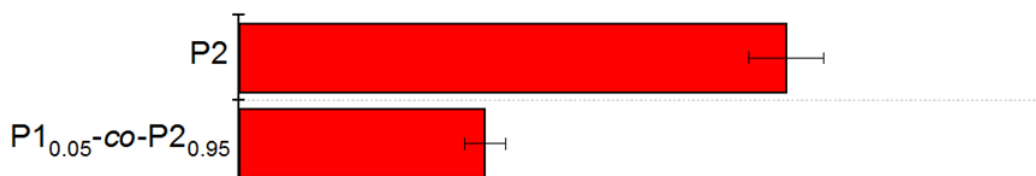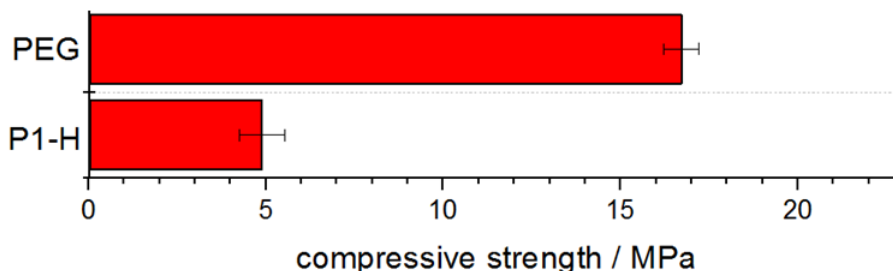
Figure 1.64. Compressive Strength of P1-H, P1-H$_{0.80}$-*co*-P2-H$_{0.20}$ (M$_n$ 6k and 8k), P1-H$_{0.60}$-*co*-P2-H$_{0.40}$, P1$_{0.05}$-*co*-P2$_{0.95}$, and P2.

5 References

1.   Binder, W. H.; Zirbs, R., Supramolecular polymers and networks with hydrogen bonds in the main-and side-chain. In *Hydrogen bonded polymers*, Springer: 2006; pp 1-78.

2.   Folmer, B. J. B.; Sijbesma, R. P.; Versteegen, R. M.; van der Rijt, J. A. J.; Meijer, E. W., Supramolecular Polymer Materials: Chain Extension of Telechelic Polymers Using a Reactive Hydrogen-Bonding Synthon. **2000,** *12* (12), 874-878.

3.   Aida, T.; Meijer, E. W.; Stupp, S. I., Functional Supramolecular Polymers. **2012,** *335* (6070), 813-817.

4.   Lange, R. F. M.; Van Gurp, M.; Meijer, E. W., Hydrogen-bonded supramolecular polymer networks. **1999,** *37* (19), 3657-3670.

5.   Khlobystov, A. N.; Blake, A. J.; Champness, N. R.; Lemenovskii, D. A.; Majouga, A. G.; Zyk, N. V.; Schröder, M., Supramolecular design of one-dimensional coordination polymers

based on silver(I) complexes of aromatic nitrogen-donor ligands. *Coordination Chemistry Reviews* **2001,** *222* (1), 155-192.

6.   Steed, J. W.; Atwood, J. L., *Supramolecular chemistry*. John Wiley & Sons: 2013.

7.   Yan, X.; Wang, F.; Zheng, B.; Huang, F., Stimuli-responsive supramolecular polymeric materials. *Chemical Society Reviews* **2012,** *41* (18), 6042-6065.

8.   Grabowski, S. J., *Hydrogen bonding: new insights*. Springer: 2006; Vol. 3.

9.   Yang, Y.; Urban, M. W., Self-healing polymeric materials. *Chemical Society Reviews* **2013,** *42* (17), 7446-7467.

10.   Zhao, Q.; Qi, H. J.; Xie, T., Recent progress in shape memory polymer: New behavior, enabling materials, and mechanistic understanding. *Progress in Polymer Science* **2015,** *49-50*, 79-120.

11.   Courtois, J.; Baroudi, I.; Nouvel, N.; Degrandi, E.; Pensec, S.; Ducouret, G.; Chanéac, C.; Bouteiller, L.; Creton, C., Supramolecular soft adhesive materials. *Advanced Functional Materials* **2010,** *20* (11), 1803-1811.

12.   Cangelosi, F.; Shaw, M., A review of hydrogen bonding in solid polymers: structural relationships, analysis, and importance. *Polymer-Plastics Technology and Engineering* **1983,** *21* (1), 13-98.

13.   He, Y.; Zhu, B.; Inoue, Y., Hydrogen bonds in polymer blends. *Progress in Polymer Science* **2004,** *29* (10), 1021-1051.

14.   Król, P., Synthesis methods, chemical structures and phase structures of linear polyurethanes. Properties and applications of linear polyurethanes in polyurethane elastomers, copolymers and ionomers. *Progress in Materials Science* **2007,** *52* (6), 915-1015.

15.   Marchildon, K., Polyamides – Still Strong After Seventy Years. **2011,** *5* (1), 22-54.

16.   Zheng, Y.-R.; Tee, H. T.; Wei, Y.; Wu, X.-L.; Mezger, M.; Yan, S.; Landfester, K.; Wagener, K.; Wurm, F. R.; Lieberwirth, I., Morphology and Thermal Properties of Precision Polymers: The Crystallization of Butyl Branched Polyethylene and Polyphosphoesters. *Macromolecules* **2016,** *49* (4), 1321-1330.

17.   Bauer, K. N.; Liu, L.; Wagner, M.; Andrienko, D.; Wurm, F. R., Mechanistic study on the hydrolytic degradation of polyphosphates. *European Polymer Journal* **2018**.

18.   Tee, H. T.; Lieberwirth, I.; Wurm, F. R., Aliphatic Long-Chain Polypyrophosphates as Biodegradable Polyethylene Mimics. *Macromolecules* **2019**.

19.   Steinbach, T.; Wurm, F. R., Poly (phosphoester) s: a new platform for degradable polymers. *Angewandte Chemie International Edition* **2015,** *54* (21), 6098-6108.

20.   Bauer, K. N.; Tee, H. T.; Velencoso, M. M.; Wurm, F. R., Main-chain poly (phosphoester) s: History, syntheses, degradation, bio-and flame-retardant applications. *Progress in Polymer Science* **2017,** *73*, 61-122.

21.   Marsico, F.; Wagner, M.; Landfester, K.; Wurm, F. R., Unsaturated Polyphosphoesters via Acyclic Diene Metathesis Polymerization. *Macromolecules* **2012,** *45* (21), 8511-8518.

22.   Wunderlich, B., *Macromolecular Physics, Volume 1: Crystal Structure, Morphology, Defects*. Academic Press: 1973.

23.   Lewis, C. L.; Dell, E. M., A review of shape memory polymers bearing reversible binding groups. *Journal of Polymer Science Part B: Polymer Physics* **2016**.

24.   Lendlein, A.; Jiang, H.; Junger, O.; Langer, R., Light-induced shape-memory polymers. *Nature* **2005,** *434* (7035), 879.

25.   Jiang, H.; Kelch, S.; Lendlein, A., Polymers move in response to light. *Advanced Materials* **2006,** *18* (11), 1471-1475.

26.   Liu, G.; Ding, X.; Cao, Y.; Zheng, Z.; Peng, Y., Shape memory of hydrogen-bonded polymer network/poly (ethylene glycol) complexes. *Macromolecules* **2004,** *37* (6), 2228-2232.

27.   Li, J.; Viveros, J. A.; Wrue, M. H.; Anthamatten, M., Shape-Memory Effects in Polymer Networks Containing Reversibly Associating Side-Groups. *Advanced Materials* **2007,** *19* (19), 2851-2855.

28.   Fu, B.; Sun, X.; Qian, W.; Shen, Y.; Chen, R.; Hannig, M., Evidence of chemical bonding to hydroxyapatite by phosphoric acid esters. *Biomaterials* **2005,** *26* (25), 5104-5110.

29.   Fukegawa, D.; Hayakawa, S.; Yoshida, Y.; Suzuki, K.; Osaka, A.; Van Meerbeek, B., Chemical Interaction of Phosphoric Acid Ester with Hydroxyapatite. **2006,** *85* (10), 941-944.

30.   Maege, I.; Jaehne, E.; Henke, A.; Adler, H.-J. P.; Bram, C.; Jung, C.; Stratmann, M., Self-assembling adhesion promoters for corrosion resistant metal polymer interfaces. *Progress in Organic Coatings* **1998,** *34* (1), 1-12.

31.   Ortmann, P.; Wimmer, F. P.; Mecking, S., Long-Spaced Polyketones from ADMET Copolymerizations as Ideal Models for Ethylene/CO Copolymers. *ACS Macro Letters* **2015,** *4* (7), 704-707.

32.   Rasche, M., *Der Zugscherversuch in der Klebtechnik*. Hochschule Hannover: 2008.

Chapter 2

Electrospun Polyphosphoesters: Degradation and Drug Release

Foreword

The following chapter is based on unpublished results.

Abstract
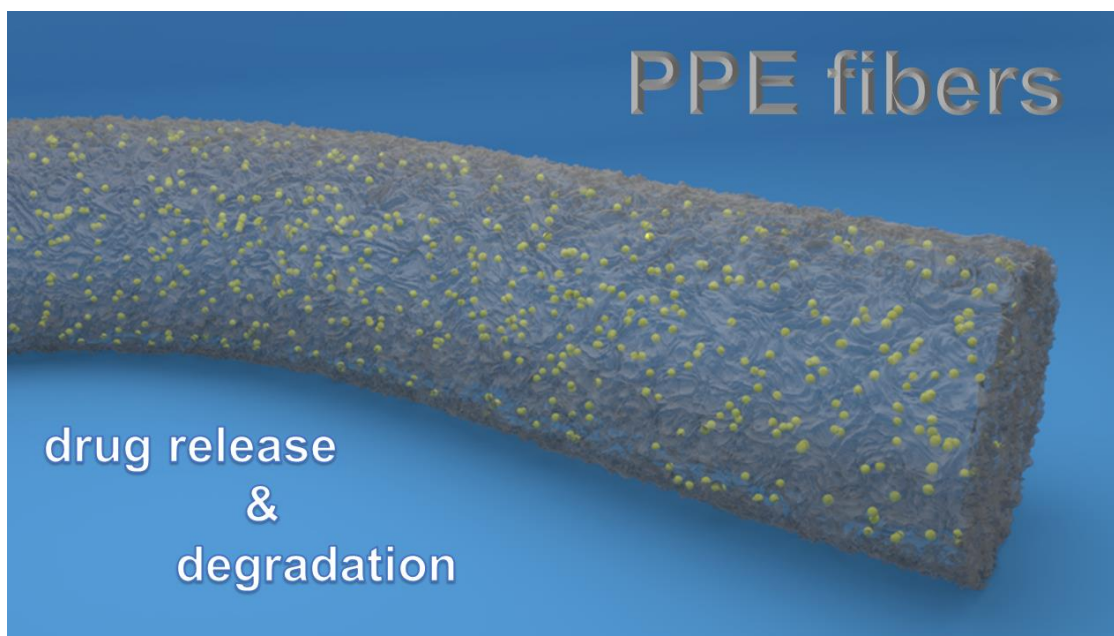
Electrospinning is a straightforward technique to produce nano- and micrometer sized materials. For the first time, PPEs were used in the electrospinning process and hydrophobic cargo was loaded into the PPE fibers. Fiber mats were produced based on semicrystalline long-chain alkyl PPEs. The effect of H-bonding from phosphoric acid diesters in the polymer chains, which act as noncovalent crosslinks, and their molecular weights were studied. Dexamethasone, an anti-inflammatory drug, was used as a hydrophobic drug which was loaded into the electrospun PPE fibers to study the release under various conditions. Degradation studies were conducted, revealing that surface erosion and the selective hydrolytic cleavage of the pendant phenyl-ester was observed at pH 14.

1   Introduction

Nowadays, electrospinning has become a popular technique due to its cost-effectiveness and versatility to engineer nano- to micron-sized fiber materials. Besides its versatility in the material section, electrospinning provides many tools to tune fiber morphology and scaffold geometry with large surface area to volume ratios of the fibrous scaffolds, which has emerged great interests for companies to exploit their innumerable applications. Nanosized particles, fibrous morphologies and other complex forms, have shown many improved interactions with cells, like adhesive, orientation and selective endocytosis.[1-3] Depending on the structure of the fiber mats, high pore volumes can be designed with different pore sizes to facilitate loading of drugs or bioactive molecules and transportation of waste or nutrients. In addition to the previously mentioned properties it is also easy to use and has therefore found its way in areas such as bioengineering,[1,4] environmental protection,[5,6] clothing,[7,8] filtration,[9,10] catalysis,[11] electronics[12] and sensors.[13,14] Numerous of natural and synthetic polymers were already electrospun into nanofibers, including fibrinogen, elastin, collagen, polyurethanes, polyesters etc.[15,16] In spite of many attractive properties of polyphosphoesters (PPEs) for biomedical applications (see below), pure PPE electrospun fibers have not been reported to date. PPEs with the repeating phosphoester bonds in the backbone and with the pentavalent phosphorus atom are structurally versatile and allows easy modification of chemical and physical properties or introduction of bioactive molecules.[17] Furthermore, they show biocompatibility and biodegradability through hydrolysis or enzymatic degradation which renders them to an suitable material class for biomedical applications.[18] Especially in the fields of drug and gene delivery, as well as tissue engineering PPEs, have attracted a lot of attention in the last decades.[19] The appealing properties of PPEs and the benefits and versatility of electrospun fibers could introduce new nano size materials for biomedical applications especially in tissue engineering applications.

Herein, we report the first electrospun polyphosphoester. The hydrophobic PPEs could be electrosprayed or electrospun into particles or fibers in micrometer size. Furthermore, we were able to prove that cargo can be electrospun with the PPE and were incorporated into the resulting fibers or particles. In addition, the degradation behavior of electrospun fiber mats was conducted at pH 7 and pH 14 to study the degradation behavior with a high surface area. This study gives a first insight into the use of hydrophobic PPEs for electrospinning and broadens applications potential applications in the biomedical field and especially for tissue engineering.

2 Results and Discussion

In order to study if hydrophobic PPEs are accessible for electrospinning, we chose **P1-H$_{0.8}$-*co*-P2-H$_{0.2}$** and **P1-H$_{0.6}$-*co*-P2-H$_{0.4}$,** due to the functionality and increased viscosity resulting from the phosphoric acid diester compared to the homopolymer of **P1**. The phosphorus diester can form strong bonds to amines or salts and allows lower polymer concentration, due to the increased viscosity from H-bonding. Furthermore, these PPEs gave more stable fiber mats due to their improved mechanical properties as shown in chapter 1.
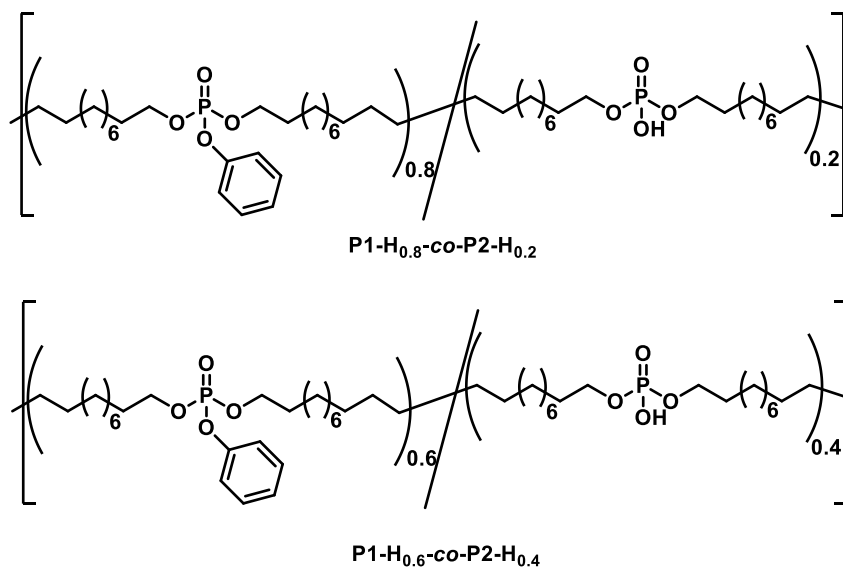
Figure 2.1. Structure of Polyphosphoesters used in this study.

2.1 Electrospinning

To investigate the suitability of **P1-H$_{0.8}$-*co*-P2-H$_{0.2}$** and **P1-H$_{0.6}$-*co*-P2-H$_{0.4}$** as polymers for the electrospinning process, characteristics of the polymer solution like molecular weight, polymer concentration, and the solvent were varied. In addition, process parameters on the machine like the voltage, tip distance, ejection volume, and inner tip diameter were kept constant. At low polymer concentrations (20-100 mg/mL) an electrospraying was observed, which resulted in the formation of PPE particles with diameters of 2.9 ± 0.3 nm. When the polymer concentration was increased to 380 mg/mL, the spraying changed into a spinning process with no break up of the polymer stream, and fibers were produced. An important parameter to achieve a successful spinning and fiber production is the molecular cohesion, which can be increased by higher molecular weights of the polymer, i.e. entanglements, of the introduction of non-covalent

interactions, e.g. H-bonds. With such parameters, the concentrations of the polymer solution can be adjusted in order to control the polymer morphology after the process. Table 2.1 shows all the varied parameters and the resulting electrospun and electrosprayed products.

Table 2.1. Preparation of particles and fibers based on PPEs by electrospinning/-spraying

Entry	Polymer	Solvent	wt % polymer	c / mg mL^{-1}	Product morphology	d / µm
1	**P1-H$_{0.8}$-co-P2-H$_{0.2}$** (M_n = 6,000)	THF	2	18	capsules	2.9 ± 0.3
2	**P1-H$_{0.8}$-co-P2-H$_{0.2}$** (M_n = 6,000)	THF	10	99	capsules	2.9 ± 0.3
3	**P1-H$_{0.8}$-co-P2-H$_{0.2}$** (M_n = 6,000)	THF	30	381	fiberlike	4.2 ± 1.7
4	**P1-H$_{0.8}$-co-P2-H$_{0.2}$** (M_n = 6,000)	THF	35	479	fibers	4.0 ± 0.2
5	**P1-H$_{0.8}$-co-P2-H$_{0.2}$** (M_n = 6,000) + diaminopropane	THF	30	381	fibers	3.2 ± 0.6
6	**P1-H$_{0.8}$-co-P2-H$_{0.2}$** (M_n = 8,000)	THF	28	346	fibers	4.0 ± 0.2
7	**P1-H$_{0.6}$-co-P2-H$_{0.4}$**	THF	20	222	particles + fibers	6.5 ± 6.4
8	**P1-H$_{0.6}$-co-P2-H$_{0.4}$**	CHCl$_3$	15	263	fibers	2.8 ± 0.3
9	**P1-H$_{0.8}$-co-P2-H$_{0.2}$** (M_n = 8,000) + 15wt% Dexamethasone	THF	28	346	fibers	2.1 ± 2.3
10	**P1-H$_{0.6}$-co-P2-H$_{0.4}$** + 15wt% Dexamethasone	THF	18	195	particles + fibers	2.4 ± 3.1

General parameters used for Electrospinning: Voltage 10 kV, Tip distance = 8 cm, inner Tip diameter = 0.4 mm, Ejection volume 0.5 mL/h

P1-H$_{0.8}$-*co*-P2-H$_{0.2}$ with a molecular weight of 6,000 g/mol produces particles with a concentration of 2 – 10wt% in tetrahydrofuran. With just 2wt% the particles are porous due to the low polymer concentration (cf. Figure 2.1, Particle 1) while a concentration of 10wt% of **P1-H$_{0.8}$-*co*-P2-H$_{0.2}$** results in a capsule-like morphology. For a fiber like product, a polymer concentration of at least 30wt% was necessary. However, with a polymer concentration of 35wt% uniform fibers could be produced. Another approach to increase the molecular cohesion was to add 1,3-diaminopropane into the polymer solution which also produced uniform polymer fibers however already at 30wt% polymer. By increasing the molecular weight of **P1-H$_{0.8}$-*co*-P2-H$_{0.2}$** to Mn 8,000 g/mol uniform fibers could be already produced in a 28wt% polymer solution in THF, which might be related to a higher fraction of entangled polymer chains. Changing the polymer to **P1-H$_{0.6}$-*co*-P2-H$_{0.4}$** with higher amount of H-bonding groups, the homogeneous solution in THF was achieved up to a concentration of 20wt%, giving a mixture of fibers and particles. At higher polymer concentrations an organogel was formed. Chloroform proved to be a better solvent for **P1-H$_{0.6}$-*co*-P2-H$_{0.4}$** and with a concentration of 15wt% (equivalent to 24wt% THF solution due to the higher density) round shaped polymer fibers with a diameter of 2.8 ± 0.3 µm could be produced. Lastly, polymer fibers with 15wt% Dexamethasone were loaded, with THF as solvent due to THF being able to dissolve both, polymer and dexamethasone.
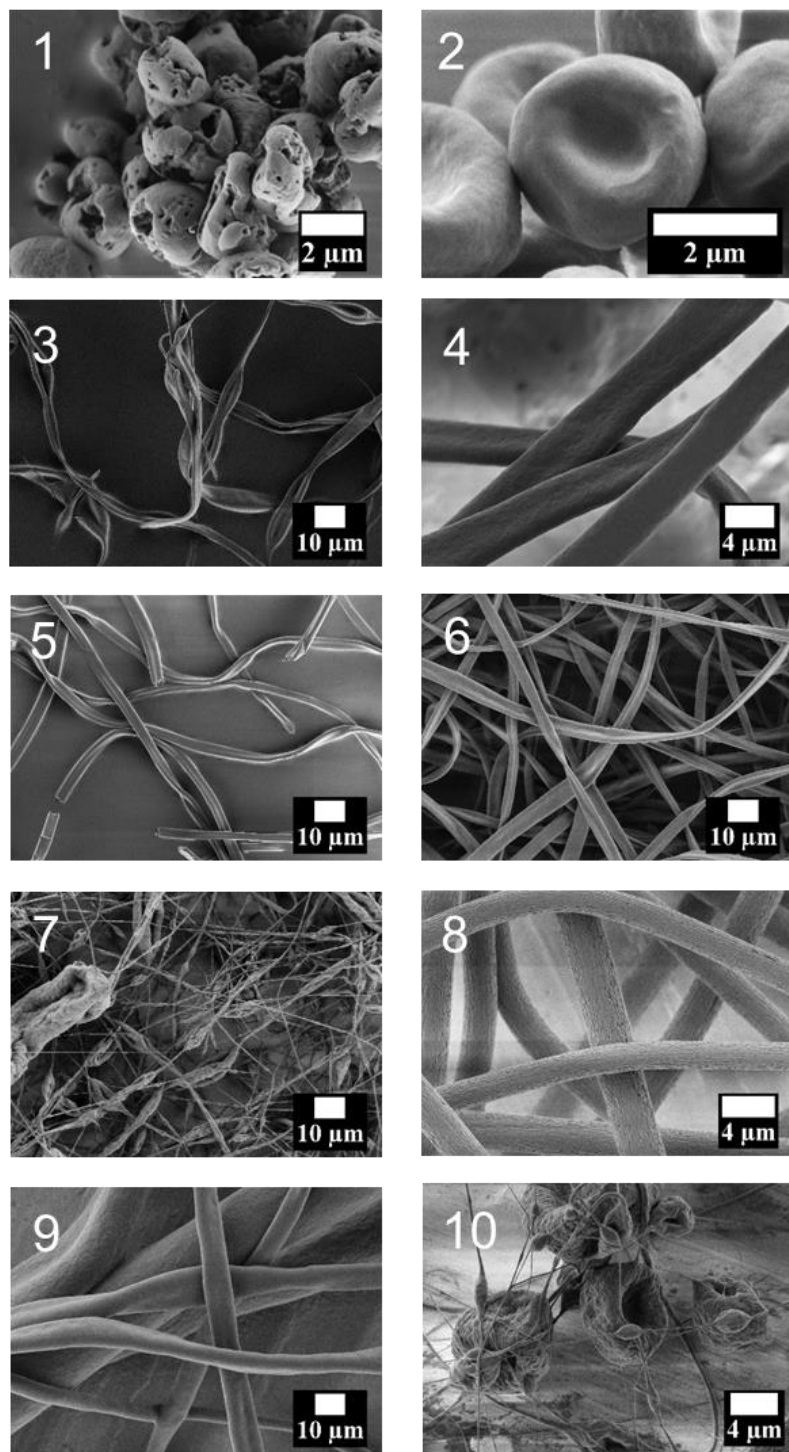
Figure 2.1. SEM pictures of the prepared PPE fibers and particles (details see Table 2.1).

2.2 Release of Dexamethasone

One major advantage of electrospinning is the high surface area of the fiber mats produced by this technique. The high surface area is able to facilitate stronger interactions, faster degradation or function as storage and has a strong influence on the drug release. Here we investigated the release of the drug Dexamethasone as we expected those fiber mats to show a faster release of small molecules.[20] For the release measurements of dexamethasone, we used the fiber mats 9 and 10 with 15 wt% loading of dexamethasone with regard to the polymer amount. The in vitro release study of dexamethasone from PPE fibers 9 and 10 was performed in phosphate buffered saline (PBS) at pH 7 and 37 °C under sink conditions. Figure 2.2 shows the release profile of **P1-H$_{0.8}$-co-P2-H$_{0.2}$** (Fiber 9) and **P1-H$_{0.6}$-co-P2-H$_{0.4}$** (Fiber 10). The release of dexamethasone from **P1-H$_{0.8}$-co-P2-H$_{0.2}$** shows a burst release of 56 % in the first 4 hours due to diffusion of dexamethasone out of the polymer matrix. For poly(lactic-co-glycolic acid) (PLGA) it has already been reported that the release of small molecules or therapeutic agents takes in the early phases mainly through diffusion, while in later phases the release is mediated by diffusion and degradation.[21, 22] No further release of dexamethasone was found after the burst release up to 28 days, showing that these PPE fibers release 50 % of dexamethasone through diffusion due to the high surface area. The plateau after the burst release indicates that the polymer fibers were stable at pH 7 and 37 °C. Similar results were found for **P1-H$_{0.6}$-co-P2-H$_{0.4}$** with a burst release of 45 % within the first day and no further release until 28 days. Due to the high surface area of these electrospun PPE fibers, they might be interesting for application in which a burst release is advantageous,[23] however, it seems that no degradation occurs under those conditions and residual drug stays in the PPE fibers.
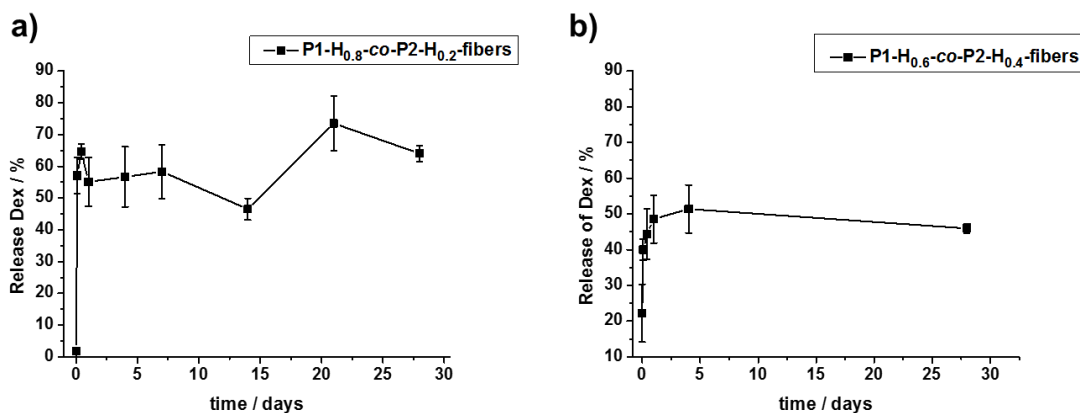
Figure 2.2. Release of Dexamethasone over a time frame of 28 days. (a) P1-H$_{0.8}$-*co*-P2-H$_{0.2}$ (Fiber 9). (b) P1-H$_{0.6}$-*co*-P2-H$_{0.4}$ (Fiber 10).

For comparison, we investigated the release of dexamethasone from compression molded polymer discs of **P1-H$_{0.8}$-*co*-P2-H$_{0.2}$** and PLGA (RG 502, 15-20 kDa and 50:50 composition) with 15w% Dexamethasone in PBS (pH 7.0) at 37 °C. The release of dexamethasone in **P1-H$_{0.8}$-*co*-P2-H$_{0.2}$** showed a slower release with 24 % after 1 day compared to around 50% for the fibers after 1 h. Furthermore, the release continued after 50% and kept releasing until the end of the measurement (28 days) with 82% being released. Dexamethasone was incorporated into the disk just by mixing the powders and forming the disc by pressure, in addition, the PPE polymer disc were still looking a little brittle which could be the reason for this higher release after 28 days compared to the fibers. In contrast, we observed the PLGA discs being more evenly pressed and therefore showed an even slower release of dexamethasone. The PLGA used for the discs was chosen with 50% glycolic acid to lactic acid and without carbon acid end groups which results in a material with slower degradation rates.[24, 25] However, the release kept increasing over the release measurement probably due to diffusion and degradation of PLGA with 19% being released after 28 days.
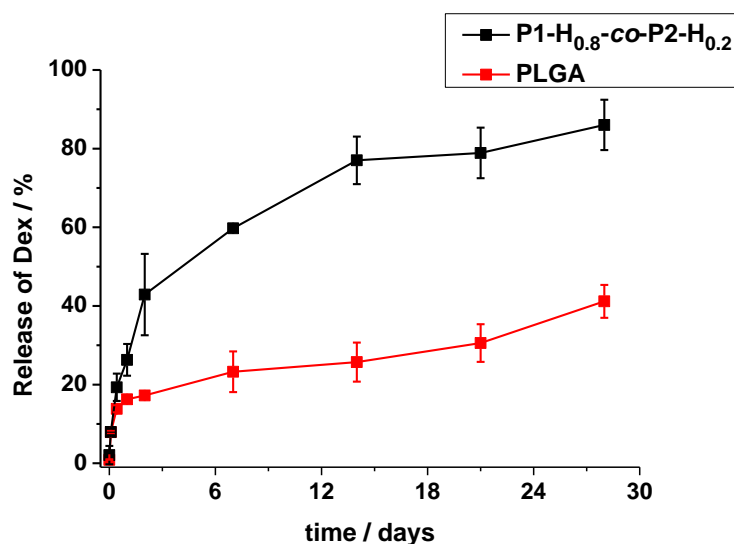
Figure 2.3. Release of Dexamethasone from P1-$H_{0.8}$-*co*-P2-$H_{0.2}$ disc and PLGA disc with 15wt% Dexamethasone.

2.3 Degradation

Since the degradation properties plays an important role in the release of drugs from electrospun fibers, we investigated the degradation behavior of electrospun PPE fibers at pH 7 and pH 14. Therefore we conducted weight loss measurements of electrospun fibers. The polymer fibers (6 and 8) were immersed in 4 mL solutions at pH 7 and pH 14 at 37 °C. Figure 2.4 and 2.5 shows the SEM images and photographs of fibers 6 and 8 from Table 2.1 after 1 and 3 months. Only **P1-$H_{0.6}$-*co*-P2-$H_{0.4}$** at pH 14 showed a significant macroscopic change. All other fiber mats were just slightly broken or fully intact. SEM images showed no distinct change of the fiber mats at pH 7, indicating no degradation under this condition. The surface for fiber 6 and 8 at pH 14 seems to be rougher after the measurement which could be due to surface erosion of those films.
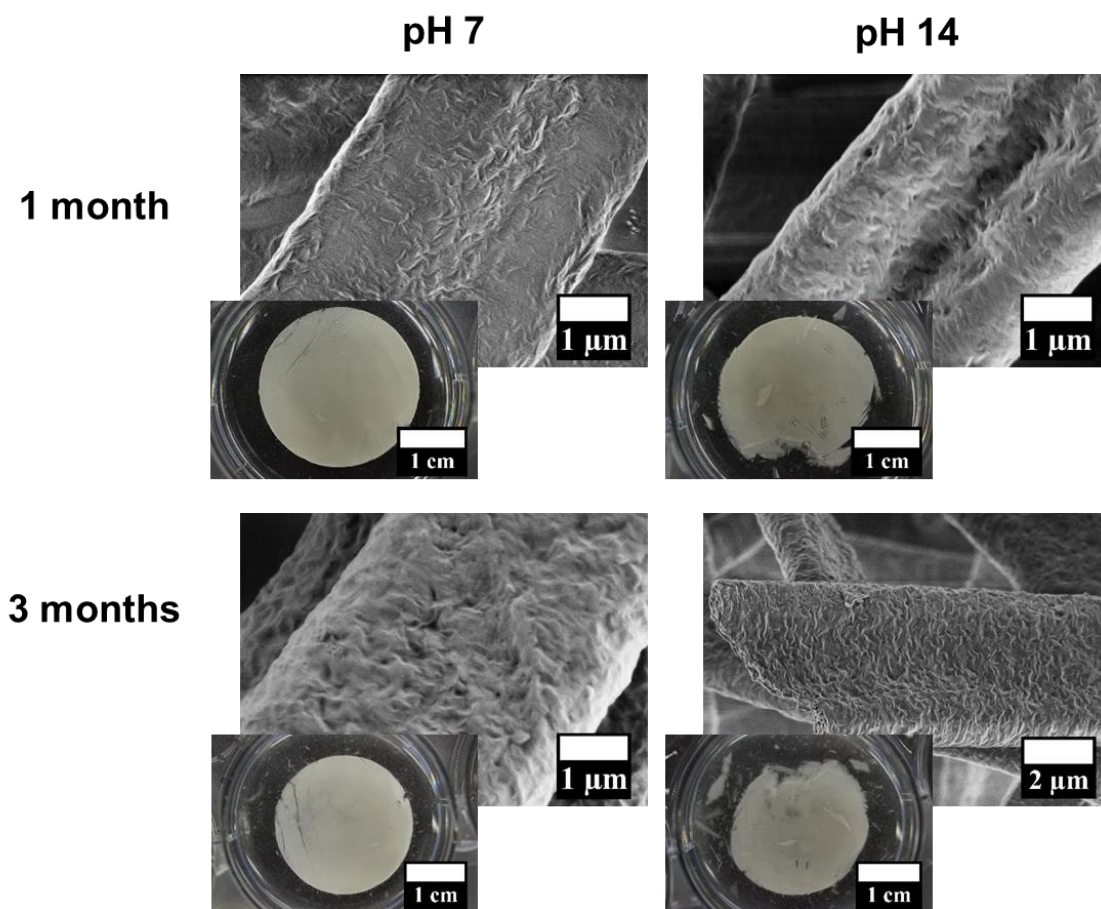
Figure 2.4. SEM images and photographs of P1-H$_{0.8}$-*co*-P2-H$_{0.2}$ (Fiber 6) after 1 and 3 months at pH 7 and pH 13 at 37 °C.
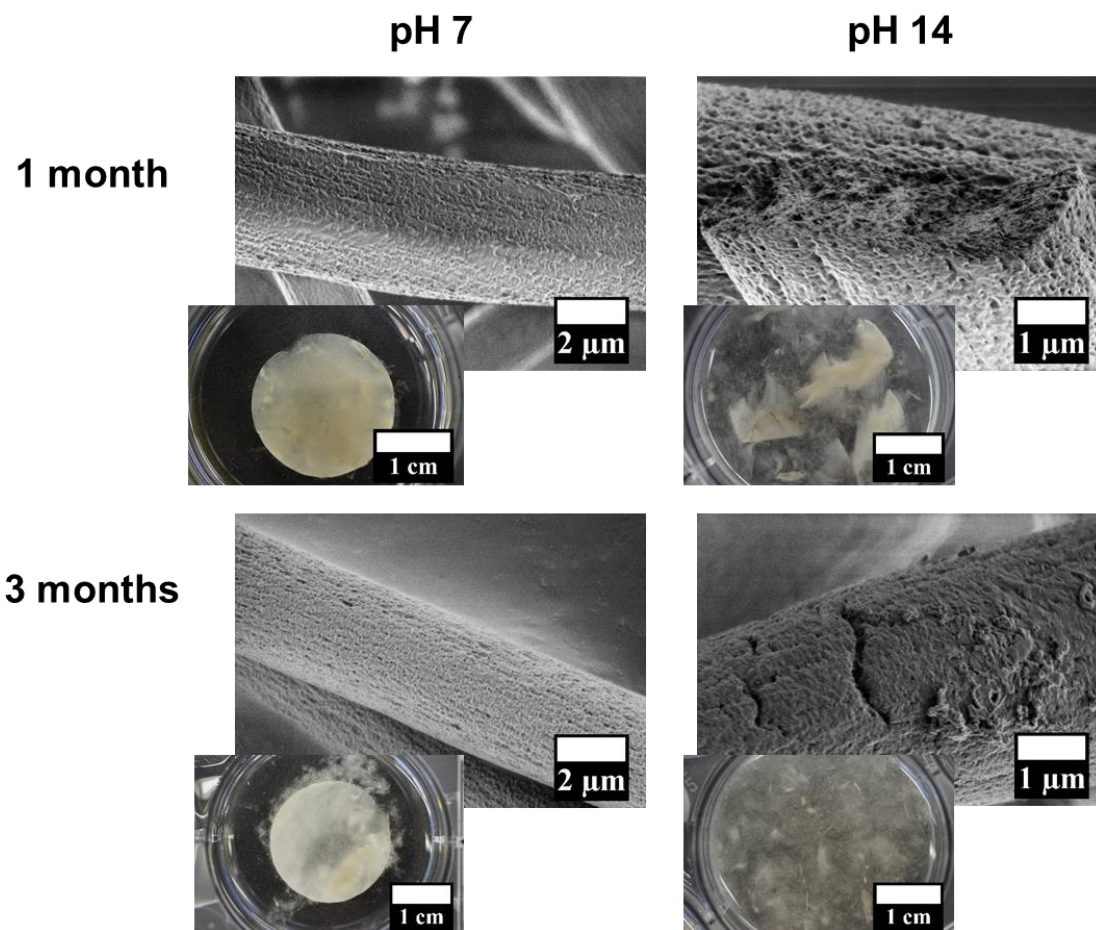
Figure 2.5. SEM images and photographs of P1-H$_{0.6}$-*co*-P2-H$_{0.4}$ (Fiber 8) after 1 and 3 months at pH 7 and pH 14 at 37 °C.

Weight loss determination after degradation measurements were not possible due to the high electrostatic repulsion leading to negative or an extraordinary high weight of the polymer fiber mats. pH measurement of the residual solution showed no pH change of the fiber mats in pH 7, however, at pH 14 we found for fibers 6 and 8 a decrease of pH to 13 and 10 respectively. The higher pH drop for Fiber 8 could be explained with an already higher concentration of phosphoric acid diester and therefore also a higher hydrophilicity of this polymer. NMR measurement to investigate degradation products of Fiber 6 and 8 at pH 13 could not be conducted due to the insolubility of those fibers, which indicates side-chain degradation towards the phosphoric acid diester which is a highly insoluble polymer (cf. Chapter 3). HPLC measurements of **P1-H$_{0.6}$-*co*-P2-H$_{0.4}$** fibers before and after degradation for 3 months at pH 14 showed no significant change for **P1-H$_{0.6}$-*co*-P2-H$_{0.4}$** with both signals at an elution volume of around 10 mL indicating no

backbone hydrolysis (Figure 2.16). Furthermore, after degradation, the signal for phenol at 4.3 mL elution volume was found and proved the side-chain degradation.

3 Summary

In this study, we prepared the first full PPE fibers by electrospinning. Material properties like molecular weight of polymers, amount of Hydrogen bonding groups or the addition of small molecules were changed and the effect on electrospun PPE fibers studied. Furthermore, by decreasing the polymer concentration polymer particles could be electrosprayed. Electrospinning with the hydrophobic drug dexamethasone was possible and release measurements showed a burst release of 50% in the first few hours due to diffusion out of the high surface area of those fiber mats. Further release did not occur due to the stability of the PPE fibers at pH 7. Degradation measurements of PPE fibers were conducted at pH 7 and pH 14 and showed a drop in pH at morphology changes at pH 14. However, qualitative determination of the degradation by weight loss measurement and NMR studies were not possible due to electrostatic repulsion and insolubility. These fibers might be interesting for surface coating of metallic implants whereas they could release drugs with antibiotic or anti-inflammatory effect, influence cell growth and being potentially degradable by human enzymes for polyphosphoesters.

4 Experimental

4.1 General Information

All Solvents and chemicals were purchased from Sigma Aldrich, Acros Organics, or Fluka and used as received unless otherwise stated. Triethylamine was distilled from calcium hydride and stored over molecular sieves (4Å) under argon prior to use. Dry solvents were purchased from Acros Organics or Sigma Aldrich and stored with a septum and over molecular sieves. Deuterated solvents, PLGA (RG 502), PBS – Phosphate buffered saline (powder), Grubbs catalyst 1st generation, Hoveyda–Grubbs catalyst 1st generation and Pd/C(10wt%) were purchased from Sigma Aldrich and used as received. Deionized water was used for preparing buffers and NaOH solutions.

4.2 Instrumentation and Characterization Techniques

SEC. SEC measurements were performed in THF with a PSS SecCurity system (Agilent Technologies 1260 Infinity). Sample injection was performed by a 1260-ALS autosampler (Waters) at 30 °C. SDV columns (PSS) with dimensions of 300×80 mm, 10 μm particle size, and pore sizes of 106, 104, and 500 Å were employed. The DRI Shodex RI-101 detector (ERC) and UV−vis 1260-VWD detector (Agilent) were used for detection. Calibration was achieved using polystyrene standards provided by Polymer Standards Service.

NMR. For nuclear magnetic resonance analysis ^{1}H, ^{13}C, and ^{31}P NMR spectra of the monomers and polymers were recorded on a Bruker AVANCE III 300, 500, or 700 MHz spectrometer. All spectra were measured in CDCl$_3$, CDCl$_3$/MeOD (7:3 or 4:2) or pyridine-d_5 at 298 K. The spectra were calibrated against the solvent signal and analyzed using MestReNova 8 from Mestrelab Research S.L.

DSC. The thermal properties of the synthesized polymers have been measured by differential scanning calorimetry (DSC) on a Mettler Toledo DSC 823 calorimeter. Three scanning cycles of heating-cooling were performed in an N$_2$ atmosphere with a heating and cooling rate of 10 °C min^{-1}.

SEM. SEM investigations were performed by using a LEO 1530 GEMINI. The characterizations were carried out by applying the low-voltage approach. The fibers were deposited with the alumina or silver foil on conductive carbon tape.

HPLC. The amounts of dexamethasone released were determined by HPLC analysis. The HPLC system consisted of an Agilent Technologies Series 1200 setup equipped with a degasser, Quaternary pump, DAD detector (Agilent Technologies, Santa Clara, USA) and an ELSD detector Varian 385-LC . The separation of dexamethasone was achieved by using a reverse phase column (Agilent Eclipse C18) at 20 °C. The mobile phase was composed of THF(46%) and water containing 0.1% trifluoroacetic acid (54%). After 3 min by this isocratic mixture, a gradient is started up to 100% THF to eluate all other components. The eluent flow rate was 1 mL/min. The detection wavelength was monitored at 254 nm.

The elution volume of Phenol and **P1-H$_{0.6}$-*co*-P2-H$_{0.4}$** before and after degradation were determined by the HPLC system consisted of an Agilent Technologies Series 1200 setup equipped with a degasser, Quaternary pump, DAD detector (Agilent Technologies, Santa Clara, USA) and an ELSD detector Varian 385-LC . The separation of phenol was achieved by using a Chromolith Performance C18 HPLC column and a Macharey Nagel Gravity SB column was used for **P1-H$_{0.6}$-**

co-**P2-H$_{0.4}$** before and after degradation at 20 °C. The mobile phase was composed of THF(90%) and water containing 0.1% trifluoroacetic acid (10%) for phenol and THF(40%) and water containing 0.1% trifluoroacetic acid (60%) for **P1-H$_{0.6}$-*co*-P2-H$_{0.4}$**. After 10 min by this isocratic mixture, a gradient is started up to 100% THF to eluate all other components. The eluent flow rate was 1 mL/min. The detection wavelength was monitored at 260 nm.

4.3 Synthetic Procedures

4.3.1 Monomer Synthesis

*Bis-(undec-10-en-1-yl) phenylphosphate (**M1**)*
See Chapter 1.
*Bis-(undec-10-en-1-yl) phosphate (**M2**)*
See Chapter 1.

4.3.2 Polymer synthesis

P1$_{0.8}$-*co*-P2$_{0.2}$ (6,000 g mol^{-1})
In a vacuum reactor **M1** (38.43 g, 80.3 mmol), 8.08 g (20.1 mmol) **M2** and 248 mg Grubbs catalyst 1st generation (0.3 mol%) were mixed under an argon atmosphere. Polymerization was carried out at reduced pressure (first membrane pump (1.15 h, 50 mbar) then oil pump (5 mbar)) to remove ethylene gas evolving during the metathesis reaction, at 65 °C for 1 h and 85 °C for 48 h. The crude mixture was dissolved in CH_2Cl_2, treated with *tris*-(hydroxymethyl) phosphine (10 eq with respect to the catalyst) and 2 mL of Et_3N. After stirring for 1 h water was added in the same volume to the organic phase and the solution was stirred overnight. The organic layer was washed twice with 5 % aqueous HCl and brine to remove the catalyst residue. The water layer was extracted with CH_2Cl_2 several times until the emulsion disappeared and the water layer got clear. The combined organic phase was dried over sodium sulfate (Na_2SO_4), filtered and concentrated at reduced pressure to yield 95%. ^1H NMR: (300 MHz, $CDCl_3$, 298 K): δ = 7.37-7.26 (m), 7.24 – 7.09 (m), 5.43 – 5.25 (m), 4.21 – 4.05 (m), 4.06 – 3.93 (m), 2.08 – 1.85 (m), 1.76 – 1.59 (m), 1.46 – 1.12 (m) ppm. ^{13}C NMR (75 MHz, $CDCl_3$, 298 K) δ = 130.31, 129.85, 129.65, 124.90, 120.00, 119.94, 68.60, 68.52, 32.61, 30.26, 30.17, 29.66, 29.53, 29.50, 29.46, 29.41, 29.17, 29.09, 25.38 ppm. ^{31}P NMR (121 MHz, $CDCl_3$, 298 K) δ = 1.14, -6.15 ppm.
P1$_{0.8}$-*co*-P2$_{0.2}$ (8,000 g mol^{-1})

See Chapter 1.

P1$_{0.6}$-*co*-P2$_{0.4}$

See Chapter 1.

P1-H$_{0.8}$-*co*-P2-H$_{0.2}$ (6,000 g mol^{-1})

A 1 L Schlenk flask was charged with 40 g **P1$_{0.8}$-*co*-P2$_{0.2}$** (6,000 g mol^{-1}) and dissolved in 400 mL toluene. The air was removed by reduced pressure and flushing the schlenk flask with argon. 4.2 g (10 wt%) of 10 % Pd/C catalyst were added, the schlenk flask was evacuated and flushed with hydrogen from a balloon. Hydrogenation was then performed with a hydrogen balloon under vigorous stirring at room temperature until ^{1}H NMR showed the removal of the double bond signals. The solution was filtered over celite and the polymer was obtained as a solid after solvent evaporation in a yield of 89 %. ^{1}H NMR: (300 MHz, CDCl$_3$, 298 K): δ = 7.42 – 7.26 (m), 7.26 – 7.09 (m), 4.25 – 4.04 (m), 4.06 – 3.91 (m), 1.79 – 1.56 (m), 1.47 – 1.12 (m) ppm. ^{13}C NMR (75 MHz, CDCl$_3$, 298 K) δ = 129.65, 124.90, 120.01, 119.95, 68.61, 68.53, 30.27, 30.18, 29.73, 29.68, 29.58, 29.52, 29.12, 25.39 ppm. ^{31}P {H} NMR (121 MHz, CDCl$_3$, 298 K): δ = 1.19, -0.69, -6.14 ppm.

P1-H$_{0.8}$-*co*-P2-H$_{0.2}$ (8,000 g mol^{-1})

See Chapter 1.

P1-H$_{0.6}$-*co*-P2-H$_{0.4}$

See Chapter 1.

4.4   Electrospinning

The electrospinning experiments were performed with a commercial platform (ES1a, Electrospinz) equipped with a positive electrode applied to the spinneret and a counter electrode covered with aluminum or silver foil. The flow of the polymer solution was adjusted to 0.5 mL/h using a syringe pump (Bioblock, Kd Scientific). The spinning tip (high-density polypropylene, inner diameter 0.4 mm) and a syringe (1 mL) made of plastic were connected with silicone rubber tubing. Experiments conducted at ~23 C showed that optimal results were obtained using a voltage of 10 and a tip collector distance of either 8 cm. For degradation of **P1-H$_{0.8}$-*co*-P2-H$_{0.2}$** and **P1-H$_{0.6}$-*co*-P2-H$_{0.4}$**, fiber mats were punched out with a diameter of 22 mm and 19 mm from the electrospun fibers on the silver foil. For the release of dexamethasone, fiber mats were punched out from electrospun fibers on the silver foil with a diameter of 13 mm.

4.5   Fabrication of polymeric disc

The compression molding method was applied to fabricate the drug-loaded polymeric discs by means of 3 mm radius of mold and press (PW 40 E Lab Press) under 707.5 bar for 5 seconds. Briefly, **P1-H$_{0.8}$-*co*-P2-H$_{0.2}$** (6,000), PLGA, dexamethasone were physically mixed with a vortex shaker (IKA Vortex Genius 3) and the homogenous powders were weighed (3 mg) and fabricated for polymeric discs.
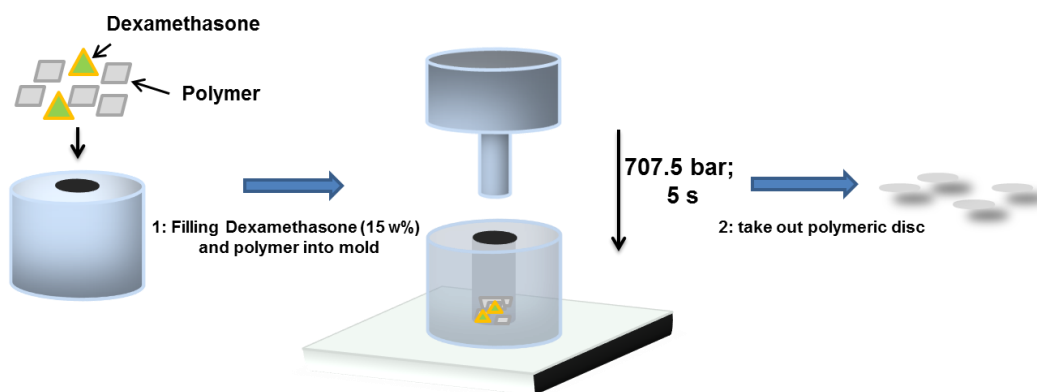
Scheme 2.1. Compression molding for drug loaded polymer discs.

4.6   In vitro release test

An *in vitro* release test was performed by placing the discs or fiber mats into vials and adding 10 ml of phosphate-buffered saline (PBS, pH 7.0). The sample vials were stored at 37 ◦C and at the scheduled time, the release media were taken out from the vials with a pipette. All analyses were carried out with each sample taken out from the vials. The drug concentration was plotted against release time. The average of 3 samples were determined for each measurement point.

4.7   Degradation studies

The degradation experiment of PPE fiber mats were done at 37 °C by immersing each polymer film with the silver foil in 4 mL 0.1 M DPBS solution (pH 7) or 2 N NaOH solution (pH 14). The coverslips were picked up over 1 month, 2 months and 3 months, washed with distilled water and dried in vacuum. The pH of the solutions were recorded with a SevenExcellence Cond meter S700 equipped with an InLab Routine Pro pH electrode (pH 0 – pH 14) when the samples were picked up. The average of 3 samples were determined for each measurement point.

4.8 ^{1}H, ^{13}C, ^{31}P NMR spectra
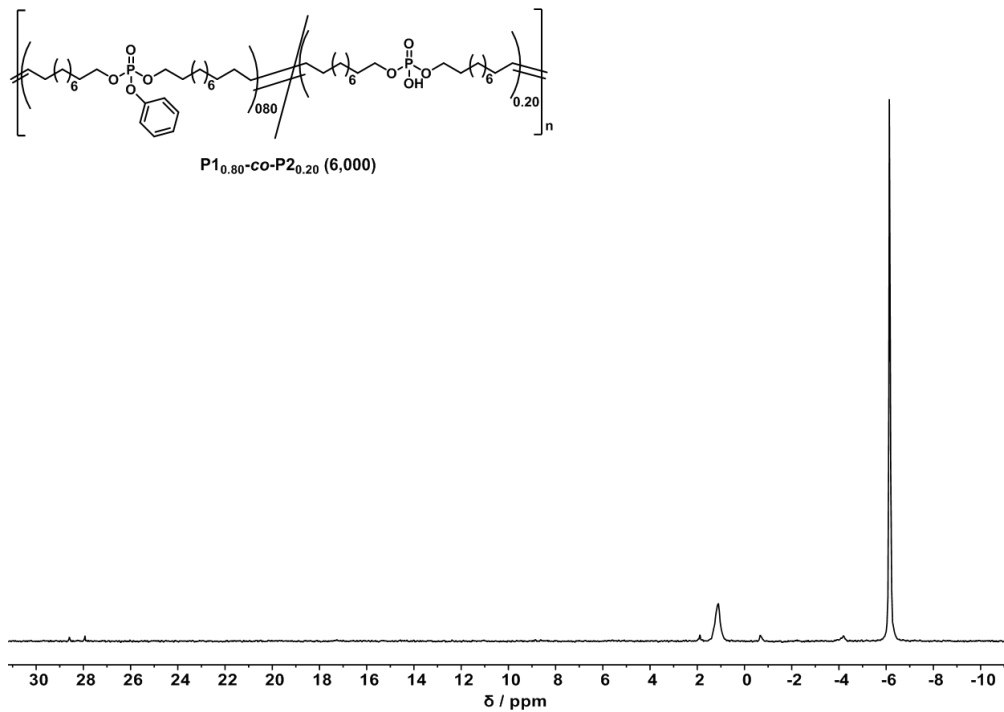
Figure 2.6. ^{31}P (121 MHz) NMR spectra of **P1$_{0.8}$-*co*-P2$_{0.2}$** in CDCl$_3$ at 298 K.
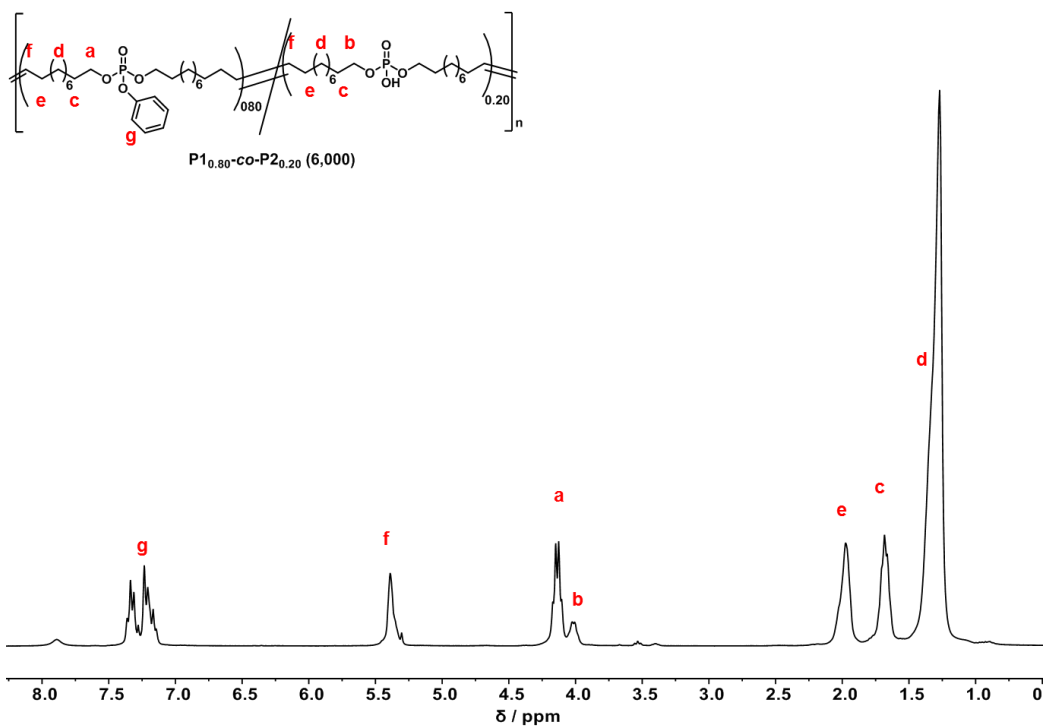
Figure 2.7. ¹H (300 MHz) NMR spectra of $P1_{0.8}$-*co*-$P2_{0.2}$ in $CDCl_3$ at 298 K.
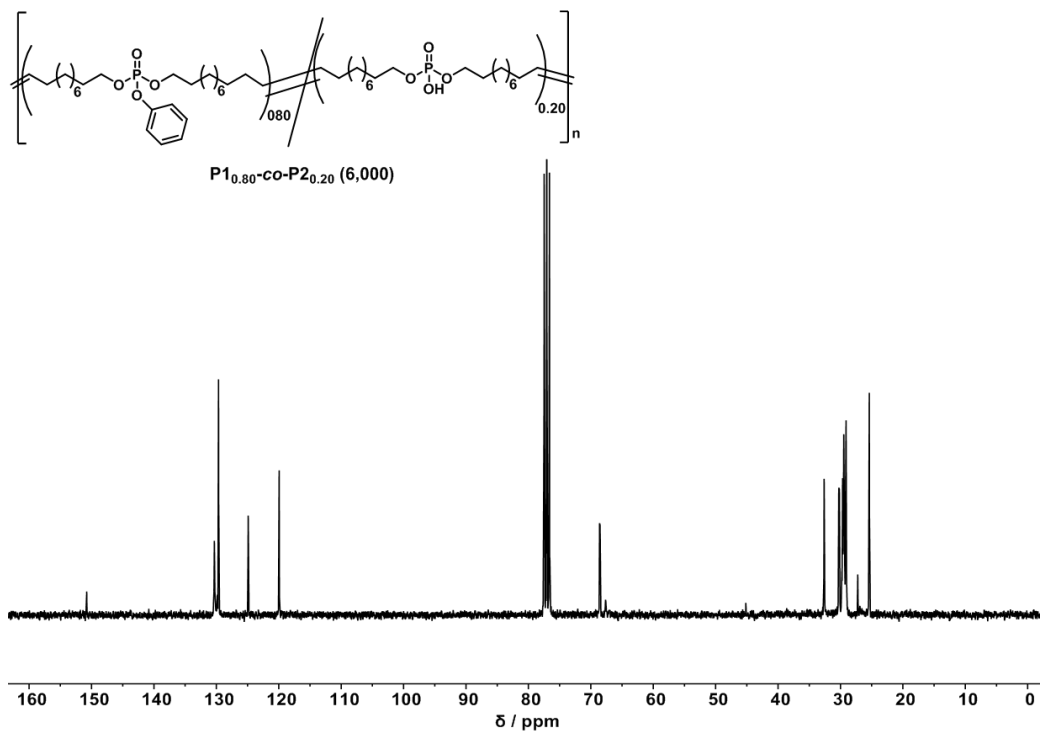
Figure 2.8. ¹H (75 MHz) NMR spectra of $P1_{0.8}$-*co*-$P2_{0.2}$ in $CDCl_3$ at 298 K.
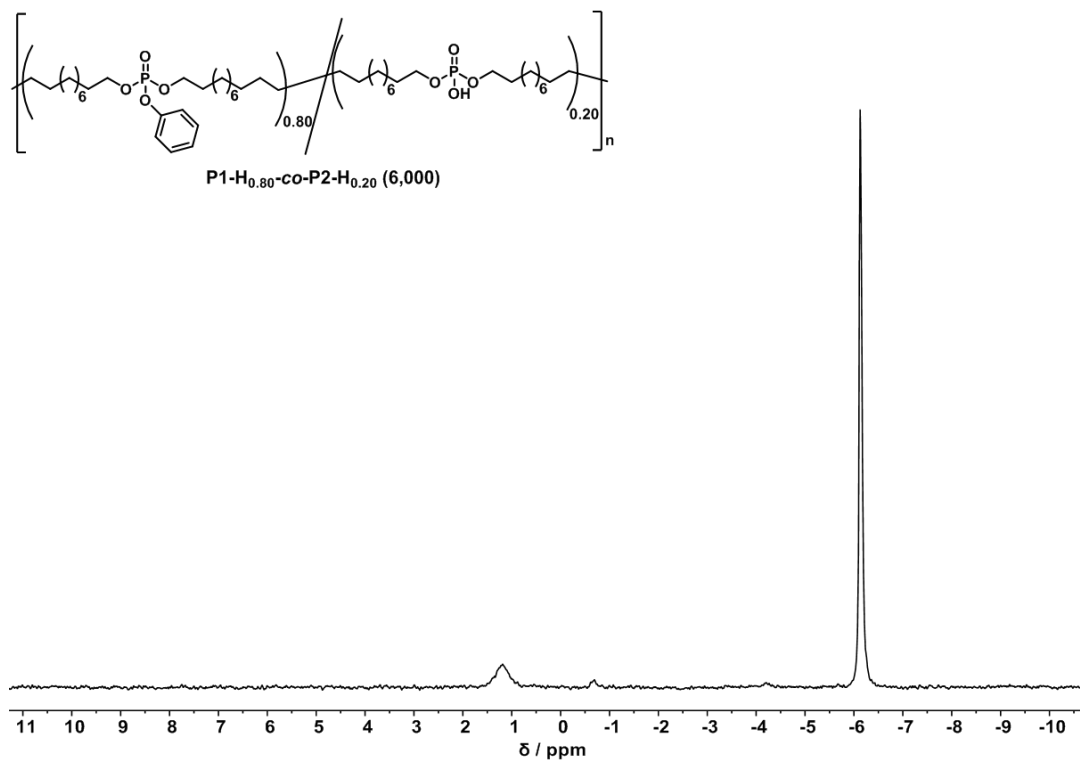
Figure 2.9. ^{31}P (121 MHz) NMR spectra of **P1-H$_{0.8}$-*co*-P2-H$_{0.2}$** in CDCl$_3$ at 298 K.
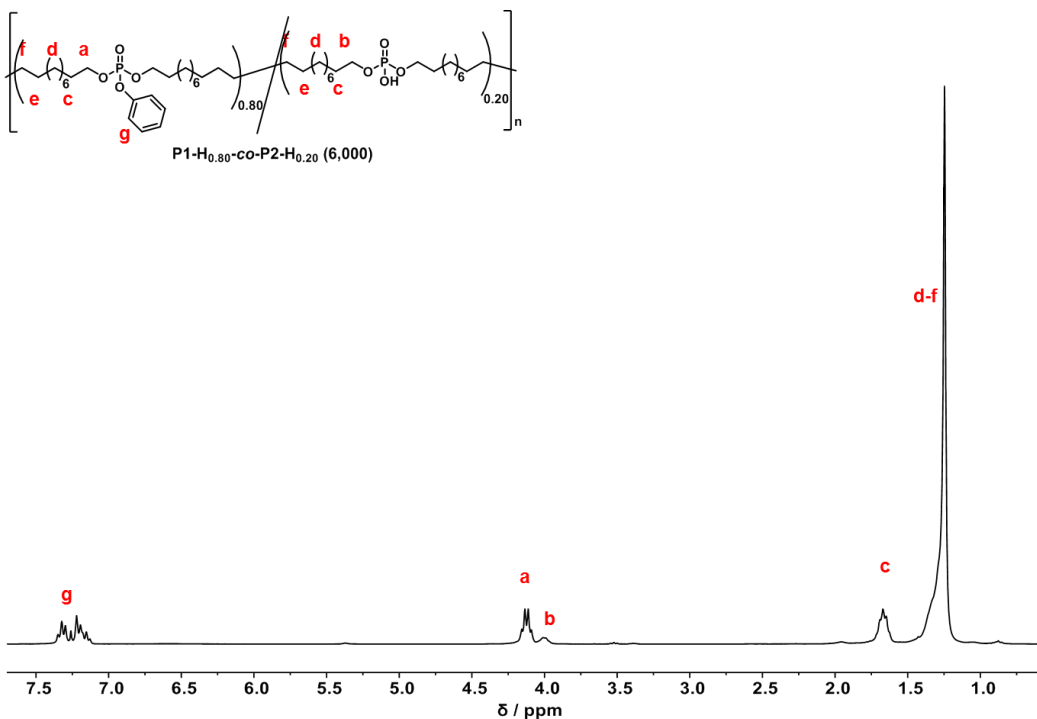
Figure 2.10. ^{1}H (300 MHz) NMR spectra of **P1-H$_{0.8}$-*co*-P2-H$_{0.2}$** in CDCl$_3$ at 298 K.
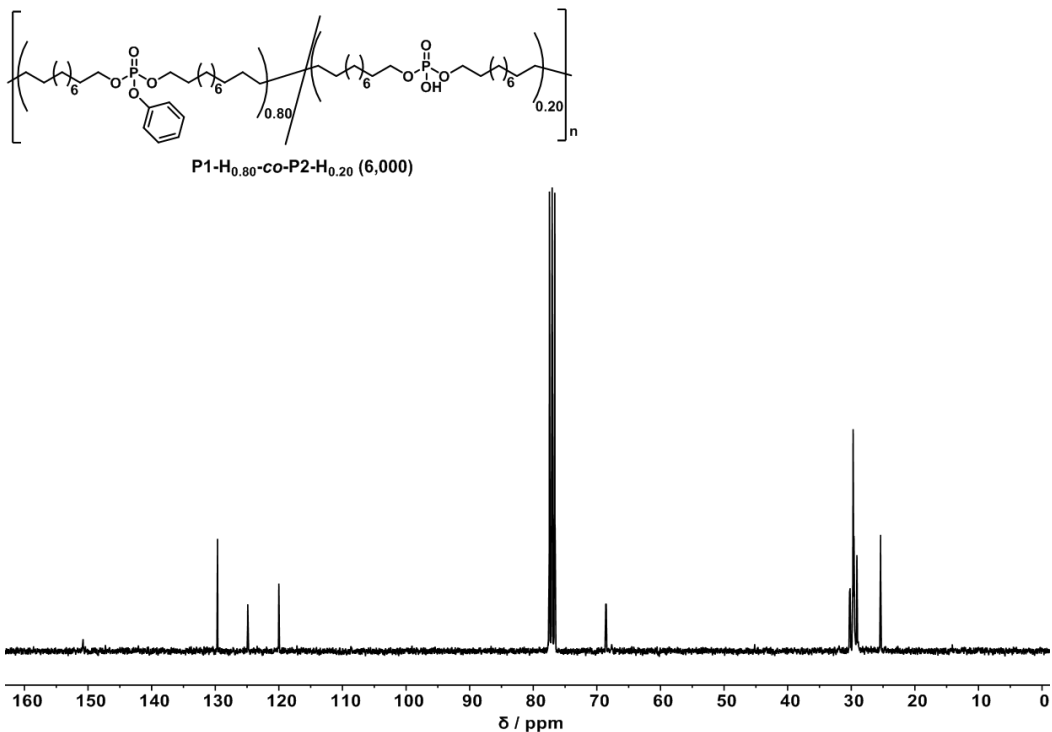
Figure 2.11. ^{1}H (75 MHz) NMR spectra of **P1-H$_{0.8}$-*co*-P2-H$_{0.2}$** in CDCl$_3$ at 298 K.

4.9   Size exclusion chromatography
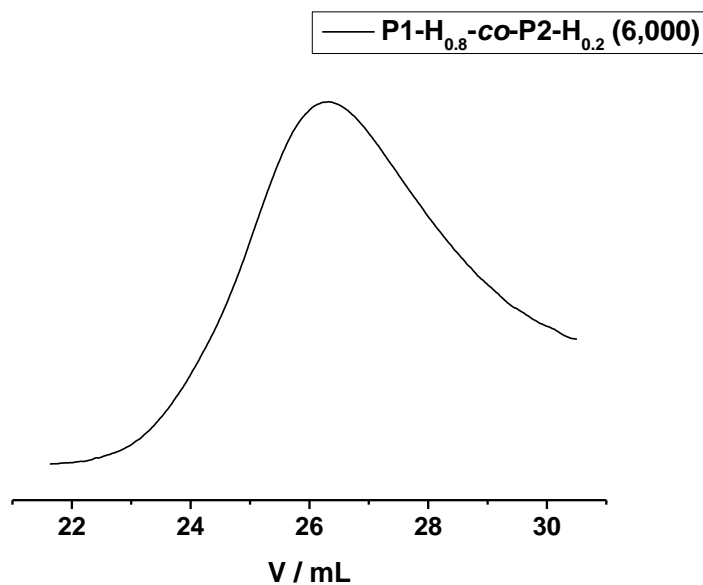
Figure 2.12. SEC Elugram of P1-H$_{0.80}$-co-P2-H$_{0.20}$ in THF (RI detection).

4.10   DSC, TGA
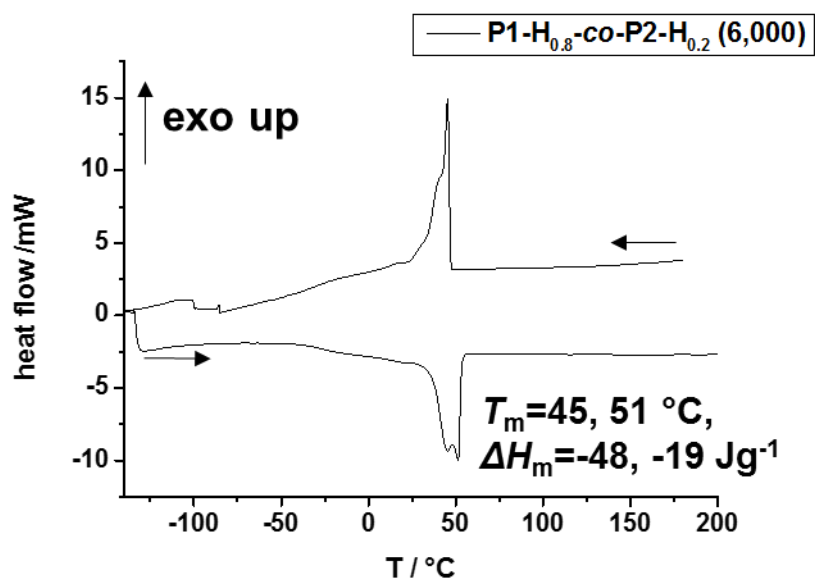
Figure 2.13. DSC of P1-H$_{0.8}$-co-P2-H$_{0.2}$ with a heating (second run) and cooling rate of 10 K min^{-1}.
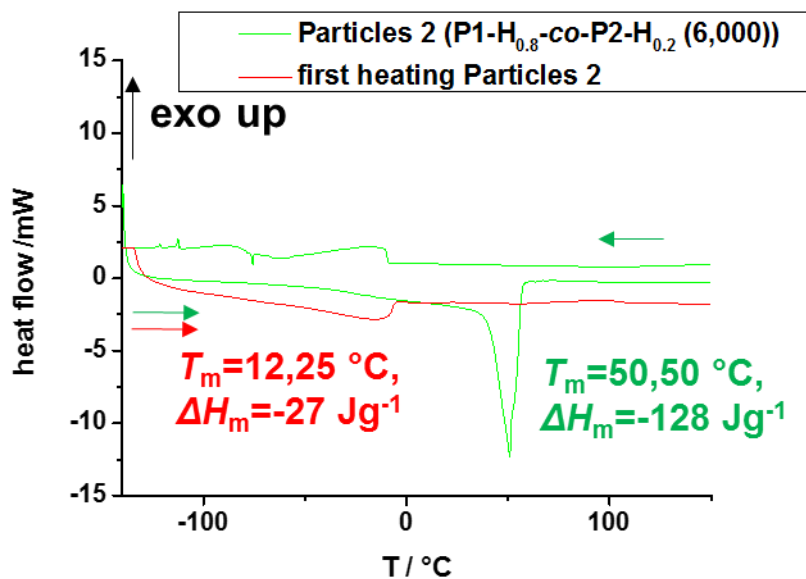
Figure 2.14. DSC of P1-H$_{0.8}$-*co*-P2-H$_{0.2}$ (Particles 2) with a heating (first run red) and cooling rate of 10 K min^{-1}.
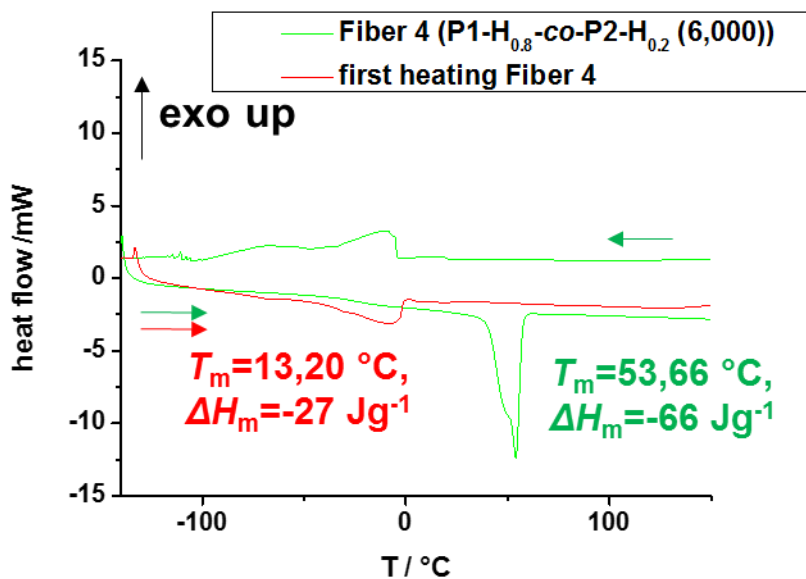
Figure 2.15. DSC of P1-H$_{0.8}$-*co*-P2-H$_{0.2}$ (Fiber 4) with a heating (first run red) and cooling rate of 10 K min^{-1}.

4.11 HPLC
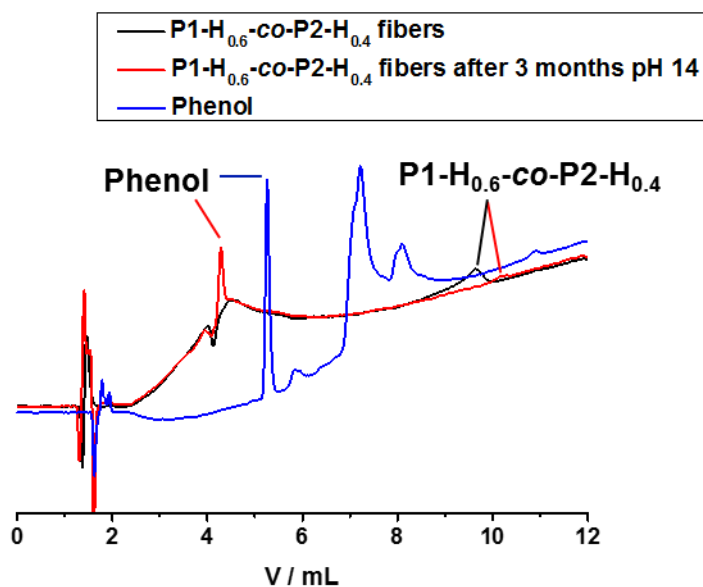
Figure 2.16. HPLC of Phenol and P1-H$_{0.6}$-*co*-P2-H$_{0.4}$ (Fiber 8) before and after 3 months at pH 14. The difference in the elution volume of phenol (red and blue curve) results from different polarity in the mobile phase (more polar for P1-H$_{0.6}$-*co*-P2-H$_{0.4}$ after 3 months at pH 14, in order to lower the elution time of the polymer; see chapter 4.2).

5   References

1.   Li, W.-J.; Laurencin, C. T.; Caterson, E. J.; Tuan, R. S.; Ko, F. K., Electrospun nanofibrous structure: A novel scaffold for tissue engineering. **2002,** *60* (4), 613-621.

2.   Gerardo-Nava, J.; Führmann, T.; Klinkhammer, K.; Seiler, N.; Mey, J.; Klee, D.; Möller, M.; Dalton, P. D.; Brook, G. A., Human neural cell interactions with orientated electrospun nanofibers in vitro. **2009,** *4* (1), 11-30.

3.   Jiang, W.; Kim, B. Y. S.; Rutka, J. T.; Chan, W. C. W., Nanoparticle-mediated cellular response is size-dependent. *Nature Nanotechnology* **2008,** *3*, 145.

4.   Pham, Q. P.; Sharma, U.; Mikos, D. A. G., Electrospinning of Polymeric Nanofibers for Tissue Engineering Applications: A Review. **2006,** *12* (5), 1197-1211.

5.   Thavasi, V.; Singh, G.; Ramakrishna, S. J. E.; Science, E., Electrospun nanofibers in energy and environmental applications. **2008,** *1* (2), 205-221.

6.   Ramakrishna, S.; Fujihara, K.; Teo, W.-E.; Yong, T.; Ma, Z.; Ramaseshan, R., Electrospun nanofibers: solving global issues. *Materials Today* **2006,** *9* (3), 40-50.

7.   Huang, Z.-M.; Zhang, Y. Z.; Kotaki, M.; Ramakrishna, S., A review on polymer nanofibers by electrospinning and their applications in nanocomposites. *Composites Science and Technology* **2003,** *63* (15), 2223-2253.

8.   Gorji, M.; Jeddi, A. A. A.; Gharehaghaji, A. A., Fabrication and characterization of polyurethane electrospun nanofiber membranes for protective clothing applications. **2012,** *125* (5), 4135-4141.

9.   Gopal, R.; Kaur, S.; Ma, Z.; Chan, C.; Ramakrishna, S.; Matsuura, T., Electrospun nanofibrous filtration membrane. *Journal of Membrane Science* **2006,** *281* (1), 581-586.

10.   Qin, X.-H.; Wang, S.-Y., Filtration properties of electrospinning nanofibers. **2006,** *102* (2), 1285-1290.

11.   Cavaliere, S.; Subianto, S.; Savych, I.; Jones, D. J.; Rozière, J. J. E.; Science, E., Electrospinning: designed architectures for energy conversion and storage devices. **2011,** *4* (12), 4761-4785.

12.   Miao, J.; Miyauchi, M.; Simmons, T. J.; Dordick, J. S.; Linhardt, R. J., Electrospinning of Nanomaterials and Applications in Electronic Components and Devices. *Journal of Nanoscience and Nanotechnology* **2010,** *10* (9), 5507-5519.

13.   Wang, X.; Drew, C.; Lee, S.-H.; Senecal, K. J.; Kumar, J.; Samuelson, L. A., Electrospun Nanofibrous Membranes for Highly Sensitive Optical Sensors. *Nano Letters* **2002,** *2* (11), 1273-1275.

14.   Agarwal, S.; Greiner, A.; Wendorff, J. H., Functional materials by electrospinning of polymers. *Progress in Polymer Science* **2013,** *38* (6), 963-991.

15.   Gunn, J.; Zhang, M., Polyblend nanofibers for biomedical applications: perspectives and challenges. *Trends in Biotechnology* **2010,** *28* (4), 189-197.

16.   Kishan, A. P.; Cosgriff-Hernandez, E. M., Recent advancements in electrospinning design for tissue engineering applications: A review. **2017,** *105* (10), 2892-2905.

17.   Wang, Y.-C.; Yuan, Y.-Y.; Du, J.-Z.; Yang, X.-Z.; Wang, J., Recent Progress in Polyphosphoesters: From Controlled Synthesis to Biomedical Applications. **2009,** *9* (12), 1154-1164.

18.   Steinbach, T.; Wurm, F. R., Poly (phosphoester) s: a new platform for degradable polymers. *Angewandte Chemie International Edition* **2015,** *54* (21), 6098-6108.

19.   Bauer, K. N.; Tee, H. T.; Velencoso, M. M.; Wurm, F. R. J. P. i. P. S., Main-chain poly (phosphoester) s: History, syntheses, degradation, bio-and flame-retardant applications. **2017,** *73*, 61-122.

20.   Subbiah, T.; Bhat, G. S.; Tock, R. W.; Parameswaran, S.; Ramkumar, S. S., Electrospinning of nanofibers. **2005,** *96* (2), 557-569.

21.   Shah, S. S.; Cha, Y.; Pitt, C. G., Poly (glycolic acid-co-dl-lactic acid): diffusion or degradation controlled drug delivery? *Journal of Controlled Release* **1992,** *18* (3), 261-270.

22.   Avgoustakis, K.; Beletsi, A.; Panagi, Z.; Klepetsanis, P.; Livaniou, E.; Evangelatos, G.; Ithakissios, D. S., Effect of copolymer composition on the physicochemical characteristics, in vitro stability, and biodistribution of PLGA–mPEG nanoparticles. *International Journal of Pharmaceutics* **2003,** *259* (1), 115-127.

23.   Huang, X.; Brazel, C. S., On the importance and mechanisms of burst release in matrix-controlled drug delivery systems. *Journal of Controlled Release* **2001,** *73* (2), 121-136.

24.   Anderson, J. M.; Shive, M. S., Biodegradation and biocompatibility of PLA and PLGA microspheres. *Advanced Drug Delivery Reviews* **1997,** *28* (1), 5-24.

25.   Park, T. G., Degradation of poly(lactic-co-glycolic acid) microspheres: effect of copolymer composition. *Biomaterials* **1995,** *16* (15), 1123-1130.

Chapter 3

Selective hydrolysis of phosphoester side or main-chain in long-chain aliphatic PPEs

Foreword

The following chapter is based on unpublished results.

Abstract
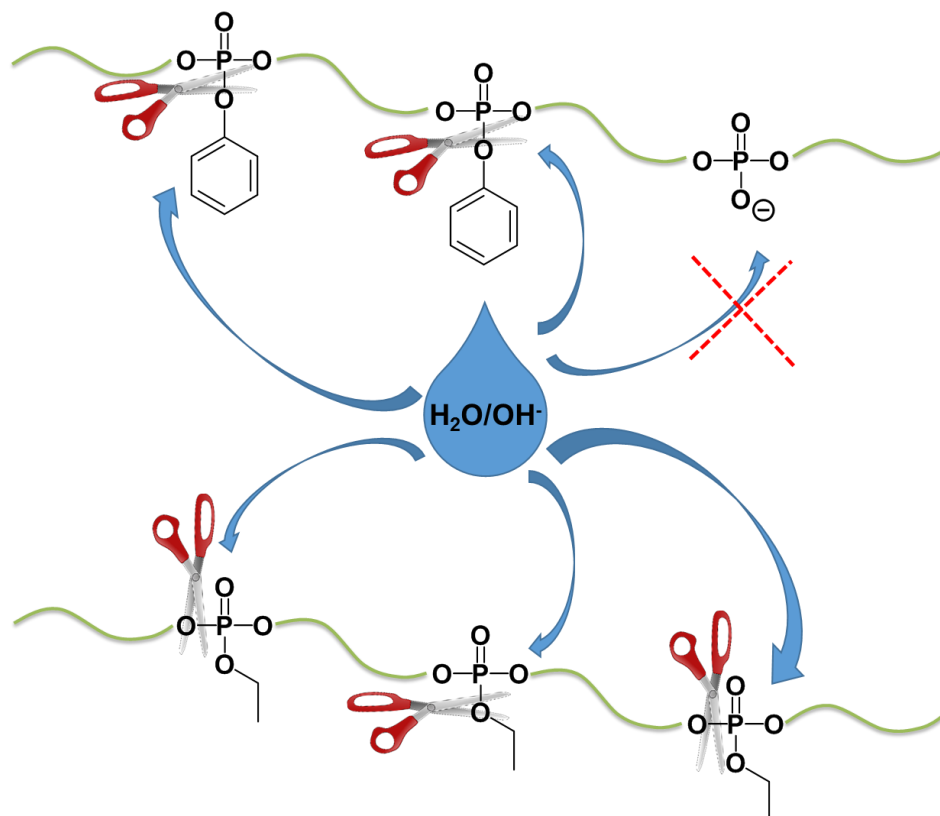
Acyclic diene metathesis polymerization of long-chain diene alkyl phosphoesters offers a fast access to functional and potentially degradable polyethylene mimics. The degradation behavior of such hydrophobic polyphosphoesters (PPEs) is, however, not well studied and by tailoring of the ester stabilities, a precise cleavage of the side or the main chain should be feasible. Herein, we study the hydrolysis at pH 7 and pH 14 of long-chain alkyl polyphosphoesters with phenoxy and ethoxy side chains (Figure 3.1). The degradation is followed by weight loss measurements and differential scanning calorimetry. We show that harsh basic conditions are necessary for hydrolysis to phosphoric acid diesters and precise side group hydrolysis is possible by using

aromatic phosphoesters side groups. Furthermore, we find that PPEs with an ethoxy side chain can form pyrophosphates with main chain hydrolysis under basic conditions. Our findings help to develop novel PE mimics based on polyphosphoesters with a precise degradation profile.

1 Introduction

With the rising ecological and health concern, biodegradable polymers have attracted great interest in the last decades in fundamental research as well as in technology, due to their high potential in addressing environmental concerns and potential in biomedical applications. The use of biodegradable polymers has grown significantly in packaging, agriculture, fibers, surgical suture, tissue engineering, controlled drug delivery, and gene therapy.[1-7] Besides all properties the materials have to bring along for their applications, biodegradability is one of the most fundamental and essential property to bring no extra burden on today's severe environmental issue.[8] Furthermore, for biomedical applications, it can be a required design variable to be addressed as biodegradability permits, for example, spatiotemporal control release of the cargo molecule in controlled drug delivery applications[9] or allows infiltration of blood cells and provides space for proliferating cells in tissue engineering applications.[10] Therefore the biodegradation rate is an essential parameter for specific applications which is not only depended on the chemical structure of the polymer but also multiscale structures like crystal size, crystallinity, crystal modifications, and molecular alignment. For semicrystalline polyesters, it is known that the degradation in aqueous media occurs first in the amorphous region by random hydrolytic scission of ester bonds. When most of the amorphous parts are degraded, the crystalline domains are under hydrolytic attack from the edges towards the center.[11] Therefore the molecular alignment of the polymer in crystalline domain is important for the degradable segments to be accessible for hydrolytic attack. Long chain aliphatic polyphosphoesters (PPEs) are reported to be semicrystalline and have a similar lamellar crystalline structure as polyethylene with a pseudohexagonal crystal structure.[12] However, compared to the polyolefin counterpart, these PPEs are potentially degradable due to phosphoesters located in the polymer backbone. Crystal structure analysis revealed that in single crystals the phosphoesters in the backbone are located in the chain folding end with the side group outside of the lamellae. For larger crystals or melt grown crystals, the lamellae thickness is close to an extended chain crystal with 20 CH_2 units with possibly no chain folding similar to a fringed micelle with the phosphate defects urged into the amorphous phase making those phosphates accessible to hydrolysis. Baran and Penzcek made

thorough investigations on the hydrolysis of PPEs and found out, that an nucleophilic attack of OH⁻ on polyphosphoesters resulted in similar rates for the cleavage of side and main chain.[13] Herein, we present the degradation of long-chain aliphatic PPEs as polymer films with different side groups in order to control the degradation profile. Therefore the degradation of PPEs with various amount of phenoxy side chains were measured and compared to analog ethoxylated-PPE. Different conditions were used to evaluate the degradation of these hydrophobic PPE films. Strong basic conditions at pH 14 and neutral conditions at pH 7.4 in PBS buffer.

2   Results and Discussion

Different PPEs were prepared by ADMET polymerization (Figure 3.1). **P1-H** carried a phenolic ester as pendant chain, while two aliphatic phosphoesters built up the main chain. Aromatic esters are known exhibit higher rates in hydrolytic degradation compared to aliphatic esters. This should lead to a selective cleavage of the pendant chains. Additionally, due to the resulting negative charge of the produced phosphodiester after the first hydrolysis step, a further degradation should only occur under very harsh conditions. Copolymers **P1-H$_{0.8}$-*co*-P2-H$_{0.2}$** and **P1-H$_{0.6}$-*co*-P2-H$_{0.4}$** were chosen as they have the same phenoxy side chains, however, vary in their hydrophilicity which should alter the hydrolysis kinetics of the pendant ester groups (see below). In contrast, **P3-**

H with the ethoxy side groups, we expected similar rates for the hydrolysis of the main and the side chains.

P1-H

P1-H$_{0.8}$-*co*-P2-H$_{0.2}$

P1-H$_{0.6}$-*co*-P2-H$_{0.4}$

P3-H
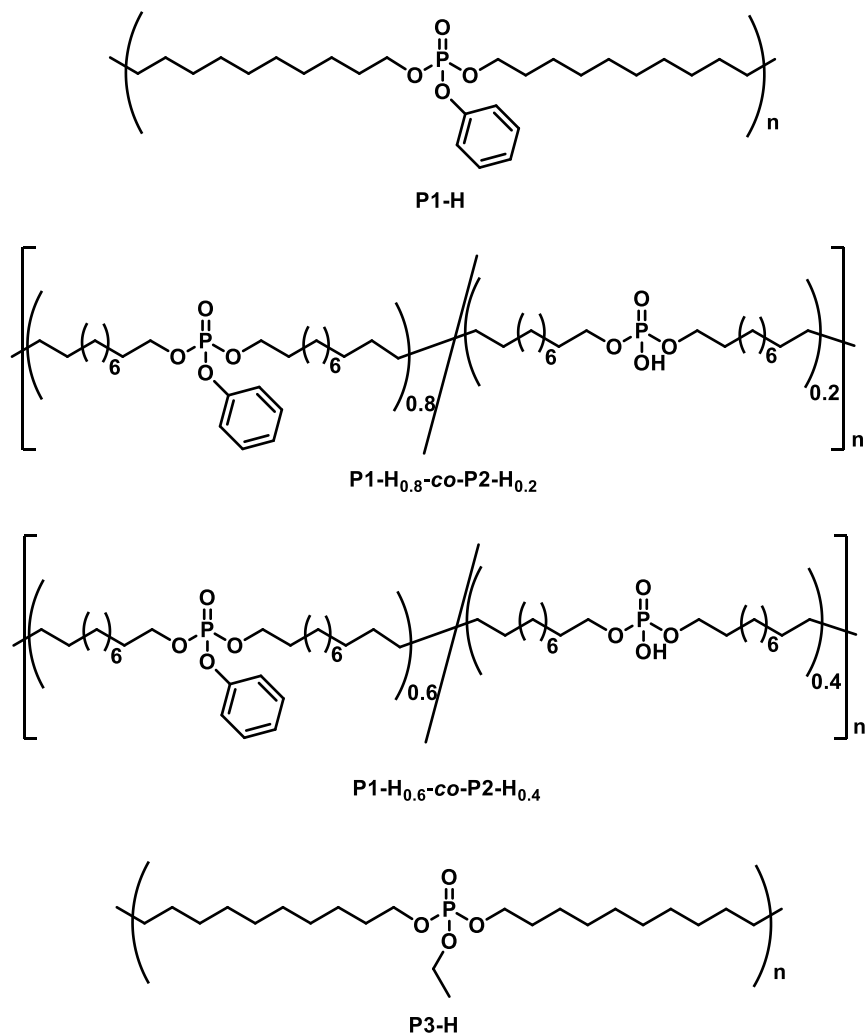
Figure 3.1. Structure of polyphosphoesters used in this study.

Solid State Characterization. The X-ray diffractogram of **P1-H**, **P1-H$_{0.8}$-co-P2-H$_{0.2}$**, **P1-H$_{0.6}$-co-P2-H$_{0.4}$**, and **P3-H** showed a similar degree of crystallinity and crystal structure between the polymers used for the degradation measurements (Figure 3.2). The crystallization behavior of such long alkyl-chain PPEs have been already studied in our group and are considered to have a similar semicrystalline bulk structure as polyethylene with a pseudohexagonal crystal structure.[12,14] All polymers in this study have a peak position at 2Θ of 21.7° which corresponds to a lattice

spacing of 0.41 nm and indicates that the crystal lattice is slightly inflated compared to the orthorhombic phase of PE which exhibits an XRD peak at $2\Theta = 20.5°$.[15]
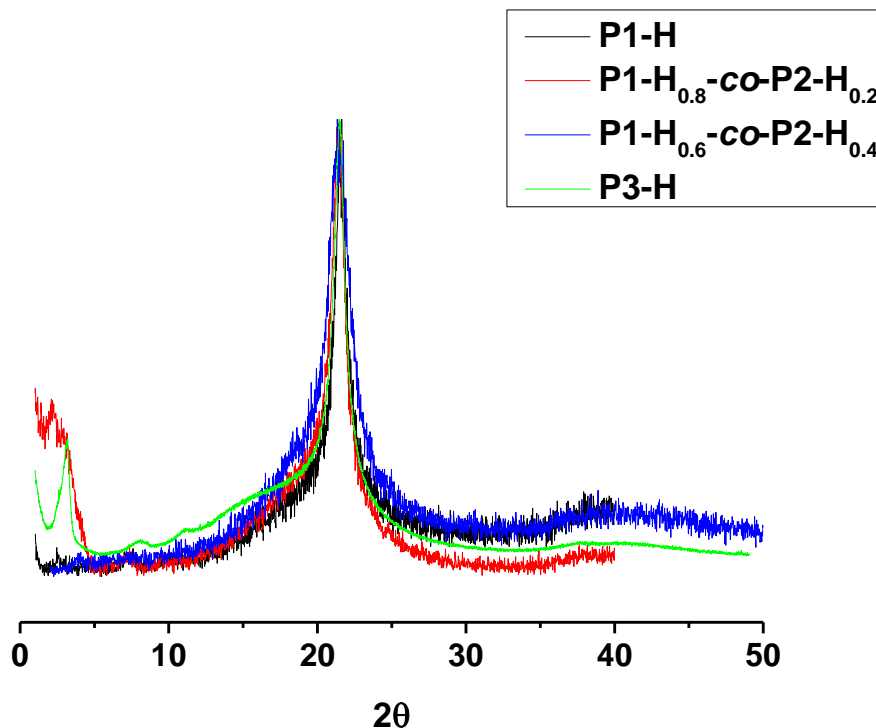
Figure 3.2. X-ray diffractograms of P1-H, P1-H$_{0.8}$-co-P2-H$_{0.2}$, P1-H$_{0.6}$-co-P2-H$_{0.4}$, and P3-H.

Polymer films were prepared by solution casting of chloroform solutions on microscope coverslips. The polymer films prepared in this study where all waxy to brittle solid films. They were immersed into the respective solution with pH 7 and 14 and their degradation was studied by DSC and weight loss measurement. After 8 weeks, the degradation products were dried and analyzed by DSC. Macroscopically, the degradation products appeared to be more brittle films or as broken particles. The changes of the melting transitions and the crystallinity of the polymer

films after degradation were determined by differential scanning calorimetry (DSC) and are shown in Figure 3.3.
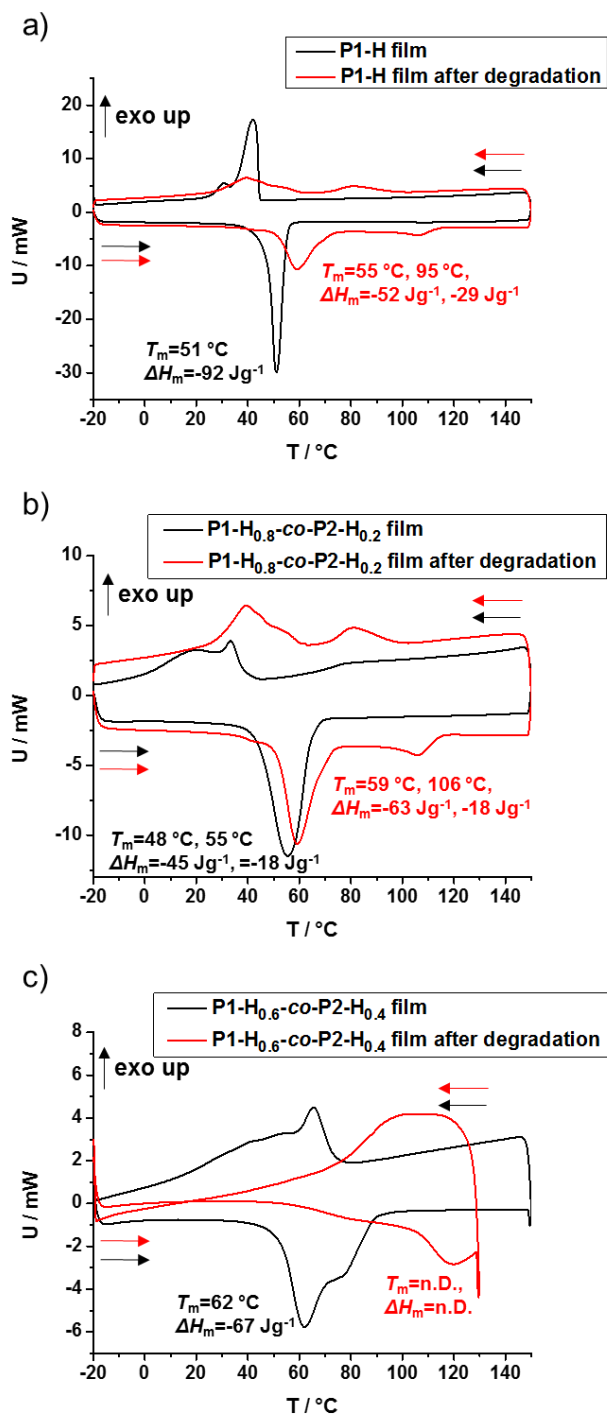
Figure 3.3. DSC of polymer films before and after degradation. (a) P1-H film. (b) P1-H$_{0.8}$-co-P2-H$_{0.2}$ film. (c) P1-H$_{0.6}$-co-P2-H$_{0.4}$ film.

Comparing the DSC curves in Figure 3.3 it is noticeable that in all cases, the melting temperature (T_m) is increased after degradation at pH 14. The data in Table 3.1, extracted from the DSC measurements, shows that **P1-H** films exhibit the highest crystallinity with 31% while the copolymer films exhibit similar crystallinity with around 22%. After degradation, we can see a decrease in crystallinity for **P1-H** films to 24% and an increase in crystallinity for **P1-H$_{0.8}$-*co*-P2-H$_{0.2}$** films to 24% for both polymers. The thermal data for **P1-H$_{0.6}$-*co*-P2-H$_{0.4}$** films after degradation could not be evaluated due to decomposition after 130 °C. NMR data of the polymer films after degradation could not be conducted due to the insolubility of the polymer films after the degradation process. However, the data indicates a sidechain ester hydrolysis due to the increased melting temperature and the insolubility of the polymer films afterward. The only similar PPE which was not soluble was **P2** reported in Chapter 1. Furthermore, phosphoester hydrolysis on the backbone should increase the solubility of the polymers. The increase of T_m ascends with higher composition of **P2** indicates a surface erosion of our polymer films, due to the high hydrophobicity of those long-chain PPEs.

Table 3.1. Thermal data acquired from DSC.

Sample	T_m/°C	T_c/°C	ΔH_m/J g^{-1}	crystallinity /%
P1-H film	51	42; 31	92	31
P1-H film after degradation	55; 95	94; 41	81	24
P1-H$_{0.8}$-*co*-P2-H$_{0.2}$ film	48, 55	48; 43	63	22
P1-H$_{0.8}$-*co*-P2-H$_{0.2}$ film after degradation	59, 106	81; 39	81	24
P1-H$_{0.6}$-*co*-P2-H$_{0.4}$ film	62	65	67	23
P1-H$_{0.6}$-*co*-P2-H$_{0.4}$ film after degradation	n.D.	n.D.	n.D.	n.D.

Determined by DSC with heating/cooling rate of 10 K min^{-1}. Peak T_m determined from the first heating run. [d] From DSC measurements, calculated *vs.* 100 % crystalline polyethylene (293 J g^{-1}).[16]

Weight loss determination of polymer films. Degradation of the PPEs was measured by weight loss of polymer films. The polymer films were immersed into PBS buffer at pH 7.4 and at high basic conditions at pH 14. The weight loss was measured over a period of several weeks. The polymer films on the glass coverslips were immersed into 4 mL aqueous solution of the specific degradation condition at 37 °C. After 4 and 8 weeks the polymer films were taken out, dried and the weight measured. Photos of all polymer films after 2 months immersion are shown in Figure 3.5. Changes to the polymer films were only detected for the polymer films at pH 14. The films were partially fragmented.

Figure 3.4a shows the weight changes of the polymer films at pH 7 and pH 14. As the fragments are not water soluble, only the release of phenol from the polymer film could be measured by weight loss (which is soluble under these conditions). Thus, the weight loss should increase with increasing amount of **phenolic esters** the polymer and the exact theoretical weight loss from cleavage of the phenoxy side chain can be calculated.

a)

b)

P1-H film: 0.13 mmol Phenoxy; weight loss $\triangleq$ 0.18 mmol Phenyl
P1-H$_{0.8}$-*co*-P2-H$_{0.2}$ film: 0.11 mmol Phenoxy; weight loss $\triangleq$ 0.14 mmol Phenyl
P1-H$_{0.6}$-*co*-P2-H$_{0.4}$ film: 0.09 mmol Phenoxy; weight loss $\triangleq$ 0,09 mmol Phenyl
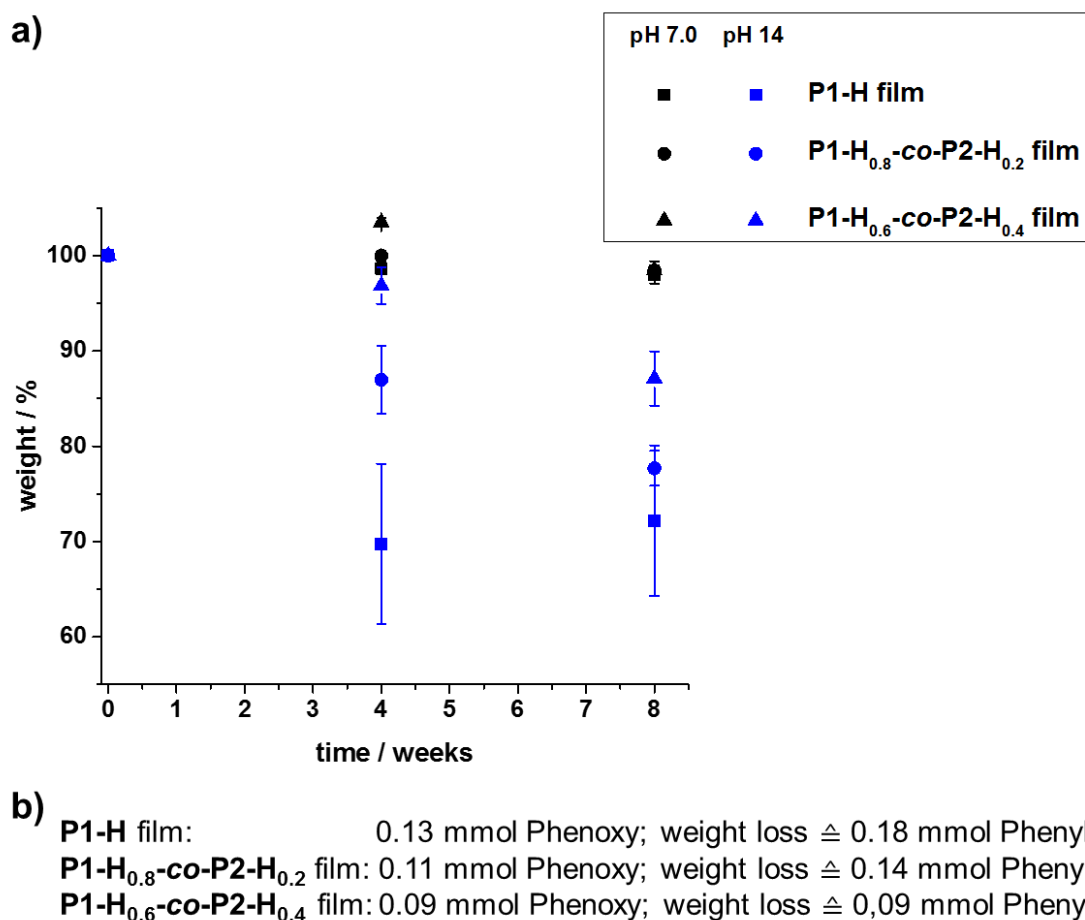
Figure 3.4. (a) Mass loss of P1-H, P1-H$_{0.8}$-co-P2-H$_{0.2}$ and P1-H$_{0.6}$-co-P2-H$_{0.4}$ films under neutral (black) and basic conditions (blue) over a time frame of 2 months. (b) Amount of phenoxy groups in polymer films and calculated amount of phenoxy groups determined by weight loss at pH 14.

At pH 7.0 no significant weight loss can be detected for **P1-H**, **P1-H$_{0.8}$-*co*-P2-H$_{0.2}$**, and **P1-H$_{0.6}$-*co*-P2-H$_{0.4}$**. At pH 14 a clear weight loss for all polymer films was detected. However, after 8 weeks the weight loss did not overcome 30% and showed a remaining weight of 72%, 78% and 87% for **P1-H**, **P1-H$_{0.8}$-*co*-P2-H$_{0.2}$**, and **P1-H$_{0.6}$-*co*-P2-H$_{0.4}$** respectively. Noticeable is the decreasing weight loss with decreasing amount of phenoxy side chain in the polymer. Calculation of the amount of phenoxy side chain in the polymer films of **P1-H**, **P1-H$_{0.8}$-*co*-P2-H$_{0.2}$** and **P1-H$_{0.6}$-*co*-P2-H$_{0.4}$** and comparing this to the weight loss as phenol, shows that the weight loss corresponded to the weight of the phenoxy side chains in the respective polymers (Figure 3.4b and Scheme 3.1).
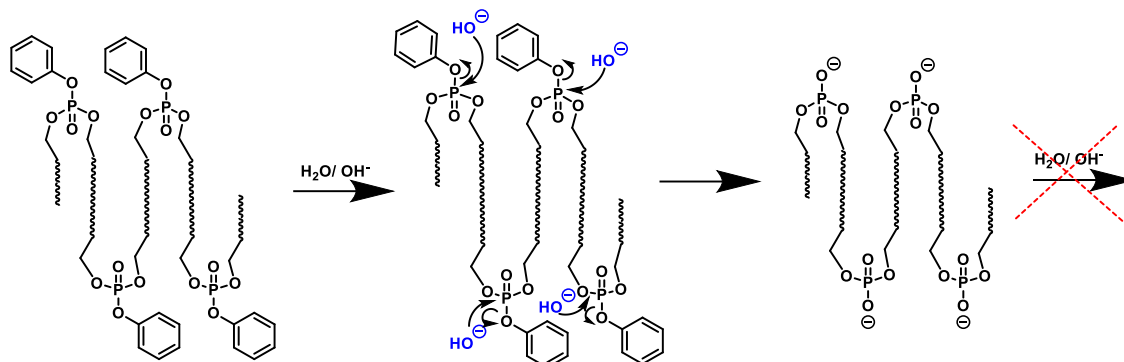
Scheme 3.1. Hydrolysis mechanism of P1-H under basic conditions.
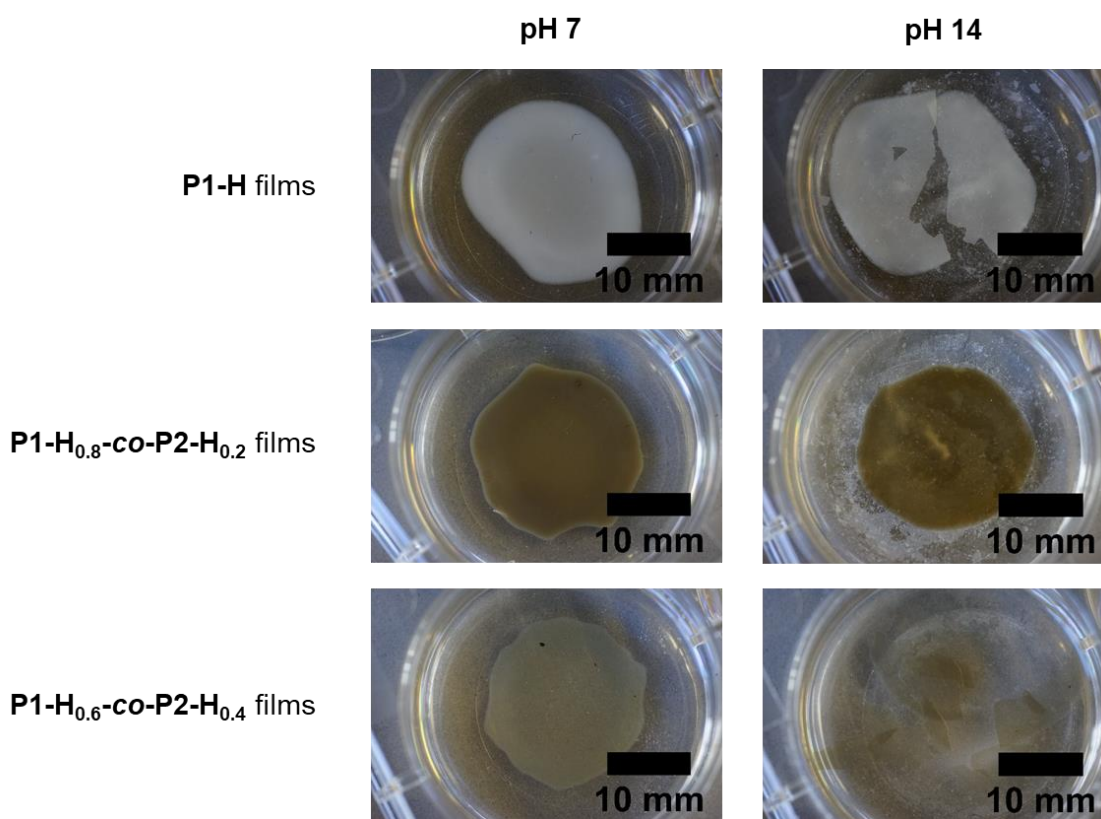
Figure 3.5. Photos of P1-H, P1-H$_{0.8}$-co-P2-H$_{0.2}$, and P1-H$_{0.6}$-co-P2-H$_{0.4}$ films after 2 months degradation measurements in pH 7 and pH 14.

Scanning electron microscope (SEM) images of the same polymer films showed that **P1-H** had a smoother surface at pH 7 as no degradation occurs. After immersing the film at pH 14 all polymers proved a similar rough surface indicating the degradation of the polymer.
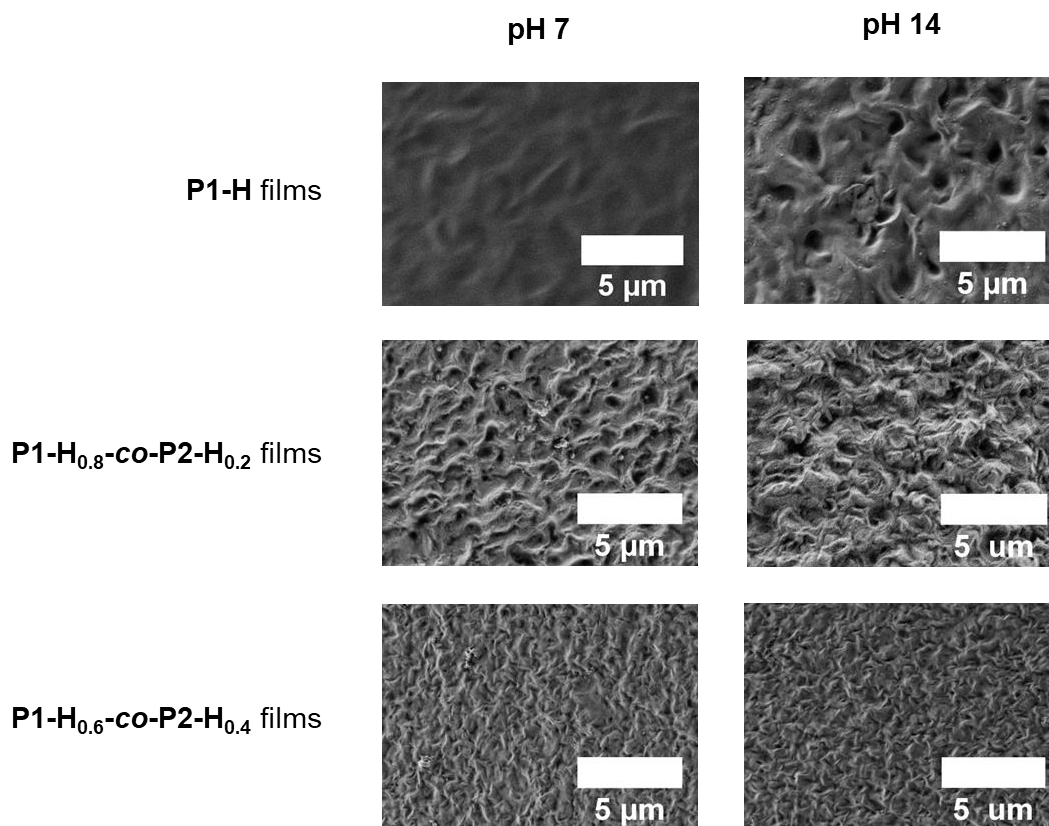
Figure 3.6. SEM images of P1-H, P1-H$_{0.8}$-co-P2-H$_{0.2}$ and P1-H$_{0.6}$-co-P2-H$_{0.4}$ films after 2 months degradation measurement in pH 7 and pH 14.

P3-H carrying the ethoxy side chain was also immersed in 2 N NaOH (pH 14) for 3 months for comparison of the degradation behavior when all phosphoester bonds are aliphatic. The films were fragmented into small pieces and in contrast to **P1-H**, the degradation products were still soluble in organic solvents.

DSC of polymer films before and after degradation proves that the degradation happens also in the crystalline part. The melting point of the Et-PPE film before degradation was $T_m = 55$ °C ($\Delta H_m = 77$ J/g) and changed to $T_m = 85$ °C ($\Delta H_m = -38$ J/g) (Figure 3.7).
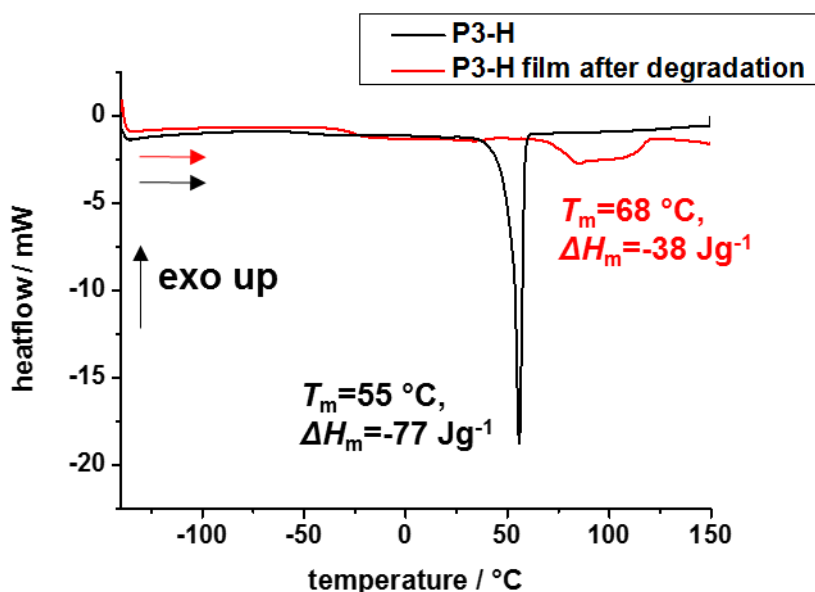
Figure 3.7. DSC of P3-H films before and after degradation at pH 14.

Due to the amphiphilic nature of these PPEs, we assume separation of the polar phosphoester groups from the apolar aliphatic main chain which brings the phosphoester groups close together and determines the degradation products. The separation is especially the case in the crystalline part of the polymer when the polymer chains form lamellae. Therefore, when the side chain is cleaved the phosphate will turn into the diester and the phosphate group does not gain any freedom, so no further reaction will happen as proven by the degradation of **P1-H**. However, since **P3-H** has no aromatic esters 66% of the hydrolysis will be in the main chain. Herein, the HMBC experiment showed the distinct peaks for pyrophosphates at -13 ppm in the ^{31}P NMR. Scheme 3.2 shows the proposed hydrolysis mechanism of P3-H under basic conditions.
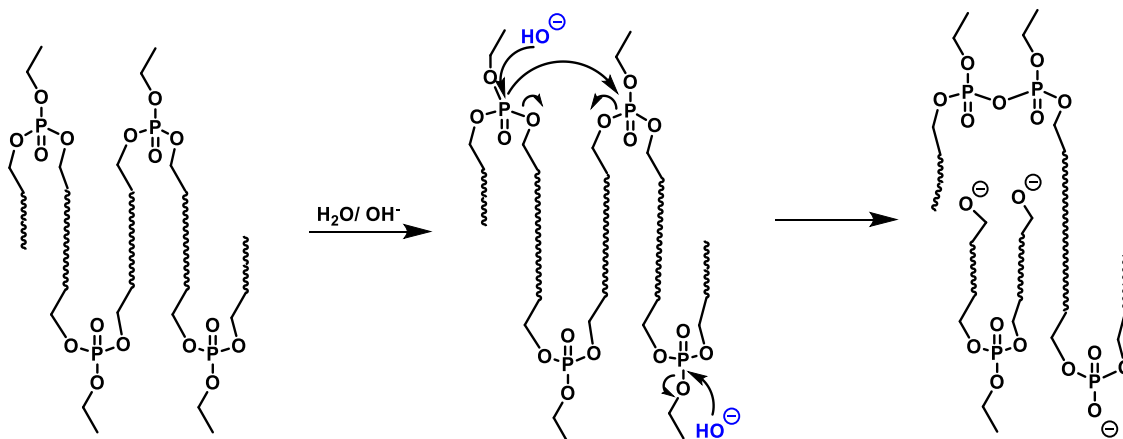
Scheme 3.2. Proposed hydrolysis mechanism of P3-H under basic conditions.

Figure 3.8 shows the Heteronuclear Multiple Bond Correlation (HMBC) NMR measurements of **P3-H** after 3 months at pH 14. Several products can be identified, such as diesters from side or main chain hydrolysis, unaltered phosphotriesters and pyrophosphates. Under basic conditions, the nucleophilic attack of the OH⁻ takes place on the central phosphorous atom resulting in similar rates for the cleavage of side and main chain.
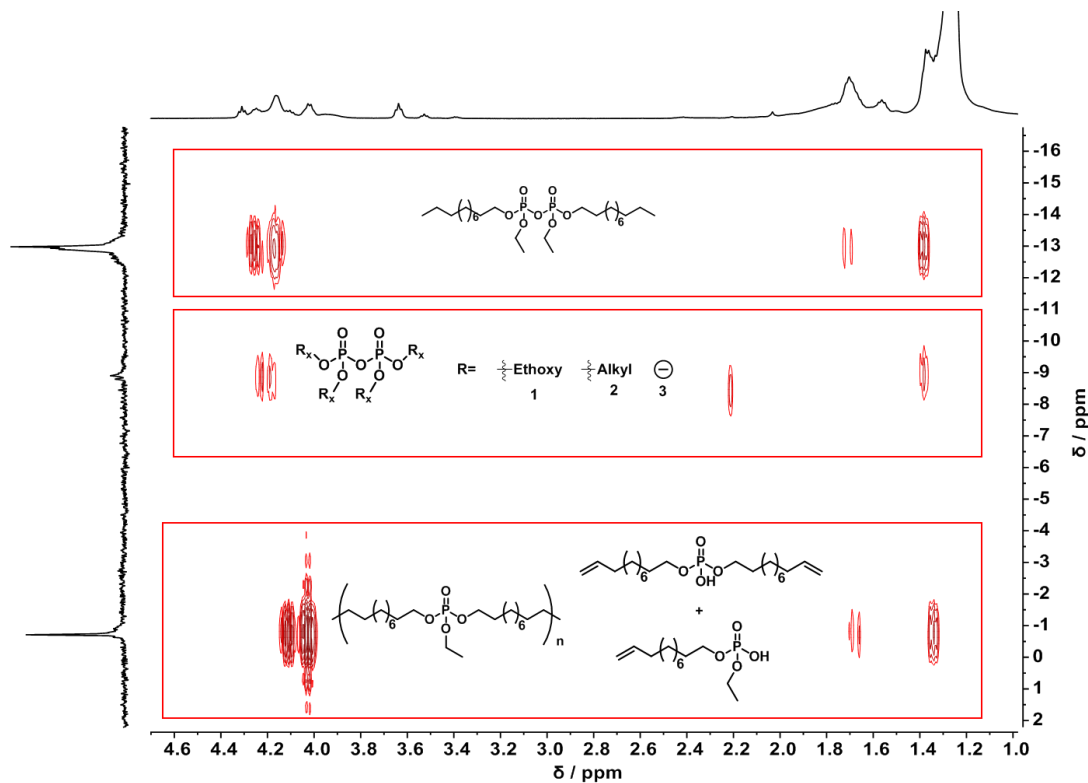
Figure 3.8. ^{1}H-^{31}P HMBC NMR spectrum of P2-H film after degradation at pH 13.

3   Summary

We studied the hydrolytic degradation of films of semicrystalline PPEs. These PE-mimics have a similar bulk morphology as PE, however, due to the phosphate groups allow hydrolysis of the materials. We investigated PPEs with aromatic and aliphatic pendant esters with respect to their hydrolysis. Polymer films were prepared by solution casting and did not show any degradation at pH 7. PPEs with the phenoxy side chain showed only side chain hydrolysis at pH 14 while **P3-H** with aliphatic phosphoesters only showed random hydrolysis of side and main chain ester bonds. Furthermore, the formation of pyrophosphates was observed for main chain hydrolysis due to the obtained mobility and the vicinity of other phosphates in the bulk. This knowledge will be further used to prepare degradable PE-mimics with precise chain scission for future applications.

4   Experimental Section

4.1   General Information

All Solvents were purchased from Sigma Aldrich or VWR and used as received. Dry solvents were purchased from Acros Organics or Sigma Aldrich and stored with a septum and over molecular sieves. $CDCl_3$ and CD_2Cl_2 was purchased from Sigma Aldrich. Catalysts, and all other chemicals were purchased from Sigma Aldrich and used as received unless otherwise stated.

4.2   Instrumentation and Characterization Techniques

NMR. Heteronuclear Multiple Bond Correlation (HMBC) NMR spectra of the monomers and polymers were recorded on a Bruker AVANCE III 500 MHz spectrometer. All spectra were measured in $CDCl_3$ at 298 K. The spectra were calibrated against the solvent signal and analyzed using MestReNova 8 from Mestrelab Research S.L.

DSC. The thermal properties of the polymer films and films after degradation have been measured by differential scanning calorimetry (DSC) on a Mettler Toledo DSC 823 calorimeter. Three scanning cycles of heating-cooling were performed in an N_2 atmosphere with a heating and cooling rate of 10 °C min^{-1}.

SEM. SEM investigations were performed by using a LEO 1530 GEMINI. The characterizations were carried out by applying the low-voltage approach. The fibers were deposited with the alumina or silver foil on conductive carbon tape.

4.3   Synthetic Procedures

4.3.1   Monomer Synthesis

*Bis-(undec-10-en-1-yl) phenylphosphate (**M1**)*

See Chapter 1.

*Bis-(undec-10-en-1-yl) phosphate (**M2**)*

See Chapter 1.

*Bis-(undec-10-en-1-yl) ethylphosphate (**M3**)*

A 1000 mL schlenk flask, equipped with a dropping funnel, was charged with ethyl dichlorophosphate (120 g, 0.74 mol), dissolved in dry CH_2Cl_2 (150 mL) under an argon atmosphere. The solution was cooled to 0 °C with an ice-bath. 50 mL dry CH_2Cl_2 and 1.8

equivalents of Et_3N (183.66 mL) and 266 mL 10-Undecen-1-ol were dropped over a period of 1 h via the dropping funnel. After the addition, 0.01 equivalents of 4-*N,N*- dimethylaminopyridine (0.9 g) was added and the reaction was stirred overnight at room temperature. The crude mixture was concentrated at reduced pressure, dissolved in diethyl ether and filtered. The organic phase was washed twice with 10 % aqueous hydrochloric acid (HCl) solution and twice with brine. The organic layer was dried over sodium sulfate, filtered, concentrated at reduced pressure, and purified by chromatography over neutral alumina using dichloromethane as eluent to give a clear yellowish liquid (yield: 53 %, $R_f(AlOx)$: 0.5 (PE/EtOAc = 8/2)). ^{1}H NMR (250 MHz, $CDCl_3$, 298 K): δ = 5.79 (ddt, J_1= 16.9 Hz, J_2 = 10.2 Hz, J_3 = 6.7 Hz, 2H, CH2=C*H*-), 5.06-4.87 (m, 4H, C*H2*=CH-), 4.18-3.94 (m, 6H, -OPO3-C*H2*-), 2,06-1.98 (m, 4H, =CH-C*H2*-), 1.70-1.63 (m, 4H, -OPO3-CH2-C*H2*-), 1.38-1.27 ppm (m, 27H). ^{13}C {H} NMR (176 MHz, $CDCl_3$, 298 K): δ = 139.27, 114.25, 67.78, 63.76, 33.91, 30.41, 29.54, 29.23, 29.03, 25.56, 16.30 ppm. ^{31}P {H} NMR (283 MHz, CDCl3, 298 K): δ = -0.71 ppm.

4.3.2 Polymer synthesis

P1$_{0.80}$-*co*-P2$_{0.20}$

See Chapter 1.

P1$_{0.60}$-*co*-P2$_{0.40}$

See Chapter 1.

P1-H$_{0.80}$-*co*-P2-H$_{0.20}$

See Chapter 1.

P1-H$_{0.60}$-*co*-P2-H$_{0.40}$

See Chapter 1.

P3

In a vacuum reactor, 70 g of **M2** and the Grubbs catalyst 1st generation (0.3 mol%) were mixed under an argon atmosphere. Polymerization was carried out at reduced pressure (first membrane pump (5 h, 50 mbar) then oil pump (0.07 mbar)) to remove ethylene gas evolving during the metathesis reaction, at 65 °C for 1 h and 85 °C for 48 h. The crude mixture was dissolved in CH_2Cl_2, treated with *tris*-(hydroxymethyl) phosphine (10 eq with respect to the catalyst) and 2 mL of Et_3N. After stirring for 1 h water was added in the same volume to the organic phase and the solution was stirred overnight. The organic layer was washed twice with a mixture of 100 mL 5 %

aqueous HCl and 100 mL brine and then washed twice with brine. The water layer was extracted with ethyl acetate or diethyl ether several times until the emulsion disappeared and the water layer got clear. The organic layer was dried over sodium sulfate (Na_2SO_4), filtered and dried at reduced pressure. (yield: 93 %). Number-average molecular weight, weight-average molecular weight and molecular weight distribution are $9.3 \cdot 10^3$ g/mol, $23.1 \cdot 10^3$ g/mol and $M_w/M_n = 2.5$. ^{1}H NMR (250 MHz, $CDCl_3$, 298 K, ppm): δ = 5.53-5.27 (m, 2H, -C*H*=C*H*-), 4.21-3.90 (m, 6H, -OPO3-C*H*2-), 2.13-1.85 (m, 2H =CH-C*H*2-), 1.75-1.53 (m, 2H -OPO3-CH2-C*H*2-), 1.48-1.16 ppm (m, 27H). ^{13}C {H} NMR (125 MHz, $CDCl_3$, 298 K): δ = 130.32, 130.30, 130.26, 129.87, 129.83, 129.79, 67.65, 63.58, 32,61, 30.30, 29.65, 29.62, 29.49, 29.43, 29.38, 29.16, 25.46, 16.17 ppm. ^{31}P {H} NMR (202 MHz, $CDCl_3$, 298 K): δ = -0.71 ppm.

P3-H

A schlenk flask was charged with Et-PPE and dissolved in toluene (ca. 12 wt%). The air was removed by reduced pressure and flushed with argon. 10 wt% of 5 % Pd/C catalyst was added followed by removing the argon by reduced pressure and flushing with hydrogen by a balloon. Then via septum and syringe hydrogen was bubbled into the solution. Hydrogenation was then performed with a hydrogen balloon under vigorous stirring at room temperature until NMR showed no signals of double bonds. The solution was filtered over celite and the polymer was obtained as a solid after solvent evaporation with a yield of 89 %. Number-average molecular weight, weight-average molecular weight and molecular weight distribution are $9.9 \cdot 10^3$ g/mol, $23.1 \cdot 10^3$ g/mol and $M_w/M_n = 2.3$. ^{1}H NMR (300 MHz, $CDCl_3$, 298 K): δ = 4.23-3.91 (m, 6H, -OPO3-C*H*2-), 1.82-1.58 (m, 4H -OPO3-CH2-C*H*2-), 1.31-1.22 ppm (m, 37H). ^{13}C {H} NMR (176 MHz, $CDCl_3$, 24 °C): δ = 67.73, 63.65, 30.37, 29.78, 29.73, 29.68, 29.23 25.53, 16.23 ppm. ^{31}P {H} NMR (283 MHz, $CDCl_3$, 298 K): δ = -0.74 ppm.

4.4 Degradation Studies

Polymer films were prepared by casting 0.18 mL of a **P1-H**, **P1-H$_{0.8}$-co-P2-H$_{0.2}$**, **P1-H$_{0.6}$-co-P2-H$_{0.4}$** and 0.2 mL **P3-H** chloroform solution (120 mg/mL) onto circle Microscope coverslips with 25 mm diameter. The samples were dried at room temperature for 3 h and then dried in vacuum at 40 °C for 16 h. The weights of the films were about 20 mg. The degradation experiment of polymer films was done at 37 °C by immersing each polymer film with the coverslips in 4 mL 0.1 M DPBS solution (pH 7) or 2 N NaOH solution (pH 14). The coverslips were picked up over 2 weeks, 4 weeks and 8 weeks, washed with distilled water and dried in vacuum. The weights of

the Microscope coverslips were measured before film casting and the weight of the coverslips with the polymer before and after degradation studies as well as the pH of the solutions were recorded with a SevenExcellence Cond meter S700 equipped with an InLab Routine Pro pH electrode (pH 0 – pH 14). The average weight of 3 samples were determined for each measurement point. Precipitated particles were collected by 3 times washing with water and centrifugation at 4000 rpm for 10 minutes and finally lyophilized to determine the weight.

4.5   ¹H, ¹³C, ³¹P NMR spectra

4.5.1   Monomer NMR spectra
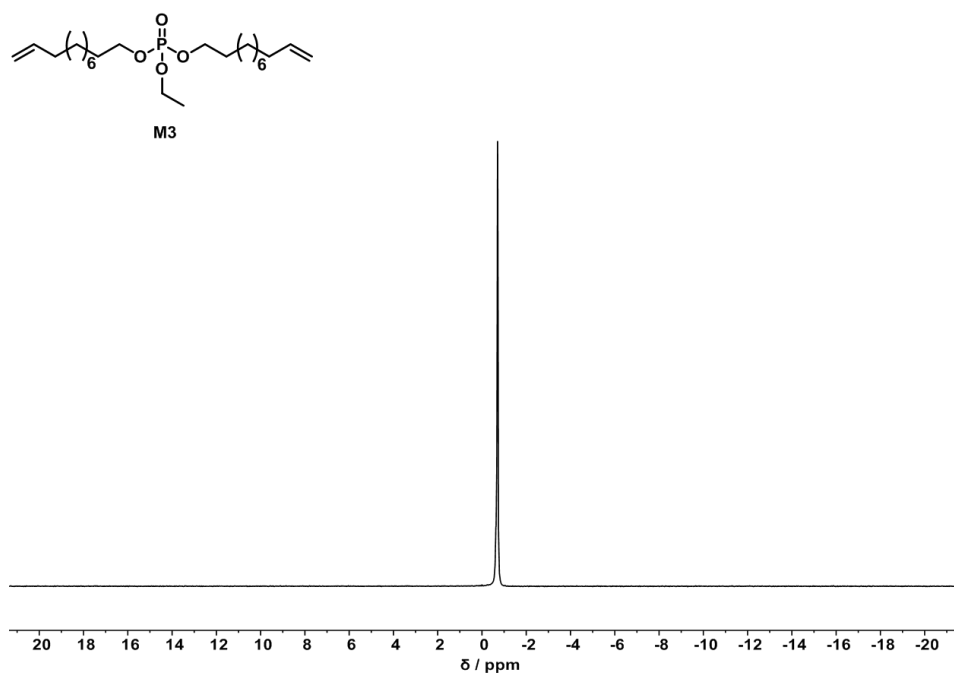
Figure 3.9. ³¹P (283 MHz) NMR spectra of M3 in CDCl₃ at 298 K.

Figure 3.10. ^{1}H (250 MHz) NMR spectra of M3 in CDCl$_3$ at 298 K.

Figure 3.11. ^{13}C (176 MHz) NMR spectra of M3 in CDCl$_3$ at 298 K.

4.5.2 Polymer NMR Spectra

Figure 3.12. ^{1}H (250 MHz) NMR spectra of P3 in CDCl$_3$ at 298 K.

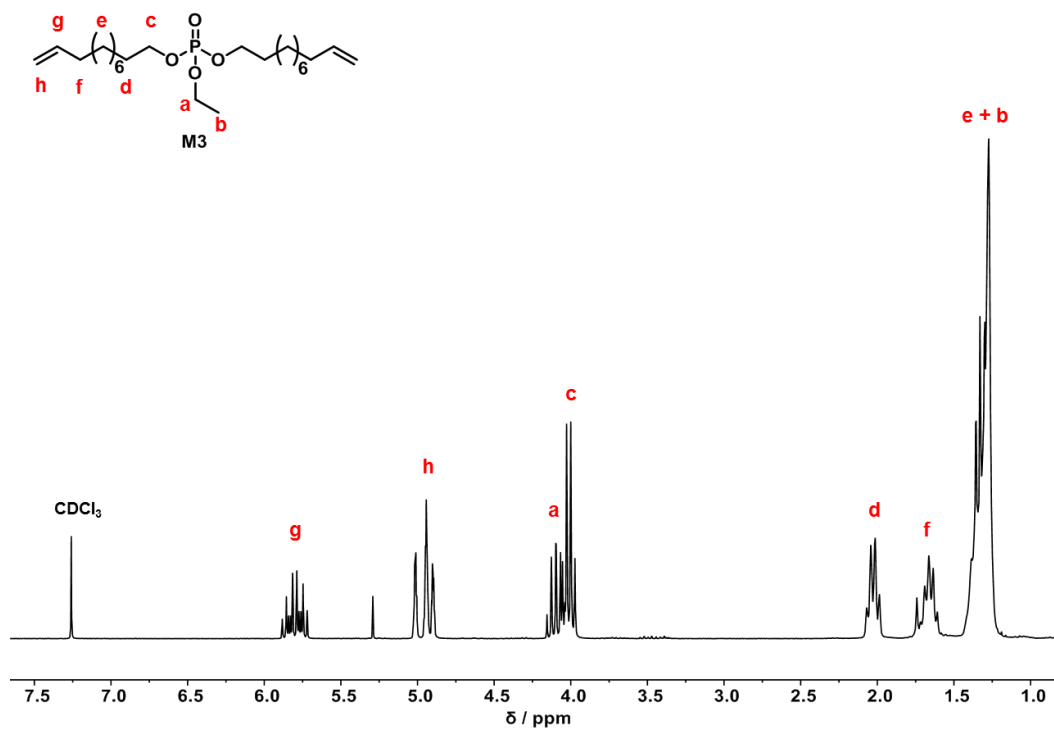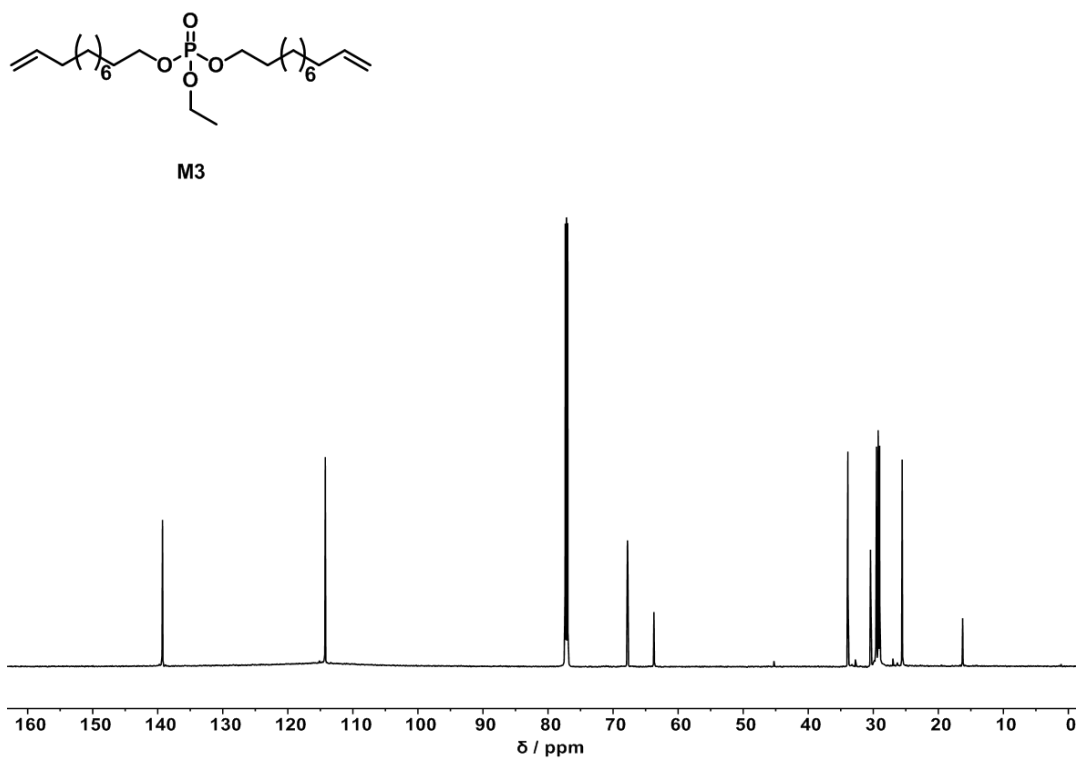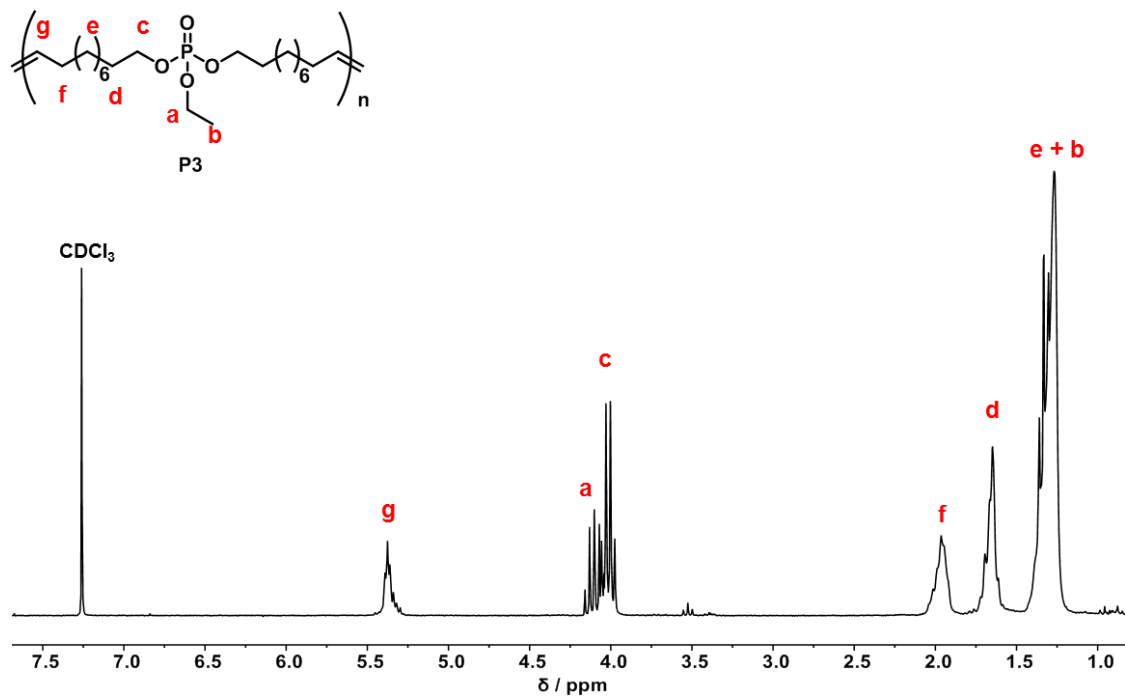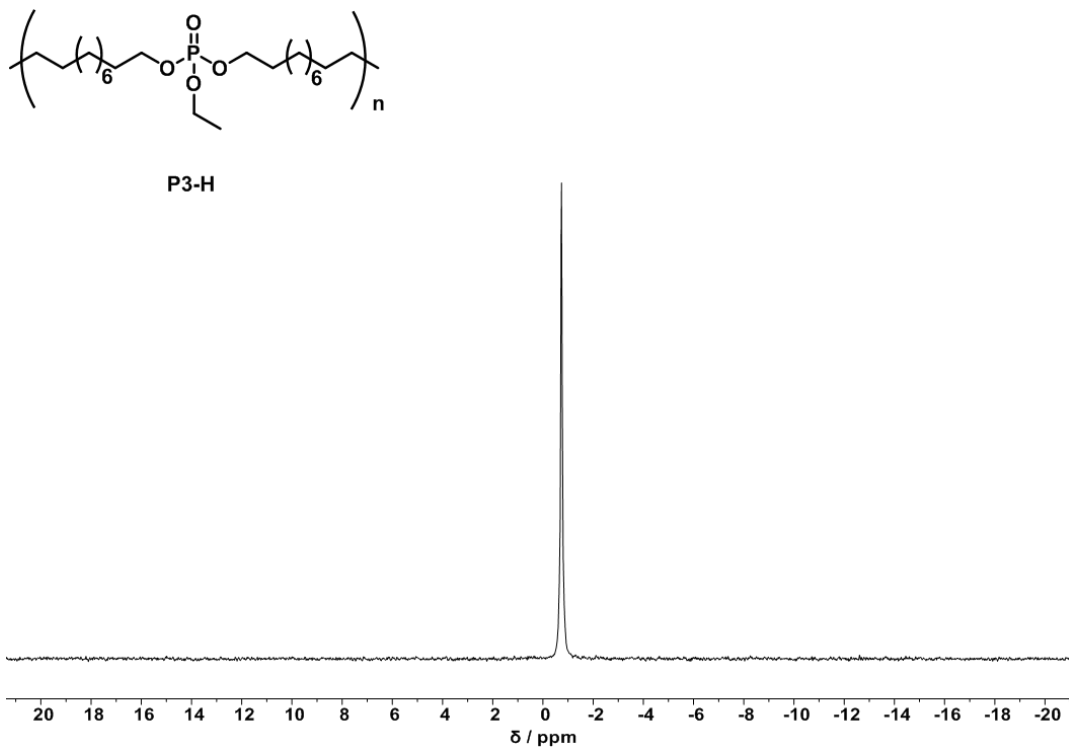**Figure 3.13.** ^{31}P (121 MHz) NMR spectra of P3-H in CDCl$_3$ at 298 K.
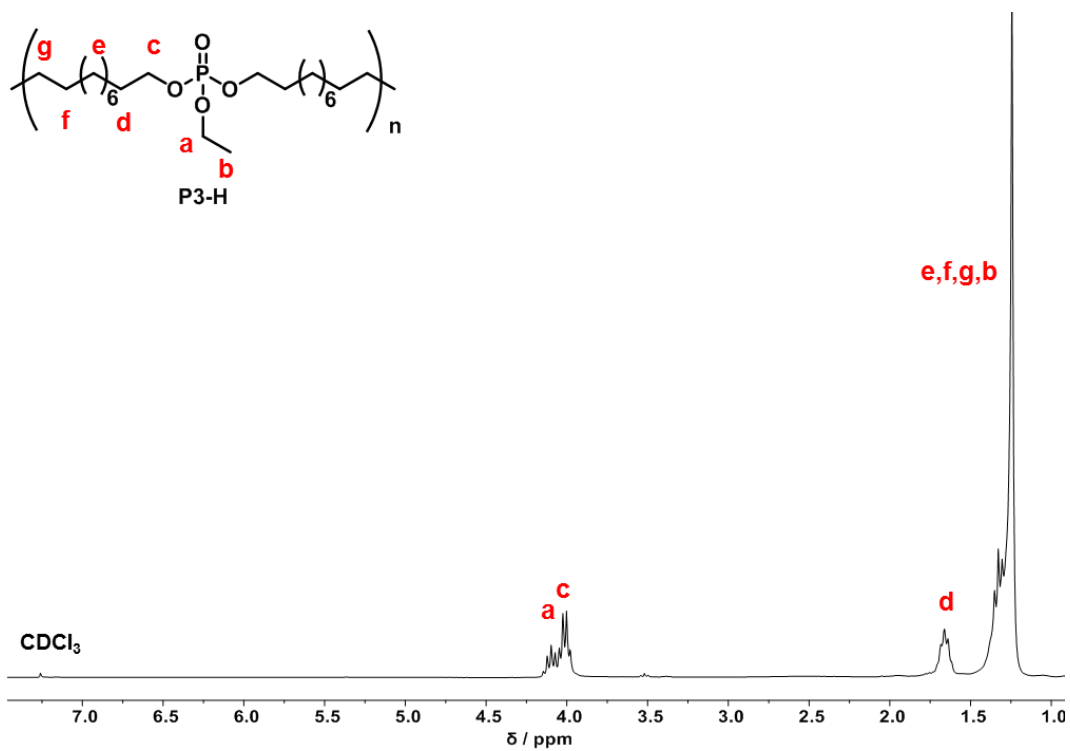
Figure 3.14. ^{1}H (300 MHz) NMR spectra of P3-H in CDCl$_3$ at 298 K.
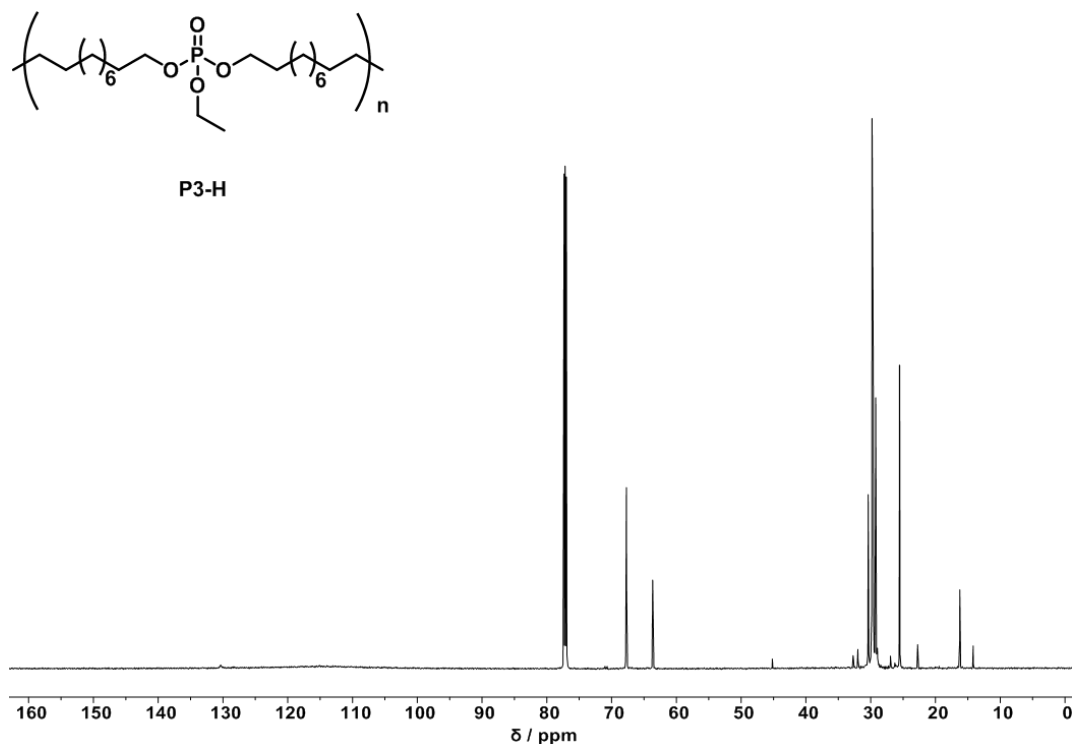
Figure 3.15. ^{13}C (176 MHz) NMR spectra of P3-H in CDCl$_3$ at 298 K.

5 References

1. Nair, L. S.; Laurencin, C. T., Biodegradable polymers as biomaterials. *Progress in Polymer Science* **2007,** *32* (8), 762-798.

2. Lucke, A.; Teßmar, J.; Schnell, E.; Schmeer, G.; Göpferich, A., Biodegradable poly(d,l-lactic acid)-poly(ethylene glycol)-monomethyl ether diblock copolymers: structures and surface properties relevant to their use as biomaterials. *Biomaterials* **2000,** *21* (23), 2361-2370.

3. Temenoff, J. S.; Mikos, A. G., Injectable biodegradable materials for orthopedic tissue engineering. *Biomaterials* **2000,** *21* (23), 2405-2412.

4. Gross, R. A.; Kalra, B., Biodegradable Polymers for the Environment. **2002,** *297* (5582), 803-807.

5. Siracusa, V.; Rocculi, P.; Romani, S.; Rosa, M. D., Biodegradable polymers for food packaging: a review. *Trends in Food Science & Technology* **2008,** *19* (12), 634-643.

6. Amass, W.; Amass, A.; Tighe, B., A review of biodegradable polymers: uses, current developments in the synthesis and characterization of biodegradable polyesters, blends of biodegradable polymers and recent advances in biodegradation studies. **1998,** *47* (2), 89-144.

7. Martina, M.; Hutmacher, D. W., Biodegradable polymers applied in tissue engineering research: a review. **2007,** *56* (2), 145-157.

8. Grubbs, R. B.; Grubbs, R. H., 50th Anniversary Perspective: Living Polymerization—Emphasizing the Molecule in Macromolecules. *Macromolecules* **2017,** *50* (18), 6979-6997.

9. Pillai, O.; Panchagnula, R., Polymers in drug delivery. *Current Opinion in Chemical Biology* **2001,** *5* (4), 447-451.

10.   Gunatillake, P. A.; Adhikari, R. J. E. C. M., Biodegradable synthetic polymers for tissue engineering. **2003,** *5* (1), 1-16.

11.   Li, S., Hydrolytic degradation characteristics of aliphatic polyesters derived from lactic and glycolic acids. **1999,** *48* (3), 342-353.

12.   Zheng, Y.-R.; Tee, H. T.; Wei, Y.; Wu, X.-L.; Mezger, M.; Yan, S.; Landfester, K.; Wagener, K.; Wurm, F. R.; Lieberwirth, I., Morphology and Thermal Properties of Precision Polymers: The Crystallization of Butyl Branched Polyethylene and Polyphosphoesters. *Macromolecules* **2016,** *49* (4), 1321-1330.

13.   Baran, J.; Penczek, S. J. M., Hydrolysis of polyesters of phosphoric acid. 1. Kinetics and the pH profile. **1995,** *28* (15), 5167-5176.

14.   Bauer, K. N.; Tee, H. T.; Lieberwirth, I.; Wurm, F. R. J. M., In-chain poly (phosphonate) s via acyclic diene metathesis polycondensation. **2016,** *49* (10), 3761-3768.

15.   Uehara, H.; Kanamoto, T.; Kawaguchi, A.; Murakami, S. J. M., Real-time X-ray diffraction study on two-stage drawing of ultra-high molecular weight polyethylene reactor powder above the static melting temperature. **1996,** *29* (5), 1540-1547.

16.   Wunderlich, B., *Macromolecular Physics, Volume 1: Crystal Structure, Morphology, Defects*. Academic Press: 1973.

17.   Marten, E.; Müller, R.-J.; Deckwer, W.-D., Studies on the enzymatic hydrolysis of polyesters I. Low molecular mass model esters and aliphatic polyesters. *Polymer Degradation and Stability* **2003,** *80* (3), 485-501.

Chapter 4

Aliphatic long-chain polypyrophosphates as biodegradable polyethylene-mimics

Forword

Authors: Hisaschi T. Tee, Ingo Lieberwirth, Frederik R. Wurm.

Abstract
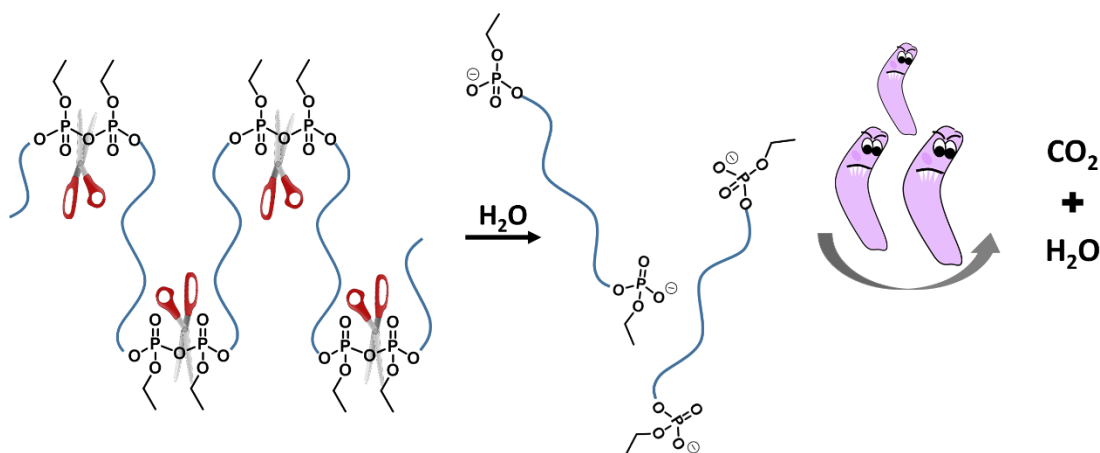
Biodegradable polyethylene-mimics have been synthesized by the introduction of pyrophosphate-groups into the polymer backbone allowing not only hydrolysis of the backbone but also further degradation by microorganisms. Due to cost, low weight and good mechanical properties, the use of polyolefins has increased significantly in the last decades and has created many challenges in terms of disposal and their environmental impact. The durability and resistance to degradation make polyethylene difficult or impossible for nature to assimilate thus making the degradability of polyolefins to an essential topic of research. The biodegradable polypyrophosphate was prepared via acyclic diene metathesis polymerization of a diene monomer. The monomer is accessible via a three-step synthesis, in which the pyrophosphate was formed in the last step by DCC-coupling of two phosphoric acid derivatives. This is the first report of a pyrophosphate group localized in an organic polymer backbone. The polypyrophosphate was characterized in detail by NMR spectroscopy, size exclusion chromatography, FTIR spectroscopy, differential scanning calorimetry, and thermogravimetry. X-ray diffraction was used to compare the crystallization

structure in comparison to analog polyphosphates and showing poly(ethylene)-like structures. In spite of its hydrophobicity and water-insolubility, the pyrophosphate groups exhibited fast hydrolysis resulting in polymer degradation when films were immersed in water. Additionally, the hydrolyzed fragments were further biodegraded by microorganisms, rendering these PE-mimics as potential candidates for fast release of hydrophobic cargo, e.g. in drug delivery applications.

1   Introduction

Polyethylene (PE) is the most produced commodity polymer today.[1] With the invention of Karl Ziegler in the last century,[2] perfectly linear PE was accessible that changed our everyday life drastically.[3] PE and other polyolefins are resistant to most chemicals and environmental conditions, they do not degrade hydrolytically or by enzymes.[4] The durability of PE is an attractive feature and has driven its success in light-weight materials, packaging but also in biomedical applications, e.g. for long-term implants.[5] However, if littered in nature, PE plastic parts do not degrade over a period of decades to centuries.[4]

Biodegradable alternatives to commodity polymers are discussed today heavily for packaging applications.[6] In contrast, in the biomedical field, degradable polymers have found already several applications if degradation of the device is desired, e.g. for sustained drug release,[7] temporary prostheses,[8] or tissue engineering.[9] For such uses, polyesters, polyamides, or polysaccharide-derivatives and others have been applied, which can be degraded by different enzymes *in vivo*.[10] Furthermore, the biocompatibility of the polymer but also of its degradation products are crucial for the use in the biomedical field.[11]

Combining properties of PE, such as crystallinity and thermoplasticity, with controlled degradation would be a desirable platform for biomedicine and the plastic sector. Others and we have prepared potentially degradable PE-mimics, which are polymers based on long aliphatic alkyl chains, which are spaced by heteroatom linkages that may allow degradation into smaller fragments.[12] For full biomineralization, these smaller fragments should eventually be resorbed by the body or degraded by microorganisms.[13, 14] Such potentially degradable groups, esters, and acetals, for example, have been installed into PE-mimics already,[15, 16] but polymers did not or only very slowly degrade.[16] Recently, we have prepared PE-mimics with phosphoesters/-amide-linkages between the aliphatic chains, since their degradation rate might be adjusted by variation of the binding motif.[17] Polyphosphorodiamidates were found to be much more hydrolysis-labile

than polyphosphoesters.[18] However, in such nonpolar PE-mimics, degradation under physiological or environmental conditions is very slow, rendering them as too stable for certain applications, in which degradation is demanded.[19] Recently, Mecking and coworkers synthesized long-chain polyphosphoesters by polyesterification and reported that a low number of pyrophosphate-linkages were formed during the process. These bonds – undesired in polyphosphoesters (PPEs) – were however responsible for a partial degradation of the materials at mild hydrolysis conditions. Immersing polymer films in basic or acidic conditions, cleavage occurred selectively in anhydride groups and the phosphoester bonds remained intact during the course of their study.[19] To date, no polypyrophosphates have been reported as degradable mimics for PE with a potentially very fast hydrolysis.

Herein, we present a fully biodegradable aliphatic polypyrophosphate PE-mimic. The hydrophobic and semicrystalline PE-like material exhibited fast hydrolysis rates under mild conditions. Additionally, we proved that microorganisms occurring in activated sludge from the sewage plant further degraded the degradation products after hydrolysis. The readily cleavable pyrophosphate group was introduced to the monomer, which was polymerized by acyclic diene metathesis polycondensation without cleaving of the pyrophosphate bond. Hydrogenation of the unsaturated product from the ADMET polycondensation was carried out without any further catalyst addition by a modified Grubbs catalyst to produce the saturated PE-mimic. This is the first example of a PE-mimic with very fast hydrolysis conditions of polymer films. The degradation products are soluble in neutral and basic aqueous solution and undergo further microbial degradation, which renders polypyrophosphates an interesting class of polymers for degradation on demand in biomedical or other packaging applications where fast dissolution of the matrix is desired.

2   Results and Discussion

Monomer Synthesis. We prepared a novel pyrophosphate-monomer (**1**) for the ADMET polycondensation via a three-step synthesis (Scheme 4.1). The first step was the esterification of ethyl dichlorophosphate with one equivalent of 10-undecen-1-ol in the presence of triethylamine (Et_3N) to produce ethyl undec-10-en-1-yl phosphorochloridate (**1a**). The resulting **1a** was then hydrolyzed to the free phosphoric acid derivative (**1b**). The A_2-type pyrophosphate monomer was obtained by coupling of two molecules of **1b** with dicyclohexylcarbodiimide similar to a literature protocol[20] to give **1** as an off-white oil (Scheme 4.1).
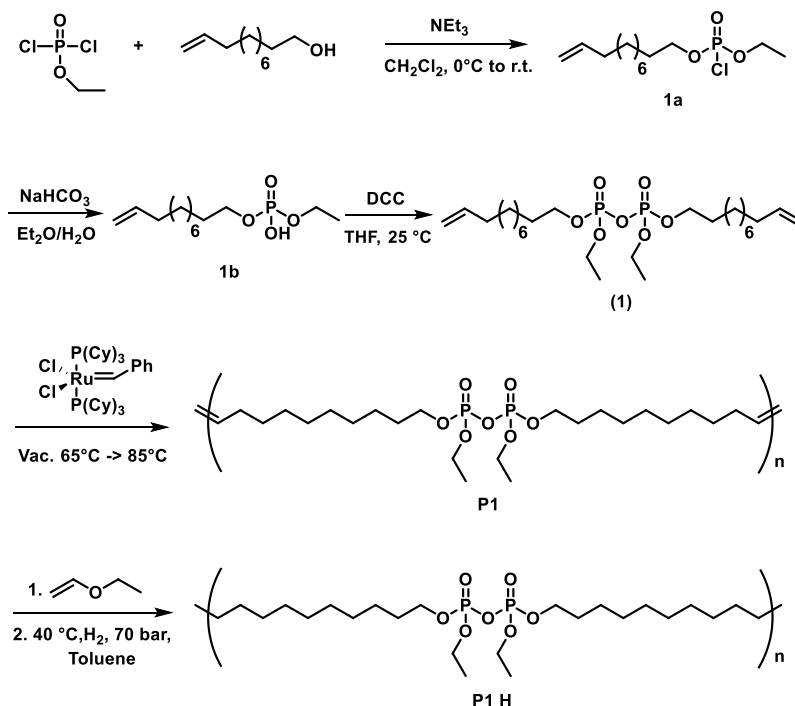
Scheme 4.1. Synthesis of monomer 1 and its subsequent polymerization by acyclic diene metathesis (to P1) and hydrogenation (to P1-H).

The monomer was obtained in high purity after column chromatography. The ^{1}H NMR spectrum of **1** shows at 5.7 ppm and 4.9 ppm the signals for the terminal double bond and at 4.2 ppm the protons next to the pyrophosphate. The upfield signals at 2.0 ppm, 1.6 ppm, and 1.3 ppm are resulting from the protons of the β-carbon of the pyrophosphate, the protons adjacent to the double bond and the remaining protons of the alkyl groups (Figure 4.1a). ^{31}P NMR spectroscopy proved the formation of the pyrophosphate as a single resonance at -12.95 ppm, which is a typical chemical shift for aliphatic pyrophosphates (Figure 4.1a).[21] For comparison, we prepared the phosphate analog bis-(undec-10-en-1-yl) ethyl phosphate **(3)** and polymerized it according to the literature.[22]
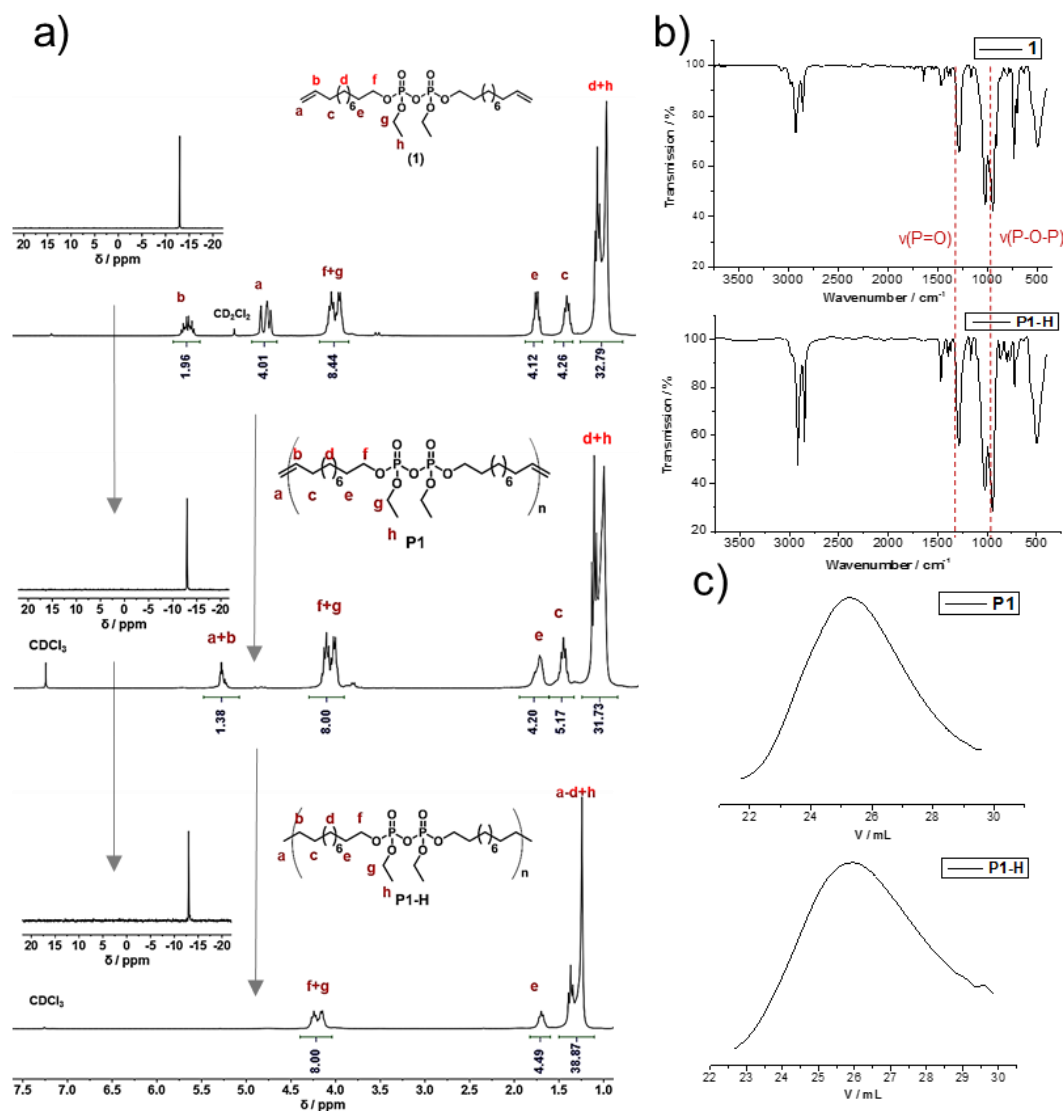
Figure 4.1. Characterization data of pyrophosphate monomer and polymers. (a) ^{1}H and ^{31}P (inset) NMR spectra of 1, P1, and P1-H with peak assignments (measured in CDCl$_3$ or CD$_2$Cl$_2$, 300 MHz, 298K), (b) IR spectra of 1 and P1-H, (c) GPC elugrams of P1 and P1-H in THF (RI detection).

ADMET polymerization. During the last years, acyclic diene metathesis (ADMET) was established as a reliable method for the synthesis of PPEs, allowing the adjustment of main- and side-chains with the high functional group tolerance of olefin metathesis with modern Grubbs-type catalysts.[23, 24] We polymerized **1** and **3** via ADMET polycondensation with Grubbs catalyst 1st to the respective unsaturated polymers (**P1** and **P3**, characterization data of **P3** can be found in the Supporting Information). After polymerization, the addition of ethyl vinyl ether did not only terminate the reaction but also generated an active Ru-catalyst for hydrogenation.[25] The

hydrogenation was performed without any further addition of catalyst at a hydrogen pressure of 70 bar for ca. 24 h to yield the hydrogenated polymers **P1-H** and **P3-H** (Scheme 4.1 and Scheme 4.2). Successful polymerization was proven by ^{1}H NMR spectroscopy with the formation of the internal double bonds in the backbone at 5.3 ppm and the disappearance of the terminal double bonds at 4.9 and 5.7 ppm (Figure 4.1a). GPC showed an apparent molecular weight of M_n=13,000 g mol^{-1} (M_w/M_n= 1.9) for **P1**. Additionally, the NMR spectra prove that the pyrophosphate group remained untouched during the ADMET procedure and the subsequent hydrogenation: The resonances for the methylene groups next to the pyrophosphate at 4.2 ppm in the ^{1}H NMR spectra remain unchanged. In addition, no change of the ^{31}P NMR resonance at -12.95 ppm after polymerization and hydrogenation was detected (Figure 4.1a). After hydrogenation, the double bond resonances disappeared from the ^{1}H NMR spectra and only the protons around the pyrophosphate at 4.2 and 1.7 ppm and the protons from the alkyl chains at 1.2 ppm remained; GPC detected an apparent molecular weight of M_n= 9,000 g mol-1 (M_w/M_n= 1.9) for **P1-H**.

Solid State Characterization. The thermal stability of both synthesized polymers was examined by thermal gravimetric analysis (TGA). The polypyrophosphate (**P1-H**) proved a distinctively lower thermal stability compared to the polyphosphate (**P3-H**). **P1-H** showed an onset of degradation at ca. 280 °C, while **P3-H** started to decompose at ca. 320 °C. The char-yields of both polymers are in agreement with the phosphate weight content.

The crystallinity as an important factor for many properties of PE in dependency to the molecular weight has been reported.[26, 27] Therefore, as PE-mimics, the crystallinity of **P1-H** and **P3-H** are important properties, which were analyzed by DSC. Both polymers are solid powders at room temperature. **P1-H** exhibited a melting endotherm at T_m(**P1-H**) = 38 °C with a melting enthalpy of ΔH_m = - 67 J g^{-1}, while **P3-H** showed a distinct higher melting event at T_m of 51 °C with a similar melting enthalpy of ΔH_m = -69 J g^{-1}), indicating a similar degree of crystallinity. Compared to 100% crystalline polyethylene with ΔH_m = 293 J g^{-1} the crystallinity of **P1-H** and **P3-H** are 23% and 24% respectively. However, the lower melting point of **P1-H** is appointed to the size of the pyrophosphate group compared to the phosphate group, which both act as defects during the crystallization of the polymers. The crystallization behavior of PPEs has already been studied in our group and has been compared to polyethylene.[28] PPEs with such a long alkyl-chain are considered to have a similar lamellar crystalline structure as polyethylene with a pseudohexagonal crystal structure. In agreement to the results by DSC measurement, the XRD measurement showed a similar degree of crystallinity and a similar crystal structure between both polymers (Figure

4.2c) and towards PE. In detail, a lattice spacing of 0.43 nm and 0.41 nm can be found by XRD with the peak positions at 2Θ of 21.32° and 21.70° for **P1-H** and **P3-H**, respectively. The appearance of the pseudohexagonal phase indicated, that the crystal lattice of **P1-H** and **P3-H** are slightly inflated compared to the orthorhombic phase of PE which exhibits an XRD peak at 2Θ = 20.5°.[29]
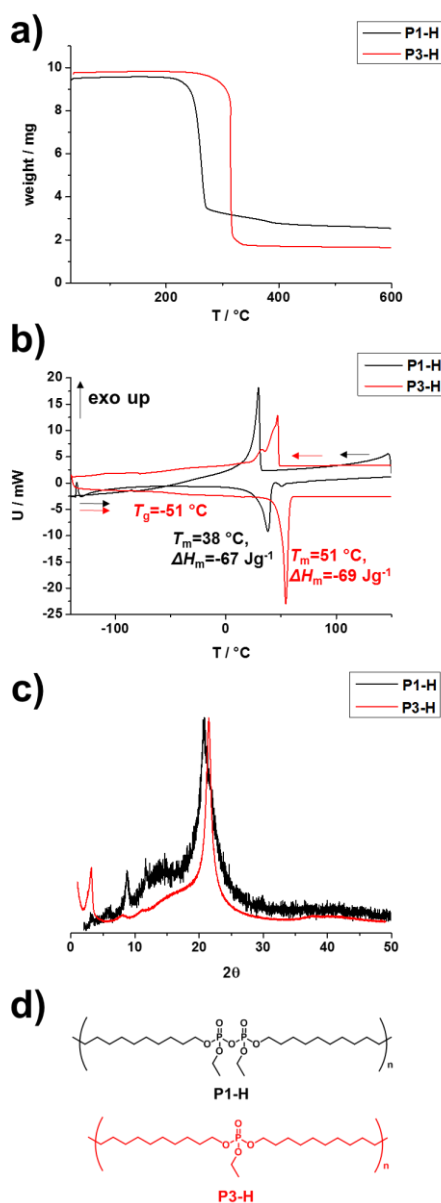

Figure 4.2 Bulk properties of polypyrophosphates and analog polyphosphates. (a) TGA of P1-H and P3-H with a heating rate of 10 K min^{-1}. (b) DSC of P1-H and P3-H with a heating (second run) and cooling rate of 10 K min^{-1}. (c) X-ray diffractograms of P1-H and P3-H. (d) Structure of P1-H and P3-H.

Polymer Degradation. PPEs are potential candidates for the development of degradable materials as they can be degraded either hydrolytically or in the presence of enzymes, e.g. by phosphodiesterase I.[30-33] The mechanism of hydrolysis of PPEs depends on their structure and either random hydrolysis of the main and side chain esters or a backbiting mechanism were reported.[34]

To evaluate hydrolysis of the PPPs, we cast polymer films, immersed them into aqueous buffer solutions with different pH values, and analyzed their weight loss. Molecular information during the degradation was collected from the ^{31}P NMR spectra after dissolving the dried films after certain incubation time in CDCl₃. The degradation of **P1-H** and the analog **P3-H** was studied at basic, acidic, and neutral conditions at 37 °C (Figure 4.3). Fastest degradation and dissolution of the **P1-H** films occurred under basic conditions (pH = 13); a rapid weight loss resulted in the complete dissolution of the film after 2 h (Figure 4.3 c & d). When **P1-H** films were immersed into a PBS solution at pH 7.0, the polymer films initially swelled and an increased mass was obtained. After 4 h, however, a rapid weight loss was detected until total dissolution after 7 h. This rapid weight loss might be rationalized with the degradation products dissolving over time, where the swollen polymer film reaches a state not stable enough to keep the integrity of the film, followed by quick disassembly. ^{31}P NMR of the dried films clearly proved the hydrolysis of the pyrophosphate bond during the overall investigation. In addition, the degradation time from the ^{31}P NMR spectra for full hydrolysis of the pyrophosphate bonds was comparable to the full weight loss of the **P1-H** films. When the films were immersed into an acidic solution (pH=0), no weight-loss of the **P1-H** films could be measured and the film became opaque during the treatment (Figure 4.3b). ^{31}P NMR spectra of the dried polymer films confirmed, however, a decreasing pyrophosphate signal and an increasing phosphoric acid signal over time (Figure 4.14 and 4.15). In addition, the degradation rate was slower compared to basic or neutral conditions (Figure 4.3d). We assume that under acidic conditions the water-insoluble and partially protonated degradation product was formed, which exhibits higher crystallinity and turned the film opaque. DSC measurement from the dried film after degradation confirmed a higher crystallinity compared to the initial casted polymer film (Figure 4.3c). **P1-H** films before degradation exhibited several melting events between 35-60°C (and ΔH= -74 J g⁻¹, measured from the first heating run), while the degraded film melted at 102°C with a higher melting enthalpy of ΔH=147 J g⁻¹ indicating the formation of crystals of the **P1-H** degradation products.

Interestingly, in organic solution, the degradation of **P-1H** was at least one order of magnitude slower than in the films. We dissolved **P1-H** in 0.5 mL/0.1 mL THF-d_8/D₂O and added 0.05 mL

trifluoroacetic acid or diisopropylethylamine as a base (Figure 4.3e). Degradation was studied over a period of several months. Under acidic conditions, **P1-H** degraded completely after 2 months ($t_{1/2}$= 7.6 days). Under basic conditions, a $t_{1/2}$= 17.6 days under these conditions was determined. In addition, an equilibrium between pyrophosphate and phosphate was reached after 3 months (Figure 4.3e). Even if pH-values are hard to compare between water and an organic solvent, the slower degradation kinetics of **P1-H** in solution compared to the polymer film might be rationalized by aggregation of the polymer in solution. The solution of **P1-H** in THF/water was a clear solution, but dynamic light scattering proved the formation of aggregates (>1 µm), in which the polar pyrophosphate might be protected against hydrolysis, while in the crystal lattice they are exposed to the surface and the solvent.
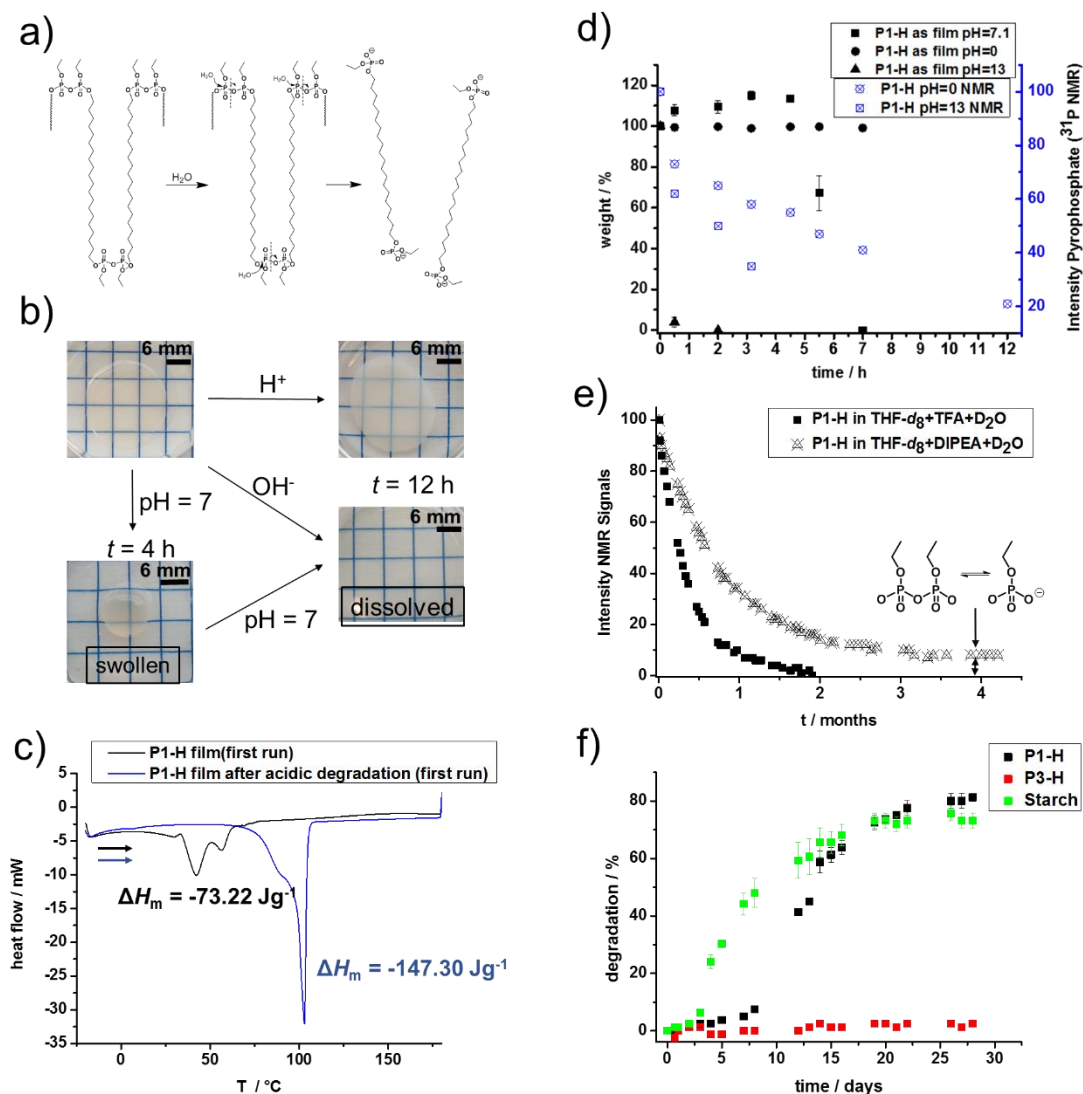
Figure 4.3 Degradation studies of P1-H. (a) Scheme of P1-H hydrolysis. (b) P1-H film before and after neutral, acidic, and basic hydrolysis. (c) DSC of P1-H film before and after acidic degradation. (d) Mass loss of P1-H films under acidic, basic, and neutral conditions (black) and ^{31}P NMR intensity of pyrophosphate P1-H films under acidic and neutral conditions (blue). (e) Degradation of P1-H in 0.5 mL THF-d_8 with 0.1 mL D$_2$O and 0.05 mL TFA or DIPEA. (f) Biodegradation of P1-H, P3-H, and starch in aqueous conditions with microorganisms from activated sludge.

Polymer films of **P3-H** did not show any degradation under neutral conditions at 37 °C. In addition, no weight loss was recorded when **P3-H** was immersed at pH 13 and 37 °C. In order to collect data about molecular degradation ^{1}H-^{31}P HMBC NMR spectrum of **P3-H** film after

degradation at pH 13 was collected and showed more than 70 % hydrolysis to the diester (Chapter 3 Figure 3.7).

As the polyprophosphate PE mimics undergo rapid backbone degradation by hydrolysis, we evaluated the biodegradability of **P1-H** (as powder) in an aqueous environment with activated sludge from the sewage plant (kindly provided from the "Wirtschaftbetrieb Mainz" and the plant in Mainz-Mombach). As the medium possessed a pH-value of 7.4, we expected a fast polymer backbone hydrolysis under these conditions. The resulting fragments should be biodegradable and ensure a full biomineralization of **P1-H**. Figure 4.3f shows the biodegradation of **P1-H** compared to **P3-H**, which does not undergo a backbone degradation at pH 7.4 (and acts as a negative control) and starch (as a positive control). The biodegradation was measured following the OECD 301F guideline with the Oxitop system measuring the biochemical oxygen demand (BOD) over a period of 28 days.[35] All tests were carried out in duplicate and the maximum error was ± 6%. The BOD of starch after 28 d, reached a degradation of 73%. The BOD determined for **P1-H** reached a degradation of 81% after 28 d, which resembles the material as "readily biodegradable", a term considered for chemicals with greater than 60% biodegradation after 28 days.[35] Initially, a lag time was detected, which might be due to hydrolysis of the polymer and consumption of other nutrients in the mixture by the microorganisms. When **P1-H** was hydrolyzed to smaller fragments, the microorganisms were able to further mineralize them, resulting in an increase of the BOD value. Under the same conditions, **P3-H** showed negligible biodegradation with 3% which is in the error value, which is probably attributed to the phosphoester bond, which does not undergo hydrolysis at neutral conditions. As the polymer itself is very hydrophobic, degradation by microorganisms from the sewage plant seems to be very low.

3   Summary

We prepared the first pyrophosphate-containing polyethylene mimic, which is readily biodegradable. The polymer was prepared by acyclic diene metathesis polycondensation of **1**, followed by hydrogenation. The unsaturated semicrystalline polymer (**P1-H**) was water-insoluble, but undergoes rapid backbone hydrolysis under neutral, basic, or acidic conditions, when polymer films were immersed in water. The resulting degradation products were further identified as readily biodegradable by microorganisms according to the OECD 301F guideline. **P1-H** is the first long-chain polyphyrophosphate that resembles the crystallinity of polyethylene but is readily degraded. These materials might be interesting for a quick release under mild conditions in the

biomedical field or also for advanced packaging. In addition, they broaden the field of phosphorus-containing polymers with a very labile linkage in the main chain, compared to structurally very similar polyphosphoesters. A combination of pyrophosphate- and phosphate-based polymers might also be used in order to control degradation and/ or release rates.

4 Experimental

4.1 General information

Materials. All Solvents and chemicals were purchased from Sigma Aldrich, Acros Organics, or Fluka and used as received unless otherwise stated. Triethylamine was distilled from calcium hydride and stored over molecular sieves (4Å) under argon prior to use. Dry solvents were purchased from Acros Organics or Sigma Aldrich and stored with a septum and over molecular sieves. Deuterated solvents, Grubbs catalyst 1st generation and Pd/C(10wt%) were purchased from Sigma Aldrich and used as received. Deionized water was used for preparing buffers, NaOH and HCl solutions. Activated sludge was provided by "Wirtschaftsbetrieb Mainz".

4.2 Instrumentation and characterization techniques

SEC. For the polypyrophosphates and polyphosphoesters, SEC measurements were performed in THF with a PSS SecCurity system (Agilent Technologies 1260 Infinity). Sample injection was performed by a 1260-ALS autosampler (Waters) at 30 °C. SDV columns (PSS) with dimensions of 300×80 mm, 10 μm particle size, and pore sizes of 106, 104, and 500 Å were employed. The DRI Shodex RI-101 detector (ERC) and UV−vis 1260-VWD detector (Agilent) were used for detection. Calibration was achieved using poly(styrene) standards provided by Polymer Standards Service.

NMR. For nuclear magnetic resonance analysis ^{1}H, ^{13}C, and ^{31}P NMR spectra of the monomers and polymers were recorded on a Bruker AVANCE III 300, 500, or 700 MHz spectrometer. All spectra were measured in CDCl$_3$ at 298 K. The spectra were calibrated against the solvent signal and analyzed using MestReNova 8 from Mestrelab Research S.L.

DSC. The thermal properties of the synthesized polymers have been measured by differential scanning calorimetry (DSC) on a Mettler Toledo DSC 823 calorimeter. Three scanning cycles of heating-cooling were performed in an N$_2$ atmosphere (30 mL/min) with a heating and cooling rate of 10 °C min^{-1}.

TGA. TGA was measured on a Mettler Toledo ThermoSTAR TGA/SDTA 851-Thermowaage in a nitrogen atmosphere. The heating rate was 10 °C min^{-1} in a range of temperature between 25 and 600−900 °C.FTIR spectra were recorded in transmission mode accomplished with a Bruker Tensor II (Platinum ATR).

BOD. BOD Measurements were performed with 2 OxiTop IS 6 Systems and the biochemical oxygen demand (BOD) was documented at a daily rate.

4.3   Synthetic Procedures

*Ethyl undec-10-en-1-yl phosphorochloridate (**1a**)*

50 mL Ethyldichlorophosphate ((67.7 g, 0.42 mol) and 150 mL dry DCM were charged into a 1000 mL Schlenk flask equipped with a 500 mL dropping funnel under Argon atmosphere and cooled down to 0 °C with an ice bath. 38.4 mL Triethylamine, 55 mL 10-Undecen-1-ol and 150 mL dry DCM were mixed in the dropping funnel and added dropwise over a period of 2 h. The reaction was then stirred overnight at room temperature. The crude mixture was filtered, concentrated at reduced pressure, dissolved in diethyl ether and filtered again to give a clear yellowish liquid with a yield of 84 %. ^{1}H NMR (300 MHz, CDCl$_3$, 298 K) δ = 5.81 (ddt, *J* = 17.0, 10.2, 6.7 Hz, 1H, CH2=C*H*-), 5.15 – 4.81 (m, 2H, C*H2*=CH-), 4.20 – 3.96 (m, 4H, -OPO3-C*H2*-), 2.15 – 1.93 (m, 2H, =CH-C*H2*-), 1.86 – 1.58 (m, 2H, -OPO3-CH2-C*H2*-), 1.51 – 1.14 ppm (m, 15H). ^{31}P {H} NMR (121 MHz, CDCl$_3$, 298 K): δ = 1.10 ppm.

*Ethyl undec-10-en-1-yl hydrogen phosphate (**1b**)*

Ethyl undec-10-en-1-yl phosphorochloridate (68.7 g, 0.23 mol) was dissolved in 150 mL Et$_2$O and charged into a 1000 mL round bottom flask. 100 mL of deionized water and 100 mL saturated NaHCO$_3$ solution was added to the solution and stirred overnight. The aqueous phase was removed and 150 mL of saturated NaHCO$_3$ solution was added again to the organic phase and stirred for 16 h. The mixture was acidified with the old aqueous phase until phase separation occurred. The separated organic phase was dried with sodium sulfate, filtered and the organic solvent was removed under reduced pressure to give an orange liquid with a yield of 80 %. ^{1}H NMR (300 MHz, CDCl$_3$, 298 K) δ = 5.98 – 5.66 (m, 1H), 4.97 (dd, *J* = 18.4, 13.7 Hz, 2H), 4.47 – 3.91 (m, 4H), 2.05 (q, *J* = 7.0 Hz, 2H), 1.71 (dt, *J* = 14.1, 6.6 Hz, 2H), 1.60 – 1.19 (m, 17H). ^{31}P {H} NMR (121 MHz, CDCl$_3$, 298 K): δ = 1.18.

*Bis(Ethyl undec-10-en-1-yl) pyro phosphate (**1**)*

60,2 g (0.216 mol) of Ethyl undec-10-en-1-yl hydrogen phosphate was charged into a 1000 mL Schlenk flask and dissolved in 480 mL dry THF under an argon atmosphere. 23 g (0.111 mmol) *N, N'*-Dicyclohexylcarbodiimid(DCC) were dissolved in 100 mL dry THF and then added to the phosphodiester. After stirring for 1 h, the precipitated 1,3-dicyclohexylurea (DCU) was filtered off and the solvent evaporated at reduced pressure. The crude was dissolved in DCM and stored at 278 K overnight. Residual DCU was then filtered off, concentrated at reduced pressure and purified by chromatography over silica using DCM and ethyl acetate as solvents (yield: 15 %, R_f: 0.25 (DCM/EtOAc = 9/1)). ^{1}H NMR (300 MHz, CDCl$_3$, 298 K) δ = 5.81 (ddt, J = 16.9, 10.2, 6.6 Hz, 2H, CH2=C*H*-), 5.13 – 4.78 (m, 4H, C*H*2=CH-), 4.37 – 4.09 (m, 8H, -OPO3-C*H*2-), 2.18 – 1.86 (m, 4H, =CH-C*H*2-), 1.85 – 1.58 (m, 4H, -OPO3-CH2-C*H*2-), 1.56 – 1.13 ppm (m, 30H). ^{31}P {H} NMR (121 MHz, CDCl$_3$, 298 K): δ = -12.95 ppm.

P1.

Into a flame-dried 100 mL glass reactor equipped with a stir bar, the monomer ethyl undec-10-en-1-yl pyrophosphate (8.84 g) was added and any residual solvent/moisture was removed under vacuum. Grubbs catalyst 1st generation (41.3 mg, 0.3 mol%) was added under an argon atmosphere. Polymerization was carried out at reduced pressure to remove ethylene gas evolving during the metathesis reaction, at 40 °C for 2 h and 60 °C for 1 h. Then, 4 mg of Grubbs catalyst 1st generation was added before the reaction was stirred at 80 °C for additional 8h. The polymerization was terminated with an excess of ethyl vinyl ether (5 mL) and 20 mL dry toluene and stirred for 1 h at room temperature. The addition of ethyl vinyl ether produced also an active catalyst for hydrogenation (visible by a color change to orange). The mixture was concentrated at reduced pressure and redissolved in toluene to evaporate residual ethyl vinyl ether. The unsaturated polymer was not further purified and used directly in the hydrogenation reaction (see below). A sample for analysis was taken: M_n= 13 · 10^3 g/mol, M_w=25.0 · 10^3 g/mol and M_w/M_n = 1.9. ^{1}H NMR (300 MHz, CDCl$_3$, 298 K) δ = 5.53 – 5.25 (m, 2H, C*H*=C*H*), 4.44 – 4.05 (m, 8H, -OPO3-C*H*2-), 2.14 – 1.86 (m, 4H, =CH-C*H*2-), 1.83 – 1.59 (m, 4H, -OPO3-CH2-C*H*2-), 1.51 – 1.18 ppm (m, 30H). ^{31}P {H} NMR (121 MHz, CDCl$_3$, 298 K): δ = -12.95 ppm.

P1-H

8.5 g of **P1** was dissolved in 30 mL toluene and degassed by bubbling argon into the stirring solution for 10 minutes. A high-pressure reactor was then charged with the solution and flushed twice with hydrogen. Hydrogenation was performed with vigorous stirring under a hydrogen

pressure of 70 bar at 40 °C for 36 h. The solvent was evaporated by reduced pressure to give the solid polymer in quantitative yield. Number-average molecular weight, weight-average molecular weight and molecular weight distribution are $9 \cdot 10^3$ g/mol, $17 \cdot 10^3$ g/mol and $M_w/M_n = 1.9$. ^{1}H NMR (300 MHz, CDCl$_3$, 298 K) δ = 4.29 – 4.03 (m, 8H, -OPO3-C*H*2-), 1.80 – 1.55 (m, 4H, -OPO3-CH2-C*H*2-), 1.44 – 1.12 ppm (m, 40H). ^{13}C NMR (75 MHz, CDCl$_3$, 298 K) δ = 69.29, 65.31, 31.46 – 28.98 (m), 25.47, 16.14 ppm (t, *J* = 3.6 Hz). ^{31}P {H} NMR (121 MHz, CDCl$_3$, 298 K): δ = -13.00 ppm.

Bis-(undec-10-en-1-yl) ethylphosphate (3)

See chapter 3.

Poly(icos-10-en-1,20-diylethylphosphate) (P3)

See Chapter 3.

Poly(ethyldiundecylphosphate) (P3-H)

See Chapter 3.

4.4   Degradation Studies

4.4.1   Hydrolytic degradation

Polymer films were prepared by casting 0.22 mL of a **P1-H** dichloromethane solution (120 mg/mL) and 0.2 mL of **P3-H** chloroform solution (120 mg/mL) onto circle Microscope coverslips with 25 mm diameter. The samples were dried at room temperature for 1 h and then dried in vacuum at 30 °C until a constant weight was achieved. The weights of the films were about 17-27 mg.

The degradation experiment of polymer films was done at 37 °C by immersing each polymer film with the coverslips in 4 mL 2 N HCl solution (pH -0.25), DPBS solution (pH 7.4) or 2N NaOH solution (pH 12.94). The coverslips were picked up over predetermined time intervals, washed with distilled water and dried in vacuum. The weights of the Microscope coverslips were measured before film casting and the weight of the coverslips with the polymer before and after degradation studies were recorded.

Degradation kinetics of P1 H in solution was achieved by dissolving 8 mg PPP in 0.5 mL THF-d^8 and adding 0.1 mL D$_2$O and 0.05 mL TFA or DIPEA.

4.4.2 Biodegradation Studies

Biodegradability was determined using the method based on Organisation for Economic Co-operation and Development (OECD) 301F guidelines[9-10]. In summary, the biological oxygen demand (BOD) for each chemical was measured using the OxiTop control manometric closed system (WTW, Germany) over 28 days. The percentage of biodegradability was determined by comparing the measured BOD and the calculated theoretical oxygen demand (ThOD) values. The BOD of the measurement was calculated in $mg \cdot L^{-1}$ according to the following equation

$$BOD = \frac{mgO_2/L \text{ uptake by the test substance} - O_2/L \text{ uptake by blank}}{mg \text{ testsubstance}/L \text{ in vessel}} = mg\,O_2/mg \text{ test substance} \quad (1)$$

where the oxygen uptake is recorded by the OxiTop system. ThOD is the oxygen required when the target compound is completely oxidized from stoichiometric considerations and calculated by

$$ThOD = \frac{[16 \cdot [2 \cdot "C" + 0.5 \cdot ("H" - "Cl" - 3 \cdot "N") + 3 \cdot "S" + 2.5 \cdot "P" + 0.5 \cdot "Na" - "O"]]}{M_{repeating\,unit}} \quad (2)$$

with the number of chemical elements in the repeating unit in the quotation marks. The concentration of test substance and the positive control was calculated by dividing the targeted oxygen consumption with the ThOD of the respective Substance. The test medium was water with 30 mg/L inoculum and nutrients were added to ensure non-limiting conditions for microbial activity and growth. The test flasks contained deionized water, nutrients, the test chemicals, and 10 mg/L allylurea. Allylthiourea is not mentioned in the OECD 301F, however it was already shown that it was an effective inhibitor against nitrification processes [Reuschenbach et al. 2003; BSB FIbel} Three different types of control flasks were also used: (1) deionized water with inoculum "inoculum blanks" with nutrients only added, (2) positive controls with deionized water, inoculum, nutrients, and a readily biodegradable polymer, cornstarch, and (3) toxicity control with nutrients, corn starch at 66 mg/L and test substance. Each chemical, positive control, and the blank was tested in duplicate, while only one flask was used as a toxicity control for each tested chemical. The inoculum used in all studies was collected from a municipal wastewater treatment system (Germany, Mainz) and aerated for 7 days at 20 °C. The mineral medium consisted of KH_2PO_4, K_2HPO_4, Na_2HPO_4, NH_4Cl, $CaCl_2$, $MgSO_4 \cdot 7\,H_2O$, $FeCL_3 \cdot 6\,H_2O$[9]. 365 mL of nutrient solution were added to every 500 mL OxiTop bottle, while the inoculum was 30 mg/L dry matter.

Each test chemical was added to the test and toxicity control flasks, while 66.2 mg/L starch was added to the positive controls and toxicity controls. Magnetic stirrer bars were also added. The screw-top measuring heads, containing sodium hydroxide pellets to adsorb produced carbon dioxide, were placed. The flasks were stirred on magnetic stirrers in an incubator cabinet in the dark at 20 °C and the oxygen consumption data via pressure loss were recorded over a 28 day period. Finally, to calculate the biodegradation percentage at the end of each test the amount of oxygen taken up by the microbial population was expressed as percent ThOD

$$\text{Degradation (\%)} = 100 \cdot \frac{\text{BOD} - \text{BOD}_{\text{blank}}}{\text{ThOD}} \qquad (3)$$

where BOD is biochemical oxygen demand of the test suspension, $\text{BOD}_{\text{blank}}$ is biochemical oxygen demand of the negative control, both in $\text{mg} \cdot \text{L}^{-1}$ and ThOD is theoretical oxygen demand of the measured compound calculated with equation (2).

4.5 Synthesis scheme of P3-H
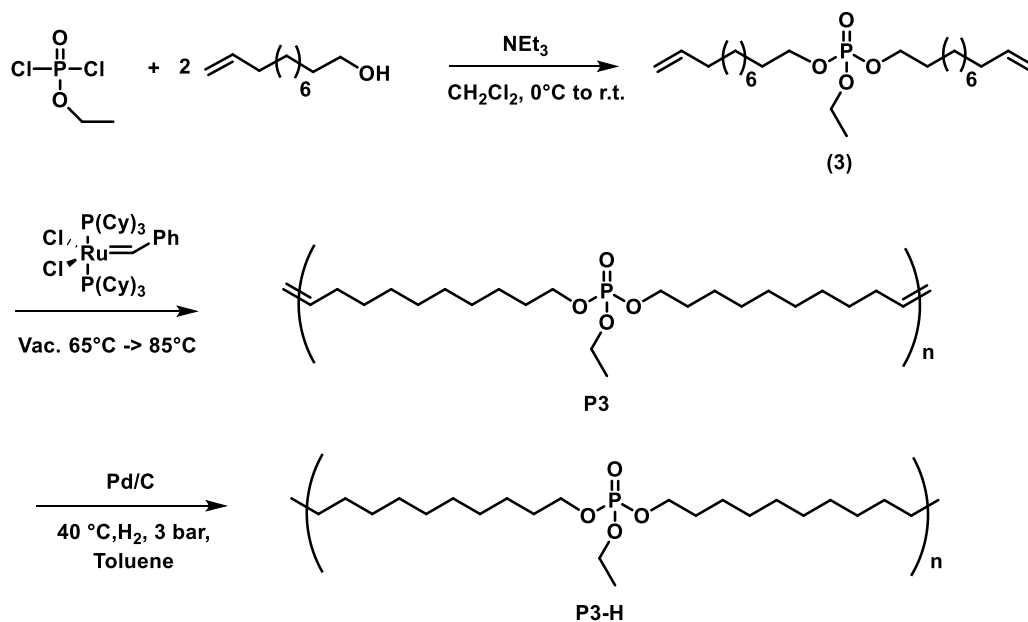
Scheme 4.2. Synthesis of monomer 3 and its subsequent polymerization by acyclic diene metathesis (to P3) and hydrogenation (to P3-H).
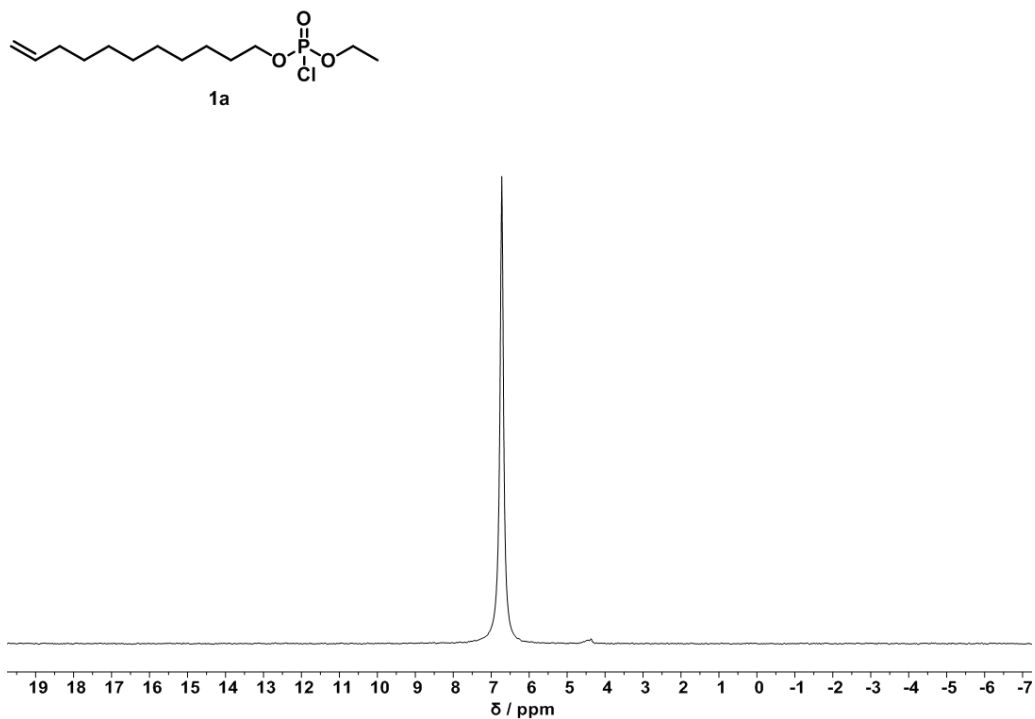
4.6 ^{1}H, ^{31}P NMR spectra

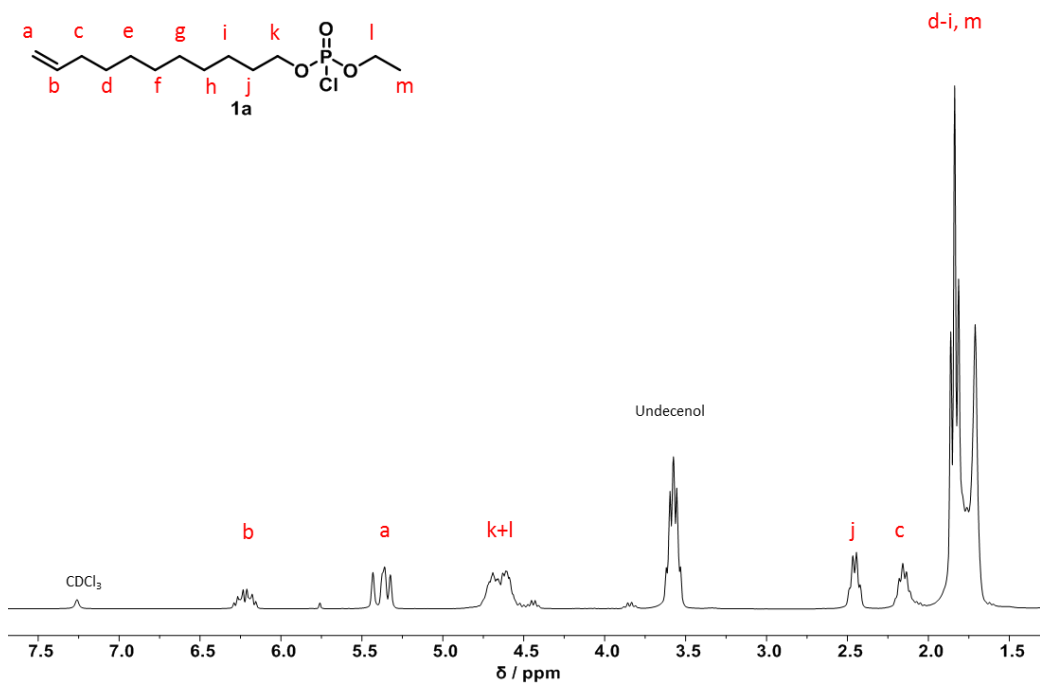**Figure 4.5.** ^{31}P NMR (121 MHz) spectra of 1a in CDCl$_3$ at 298 K.

Figure 4.6. ^{1}H (300 MHz) NMR spectra of 1a in CDCl$_3$ at 298 K.

Figure 4.7. ^{31}P NMR (121 MHz) spectra of 1b in CDCl$_3$ at 298 K.

Figure 4.8. ^{1}H (300 MHz) NMR spectra of 1b in CDCl$_3$ at 298 K.

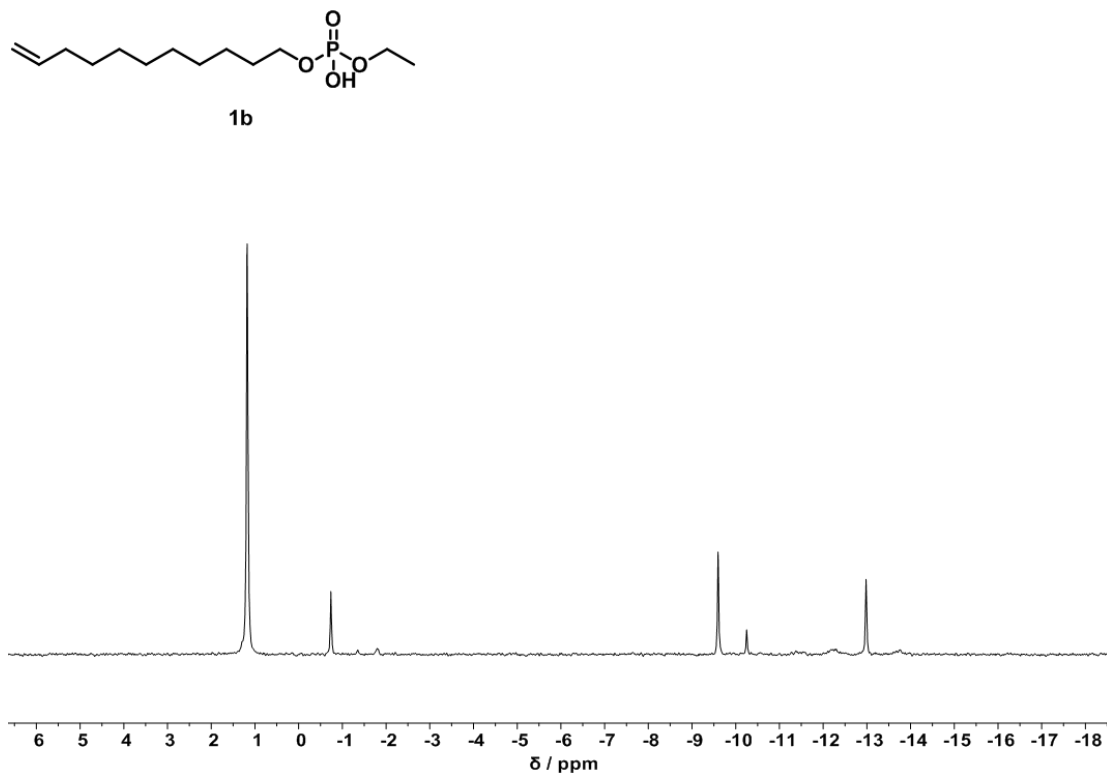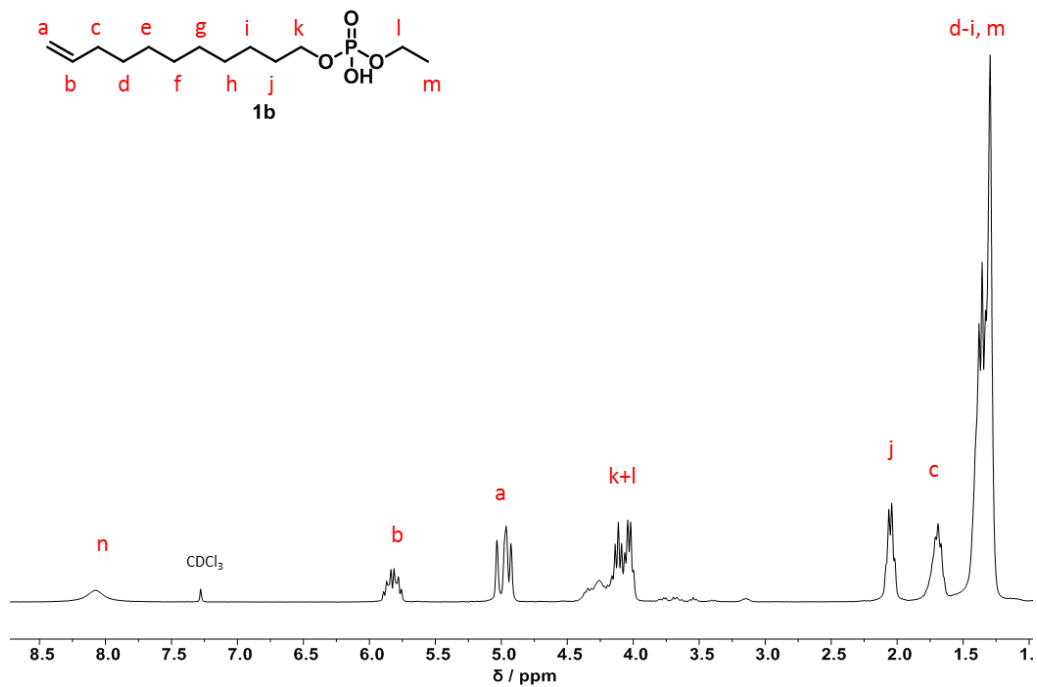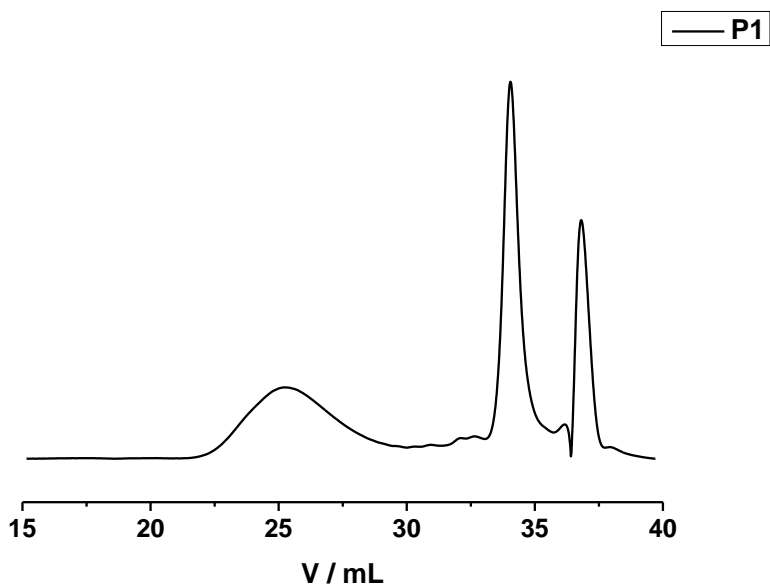## 4.7   Size exclusions chromatography

Figure 4.9. SEC elugrams (RI detection) of P1 measured in THF at 298 K.
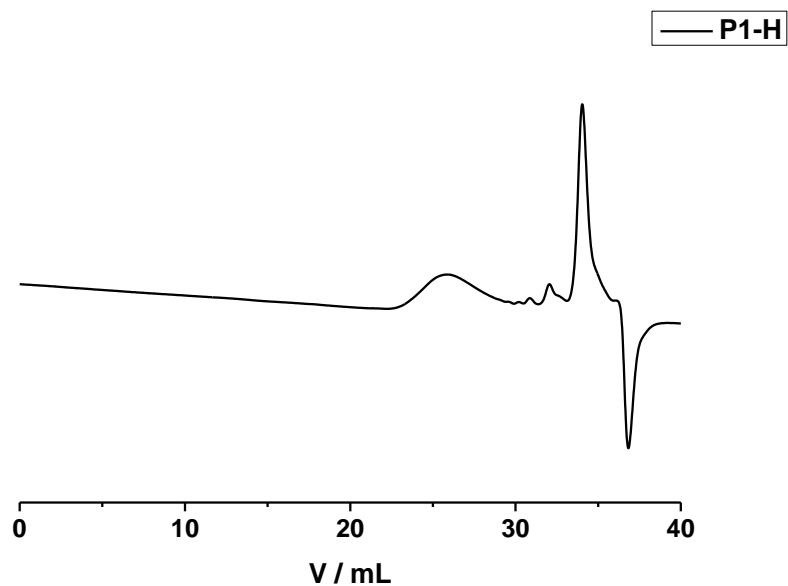

Figure 4.10. SEC elugrams (RI detection) of P1-H measured in THF at 298 K.
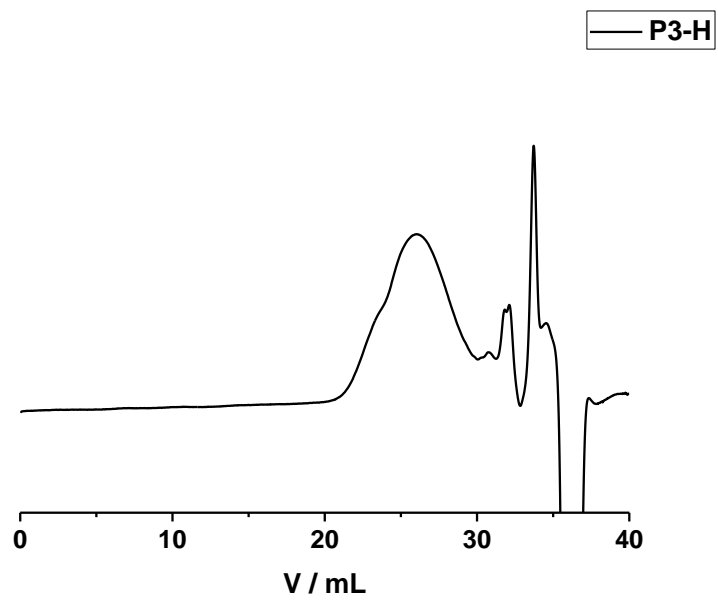
Figure 4.11. SEC elugrams (RI detection) of P3-H measured in THF at 298 K.

4.8 ^{31}P NMR of degradation studies
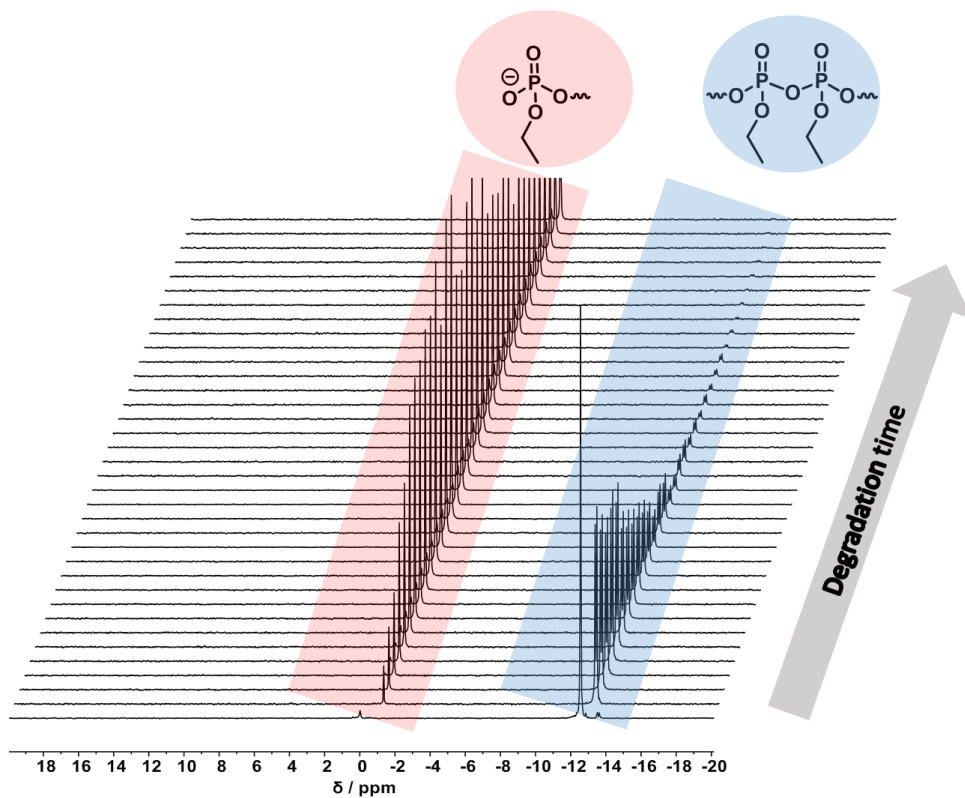
Figure 4.12. ^{31}P NMR spectra (202 MHz, 298 K) recorded within the degradation of P1-H in 0.5 mL THF-d$_8$ with 0.1 mL D$_2$O and 0.05 mL TFA.

Figure 4.13. ^{31}P NMR spectra (202 MHz, 298 K) recorded within the degradation of P1-H in 0.5 mL THF-d$_8$ with 0.1 mL D$_2$O and 0.05 mL DIPEA.

Figure 4.14. ^{31}P NMR spectra (202 MHz, 298 K) of P1-H films dissolved in CDCl$_3$ from degradation in aqueous media at pH 0.

Figure 4.15. ^{31}P NMR spectra (202 MHz, 298 K) of P1-H films dissolved in CDCl$_3$ from degradation in PBS buffer at pH 7.
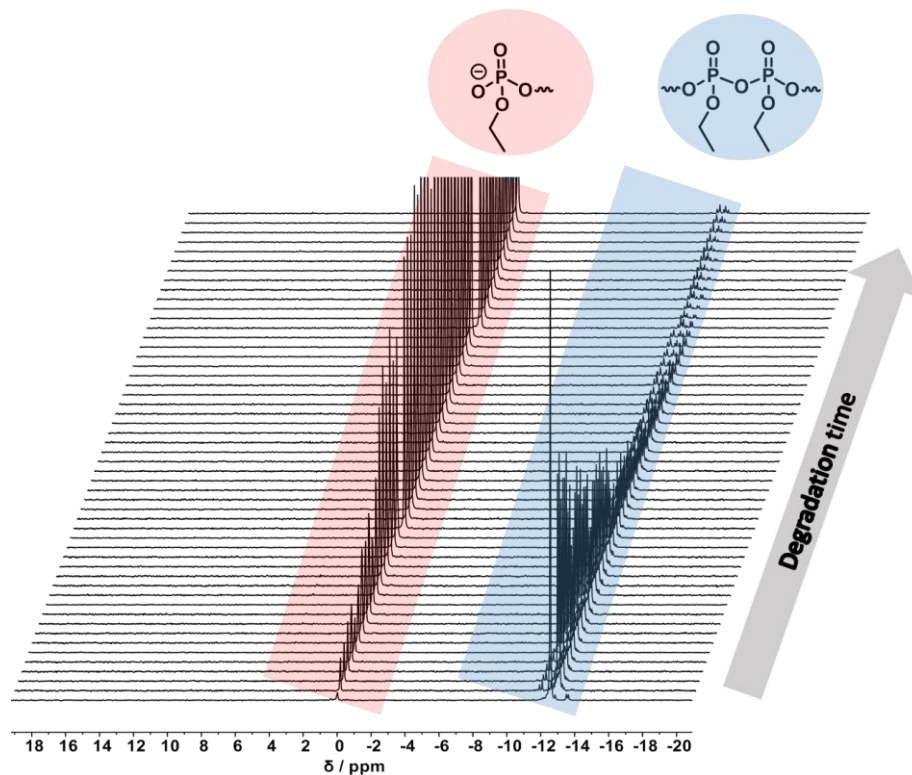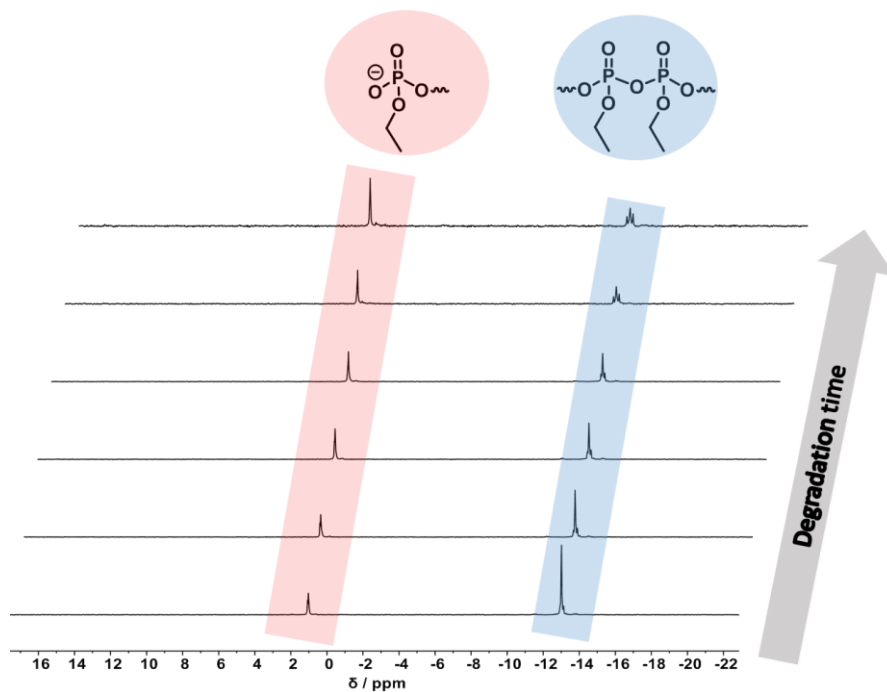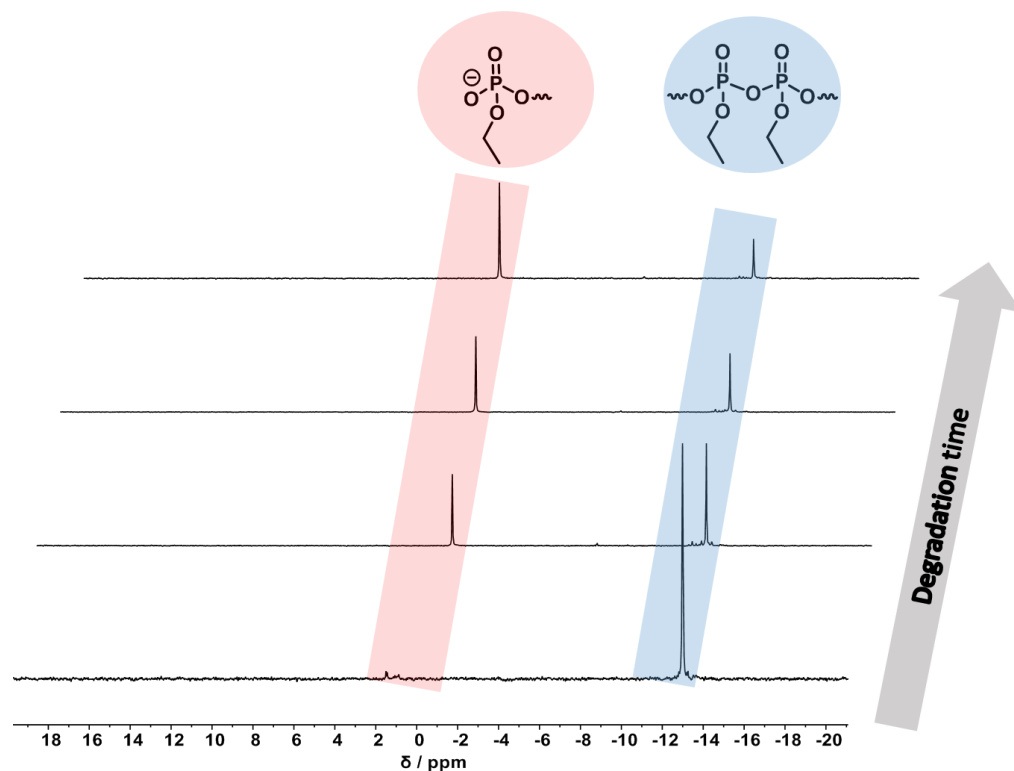
5 References

1.   Türk, O., Biogene Polyolefine: Polyethylen aus biogenem Ethanol. In *Stoffliche Nutzung nachwachsender Rohstoffe*, Springer: 2014; pp 431-438.

2.   Wilke, G., Karl Ziegler—The Last Alchemist. In *Ziegler Catalysts*, Springer: 1995; pp 1-14.

3.   Galli, P.; Vecellio, G., Polyolefins: The most promising large-volume materials for the 21st century. **2004,** *42* (3), 396-415.

4.   Austin, R., Degradation studies of polyolefins. In *Degradable Materials*, CRC Press: 2018; pp 209-236.

5.   AlMa'adeed, M. A.-A.; Krupa, I., *Polyolefin Compounds and Materials*. Springer: 2016.

6.   Haider, T.; Völker, C.; Kramm, J.; Landfester, K.; Wurm, F. R., Plastics of the future? The impact of biodegradable polymers on the environment and on society. *Angew. Chem. Int. Ed.* **2018,** *0* (doi:10.1002/anie.201805766).

7.   Jeong, B.; Bae, Y. H.; Lee, D. S.; Kim, S. W., Biodegradable block copolymers as injectable drug-delivery systems. *Nature* **1997,** *388* (6645), 860.

8.   Vert, M., Polymeric biomaterials: strategies of the past vs. strategies of the future. *Progress in Polymer Science* **2007,** *32* (8-9), 755-761.

9.   Rezwan, K.; Chen, Q.; Blaker, J.; Boccaccini, A. R., Biodegradable and bioactive porous polymer/inorganic composite scaffolds for bone tissue engineering. *Biomaterials* **2006,** *27* (18), 3413-3431.

10.   Nair, L. S.; Laurencin, C. T., Biodegradable polymers as biomaterials. *Progress in polymer science* **2007,** *32* (8-9), 762-798.

11.   Luckachan, G. E.; Pillai, C. K. S., Biodegradable Polymers- A Review on Recent Trends and Emerging Perspectives. *J. Polym. Environ.* **2011,** *19* (3), 637-676.

12.   Bauer, K. N.;   Tee, H. T.;   Velencoso, M. M.; Wurm, F. R., Main-chain poly(phosphoester)s: History, syntheses, degradation, bio-and flame-retardant applications. *Progress in Polymer Science* **2017,** *73*, 61-122.

13.   Amass, W.; Amass, A.; Tighe, B., A review of biodegradable polymers: uses, current developments in the synthesis and characterization of biodegradable polyesters, blends of biodegradable polymers and recent advances in biodegradation studies. *Polymer international* **1998,** *47* (2), 89-144.

14.   Lucas, N.; Bienaime, C.; Belloy, C.; Queneudec, M.; Silvestre, F.; Nava-Saucedo, J.-E., Polymer biodegradation: Mechanisms and estimation techniques – A review. *Chemosphere* **2008,** *73* (4), 429-442.

15.   Caire da Silva, L.; Rojas, G.; Schulz, M. D.; Wagener, K. B., Acyclic diene metathesis polymerization: History, methods and applications. *Prog. Polym. Sci.* **2017,** *69*, 79-107.

16.   Stempfle, F.; Ortmann, P.; Mecking, S., Long-Chain Aliphatic Polymers To Bridge the Gap between Semicrystalline Polyolefins and Traditional Polycondensates. *Chemical Reviews* **2016,** *116* (7), 4597-4641.

17.   Cankaya, A.; Steinmann, M.; Bülbül, Y.; Lieberwirth, I.; Wurm, F. R., Side-chain poly(phosphoramidate)s via acyclic diene metathesis polycondensation. *Polym. Chem.* **2016,** *7* (31), 5004-5010.

18.   Steinmann, M.;   Wagner, M.; Wurm, F. R., Poly(phosphorodiamidate)s by Olefin Metathesis Polymerization with Precise Degradation. **2016,** *22* (48), 17329-17338.

19.   Busch, H.;   Majumder, S.;   Reiter, G.; Mecking, S., Semicrystalline Long-Chain Polyphosphoesters from Polyesterification. *Macromolecules* **2017,** *50* (7), 2706-2713.

20.   Khorana, H. G.; Todd, A. R., 465. Studies on phosphorylation. Part XI. The reaction between carbodi-imides and acid esters of phosphoric acid. A new method for the preparation of pyrophosphates. *Journal of the Chemical Society (Resumed)* **1953,** (0), 2257-2260.

21.   Zhou, Y.; Yin, S.; Gao, Y.; Zhao, Y.; Goto, M.; Han, L.-B., Selective P☐P and P☐O☐P Bond Formations through Copper-Catalyzed Aerobic Oxidative Dehydrogenative Couplings of H-Phosphonates. *Angew. Chem. Int. Ed.* **2010,** *49* (38), 6852-6855.

22.   Bauer, K. N.; Tee, H. T.; Lieberwirth, I.; Wurm, F. R., In-Chain Poly(phosphonate)s via Acyclic Diene Metathesis Polycondensation. *Macromolecules* **2016,** *49* (10), 3761-3768.

23.   Marsico, F.; Turshatov, A.; Peköz, R.; Avlasevich, Y.; Wagner, M.; Weber, K.; Donadio, D.; Landfester, K.; Baluschev, S.; Wurm, F. R., Hyperbranched unsaturated polyphosphates as a protective matrix for long-term photon upconversion in air. *Journal of the American Chemical Society* **2014,** *136* (31), 11057-11064.

24.   Steinbach, T.; Alexandrino, E. M.; Wurm, F. R., Unsaturated poly (phosphoester) s via ring-opening metathesis polymerization. *Polymer Chemistry* **2013,** *4* (13), 3800-3806.

25.   Ortmann, P.; Heckler, I.; Mecking, S., Physical properties and hydrolytic degradability of polyethylene-like polyacetals and polycarbonates. *Green Chem.* **2014,** *16* (4), 1816-1827.

26.   Richards, R. B., Polyethylene-structure, crystallinity and properties. **1951,** *1* (8), 370-376.

27.   Tung, L.; Buckser, S. J. T. J. o. P. C., The effects of molecular weight on the crystallinity of polyethylene. **1958,** *62* (12), 1530-1534.

28.   Zheng, Y.-R.; Tee, H. T.; Wei, Y.; Wu, X.-L.; Mezger, M.; Yan, S.; Landfester, K.; Wagener, K.; Wurm, F. R.; Lieberwirth, I., Morphology and Thermal Properties of Precision Polymers: The Crystallization of Butyl Branched Polyethylene and Polyphosphoesters. *Macromolecules* **2016,** *49* (4), 1321-1330.

29.   Uehara, H.; Kanamoto, T.; Kawaguchi, A.; Murakami, S., Real-Time X-ray Diffraction Study on Two-Stage Drawing of Ultra-High Molecular Weight Polyethylene Reactor Powder above the Static Melting Temperature. *Macromolecules* **1996,** *29* (5), 1540-1547.

30.   Wolf, T.; Steinbach, T.; Wurm, F. R., A Library of Well-Defined and Water-Soluble Poly(alkyl phosphonate)s with Adjustable Hydrolysis. *Macromolecules* **2015,** *48* (12), 3853-3863.

31.   Wang, Y.-C.; Tang, L.-Y.; Li, Y.; Wang, J., Thermoresponsive block copolymers of poly (ethylene glycol) and polyphosphoester: thermo-induced self-assembly, biocompatibility, and hydrolytic degradation. *Biomacromolecules* **2008,** *10* (1), 66-73.

32.   Wang, Y.-C.; Tang, L.-Y.; Sun, T.-M.; Li, C.-H.; Xiong, M.-H.; Wang, J., Self-assembled micelles of biodegradable triblock copolymers based on poly (ethyl ethylene phosphate) and poly (ϵ-caprolactone) as drug carriers. *Biomacromolecules* **2007,** *9* (1), 388-395.

33.   Appukutti, N.; Serpell, C. J., High definition polyphosphoesters: between nucleic acids and plastics. *Polym. Chem.* **2018,** *9* (17), 2210-2226.

34.   Bauer, K. N.; Liu, L.; Wagner, M.; Andrienko, D.; Wurm, F. R., Mechanistic study on the hydrolytic degradation of polyphosphates. *Eur. Polym. J.* **2018,** *108*, 286-294.

35.   Oecd, *OECD Guidelines for the Testing of Chemicals*. Organization for Economic: 1994.

Chapter 5

# Polyphosphoester Hydrogels: Degradable and Cell-Repellent Alternatives to PEG-Hydrogels

Foreword

The following chapter is based on unpublished results.

The project was accomplished in cooperation with Dr. Romina Schröder[1], who did the cell studies.

[1] *Institute of Inorganic Chemistry and Analytical Chemistry, Johannes Gutenberg - University of Mainz, Mainz, Germany*

Abstract
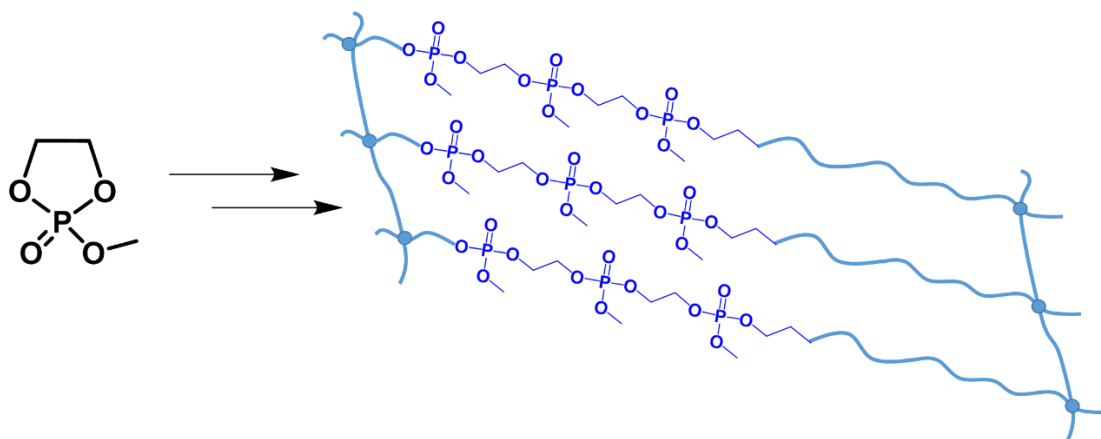
Hydrophilic PPE Hydrogels as a substitute for PEG hydrogels were prepared. In contrast to the previous chapters, this chapter uses ring-opening polymerization of cyclic phosphates in order to prepare degradable polymer gels. A photocrosslinkable, degradable, PPE, namely poly(methyl ethylene phosphoester) dimethacrylate (PMEP-DMA) was synthesized. NMR spectroscopy and infrared spectroscopy was used to characterize the macromonomer. 10 and 15wt% PMEP hydrogels (HGs) were prepared by photopolymerization of an aqueous solution of the macromonomers. The PPE gels were compared to PEG hydrogels with respect to their swelling and water content and rheology analysis demonstrated viscoelastic characteristics. In contrast to the PEG HGs, the PMEP gels proved a rapid weight loss for the 10wt% PMEP gels and a much slower weight loss for 15wt% PMEP gels during incubation in aqueous media. The release of soluble polymer chains from the network and the formation of phosphoric acid diesters during the

hydrolysis protocol was proven. Biocompatibility of the PPE gels was proven with MG-63 osteoblast cells; the PPE HGs further proved no significant cell adhesion similar to the PEG gels, which might find use in biodegradable antifouling surfaces or for drug release systems

1 Introduction

Poly(ethylene glycol) (PEG) hydrogels have showed great promises for biomedical applications as matrices for controlled release of therapeutics or as scaffolds for promoting tissue regeneration.[1-3] These PEG hydrogels are non-cytotoxic, non-immunogenic, hydrophilic and they can mask the material from the host's immune system which renders them as a great material for regenerative medicine applications.[1] However, PEG hydrogels are missing chemical versatility, given that the functionalization of the polymer is limited to the hydroxyl chain end(s).[4] Degradability of the hydrogel network is mostly achieved via ester bonds attached to the chain ends and used for crosslinking, e.g. by methacrylic acid esters. The PEG hydrogel can dissolve slowly over time, however, the non-degradable PEG chains need to be flushed or can induce bioaccumulation in the tissue.[5] One group of degradable PEG-based hydrogels is achieved by building block-copolymer components with poly(lactic acid) (PLA).[6-10] The introduction of PLA to form degradable hydrogels has found many successful applications, however this type of polymer composition can have drawbacks such as potential inflammation caused by acidic degradation products from lactic acid and poly(acrylic acid), protein denaturation due to PLA hydrophobicity and they can degrade relatively quickly in an aqueous environment due to the hydrophilicity of PEG.[11-13] Another approach to prepare degradable but also fully hydrophilic PEG hydrogels has been utilized by multiarm PEG-amine crosslinked with an ester containing amine-reactive PEG derivate.[14] Due to the to the amine reaction during the cross-linking, covalent binding of encapsulated proteins to the polymer network can occur, which limits its applications. This can be avoided by selective crosslinking chemistry of PEG-multiacrylates and PEG-dithiols to form fully hydrophilic gels.[15] However, this kind of crosslinking can lead to network nonideality because low acrylate concentration favors intramolecular reactions.[16] As a result, there is an increasing interest in polymers with similar biological and physiochemical properties with control over the polymer degradability and functionality.[17] Phosphorus containing polymers, especially polyphosphoesters (PPEs) are materials that have attracted a lot of attention for biomedical applications as they fulfill the desired properties.[18] Water-soluble PPEs have a similar stealth effect as PEG[19] and their physical properties can be controlled by the binding motif around the phosphorus atom. With the inherent ester bond in the backbone, these materials are

hydrolytically degradable and the pentavalent phosphorus atom allows a high structural and chemical versatility.

Herein, we report the first pure polyphosphoester hydrogel that exhibit all the desired protein and cell-repellent properties and also being degradable and potentially chemically tunable. Poly(methyl ethylene phosphate) (PMEP) with its high hydrophilicity was used as a PEG analog. It was synthesized by ring-opening polymerization (ROP) of the five-membered 2-methoxy-1,3,2-dioxaphospholane 2-oxide heterocycle. This polymer is known for a while, however, to our knowledge, it has never been used for the preparation of hydrogels. For the design of the photopolymerizing hydrogel, two methacrylate end groups were introduced by terminating the ROP with 2-isocyanatoethyl methacrylate.

## 2   Results and Discussion

2.1   Polymer Synthesis and Hydrogel Preparation

MEP (**1**) was polymerized by the anionic ring-opening polymerization with a mixture of 1,8-diazabicyclo[5.4.0]undec-7-ene   (DBU)   and   1-(3,5-bis(trifluoromethyl)phenyl)-3-cyclohexylthiourea (TU) as catalyst/cocatalyst system.{Clément, 2012 #307} We used PEG-diol (M_n= 400g/mol) as a difunctional initiator. The polymerization was conducted at 0 °C for 60 min and directly terminated by the addition of 2-isocyanatoethyl methacrylate to give the dimethacrylate-terminated PMEP-DMA (**P1**, M_n = 12,000 g/mol with repeating unit of 80 (determined by ^{1}H NMR), M_n = 5,700 g/mol with a PDI of 1.8 (determined by GPC) as a colorless viscous liquid (Scheme 5.1). The ^{1}H NMR spectra of **P1-DMA** exhibited the characteristic signal of the methylene groups in the backbone at 4.29 – 3.93 ppm and the methyl groups of the pendant side chain at 3.78 – 3.53 ppm as a multiplet due to coupling to the phosphorus. The signals of the initiator appear at 3.57 – 3.46 ppm. The protons at the double bond of the methacrylate group appear at 6.06 and 5.68 as singlets and the methyl group shows resonance at 1.86 ppm. ^{31}P NMR of **P1-DMA** shows the main signal at-0.20 ppm and 2 small signals at 1.10 and -1.48 ppm.

The hydrogels were then prepared by UV irradiation (15 min at 365 nm) of a 10 or 15 wt% solution of PMEP-DMA in 0.1 M PBS buffer (pH 7.4) containing 0.2% of 2-Hydroxy-4′-(2-

hydroxyethoxy)-2-methylpropiophenone. After the irradiation time, clear, colorless and soft PMEP hydrogels were obtained.
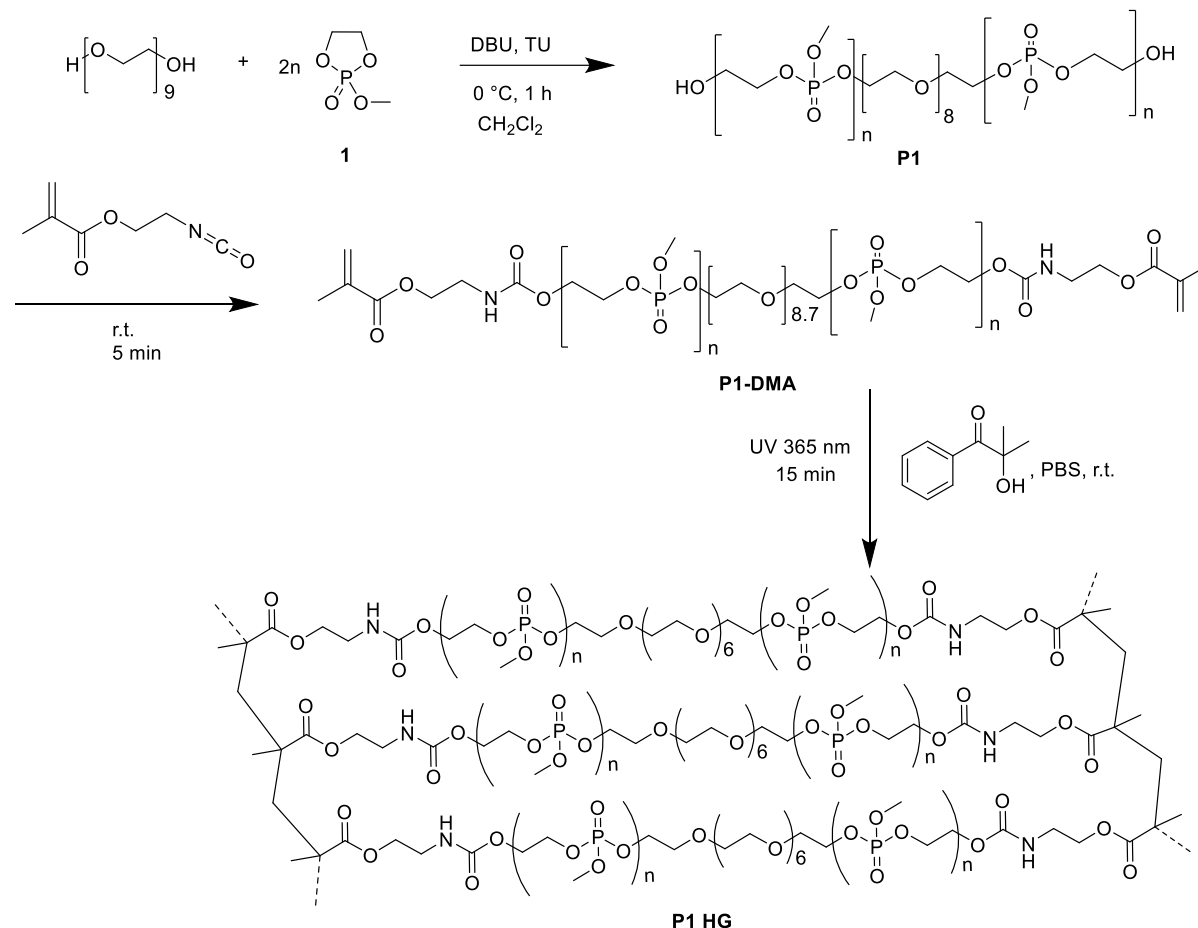
Scheme 5.1. Polymerization of MEP (1) and subsequent preparation of hydrogels.

As comparison, we also prepared PEG hydrogels, using PEG diols (4,000 g/mol or 10,000 g/mol), which were functionalized with 2-isocyanatoethyl methacrylate using a catalytic amount of dibutyltin dilaurate (Scheme 5.2).
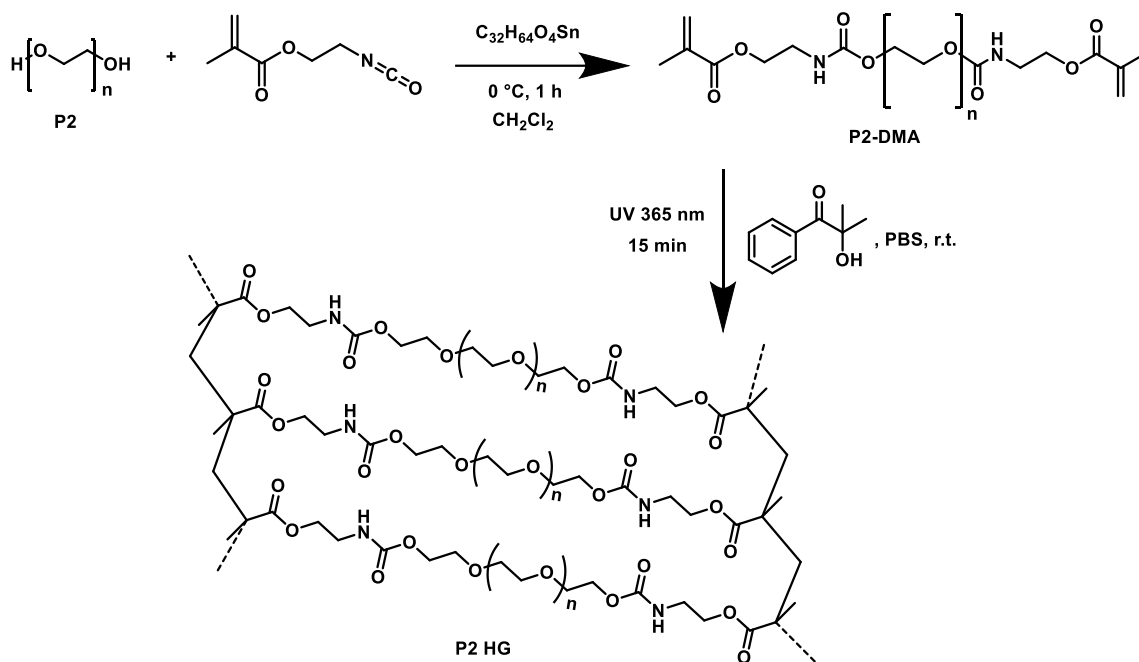
Scheme 5.2. Functionalization of P2 and subsequent preparation of hydrogels.

Crosslinking to the final hydrogels was performed in the same way as for the PMEP HGs. Compared to the flexible and transparent PMEP-HG, the PEG-hydrogels were stiffer and slightly turbid.

2.2   Characterization of the hydrogels

SEM images of lyophilized hydrogels show a strong difference of the morphology between PMEP and PEG Hydrogels. While PMEP HGs showed a clear smooth surface (Figure 5.1), PEG HGs show characteristic meshes of a three-dimensional polymer network. The difference in the morphology after lyophilization can be explained by the thermal properties of PEG and PMEP. DSC measurements proved a fully amorphous behavior for PMEP-DMA with a glass transition (T_g) of -39 °C, similar to other poly(alkyl ethylene phosphate)s.{Bauer, 2018 #308} PEG on the other side is a solid polymer with a T_m of 51 and 58 °C for PEG(4,000)-DMA and PEG(10,000)-DMA, respectively. This results in the retaining of the cellular structure after freeze-drying, while the PMEP-HGs no cellular structure can be visualized and also explains that the PEG-HGs obtained were harder and stiffer compared to the PMEP gels.
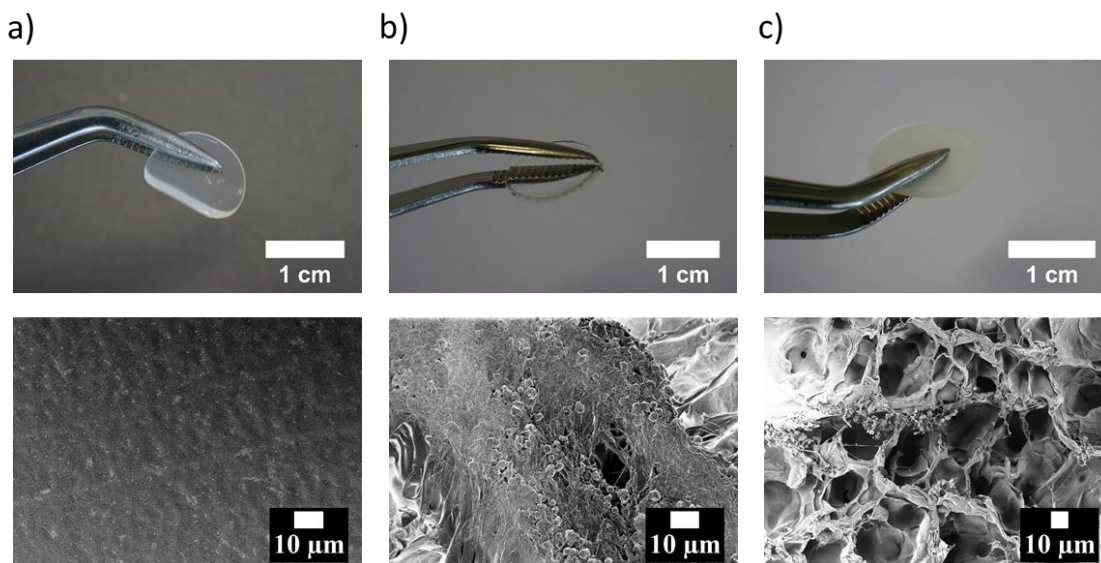
Figure 5.1. Photos of Hydrogels after polymerization and SEM images of lyophilized Hydrogels. (a) 15wt% PMEP HG, (b) 15wt% PEG(4,000) HG and (c) 15wt% PEG(10,000) HG.

IR spectra of the PMEP-DMA or PEG-DMA precursors and the corresponding hydrogels prove the successful photopolymerization (Figure 5.2). For all soluble precursors and hydrogels absorption bands at 1730 cm^{-1} for the C=O group in the urethane linkage and at 1540 cm^{-1} for the NH-vibrations were identified. With the HG synthesis, the band at 1700 cm^{-1} is getting stronger resulting from associated C=O groups in the urethane. This is due to the intermolecular urethane groups coming closer to each other by crosslinking of the methacrylates indicating successful polymerization to the gel network. For the PMEP-DMA and Hydrogel in the region of 1350 – 1150 cm^{-1} is the strong band due to stretching vibration of the P=O group. For PMEP-DMA this band is at 1350 cm^{-1} which is the P=O stretching for unassociated P=O bonds. The band for P=O stretching in the gels shifts to 1250 cm^{-1}, which is typical for associated P=O bonds and is due to hydrogen bonding of the phosphates with trapped water inside the gel. Both hydrogels showed a clear O-H vibration band at 3450 cm^{-1} resulting from residual water, trapped in the cross-linked polymer network. The hydrogel based on PMEP had a significant stronger signal for the O-H vibrations compared to the PEG-based hydrogel, which might be rationalized by the more efficient trapping of water in the amorphous hydrogel of PMEP. Three more bands resulting from phosphates in the polymer backbone can be found at 1050 cm^{-1} and 900 cm^{-1} due to asymmetric P-O-C stretching and at 800 cm^{-1} occurring from symmetric stretching of the P-O-C bond from the methoxy side-chain in PMEP. In this area, the strong band for C-O stretching can be found for PEG compounds at 1100 cm^{-1}.
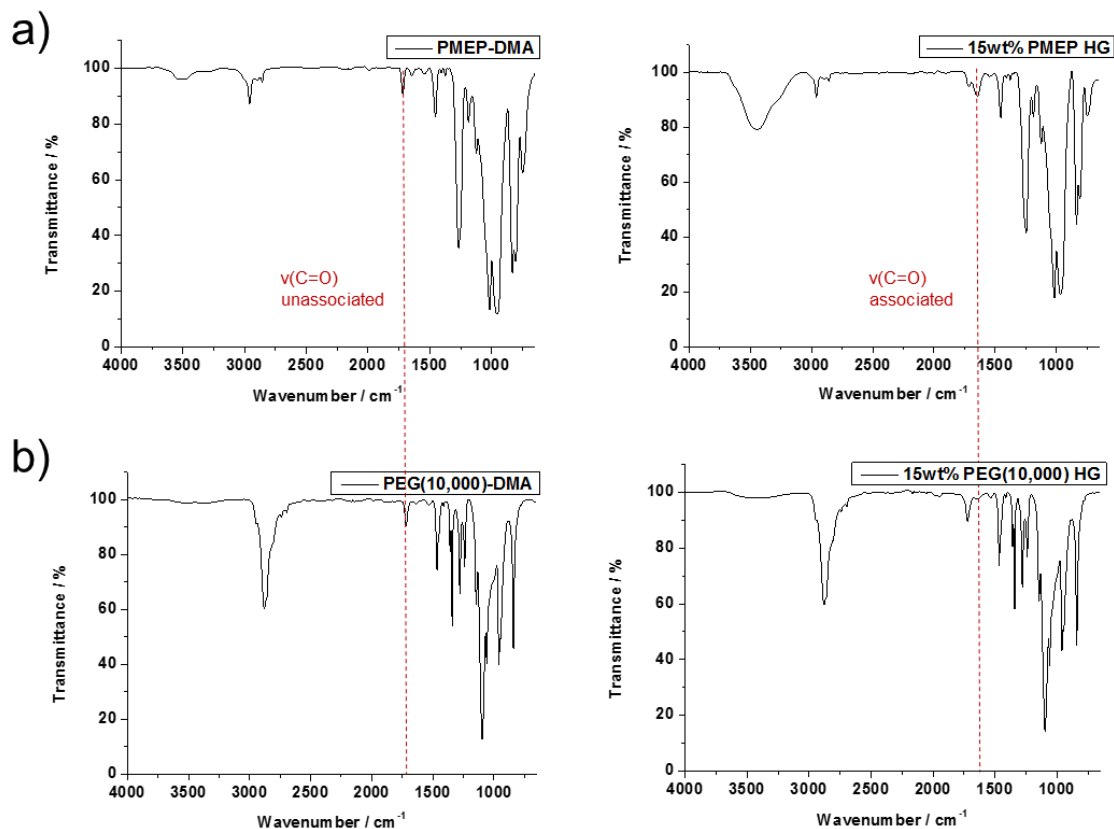
Figure 5.2. IR spectra of (a) PMEP-DMA precursor and 15 w% PMEP-hydrogel. (b) PEG(10,000)-DMA precursor and 15 w% PEG(10,000) hydrogel.

Swelling ratio. The swelling ratio of a hydrogel is an important value for various applications as it strongly influences the surface properties, mechanical properties, surface mobility as well as solute diffusion.[26] The amount of water retained by the hydrogel depends on the on the structure of the polymer network itself and on environmental conditions such as ionic strength, pH and temperature of the aqueous solution in contact with the polymer.[27] Since the physical properties can be changed with hydration, the mass swelling ratio of the gels was investigated relative to polymer concentration and swelling time. Hydrogels were immersed into DPBS and deionized water at room temperature for 6h or 26h. Then, the mass swelling ratio of the swollen mass to the dry, lyophilized mass of polymer was calculated and compared (Figure 5.3a). The swelling ratio Q was calculated according to

$$Q = \frac{w_{gel,swell,time}}{w_{gel,dry}} \tag{1}$$

where $w_{gel, swell, time}$ is the swollen hydrogel after 6 h or 26 h and $w_{gel, dry}$ is the weight of the dried hydrogel.

When comparing both PEG hydrogels with PMEP hydrogels, it is obvious that the PEG gels showed the same swelling in DPBS and in water. A slight increase in the swelling ratio seemed to occur for the 15et% PEG hydrogels after incubation compared to the "as prepared" gels. In case of PMEP HGs, a much stronger swelling compared to all PEG-hydrogels was observed for 10wt% hydrogels directly after the synthesis or after immersing into water for 6h. If the 10et% PMEP-HG was immersed into DPBS, the swelling ratio decreased to similar values as PEG-hydrogels, probably to interactions with the salt ions in DPBS. For longer incubation times, the 10et PMEP-HGs became too soft and the swelling ratio could not be determined. The 15wt% PMEP hydrogels proved to be mechanically more stable and exhibited a similar swelling after the crosslinking and after immersing them into pure water. The gels, incubated in DPBS proved a significantly lower swelling ratio, compared to the PEG hydrogels, probably attributed to stronger interactions of the polyphosphoester backbone with salt ions compared to the polyether backbone. The difference in the swelling ratios in pure water of PMEP HGs compared to PEG HGs might be rationalized also by the higher hydrophilicity of PMEP compared to PEG, which was confirmed by calculation of the theoretical logP value or by the elution time via rpHPLC (Figure 5.20).
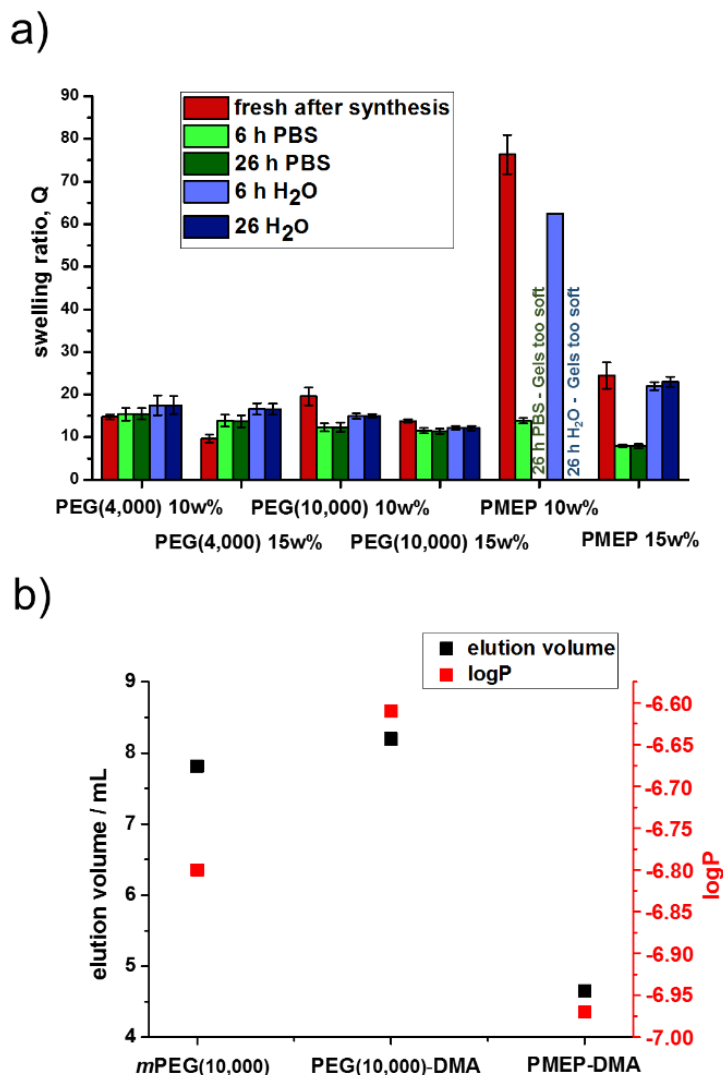
a)

b)

Figure 5.3. (a) Swelling ratio of all Hydrogels after 6 and 26 h equilibration in deionized water or 0.1 M PBS buffer. (b) Determination of the hydrophilicity of PMEP and PEG via reverse-phase HPLC (rpHPLC) and calculated logP-values.

Mechanical Properties. Mechanical properties of hydrogels are known to influence cell function and differentiation and thus are important for application on tissue engineering.[23-25] To investigate the mechanical properties, the hydrogels were tested using oscillatory shear rheology to measure the storage (G′, elastic component) and loss moduli (G″, viscous component) as a function of either strain or frequency. The profiles of PMEP-HG, PEG(4,000)-HG, and PEG(10,000)-HG as 10 and 15wt% hydrogels are shown in Figure 5.4. The strain sweeps indicate that both, the linear

plateau of the viscosity-curve and elasticity-curve is for 10 and 15wt% PMEP HG 10% and 1%, PEG(4,000) HG 10% and 0.1%, PEG(10,000) HG 0.5% and 0.2% respectively. The sharp bend of the G' curve after the yield stress means brittle fracture behavior of the gels due to uneven breaking in bigger pieces under shear. With G'>G'' in the linear zone and the peak of G'' with increasing shear, proves that the hydrogels were cross-linked and due to this, first micro cracks lead to a higher elastic to viscose proportion until the gel breaks fully resulting in G''>G'. The frequency sweeps in a range from 10^{-2} to 10^{1} rad/s were then performed at low strains. The results showed for all 15wt% gels that PMEP HG has the lowest moduli of all hydrogels with G' and G'' of $2\text{-}10\cdot10^{2}$ and $1\text{-}4\cdot10^{2}$ Pa respectively. PEG(4,000) HG has the highest moduli with G'=$4\text{-}8\cdot10^{3}$ and G''=$1\cdot10^{3}$ Pa. PEG(10,000) HG with longer polymer chains and therefore less crosslinking density has lower moduli compared to PEG(4,000) HG with G'=$2\text{-}4\cdot10^{3}$ and G''=$3\text{-}15\cdot10^{2}$ Pa. The frequency sweeps of 10wt% HG showed the same trend for all the gels, but with lower elastic and viscous modulus compared to the 15wt% HG due to the lower crosslinking density. However, in comparison to the PEG HGs the 10wt% PMEP HG has a significantly higher reduction of moduli with G'=$3\text{-}10\cdot10^{1}$ and G''=$1\text{-}4\cdot10^{1}$ Pa. 10wt% PEG(4,000) HG had G'=$1\text{-}2\cdot10^{3}$ and G''=$1\text{-}8\cdot10^{2}$ Pa; PEG(10,000) HG had G'=$6\text{-}15\cdot10^{2}$ and G''=$1\text{-}7\cdot10^{2}$ Pa. The values of G' at low frequency can be used to make a point about the crosslinking density and about the stiffness of different samples. As expected PEG(4,000) HG showed the highest G' value which means it has the highest stiffness. PMEP HG and PEG(10,000) HG have similar crosslinking density, however, the difference in G' is smaller between PEG(4,000) HG and PEG(10,000) HG.
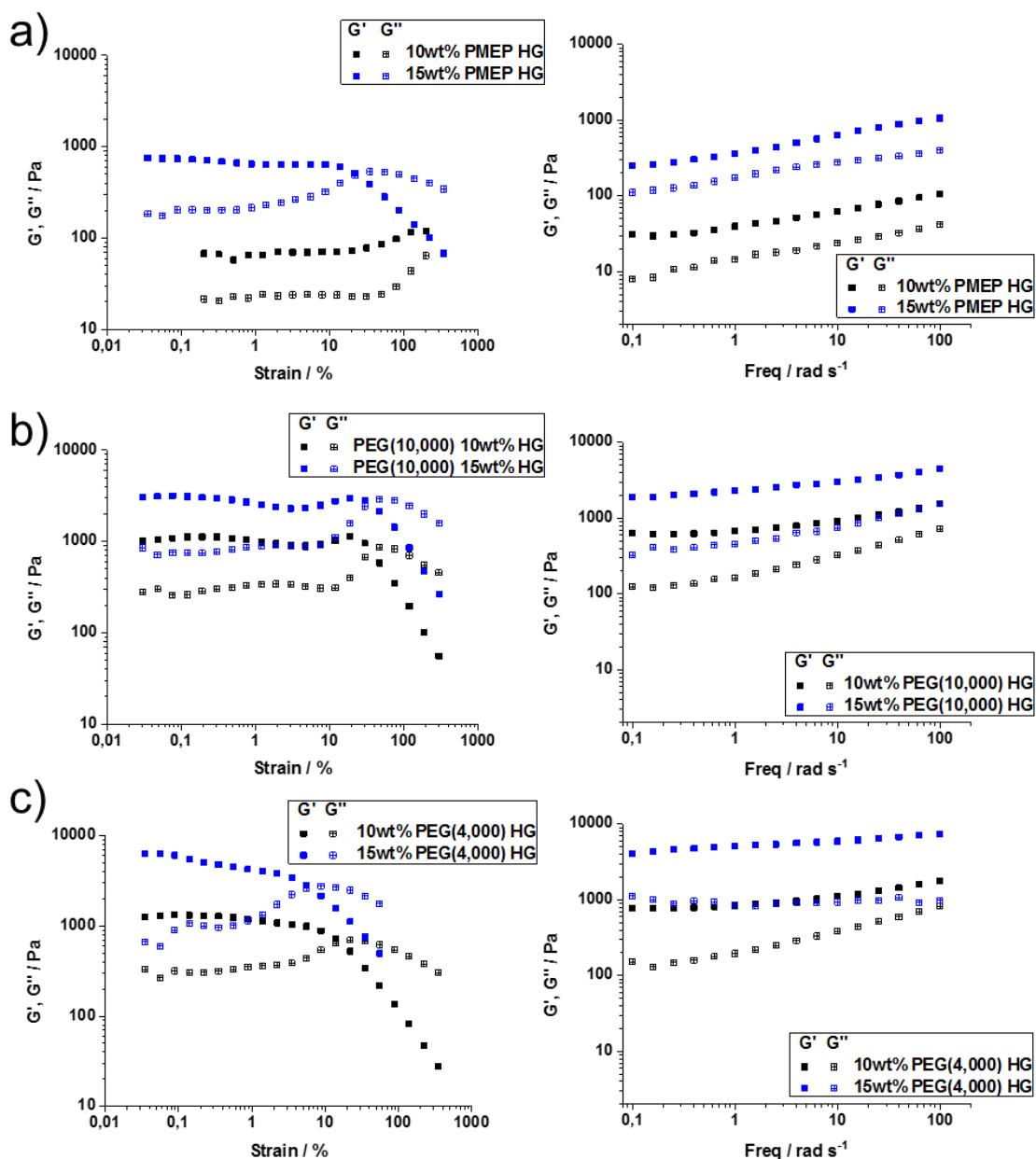
Figure 5.4. Rheological characterization of (a) 10 and 15wt% PMEP HGs, (b) 10 and 15wt% PEG(4,000) HGs and (c) 10 and 15wt% PEG(10,000) HGs after synthesis by strain sweeps at fixed frequency (1 rad/s) and frequency sweeps at constant strain.

2.3   Degradation studies

For many biomedical applications such as wound healing dressings, controlled drug release devices, cell immobilization islets, three-dimensional cell culture substrates, and bioactive scaffolds for regenerative medicine the biodegradation of the hydrogel is a preferred or a required property.[2, 28-31] In tissue engineering applications, degradable hydrogels allow the infiltration of blood vessels and provide space for proliferating cells.[32, 33] In controlled drug and gene delivery, degradation permits spatiotemporal controlled release of the cargo molecule.[34] Since the degradability of hydrogels are of importance for many applications, the biodegradability of the PMEP hydrogels were evaluated and compared to PEG hydrogels. In PMEP HGs, both the phosphoesters and the ester bond to the methacrylate could be hydrolyzed, while in the PEG HG only hydrolysis of the methacrylate would lead to gel solubilization.

The degradation of the hydrogels was determined after immersing the gels in DPBS at 37 °C over several weeks. The weight loss determinations of all gels proved a significantly faster degradation of PMEP gels compared to PEG gels (Figure 5.5a). PMEP hydrogels exhibited a clear mass loss, which was dependent on the polymer concentration used for the gel preparation. After 3 weeks, the 10wt% PMEP HG was almost completely dissolved. In case of the15wt% PMEP HG, more than 80% weight loss was observed after an incubation time of 6 weeks. In contrary, both PEG hydrogels showed only an initial weight change due to a certain swelling or de-swelling but did not degrade further under these conditions over a period of 5 weeks. The hydrolytic degradation of the PMEP hydrogel was further investigated by ^{31}P NMR spectroscopy (conducted under neutral conditions (at pH = 7.4 in 0.1 M DPBS buffer/D_2O (9:1)) (Figure 5.5b). Following the degradation process over 41 days, we can see an increasing signal for phosphotriesters at -0.2 ppm due to polymer chains released from the network by main-chain hydrolysis and dissolving into the solvent. Furthermore, at around 2 ppm, we can see besides the constant signal from the phosphate salts of DPBS an increasing signal for phosphodiesters by hydrolysis of the phosphotriesters. The signal resulting from phosphotriesters increases much stronger compared to the signal for phosphodiesters, due to dissolution of free polymer chains and degraded polymer chains, while the amount of phosphodiesters is dependent on actual hydrolysis of phosphotriesters.
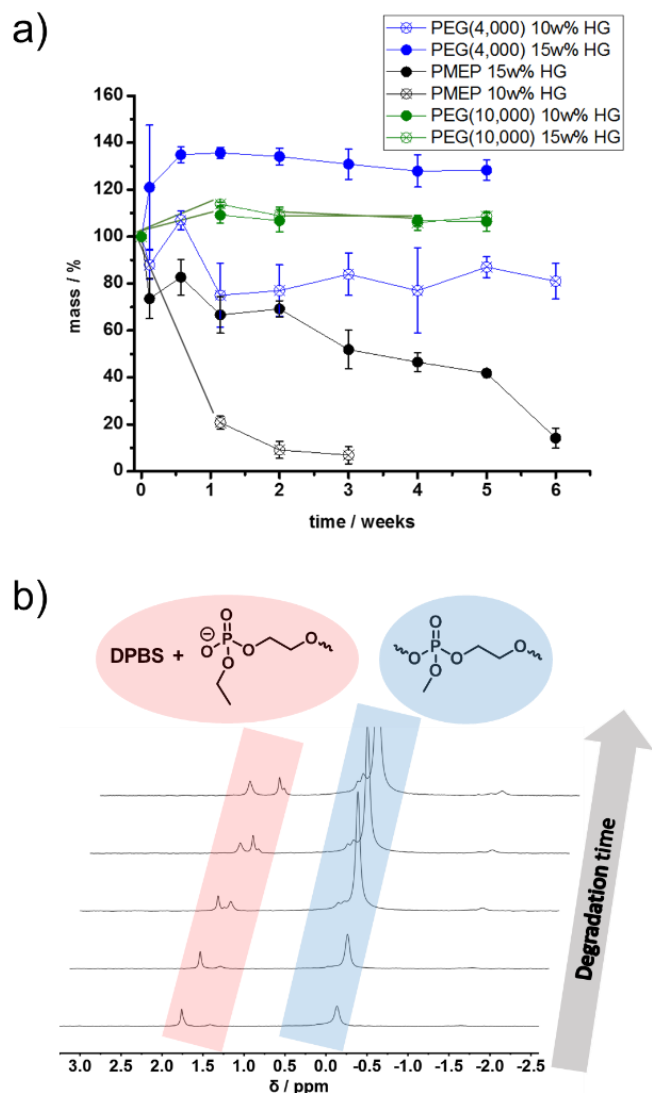
Figure 5.5. Degradation studies of PMEP HGs. (a) Mass change of Hydrogels in 0.1 M PBS buffer at 37 °C. (b) ^{31}P NMR spectra (202 MHz, 298 K, 0.1M DPBS/D$_2$O (9:1)) recorded within the degradation of PMEP HG at pH 7.4 after 0, 3, 8, 25 and 41 days.

2.4 Cell Adhesion

To demonstrate the feasibility of using PMEP HGs for tissue engineering applications the cell toxicity, biocompatibility and adherence were studied. Therefore, osteoblast cell line MG-63 were sowed over 15wt% PMEP HGs and compared to PEG-HGs and a positive control (Figure 5.6). The hydrogels proved almost no cell adherence during the conducted time frame while the positive

control showed already a significant amount of cells after 24 h. The few cells on the PMEP HGs maintained a round shape and showed no spreading on the gel substrate over time, which indicates nonadherent cells. However, the morphology of cells is dependent on the substrate these cells proliferate and adhere. Hydrogels have usually surface irregularities with small gaps (network mesh) due to the polymer network they form compared to the plain and smooth surface of cell culture plates.
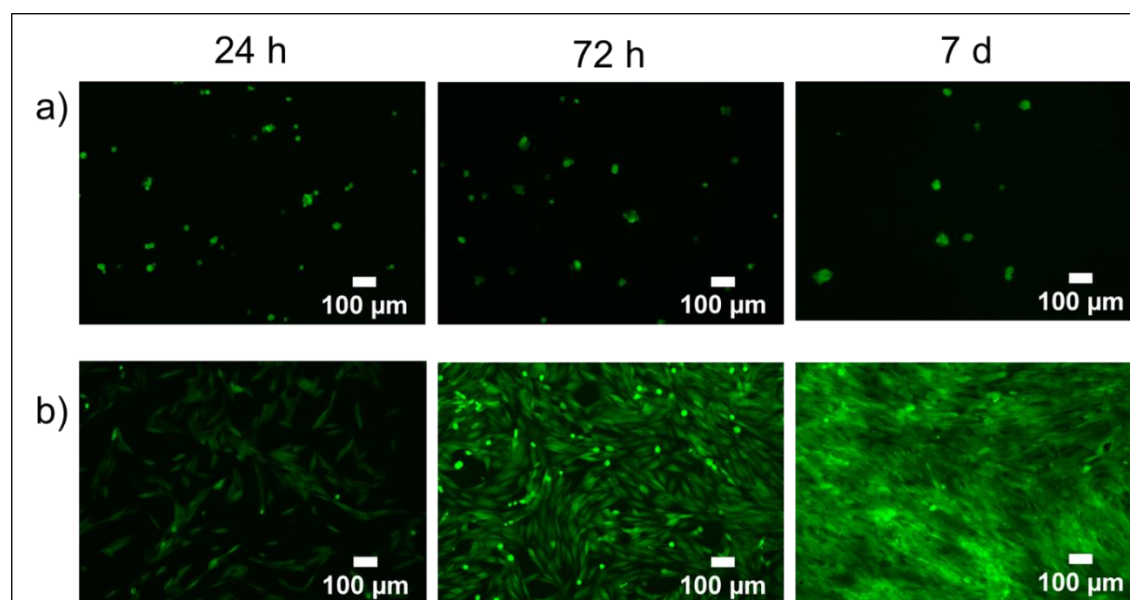

Figure 5.6. Cell adherence and viability of osteoblast cell-line MG-63 over (a) 15wt% PMEP HGs and (b) seeded into plastic wells of the cell culture plate as positive control after 24 h, 72 h and 7 days. Viable cells were indicated by green fluorescence with calcein-AM staining.

3 Summary

We prepared a strongly hydrophilic polyphosphoester hydrogel which is hydrolytically degradable, showed excellent biocompatibility and were cell-repellent. The hydrogels were prepared by the ring-opening polymerization of MEP followed by endcapping with methacrylates and crosslinking under UV-light. Clear, soft, and biodegradable PMEP hydrogels were obtained. Osteoblasts proved no adhesion to the hydrophilic PMEP and PEG hydrogels, indicating a potential use to prevent postoperative adhesions or thrombosis in damaged blood vessels after angioplasty. Further, these materials might be interesting in controlled drug and gene delivery applications or as scaffolds for regenerative medicine with the integration of adhesion peptides like RGD sequences (Arg-Gly-Asp). Because of the hydrophilicity of PMEP-MA, it is possible to synthesize pure polyphosphoester hydrogels without copolymerization of PPEs with other more

hydrophilic polymers which keeps the synthesis at low effort. However, a combination of PEG and PMEP might be used for gels to introduce degradable units and mechanical properties of PEG.

4 Experimental

Materials

All solvents and chemicals were purchased from Sigma Aldrich, Acros Organics, or Fluka and used as received unless otherwise stated. DBU was distilled from calcium hydride and stored over molecular sieves (4Å) under argon prior to use. Dry solvents were purchased from Acros Organics or Sigma Aldrich and stored with a septum and over molecular sieves. Deuterated solvents were purchased from Sigma Aldrich and used as received. 2-Chloro-1,3,2-dioxaphospholane 2-oxide (COP) and DPBS - Dulbecco's Phosphate-Buffered Saline was bought from Sigma Aldrich.

Instrumentation and Characterization Techniques

SEC. Size exclusion chromatography measurements were performed in DMF (containing 1 g L^{-1} of lithium bromide as an additive) at 60 °C and a flow rate of 1 mL min^{-1} with a PSS SECurity as an integrated instrument, including a set of 3 PSS GRAM columns (porosity of 100 Å and 1000 Å) and a refractive index (RI) Detector. Calibration was carried out using polyethylene glycol standards provided by Polymer Standards Service.

NMR. For nuclear magnetic resonance analysis ^{1}H, ^{13}C, and ^{31}P NMR spectra of the monomers and polymers were recorded on a Bruker AVANCE III 300, 500 or 700 MHz spectrometer. All spectra were referenced internally to residual proton signals of the deuterated solvent.

HPLC. The high-pressure liquid chromatography measurements were performed on an Agilent Technologies Series 1200 setup equipped with a UV detector and an ELSD detector 385-LC (both Agilent Technologies, Santa Clara, USA). The analysis of polymers was conducted using a Macherey-Nagel MN HD8 column 125/4/5 μm equipped with a 5-3 precolumn (Merck Chemicals GmbH, Darmstadt, Germany) and an eluent gradient from MeOH/water + 0.1% TFA 40/60% to 100/0% in 10 min. For each measurement, 10 μL of sample volume was injected and kept at 37 °C throughout the measurement.

DSC. The thermal properties of the synthesized polymers have been measured by differential scanning calorimetry (DSC) on a Mettler Toledo DSC 823 calorimeter. Three scanning cycles of heating−cooling were performed in a N_2 atmosphere with a heating and cooling rate of 10 °C min^{-1}.

TGA. TGA was measured on a Mettler Toledo ThermoSTAR TGA/SDTA 851-Thermowaage in a nitrogen atmosphere. The heating rate was 10 °C min^{-1} in a range of temperature between 25 and 600−900 °C.

FTIR. FTIR spectra were recorded in transmission mode accomplished with a Bruker Tensor II (Platinum ATR).

Rheology. Rheology experiments were performed on an Advanced Rheometric Expansion System (ARES, Rheometric Scientific). Plate-plate geometry was used with plate diameters of 25 mm. Oscillatory shear deformation was applied under conditions of controlled deformation amplitude. Strain sweeping at constant frequency of 1 rad/s was first performed (from 10^{-3} % to 10^2 %) for the individual hydrogels. Then the strain was fixed at a selected value in the range of linear viscoelastic response and the frequency sweeping was performed from 10^{-1} to 10^2 rad/s.

LogP. LogP values were calculated via the free online tool on www.molinspiration.com with 92 repeating units for PEG and 32 repeating units for PMEP.

SEM. SEM investigations were performed by using a LEO 1530 GEMINI. The characterizations were carried out by applying the low-voltage approach. The lyophilized gels were deposited on conductive carbon tape.

4.1 Synthesis

*2-Methoxy-2-oxo-1,3,2-dioxaphospholane (MEP) (**M1**)*

A flame-dried 1000 mL three-neck flask, equipped with a dropping funnel, was charged with 2 chloro-2-oxo-1,3,2-dioxaphospholane (50 g, 0.35 mol) dissolved in dry THF (300 mL). A solution of dry methanol (11.24 g, 0.35 mol) and dry triethylamine (35.42 g, 0.35 mol) in dry THF (45 mL) was added dropwise to the stirring solution of COP at -20 °C under an argon atmosphere. During the reaction, hydrogen chloride was formed and precipitated as triethylammonium hydrochloride. The reaction was stirred at 4 °C overnight. The salt was removed by filtration and

the filtrate concentrated *in vacuo*. The residue was purified by distillation at reduced pressure to give a fraction at 89-97 °C/0.001 mbar, obtaining the clear, colorless, liquid product MEP (37.21 g, 0.27 mol, yield: 77 %). ^{1}H-NMR (500 MHz, CDCl$_3$, 298 K): δ = 4.43 (m, 4H), 3.71 (d, 3H) ppm. ^{13}C{H} NMR (125 MHz, DMSO-d$_6$, 298 K): δ 66.57, 54.72. ^{13}C NMR (75 MHz, CDCl$_3$, 298 K) δ = 66.19, 66.16, 54.93, 54.84 ppm.^{31}P{H} NMR (202 MHz, CDCl$_3$, 298 K): δ = 17.89 ppm.

*Polymerization to PMEP-DMA (**P1-DMA**)*

N-cyclohexyl-*N*'-(3,5-bis(trifluoromethyl)phenyl)thiourea (TU) was synthesized according to literature procedure.[20] TU and the initiator PEG 400 were freeze-dried with benzene prior use. MEP (5.26 g, 7.2·10^{-3} mol), TU (1.41 g, 13.73·10^{-3} mol), PEG 400 (0.55 g, 1.37·10^{-3} mol) and 0.56 mL dry dichloromethane were introduced into a 100 mL flame dried Schlenk tube to give a total reaction concentration of 4 mol/L MEP in dichloromethane. The polymerization was initiated by rapid addition of 2.05 mL DBU (2.09 g, 13.7·10^{-3} mol) to the stirring solution with a syringe at 0 °C. The polymerization was terminated after 1 h by excess addition of 2-isocyanatoethyl methacrylate (4.27 g, 27.5·10^{-3} mol). The polymer was precipitated twice from dichloromethane into ice-cold ethyl acetate and once into ice-cold diethyl ether. 0.067 mol% hydroquinone was added, the mixture dissolved in deionized water and then freeze-dried. The polymer was obtained after freeze-drying in quantitative yield. ^{1}H NMR (300 MHz, CDCl$_3$, 298 K) δ = 6.11 (s, 2H), 5.56 (s, 2H), 4.43 – 4.11 (m, 327H), 3.93 – 3.69 (m, 239H), 3.65 – 3.56 (m, 36H), 1.91 (s, 1H) ppm. ^{13}C{H} NMR (75 MHz, CDCl$_3$, 298 K) δ = 70.53, 66.41, 66.33, 66.24, 54.70, 54.62 ppm. ^{31}P{H} NMR (121 MHz, DMSO-*d*$_6$, 298 K) δ = 1.10, -0.20, -1.52 ppm.

*PEG(4,000)-DMA and PEG(10,000)-DMA (**P2-DMA**)*

PEG-DMA was synthesized according to literature.[21] Briefly, PEG (5g, 1.25·10^{-3} mol(4,000) or 0.50·10^{-3} mol(10,000)) was added to a solution of dibutyltin dilaurate (DBTD) (2 drops) and 15 mL dry dichloromethane over freshly activated molecular sieves (ca. 6 g). The reaction was then stirred for 4 days at room temperature. The solution was precipitated twice from dichloromethane into diethyl ether. The product was isolated by filtration as a colorless powder. The PEG-DMA was dissolved in deionized water, 0.1wt% hydroquinone was added and the solution was freeze-dried to give the pure product in 92-93%.

PEG(4,000)-DMA: ^{1}H NMR (300 MHz, CDCl$_3$, 298 K) δ = 6.10 (s, 2H), 5.58 (s, 2H), 5.25-5.05 (m, 2H), 4.46 – 4.10 (m, 4H), 4.01-3.44 (m, 364H), 3.44-3.19 (m, 4H) 1.93 (s, 6H) ppm. ^{13}C NMR (75 MHz, CDCl$_3$, 298 K) δ = 126.02, 70.57, 69.57, 18.31 ppm. PEG(10,000)-DMA: ^{1}H NMR

(300 MHz, CDCl$_3$, 298 K) δ = 6.12 (s, 2H), 5.60 (s, 2H), 5.18-5.08 (m, 2H), 4.31-4.14 (m, 4H) 3.94-3.46 (m, 908H), 3.45-3.31 (m, 4H), 1.94 (s, 6H) ppm. ^{13}C NMR (75 MHz, CDCl$_3$, 298 K) δ = 118.16, 70.57 ppm.

4.2 Hydrogel formation, degradation, and swelling ratio

Hydrogel formation by photopolymerization. For the preparation of PMEP hydrogels, 500 µL of a 10 or 15 % (w/v) solution of PMEP-DMA in DPBS was mixed with 10 µL of the photoinitiator 2-hydroxy-40-(2-hydroxyethoxy)-2-methylpropiophenone used as 10% (w/v) solution in 70% ethanol (2g Initiator in 20 mL 70% EtOH).

0.1 mL of the polymer-photoinitiator solution was transferred to a 48-well plate and the same volume of isopropanol was added to remove emerging air-bubbles and to suppress capillary effects. The polymerization of all hydrogels was initiated by 365 nm UV irradiation with a DC lamp directly placed on the wellplate for 15 minutes. PMEP-DMA hydrogel for rheology was synthesized in a cylinder with 26 mm diameter with 1.06 mL polymer solution and isopropanol. All PEG hydrogels were synthesized as the PMEP hydrogels. All gels were washed three times with 1 mL deionized water at 150 rpm for 5 minutes prior use.

Hydrolytic degradation of the hydrogels.

The degradation of the hydrogels was conducted at 37 °C by immersing each gel (12 mm diameter) in 5 mL 0.1 M DPBS (pH 7.4) in closed 20 mL vials. The hydrogels were removed from the solution after predetermined time intervals, surface water was removed and the gels were freeze-dried. The weights of the lyophilized gels before (average weight of 3 samples) and after degradation were compared.

For ^{31}P NMR degradation kinetics, a full 15 w% PMEP HG with 12 mm diameter was transferred into an NMR tube and 0.5 mL DPBS/D$_2$O 9:1 were added.

Determination of the swelling ratio.

Hydrogels were immersed for 6h and 26 h in DPBS or deionized water at room temperature. Then the mass swelling ratio of the swollen mass to the dry, lyophilized mass of polymer was calculated and compared. The swelling ratio Q was calculated by dividing the mass of the swollen gel of a certain time by the mass of the lyophilized, freshly synthesized and washed gel.

4.3 Cell studies

The human osteoblast cell line MG-63 (ATCC® CRL-1427®, LGC Promochem) was used and cultured in DMEM (high glucose, Sigma–Aldrich), 10% FBS (Sigma–Aldrich) + 2 mM Glutamax I (Gibco® Thermo Fisher Scientific) + 100 U/100 μg/mL Penicillin/Streptomycin (Gibco Thermo Fisher Scientific).

Visualization and characterization of cell viability and proliferation

The biocompatibility upon exposure to vaterite was evaluated with MG-63 plated in sterile 12-well cell culture plates (Greiner bio-one Cellstar). Cells were seeded at 100,000 MG-63 cells per well. The cells were evaluated optically using fluorescence microscopy after 24 h, 72 h and 7 days. The cell culture medium was replaced on Days 3 and 6, respectively. The studies were carried out as double determinations. Cell cultures were analyzed for viability and proliferation by fluorescence microscopy (BZ-9000E BIOREVO, Keyence). Calcein-AM was used for detecting the viable cells by adding 10 μM Calcein AM (Thermo Fisher Scientific) into the culture medium and incubating for 10 min at 37 °C.[22] Calcein - AM is converted to strong green fluorescent when taken up by viable cells after intra-cellular esterases remove the acetomethoxy (AM) group.
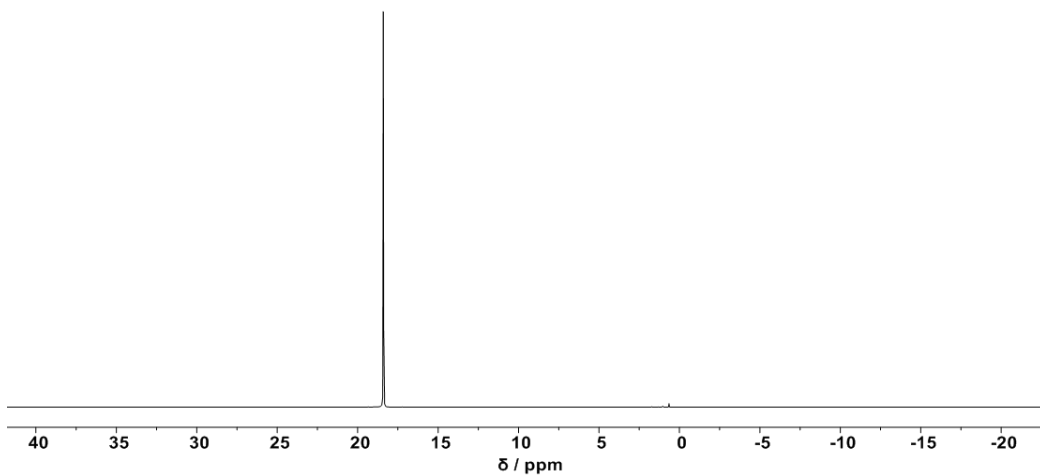
4.4 ^{1}H, ^{13}C, ^{31}P NMR spectra
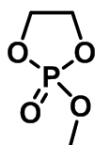
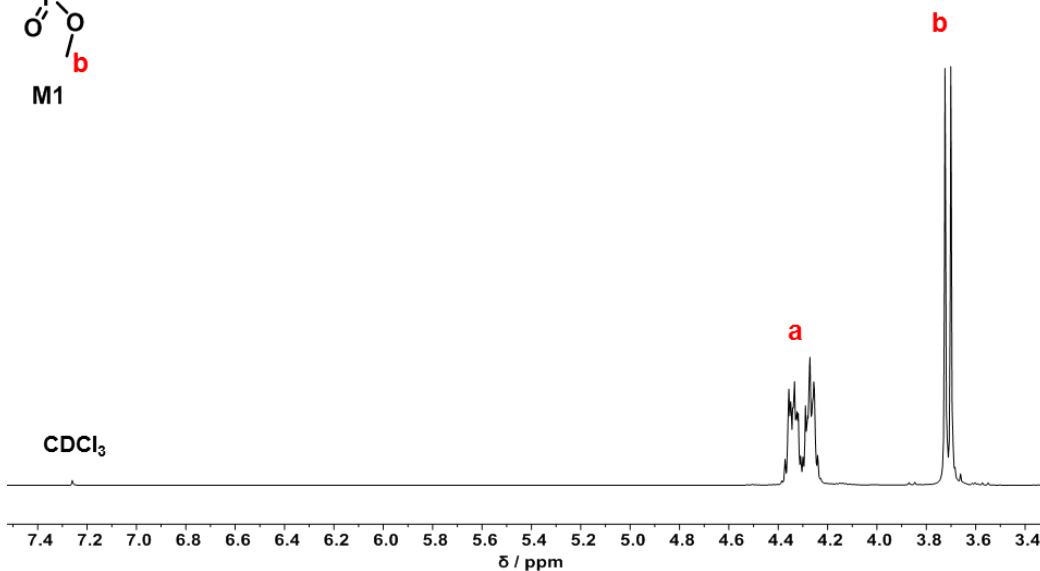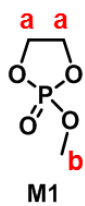**Figure 5.7. ^{31}P (202 MHz) NMR spectra of M1 in CDCl$_3$ at 298 K.**

Figure 5.8. ^{1}H (500 MHz) NMR spectra of M1 in CDCl$_3$ at 298 K.

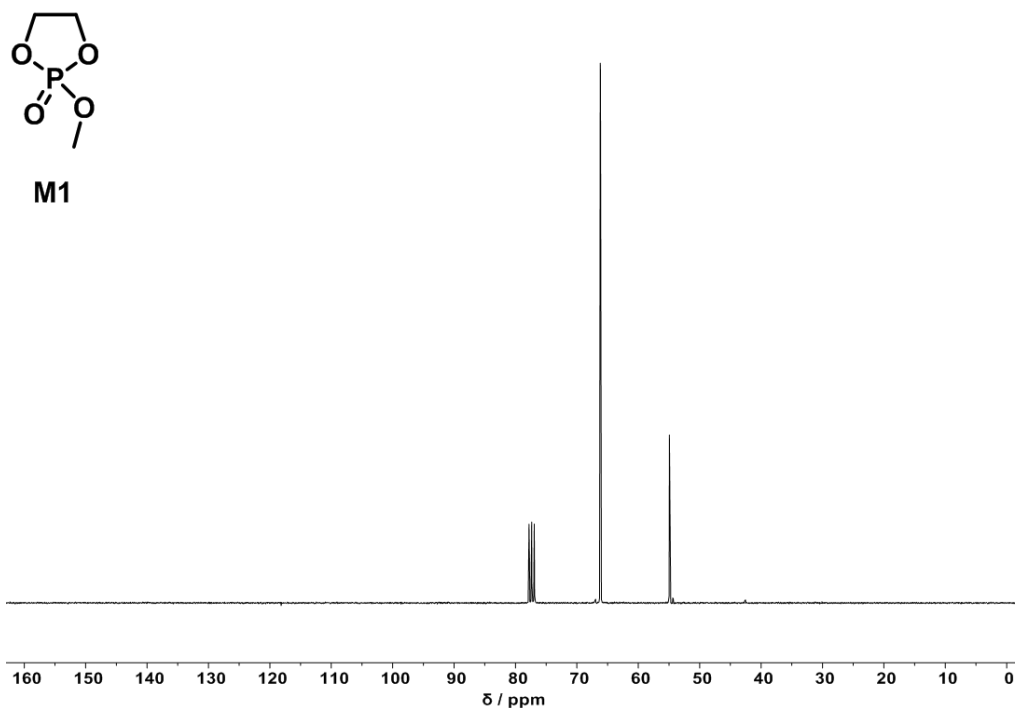**Figure 5.9.** ^{13}C (75 MHz) NMR spectra of M1 in CDCl$_3$ at 298 K.
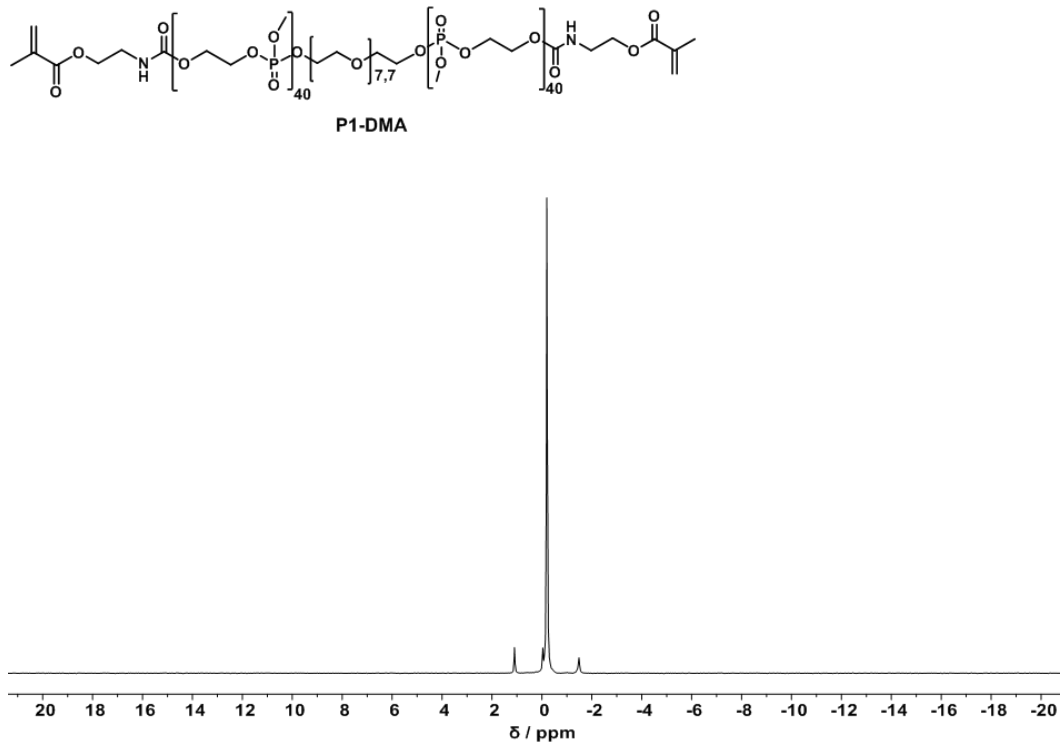
Figure 5.10. ^{31}P (121 MHz) NMR spectra of P1-DMA in CDCl$_3$ at 298 K.
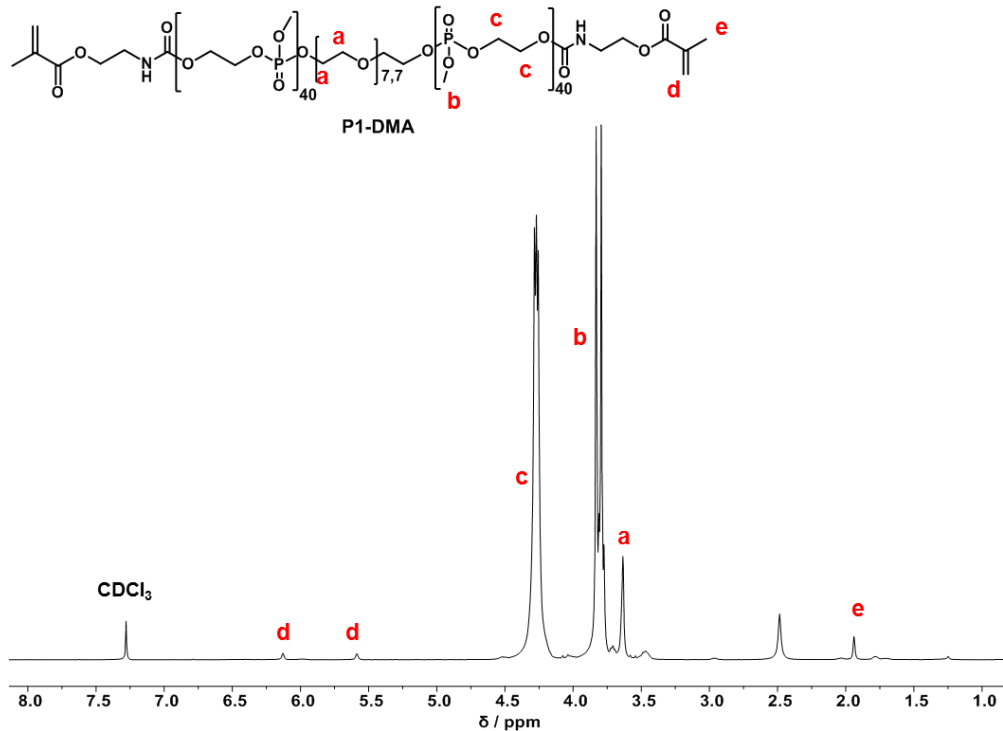
Figure 5.11. ^{1}H (300 MHz) NMR spectra of P1-DMA in CDCl$_3$ at 298 K.

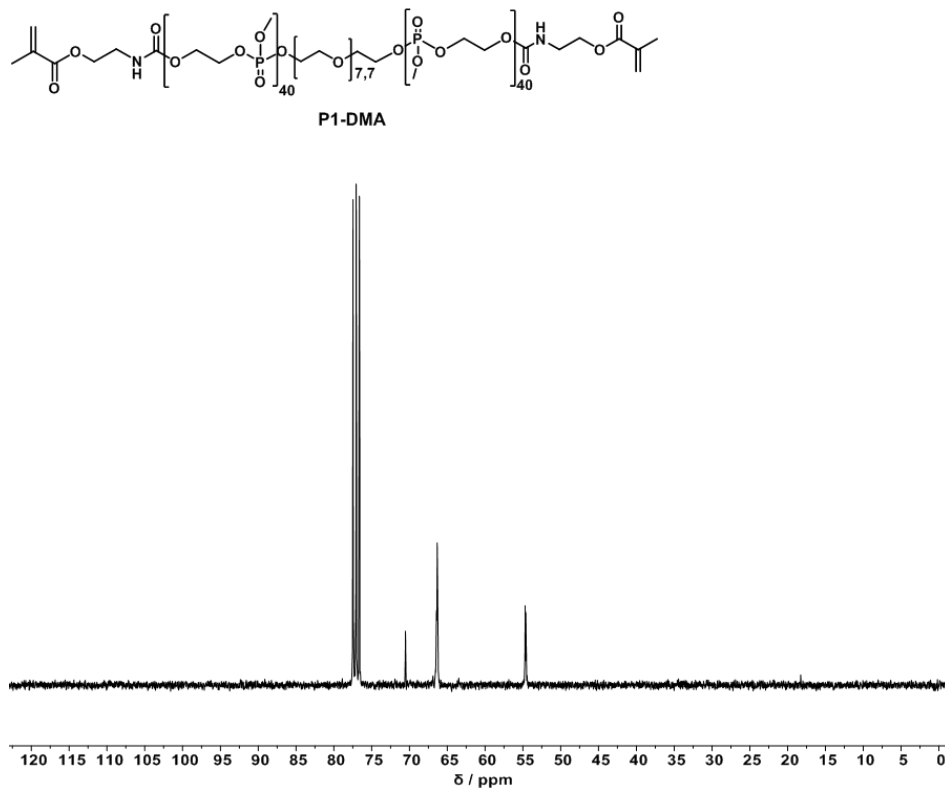**Figure 5.12.** ^{13}C (75 MHz) NMR spectra of P1-DMA in CDCl$_3$ at 298 K.
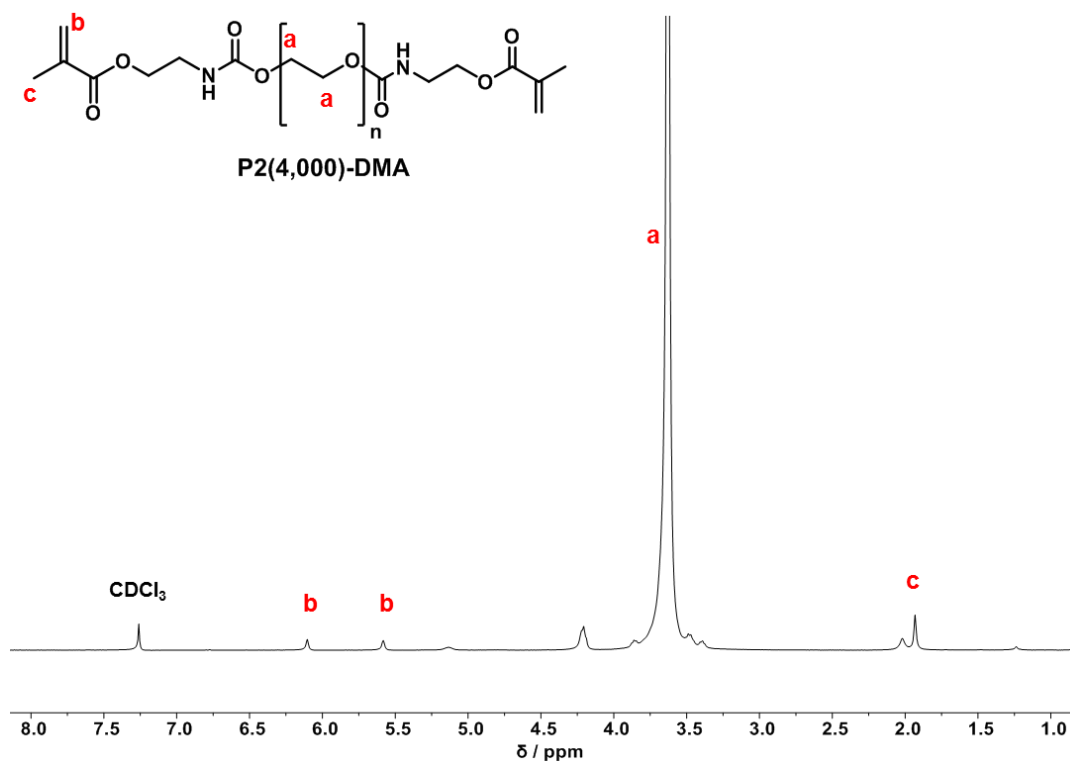
Figure 5.13. ^{1}H (300 MHz) NMR spectra of P2(4,000)-DMA in CDCl$_3$ at 298 K.
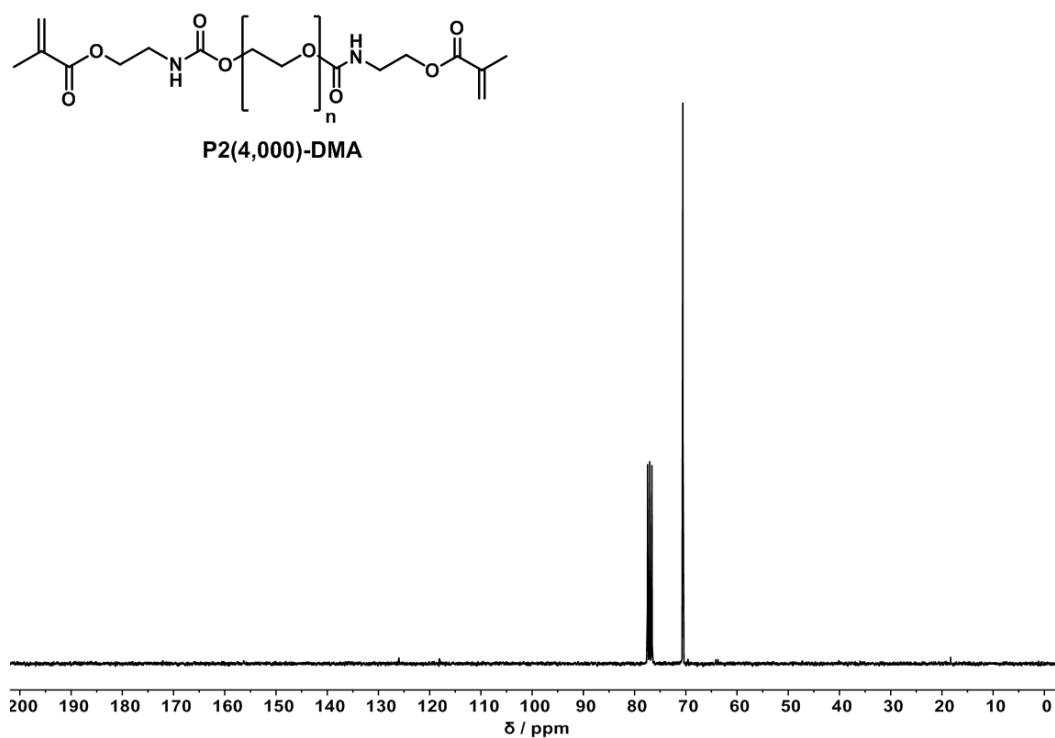
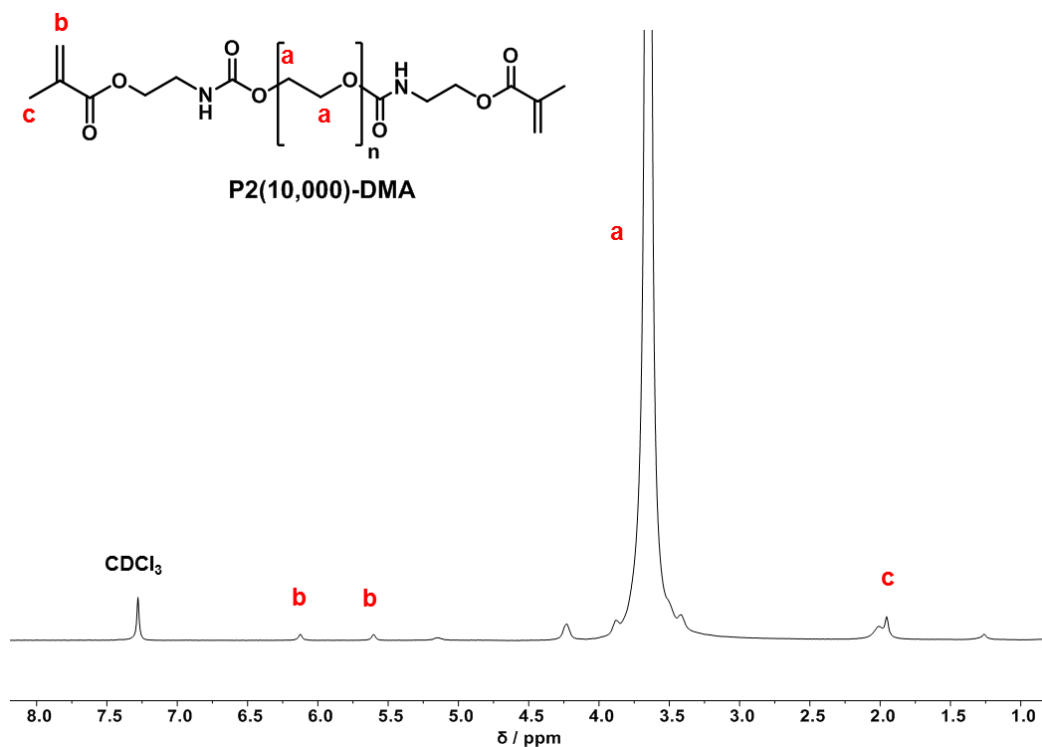**Figure 5.14.** ^{13}C (75 MHz) NMR spectra of P2(4,000)-DMA in CDCl3 at 298 K.

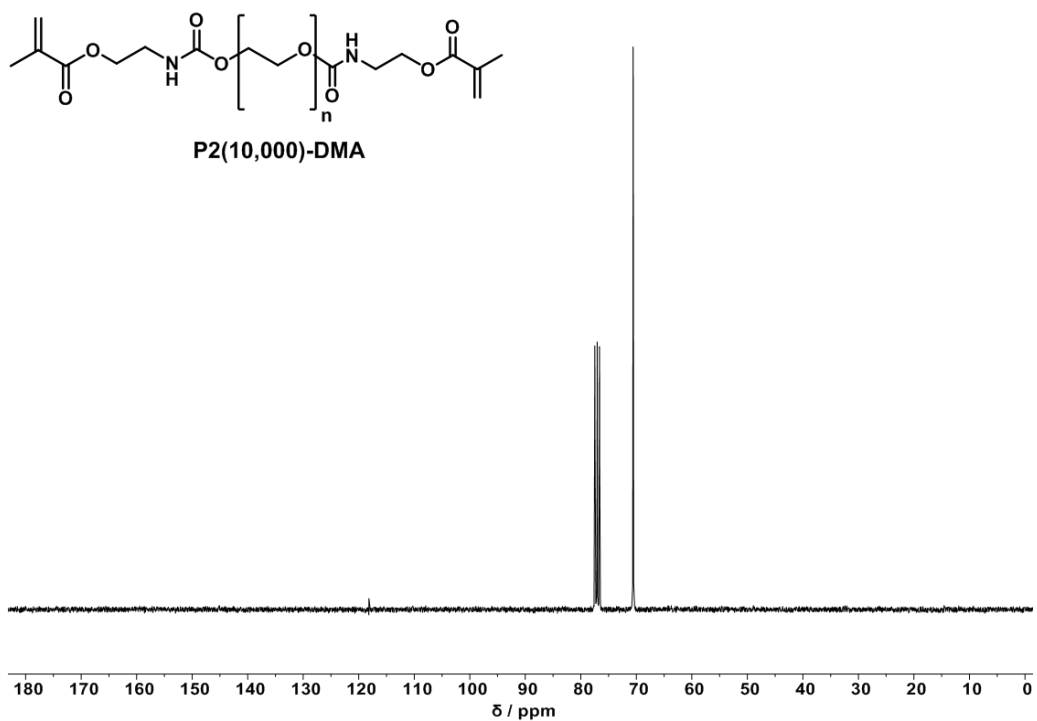**Figure 5.15.** ^{1}H (300 MHz) NMR spectra of P2(10,000)-DMA in CDCl3 at 298 K.

Figure 5.16. ^{13}C (75 MHz) NMR spectra of P2(10,000)-DMA in CDCl3 at 298 K.

4.5   IR Spectra
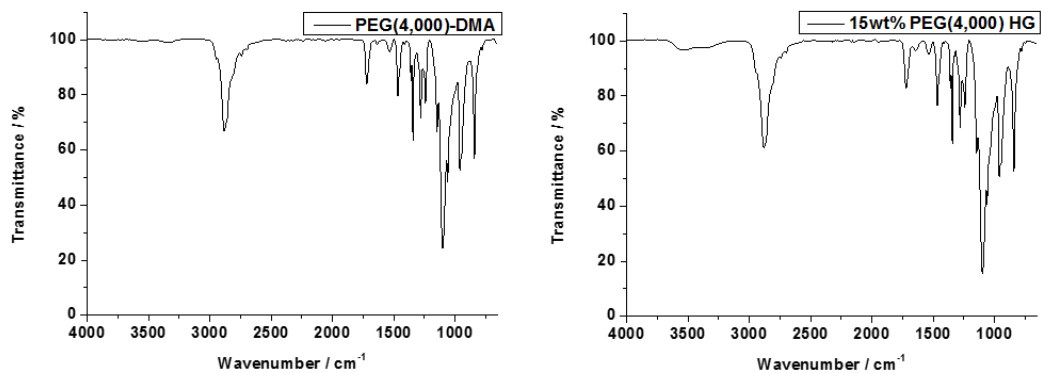
Figure 5.17. IR Spectra of PEG(4,000)-DMA and 15 w% PEG(4,000) Hydrogel
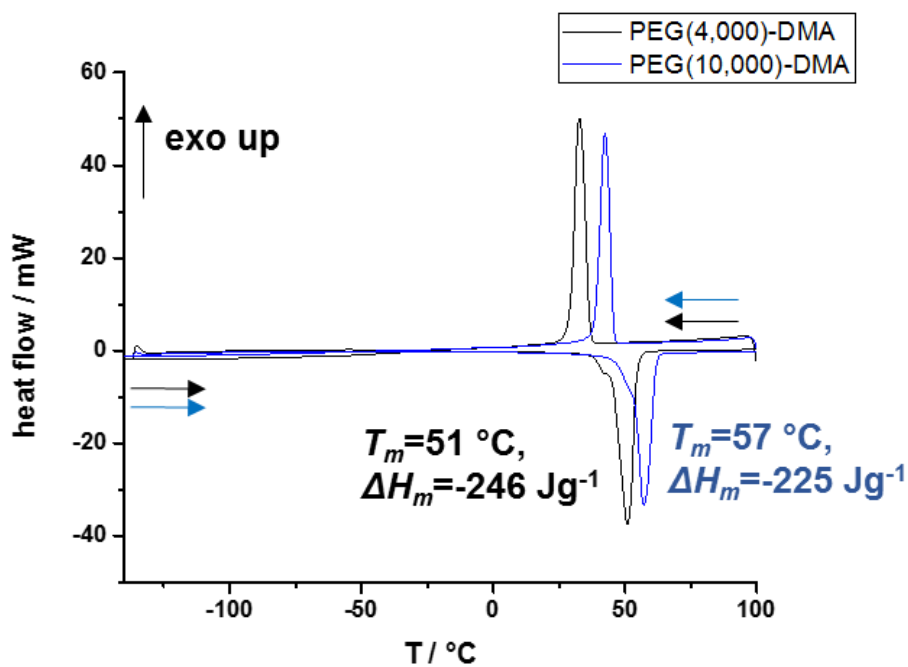
4.6   DSC

Figure 5.18. DSC of PEG(4,000)-DMA and PEG(10,000)-DMA with a heating (second run) and cooling rate of 10 K min⁻¹.
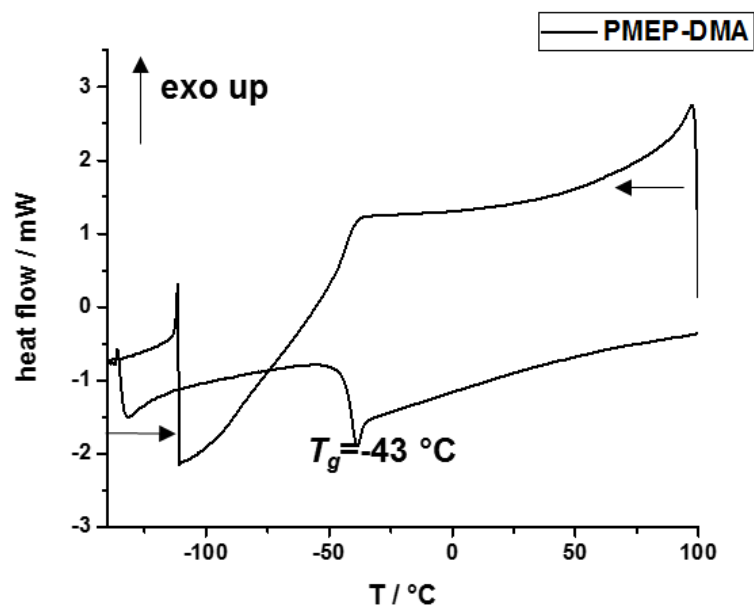
Figure 5.19. DSC of PMEP-DMA with a heating (second run) and cooling rate of 10 K min⁻¹.
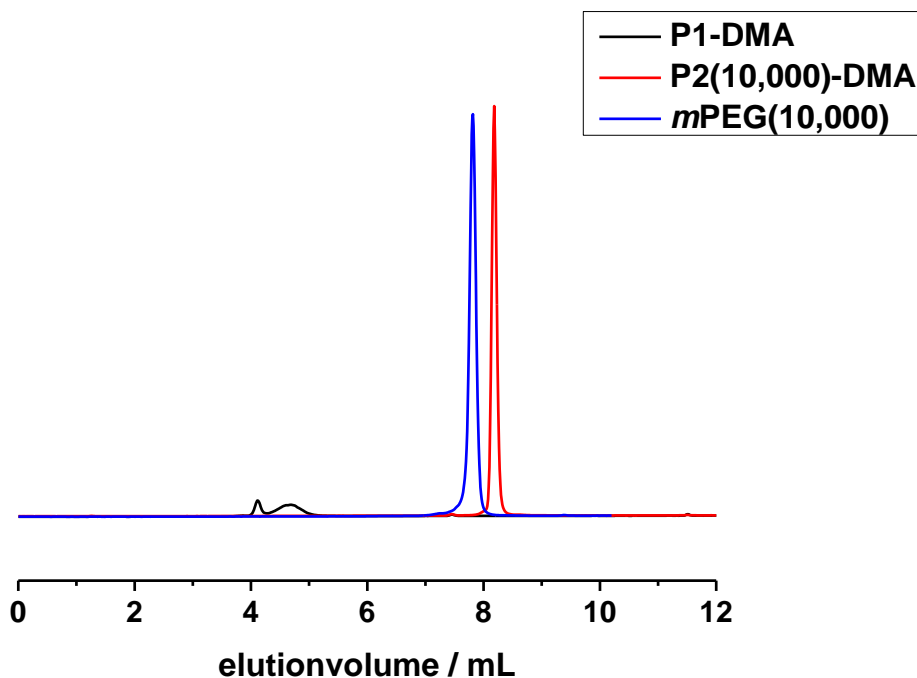
4.7 HPLC

Figure 5.20. Reverse-phase HPLC assisted determination of the hydrophilicity of P1-DMA, P2(10,000)-DMA and mPEG(10,000).

5   References

1.   Hoffman, A. S., Hydrogels for biomedical applications. *Advanced Drug Delivery Reviews* **2012,** *64*, 18-23.

2.   Drury, J. L.; Mooney, D. J., Hydrogels for tissue engineering: scaffold design variables and applications. *Biomaterials* **2003,** *24* (24), 4337-4351.

3.   Peppas, N. A.; Hilt, J. Z.; Khademhosseini, A.; Langer, R., Hydrogels in Biology and Medicine: From Molecular Principles to Bionanotechnology. **2006,** *18* (11), 1345-1360.

4.   Nuttelman, C. R.; Rice, M. A.; Rydholm, A. E.; Salinas, C. N.; Shah, D. N.; Anseth, K. S., Macromolecular monomers for the synthesis of hydrogel niches and their application in cell encapsulation and tissue engineering. *Progress in Polymer Science* **2008,** *33* (2), 167-179.

5.   Jokerst, J. V.; Lobovkina, T.; Zare, R. N.; Gambhir, S. S., Nanoparticle PEGylation for imaging and therapy. **2011,** *6* (4), 715-728.

6.   Lu, S.; Anseth, K. S., Release Behavior of High Molecular Weight Solutes from Poly(ethylene glycol)-Based Degradable Networks. *Macromolecules* **2000,** *33* (7), 2509-2515.

7.   Mason, M. N.; Metters, A. T.; Bowman, C. N.; Anseth, K. S., Predicting Controlled-Release Behavior of Degradable PLA-b-PEG-b-PLA Hydrogels. *Macromolecules* **2001,** *34* (13), 4630-4635.

8.   Molina, I.; Li, S.; Martinez, M. B.; Vert, M., Protein release from physically crosslinked hydrogels of the PLA/PEO/PLA triblock copolymer-type. *Biomaterials* **2001,** *22* (4), 363-369.

9.   Metters, A. T.; Anseth, K. S.; Bowman, C. N., Fundamental studies of a novel, biodegradable PEG-b-PLA hydrogel. *Polymer* **2000,** *41* (11), 3993-4004.

10.   Bryant, S. J.; Anseth, K. S., Controlling the spatial distribution of ECM components in degradable PEG hydrogels for tissue engineering cartilage. **2003,** *64A* (1), 70-79.

11.   Wang, D. K.; Varanasi, S.; Strounina, E.; Hill, D. J. T.; Symons, A. L.; Whittaker, A. K.; Rasoul, F., Synthesis and Characterization of a POSS-PEG Macromonomer and POSS-PEG-PLA Hydrogels for Periodontal Applications. *Biomacromolecules* **2014,** *15* (2), 666-679.

12.   Metters, A. T.; Anseth, K. S.; Bowman, C. N., Fundamental studies of biodegradable hydrogels as cartilage replacement materials. *Biomed Sci Instrum* **1999,** *35*, 33-38.

13.   Goraltchouk, A.; Freier, T.; Shoichet, M. S., Synthesis of degradable poly(l-lactide-co-ethylene glycol) porous tubes by liquid–liquid centrifugal casting for use as nerve guidance channels. *Biomaterials* **2005,** *26* (36), 7555-7563.

14.   Zhao, X.; Milton Harris, J., Novel degradable poly(ethylene glycol) hydrogels for controlled release of protein. **1998,** *87* (11), 1450-1458.

15.   Elbert, D. L.; Pratt, A. B.; Lutolf, M. P.; Halstenberg, S.; Hubbell, J. A., Protein delivery from materials formed by self-selective conjugate addition reactions. *Journal of Controlled Release* **2001,** *76* (1), 11-25.

16.   Metters, A.; Hubbell, J., Network Formation and Degradation Behavior of Hydrogels Formed by Michael-Type Addition Reactions. *Biomacromolecules* **2005,** *6* (1), 290-301.

17.   Farrugia, B. L.; Kempe, K.; Schubert, U. S.; Hoogenboom, R.; Dargaville, T. R., Poly(2-oxazoline) Hydrogels for Controlled Fibroblast Attachment. *Biomacromolecules* **2013,** *14* (8), 2724-2732.

18.   Bauer, K. N.; Tee, H. T.; Velencoso, M. M.; Wurm, F. R., Main-chain poly(phosphoester)s: History, syntheses, degradation, bio-and flame-retardant applications. *Progress in Polymer Science* **2017,** *73*, 61-122.

19.   Schöttler, S.; Becker, G.; Winzen, S.; Steinbach, T.; Mohr, K.; Landfester, K.; Mailänder, V.; Wurm, F. R. J. N. n., Protein adsorption is required for stealth effect of poly (ethylene glycol)-and poly (phosphoester)-coated nanocarriers. **2016,** *11* (4), 372.

20.   Pratt, R. C.; Lohmeijer, B. G. G.; Long, D. A.; Lundberg, P. N. P.; Dove, A. P.; Li, H.; Wade, C. G.; Waymouth, R. M.; Hedrick, J. L., Exploration, Optimization, and Application of Supramolecular Thiourea−Amine Catalysts for the Synthesis of Lactide (Co)polymers. *Macromolecules* **2006,** *39* (23), 7863-7871.

21.   Bencherif, S. A.; Srinivasan, A.; Sheehan, J. A.; Walker, L. M.; Gayathri, C.; Gil, R.; Hollinger, J. O.; Matyjaszewski, K.; Washburn, N. R., End-group effects on the properties of PEG-co-PGA hydrogels. *Acta Biomaterialia* **2009,** *5* (6), 1872-1883.

22.   Unger, R. E.; Huang, Q.; Peters, K.; Protzer, D.; Paul, D.; Kirkpatrick, C. J., Growth of human cells on polyethersulfone (PES) hollow fiber membranes. *Biomaterials* **2005,** *26* (14), 1877-1884.

23.   Engler, A. J.; Sen, S.; Sweeney, H. L.; Discher, D. E. J. C., Matrix elasticity directs stem cell lineage specification. **2006,** *126* (4), 677-689.

24.   Engler, A.; Sweeney, H.; Discher, D.; Schwarzbauer, J. J. J. o. M.; Interactions, N., Extracellular matrix elasticity directs stem cell differentiation. **2007,** *7* (4), 335.

25.   Engler, A. J.; Sen, S.; Sweeney, H. L.; Discher, D. E., Matrix Elasticity Directs Stem Cell Lineage Specification. *Cell* **2006,** *126* (4), 677-689.

26.   Peppas, N. A.; Hilt, J. Z.; Khademhosseini, A.; Langer, R. J. A. m., Hydrogels in biology and medicine: from molecular principles to bionanotechnology. **2006,** *18* (11), 1345-1360.

27.   Tanaka, T. J. S. A., Gels. **1981,** *244* (1), 124-S-17.

28.   Qiu, Y.; Park, K., Environment-sensitive hydrogels for drug delivery. *Advanced Drug Delivery Reviews* **2001,** *53* (3), 321-339.

29.   Peppas, N. A., Hydrogels and drug delivery. *Current Opinion in Colloid & Interface Science* **1997,** *2* (5), 531-537.

30.   Balakrishnan, B.; Mohanty, M.; Umashankar, P. R.; Jayakrishnan, A., Evaluation of an in situ forming hydrogel wound dressing based on oxidized alginate and gelatin. *Biomaterials* **2005,** *26* (32), 6335-6342.

31.   Jen, A. C.; Wake, M. C.; Mikos, A. G., Review: Hydrogels for cell immobilization. **1996,** *50* (4), 357-364.

32.   Kretlow, J. D.; Mikos, A. G., From material to tissue: Biomaterial development, scaffold fabrication, and tissue engineering. **2008,** *54* (12), 3048-3067.

33.   Novosel, E. C.; Kleinhans, C.; Kluger, P. J., Vascularization is the key challenge in tissue engineering. *Advanced Drug Delivery Reviews* **2011,** *63* (4), 300-311.

34.   Lin, C.-C.; Anseth, K. S. J. P. R., PEG Hydrogels for the Controlled Release of Biomolecules in Regenerative Medicine. **2009,** *26* (3), 631-643.

Appendix

1   List of publications

1.   **"**Aliphatic Long-Chain Polypyrophosphates as Biodegradable Polyethylene Mimics"

Hisaschi T. Tee, Ingo Lieberwirth, Frederik R. Wurm, *Macromolecules*, 2019, 52 (3), 1166-1172. DOI: 10.1021/acs.macromol.8b02474.

2.   "Morphology and Thermal Properties of Precision Polymers: The Crystallization of Butyl Branched Polyethylene and Polyphosphoesters"

Yi-Ran R. Zheng, **Hisaschi T. Tee**, Yujin Wei, Xi-Lin Wu, Markus Mezger, Shouke Yan, Katharina Landfester, Ken Wagener, Frederik R. Wurm, Ingo Lieberwirth, *Macromolecules*, 2016, 49 (4), 1321-1330. DOI: 10.1021/acs.macromol.5b02581.

3.   "In-Chain Poly(phosphonate)s via Acyclic Diene Metathesis Polycondensation"

Kristin N. Bauer, **Hisaschi T. Tee**, Ingo Lieberwirth, Frederik R. Wurm, *Macromolecules*, 2016, 49 (10), 3761-3768. DOI: 10.1021/acs.macromol.6b00366.

4.   "Main-chain poly(phosphoester)s: History, syntheses, degradation, bio- and flame-retardant applications"

Kristin N. Bauer, **Hisaschi T. Tee**, M. M. Velencoso, F.R. Wurm, *Prog. Polym. Sci.*, 2017. 73, 61-122. DOI: 10.1016/j.progpolymsci.2017.05.004.

5.   "Polyphosphoesters: An Old Biopolymer in a New Light. Polymers for Biomedicine: Synthesis, Characterization, and Applications"

Kristin N. Bauer, **Hisaschi T. Tee**, Evandro M. Alexandrino, Frederik R. Wurm, Polymers for Biomedicine: Synthesis, Characterization, and Applications, 2017, 191-241. DOI: 10.1002/9781118967904.ch7.

6.   "Crystallization of a polyphosphoester at the air-water interface"

Nazmul Hasan, Christian Schwieger, **Hisaschi T. Tee**, Frederik R. Wurm, Karsten Busse, Jörg Kressler, *Eur. Polym. J.*, 2018, 101, 350-357. DOI: 10.1016/j.eurpolymj.2018.03.001.

7.   "Supercooled Water Drops Do Not Freeze During Impact on Hybrid Janus Particle-Based Surfaces"

Madeleine Schwarzer, Thomas Otto, Markus Schremb, Claudia Marschelke, **Hisaschi T. Tee**, Frederik R. Wurm, Ilia V. Roisman, Cameron Tropea, Alla Synytska,. *Chem. Mater.*, 2019, 31 (1), 112-123. DOI: 10.1021/acs.chemmater.8b03183.

8.   "Non-covalent hydrogen bonds tune the mechanical properties of phosphoester polyethylene mimics"

Hisaschi T. Tee, Kaloian Koynov, Tobias Reichel, Frederik R. Wurm, *submitted*.

9.   "Polyphosphoester Hydrogels: Degradable and Cell-Repellent Alternatives to PEG-Hydrogels"

Hisaschi T. Tee, Kaloian Koynov, Frederik R. Wurm, *in preparation*.

10.   "Thermo-responsive grafted polymer brushes: influence of chemical design and wettability on adhesion underwater"

Ugo Sidoli, **Hisaschi T. Tee**, Ivan Raguzin, Jakob Mühldorfer, Frederick R. Wurm, Alla Synytska, *in preparation*.